# Experimental Validation of Computational Model for Circulating Albumin Dialysis and Optimization of Conditions

Alexander Novokhodko

A dissertation

submitted in partial fulfillment of the

requirements for the degree of

Doctor of Philosophy

University of Washington

2024

Reading Committee:

Dayong Gao, Chair

Suhail Ahmad

Jaehyun Chung

Zhiquan Shu

Program Authorized to Offer Degree:

Mechanical Engineering

University of Washington

**Abstract**

# Experimental Validation of Computational Model for Circulating Albumin Dialysis and Optimization of Conditions

Alexander Novokhodko

Chair of the Supervisory Committee:
Dayong Gao
Departments of Mechanical Engineering and Bioengineering

Traditional dialysis saves lives by removing water soluble toxins along a concentration gradient across a semi-permeable membrane. Protein bound toxins (PBTs) cannot be removed by traditional dialysis methods. By design, dialyzer pores do not allow carrier proteins like albumin or ceruloplasmin to cross the membrane. Many medical conditions such as liver failure and cholestasis are defined in part by an excess of PBTs such as bilirubin, cholic acid, copper, or manganese. End stage renal disease (ESRD) also involves the accumulation of protein bound uremic toxins (PBUTs) such as indoxyl sulfate. Removing protein bound toxins would prevent the progression of these and other diseases. PBT removal may allow recovery of the patient by reducing metabolic stress on cells in the failing organ (for example, hepatocytes in the liver). Alternatively, it may bridge the patient to a destination therapy, such as liver transplant. Finally,

for ESRD patients, adding a protein bound toxin removal mechanism may improve quality of life when ESRD is used as a destination therapy.

Devices for removing PBTs are commonly called artificial liver support systems, because this is the original intended use case. However, they have also been tested for treating cholestasis, poisonings, and chronic kidney disease (CKD).

These devices use one or more of three approaches: The first approach is a dialysate binder suspension. A material that binds the PBT of interest is added to the dialysate. The material, referred to as the binder, has an affinity for the toxin of interest. The toxin of interest crosses the dialyzer membrane, moving along a chemical gradient. It then binds to the binder molecule. The second approach is a sorbent column to remove PBTs. Here, grains of sorbent are fixed in a plastic housing. Toxin-laden blood or plasma flows directly past the sorbent column. Toxins are removed by binding to sites on the column. The third approach is to exchange toxin-laden blood, or fractions of blood, for a healthy donor blood product.

Existing devices have mixed records in clinical trials. Our group recently published promising clinical data describing Acute-on-Chronic Liver Failure (AoCLF) treatment using our Advanced Multi-Organ Replacement System (AMOR). AMOR uses a human serum albumin (HSA) binder to remove toxins from blood and a charcoal sorbent column to regenerate the HSA dialysate. This is then followed by a traditional hemodialysis system which permits the removal of excess fluid and water soluble toxins, along with pH control. Unlike previous systems, AMOR removed large quantities of excess fluid (edema) from previously hypotensive liver failure patients who were refractory to fluid removal by dialysis. To our knowledge, this is the first system to achieve notable ultrafiltration in liver dialysis.

To improve treatment with AMOR, or any other binder dialysis system, we developed and validated a computational model to predict PBT removal by binder dialysis. In this work we demonstrated its ability to accurately predict the final toxin concentration in benchtop trials with differing dialyzers, binder dialysate compositions, and flow rates.

Assays were designed for bilirubin, albumin, creatinine, cholic acid, indoxyl sulfate, manganese, and copper. These toxins are significant for hepatic failure, ESRD, inborn errors of metabolism, cholestasis, intestinal stagnant loop syndrome, and acute poisonings. Albumin was measured to study methods to prevent albumin loss. Albumin could be lost due to binding to a sorbent column, or by transfer through a ruptured dialysis membrane.

Trials were conducted to verify that albumin dialysate removes the toxins of interest in a benchtop model. The impact of flow rate on protein bound toxin removal was measured and fit using a model in which the membrane transfer coefficient of unbound toxin declines linearly with flow rate. The albumin dialysate trials were compared to negative control trials where dialysate did not contain binders. Then, the sensitivity of the system to dialysate flow rate was tested. Finally, it was shown that bovine serum albumin (BSA) at high concentration (20 g/dL) can remove bilirubin, cholic acid, and indoxyl sulfate from a human serum albumin (HSA) blood analog solution more effectively than 2 g/dL HSA or a lower (2 g/dL) BSA concentration.

Charcoal column perfusion trials were done to test the ability of the FDA-approved Adsorba 300 column to remove bilirubin. A regeneration protocol was tested to determine if column saturation can be reversed by flowing dialysate through the column. Regeneration restored the rate of toxin concentration decline to the initial rate. Future study will focus on optimizing this process, validating this conclusion, and minimizing albumin loss.

Dextrans were identified as promising alternatives to albumin for removing some PBTs. Dextrans are low cost compared to human serum albumin. Dextran 70 removed more bilirubin than dialysate with no added binder. Our pilot study suggests that anionic dextran sulphate likely removes copper. Dextran binder dialysis may offer a new, cost-effective method to remove PBTs.

Albumins from different species offer another source of novel binders to optimize binder dialysis. Porcine Serum Albumin (PSA) and BSA dialysate both removed more cholic acid than HSA dialysate from an HSA blood analog solution. For other toxins, PSA and BSA dialysates were indistinguishable from HSA regarding the amount of toxin removed.

Finally, our data suggests that the polysulfone membrane used in the Fresenius F3 dialyzer absorbs bilirubin. The quantity of bilirubin absorbed at equilibrium is measured. Better characterizing this phenomenon will enable the design of a new device for bilirubin removal using a low-risk FDA approved material. This is a critical area for further study. This includes membrane absorption of other PBTs, polysulfone rinsing and regeneration methods, and improved computational modeling of PBT removal that incorporates membrane binding.

# TABLE OF CONTENTS

# LIST OF FIGURES

# LIST OF TABLES

# ACKNOWLEDGEMENTS

I would like to thank everyone who contributed to this work. This includes my advisor, Dr. Dayong Gao, my clinical co-advisor Dr. Suhail Ahmad, the Graduate School Representative Dr. Xiaohu Gao, my committee members Dr. Jaehyun Chung and Dr. Zhiquan Shu, and current and former Gao lab members. Nanye Du, Yanyi Wang, and Shaohang Hao contributed to the albumin dialysis and charcoal column studies. Dr. Shen Ren contributed to the AU680 assay development. Ziyuan Wang contributed to pressure and temperature measurement software. Ye Jin helped with the charcoal column studies. Ruidong Ma manages our lab and keeps it clean and running smoothly. Shaohang Hao translated several important papers in Chinese. Dr. Martin Sadilek from the Bagley Hall mass spectrometry facility taught me to use the instrument there. Dr. Julia Cui and Dr. Moumita Dutta helped design the cholic acid measurement protocol. Dr. Jakub Sliwinski and Asiran Siu-Kwong Chaing helped design the copper and manganese measurement protocol. Asiran conducted many of the sample digestions. Dr. Sliwinski operated the gas chromatography-mass spectrometry instrument. My indoxyl sulfate measurement protocol is based on previous work by Dr. Runbang Tang. Girold Martelino provided assistance with clinical aspects of this research. Dr. Eli Shlizerman advised regarding the mathematical modeling aspect of this work. Dr. Forest Bohrer and Dev Narasimhan from the University of Washington's Technology Transfer Office have provided support regarding intellectual property related to this work. Kiehl Sundt provided pro-bono legal support related to the intellectual property that this work generated.

Other students in the Gao Lab were valued colleagues in my graduate school journey, contributing to projects that didn't become part of this thesis, but are of great importance to our future work. Tejoram Vivekanandan, Noah Griffaton, and Pavtir Agarwal contributed to

developing a contactless bilirubin measurement algorithm, which we are patenting. Logan Snider contributed to the development of the Advanced Multi-Organ Replacement system. Avocet Nagle-Christensen, Yuji Furukawa, and Sarmad Hassan studied optimization of rinsing fluid composition for charcoal column regeneration. Yuji Furukawa translated papers from Japanese. Enrique Liang designed a computer model of a charcoal column with an alternative geometry in support of a planned machining effort.

Carla Pagotto, Dr. Terri Butler, and Ian Johnson of the Massachusetts Institute of Technology Blueprint Engine program provided advice on commercialization of these technologies. Carla Pagotto contributed significantly to mentoring our team during business competitions. Soraya Bailey supported our team during customer discovery in National I-CORPS, serving as our team's Industry Mentor.

This work was supported by the National Science Foundation (NSF) Graduate Research Fellowship Program grant DGE-1762114. Any opinions, findings, and conclusions or recommendations expressed in this material are those of the author(s) and do not necessarily reflect the views of the National Science Foundation. The Center for Dialysis Innovation provided support for this work. The Ron and Wanda Crockett Endowed Fellowship helped support my graduate studies. I am grateful to the judges and sponsors of the Hollomon Health Innovation Challenge and Dempsey Startup Challenge for awarding our team second place prizes at these business competitions. I further acknowledge the University of Washington (UW) Engineering Innovation in Health program, CoMotion Innovation Gap Fund, and Buerk Center for Entrepreneurship, which provided funding and support for this work. Customer discovery efforts were supported by an NSF National I-CORPS grant and the UW's Regional I-CORPS grant. The Sigma Xi Scientific

Research Honor Society provided funding which supported training in new protocols for me and others in our laboratory.

I am thankful to my family and friends for being there for me during this long process.

A special thanks goes to my wife Claire Accettullo, who supported and encouraged me throughout my PhD journey, traveled with me to conferences, and provided insights when I was stuck. In particular, your insight when the computational model would not converge helped me overcome a great barrier in this work. I look forward to a long life of love, family, and future adventures together.

# Chapter 1. INTRODUCTION

## 1.1 Overview of Protein Bound Toxins

Dialysis has made it possible to remove water-soluble toxins such as urea and ammonia. However, many toxins and metabolites are carried through the bloodstream on carrier proteins such as albumin and ceruloplasmin. These toxins may form ionic bonds with the carrier protein or bind through hydrophobic Van der Waals interactions. When carrier proteins exceed the Molecular Weight Cutoff (MWCO) of the dialysis membrane, these protein bound toxins cannot diffuse across the membrane. In traditional dialysis, only a small unbound fraction rapidly equilibrates across the membrane. This is coupled with toxin binding to the membrane. Together, these factors provide insufficient clearance of protein-bound toxins.

Binding molecules in the fluid on the dialysate side rapidly bind any toxin that crosses the membrane. This reduces the free concentration of toxin in the dialysate to nearly zero. This enables the removal of more toxin along the concentration gradient from the blood side. In turn, that favors the release of more toxin from carrier proteins in blood. This process continues until the dialysate side binder becomes saturated.

Because of its role in toxin transport in the body, albumin is a commonly chosen binder, but albumin is very expensive and supply is limited (1). Currently, clinical albumin can only be acquired from the blood bank, because of a lack of regulatory confidence in the safety and purity of recombinant albumin sources. Thus, systems often recirculate albumin to maximize use efficiency.

A sorbent column of charcoal and resin can be added to the dialysate circuit. This sorbent column binds free toxin in the dialysate, enabling the release of toxin from binding sites on the

dialysate side binder. This mitigates saturation. For example, toxin from blood can be transported onto dialysate albumin across the dialyzer membrane, then to the charcoal column on the dialysate side, preventing the albumin from becoming saturated. This is the case in the Molecular Adsorbent Recirculating System (MARS). The efficiency of albumin usage could be extended further by periodically rinsing the charcoal column. For example, in the recent pilot study describing the Advanced Multi-Organ Replacement System (AMOR), bilirubin is removed from charcoal columns by rinsing (2).

Protein bound toxin removal would benefit a variety of clinical indications. A lack of validated mathematical design principles has prevented binder dialysis systems from reaching their maximal toxin removal potential. In this work, we describe a mathematical theory for the bound solute dialysis process. Then, we implement a computational model using this theory. We fit parameters using experimental data, then use other experimental results to independently validate the computational model in a variety of conditions.

## 1.2 Indications for Protein Bound Toxin Removal:

### 1.2.1 *Liver Failure*

As of 2021 liver failure is the 12$^{th}$ leading cause of death worldwide (3), and rate liver disease appears to be rising. Worldwide, the Global Burden of Disease study does not report the incidence of liver failure but reports 1.43 million deaths in 2021 from Acute-on-Chronic Liver Failure (AoCLF) and 72 thousand deaths from acute viral hepatitis. In the United States (US), the Healthcare Utilization Project (HCUP) reported 88,695 liver failures in 2021 (4). In contrast, Acute Liver Failure (ALF) qualifies for rare disease status according to the US Food and Drug Administration (FDA) definition, with an incidence of 2,000-3,000 cases annually in the US (5).

The gold standard treatment for liver failure is transplantation, but transplant organs are scarce. Even among transplant recipients, Only 10% of the global need for liver transplants is met (6). Much of that need is in developing countries. However, in the United States three year mortality without transplantation on the waiting list was 9% for adults and 3.3% for children in 2022 (7). 23.3% of adults and 15.2% of children were removed from the transplant waiting list, which could indicate recovery, or decompensation to the point where the patient is no longer transplantable. In the United States the failure rates of transplanted organ is 38.1% of deceased donor over 10 years as of 2022 (7).

Many patients on the transplant list have acute decompensation of liver and develop with multiple organ failures, these are taken off the list because of their poor clinical condition and often die. If such patients can be bridged to transplant candidacy by using liver support devices, the survival would increase. In the United States, in 2021 31% of livers from potential deceased donors were not recovered (8). Among those livers recovered, 8.7% were discarded because recipients could not be located, or reallocation was impossible after an initial recipient declined.

The number of liver failure patients that die without ever being added to the transplant waiting list is almost ten times greater than the number of patients waitlisted (9). Many patients are ineligible for transplantation due to severe clinical conditions or psychiatric comorbidities. The healthy liver removes hydrophobic, protein bound, toxins such as bilirubin and bile acids. This means dialysis alone cannot treat liver failure. Existing liver support systems are expensive and have a mixed track record. The Molecular Adsorbent Recirculating System (MARS) and plasma exchange are the only currently U.S. FDA approved artificial liver support systems (10,11).

The liver maintains health and performs complex synthetic, metabolic and excretory functions, vital for survival. With the loss of cells during hepatic failure, various toxins which are

normally removed by the liver, such as ammonia and bilirubin, accumulate in the blood (12). At the same time release of certain toxic and immunoactive substances, such as soluble B7, makes patients susceptible to infection and inflammation. Decreased protein synthesis leads to the deficiency of serum albumin and clotting factors (13). Often patients with severe disease suffer multi-organ failure (MOF) and death. However, if the protein bound toxins are removed, the liver can regenerate (14). Regeneration is a core objective of liver failure treatment.

With regards to patients who cannot be bridged to transplantation, liver support is not likely to be a destination therapy, because the liver has many functions related to coagulation and immunity that cannot be adequately replaced by detoxification alone. Thus, liver support in these patients is instead a bridge to recovery. In ALF, clinically significant results in improving transplant-free survival with plasma exchange have been documented (15). Cellular pathways for liver regeneration have been identified in AoCLF and ALF (14). Long-term survival and organ function recovery in AoCLF without transplantation is possible. For example, Qin and colleagues found 43% five-year survival in plasma exchange recipients and 31% survival in control patients in a 234 patient study where only two patients were transplanted (16). In this study, the plasma exchange conferred a significant benefit, but as discussed in Section 1.3.5.4, most plasma exchange studies in AoCLF did not report this survival benefit, but some patients do survive and recover without transplantation in test and control groups. Further research is needed into identifying good candidates for bridging to recovery in AoCLF patients and avoiding futile treatments.

### 1.2.2 *Other Indications*

Protein bound toxin removal is also beneficial in treating other diseases. Renal failure is the 11$^{th}$ leading cause of death worldwide as of 2021 (3). 14% of United States (US) adults have

chronic kidney disease (17). Globally, 4.1 million patients were estimated to be receiving dialysis treatment in 2023 (18). In 2021, a person in the United States in the 40-44 year old age bracket receiving dialysis had a life expectancy of 8.6 years for women and 9.4 years for men (17). For those lucky enough to get a transplant, challenges remain. 22.9% of deceased donor grafts in the United States fail over 5 years (17). The protein bound uremic toxin (PBUT) indoxyl sulfate is related to vascular disease and overall mortality (19). P-Cresyl sulphate, another PBUT, is associated with vascular calcification. High free P-Cresyl sulphate is associated with death (20). A small study using Fractionated Plasma Separation and Adsorption (FPSA, also known as the Prometheus system) found that it was able to remove P-Cresyl sulphate but arterio-venous conduit thrombosis was a common adverse event (21).

Another condition that could benefit from protein bound toxin removal treatment is pruritus. Pruritus is a protracted itch, affecting at least 22% of people at some point in their lifetime (22). Among patients with chronic pruritus (6 weeks or longer), 15% itch due to biliary and renal disease. Bile acid accumulation in cholestasis is associated with pruritus (23). Bile acids are protein-bound when they circulate in the bloodstream. Whether protein bound toxins account for pruritus in renal failure patients is controversial. Recent work supports removing indoxyl sulfate to alleviate pruritus, but not all reports support this link (24,25). Intractable pruritus has been treated with MARS in several case series, but no randomized controlled trials exist (26).

Similarly, case series report the use of MARS or other forms of binder dialysis to treat acute poisonings by a variety of protein bound toxins such as drugs and medications. For example, MARS has been used to treat paracetamol intoxication (27). Proper timing is important to avoid removal of beneficial molecules, such as the N-acetyl cystine used to treat the overdose (28).

Several rare diseases are caused by protein bound toxins. These include inborn errors of metabolism caused by protein bound metal ions, and those caused by protein-bound hydrophobic organic toxins such as bilirubin.

Wilson's Disease is an autosomal recessive inborn error of copper metabolism (29). The transporter ATPase ATP7B is impaired in this condition, leading to an inability to secrete copper in bile, or load copper onto the ceruloplasmin carrier protein. Instead, copper accumulates in the liver, brain, and other tissues, and is loaded onto albumin in the blood (30). Copper accumulation drives the death of liver cells. Copper also accumulates in astrocytes in the brain, damaging other cells and forming lesions, especially in the basal ganglia and brain stem. Wilson's disease caused 9,046 hospitalizations in the US from 2006 to 2011 (31). It is estimated that the prevalence of clinically significant Wilson's disease is one in 50,000 (32).

Hypermanganesemia with dystonia is an inborn error of manganese metabolism due to mutations in the SLC30A10 (solute carrier family 30, member 10) protein expressed predominantly, but not exclusively on biliary and intestinal epithelia (33,34). Manganese accumulates in the brain (particularly the basal ganglia) and liver of affected individuals, causing liver impairment and movement disorders in childhood that resemble parkinsonism without cognitive deficits. This disorder has only been described recently, and prevalence has not yet been established (35).

Both disorders of metal ion metabolism are managed with chelation. In hypermanganesemia, chelation slows or reverses disease progression in some patients (36). However, in some patients the disorder progresses despite chelation. Chelation is not consistently available in the low resource settings where the disease is most prevalent. In Wilson's disease, symptom alleviation is incomplete, with 60% of patients progressing with worsening neurological

symptoms despite chelation (37). There is some experience using MARS to treat acute decompensation of liver function in Wilson's disease (38).

Crigler-Najjar syndrome is an example of a rare disease caused by an organic protein bound toxin (bilirubin). It is caused by mutations in the bilirubin-uridine diphosphate glucuronosyltransferase gene (39). In the more severe (Type I) manifestation of the disorder, where the enzyme is completely inactive, serum bilirubin levels rise above 20 mg/dL. Excess bilirubin accumulates in tissues, including the brain as blood bilirubin levels exceed albumin binding capacity. The disease state is referred to as kernicterus, based on yellow pigmentation of brain tissue on autopsy. Bilirubin accumulation leads to brain damage, manifesting as cerebral palsy, hearing loss, and if untreated, death. The disease is estimated to occur in 0.6-1 per million live births (40).

Protein bound toxin removal is an area of great unmet clinical need. In this work, we summarize existing systems for protein bound toxin removal. Then we test the removal of five protein bound toxins (bilirubin, indoxyl sulfate, cholic acid, manganese, and copper) which represent various binding sites on albumin and various diseases. We use binder dialysis methods (such as albumin dialysis or lipid dialysis) and fixed sorbent columns (such as activated charcoal). We develop mathematical methods to predict the effectiveness of binder dialysis and validate them. This will aid in the treatment of many currently intractable diseases.

## 1.3 Existing Methods of Protein Bound Toxin Removal: Mechanical Extracorporeal Liver Support

We review systems that detoxify the blood through non-cellular means such as binder dialysis, flat bed sorbent columns, and blood component exchange. We define these devices as Extracorporeal Liver Support systems (ELSS). Other experimental devices use liver-derived cells

in an extracorporeal bioreactor to remove toxins and provide necessary factors and nutrients. These bioartificial livers will be reviewed in a separate manuscript. Stem cell therapies, therapeutic hypothermia, enterosoprtion, and colon dialysis/retention enema are beyond the scope of this review.

ELSS development began in the 1950s and 1960s. The emerging renal dialysis was not effective in toxin removal or prolonging life appreciably in liver failure (41). Since then, many systems have undergone prospective randomized controlled trials (RCTs). Some gained approval from regulatory agencies, but hurdles to clinical use remain.

The aim of ELSS is to remove toxins including protein-bound toxins, an effective ELSS should also improve the internal milieu and physiology. In transplant-eligible patients, the objective is to keep the patient alive until transplantation takes place. Patients who have become too clinically unstable to transplant but are otherwise transplant-eligible can be stabilized using ELSS to enable transplantation (2). In patients where there is no barrier to transplantation except for waitlist priority, ELSS may lower a patient's MELD score, which is used to assess transplant urgency (42). This may prevent the use of ELSS in some circumstances. These considerations can help identify the optimal transplant-eligible patients for ELSS. In transplant-ineligible patients, the objective is instead to recover liver function. The quality of life the patient will experience after therapy must be considered in these candidates. Thus, careful selection of patients is needed in both transplant-eligible and transplant-ineligible cohorts. Though survival outcome is the ultimate desirable test of the efficacy of any ELSS that justifies the high cost and use of resources, other improvement in clinical condition such as reduction in encephalopathy, improvement in renal, cardiac and pulmonary function, and relisting for transplantation are also significant beneficial

outcomes. Here we summarize ELSS devices tested in humans, their mechanisms, and current status.

### 1.3.1 *Renal Replacement Therapy:*

#### 1.3.1.1 Intermittent (IRRT) and Continuous Renal Replacement Therapy (CRRT):

As early as 1950, a Kolff-type artificial kidney was tested for ammonia removal in liver failure (41). After Hemodialysis became widely used to treat kidney failure, hemodialysis (HD), hemofiltration (HF), and hemodiafiltration (HDF) were among the first ELSS devices. Dialysis is often used in liver failure patients with renal comorbidities. However, these techniques cannot effectively remove protein bound or hydrophobic toxins which cannot cross the membrane into aqueous solution. All dialytic techniques can remove some excess fluid and improve electrolyte and pH balances. Edema is a severe manifestation of liver failure. However, the low systemic blood pressure seen in liver failure complicates fluid removal by dialysis. For example, in a recent RCT of CRRT in AoCLF patients, less than half achieved ultrafiltration targets (43). An analysis of patients with hepatorenal syndrome randomized as part of a larger kidney failure trial found no survival benefit from increased CRRT intensity (44). An RCT of AoCLF patients with septic shock and stage 3 acute kidney injury (AKI) found that starting dialysis early improved renal recovery and reduced 28-day mortality (43).

#### 1.3.1.2 Anticoagulation in Dialysis in Liver Failure Patients

Anticoagulation is a challenge in ELSS. Heparin is not recommended because of bleeding risk, heparin-induced thrombocytopenia, and unreliable activated partial thromboplastic time (aPTT) measurements (45). Low molecular weight heparins are contraindicated in renal failure, which is a common sequela of liver failure. Recent studies support the use of regional citrate anticoagulation (RCA) (46,47). Historically, concerns were raised about citrate toxicity because

citrate is metabolized in the liver. However, muscles and kidneys eliminate exogenous citrate in liver failure patients, which is consistent with recent work in CRRT (46), and MARS (47) (discussed in Section 1.3.2.2). An RCT compared 44 patients on CRRT with RCA to 45 CRRT patients without it (46). The patients had a mixture of ALF and AoCLF, with ALF predominating (84-86%). The CRRT modality was continuous veno-venous hemofiltration (CVVH). Citrate reduced filter failure rate. RCA recipients had higher rates of severe hypocalcemia, but increasing the calcium substitution rate resolved this. No elevation in systemic citrate was seen in RCA recipients 6 hours after treatment. There was no difference in 28-day mortality between the two groups. A limitation of this study is that 16 participants received citrate prior to randomization as part of their standard care. While RCA requires attention to calcium levels, this challenge is readily resolvable with existing technology, allowing the use of this anticoagulant.

#### 1.3.1.3 Peritoneal Dialysis (PD):

The history of PD in liver failure starts in the 1950s, when peritoneal lavage by the procedure of Hearn and Berry was done in liver failure patients (48) . The peritoneum has a high molecular weight cutoff. PD allows long dialysis times. Together, these factors could improve blood electrolyte balance and remove protein bound toxins across the peritoneal membrane. Risks include bleeding, blood protein loss, pulmonary complications, and severe outcomes from sudden changes in vascular tone (49,50). No RCTs of PD in ALF/AoCLF have been reported.

### 1.3.2 *Albumin Dialysis:*

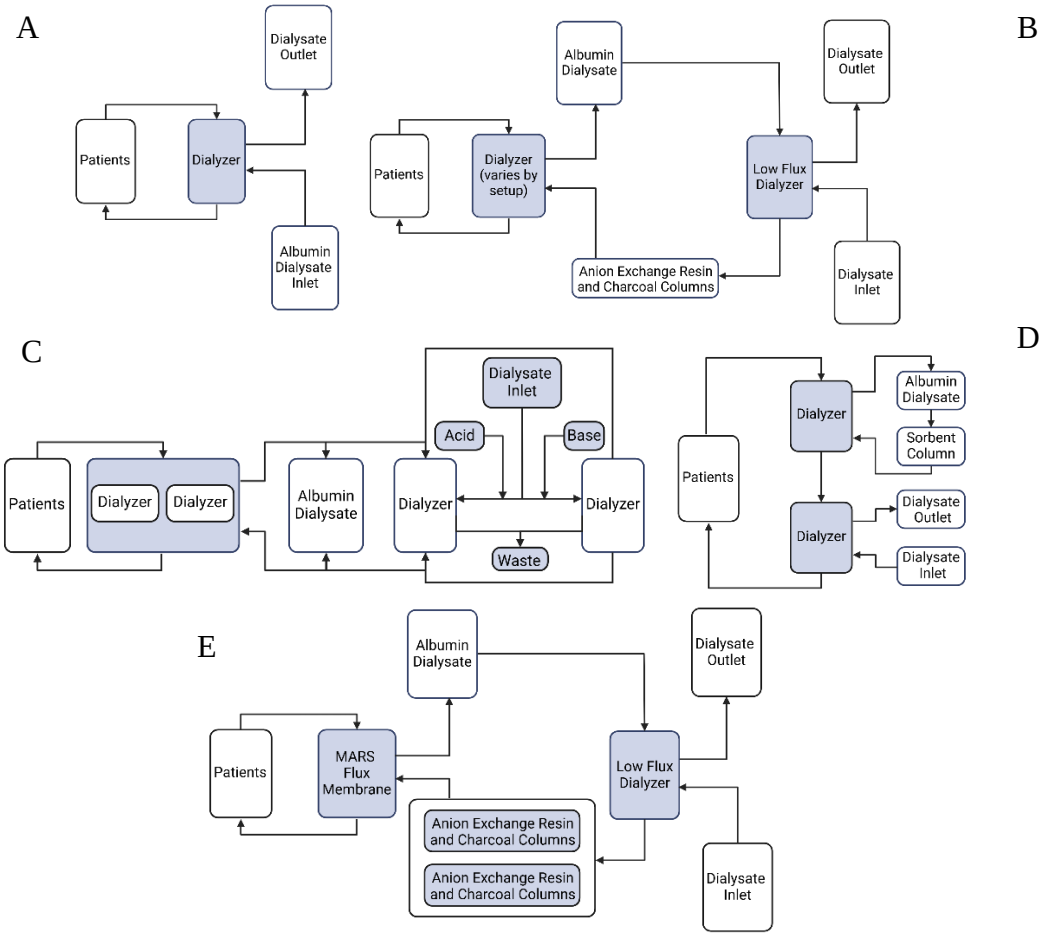


Figure 1-1: **A**: SPAD. Countercurrent flow of blood and albumin dialysate for detoxification. **B**: MARS, ECHS, and OPAL. Albumin dialysate is recycled and regenerated by sorbent columns. The three systems differ only in the sorbent columns used. **C**: ADVOS. Albumin dialysate is regenerated by pH and temperature. **D**: MAHD/AMOR. Combines closed loop mode albumin dialysis with sorbent regeneration and ultrafiltration using dialysis. **E**: HE-MARS. A modified version of MARS with duplicate sorbent columns added in parallel. Figure created with BioRender. Licenses in Appendix A.

In human serum, albumin carries many hepatic toxins such as bilirubin. Thus, adding albumin to dialysate is a reasonable approach to removing hepatic toxins. Their affinity for the dialysate albumin, along with the concentration gradient across the dialyzer, will drive the movement of toxins out of the patient. Albumin dialysate-based liver support systems are shown in Figure 1-1 and their characteristics are summarized in Table 1-1. Figure panels were created with BioRender. BioRender figure licenses are in Appendix A.

Patzer proposed a purely thermodynamic mechanism for detoxification by albumin dialysis (51). The sorbent in the dialysate ensures that the free concentration of toxin there is nearly zero. The small free fraction of toxin in the patient's blood diffuses down the strong concentration gradient. It crosses the membrane and binds dialysate albumin. This causes more of the bound toxin to detach, continuing the process. Membrane-bound albumin facilitates this process. Toxic stabilizers in commercial albumin could reduce the effectiveness of albumin dialysis (52).

Table 1-1: Summary of Albumin Dialysate Based Artificial Liver Support Systems.

| Name | Dialyzer | Treatment Duration | Albumin Circuit | Blood Flow Rate (mL/min) | Albumin Dialysate Flow Rate (mL/min) | Albumin Regeneration Method |
|---|---|---|---|---|---|---|
| **SPAD** | Any | 7.25 hr (53)<br>10 hr (54) | 192 g in 5 L (53)<br>160 g in 5 L (54) | 100-150 (53) | 11.67 (53)<br>16.67 (54) | None (single pass) |
| **MARS** | MARS Flux (55) | Up to 8 hr (53,54,56) | 100 g in 600 mL (57) | 100-150 (53,54)<br>170-500 (55)<br>100-250 (56) | 33.33 (53)<br>16.67 (54)<br>100-250 (55)<br>150 (56) | Charcoal column (AC 250) and anion exchange resin column (IE 250) (55) |
| **ECHS** | Any | Varies | 10 g/dL. Volume not stated. (58) | 10 mL/kg/min | 10 mL/kg/min | Two Adsorba 300 Columns |
| **ADVOS/ HepaWash** | Elisio-19H or Ratingen (59) | Up to 24 hr (60) | 40 g in 2 L (61,62) | 100-400 (60) | 800 (61)<br>320 (63) | 28 °C temperature in albumin circuit and pH alteration (59) |
| **AMOR/ MAHD** | Any | Up to 10 hr (2) | 100-200 g in 5 L | 200 | 20 | Adsorba 300 Column with D5NS Wash |
| **OPAL** | Any | Up to 24 hr (63) | 100 g. Volume not yet published. | 100-150 | 200 | Hepalbin, charcoal column |
| **HE-MARS** | MARS Flux (64) | 5 hr | 150 g in 750 mL | 220 | 150-180 | Same as MARS, two sets of columns |

1.3.2.1 Single Pass Albumin Dialysis (SPAD):

In SPAD each albumin molecule is carried through the dialyzer once before being discarded. Efficiency is maximized when the albumin dialysate flows counter-current to blood. This maintains a constant concentration gradient for toxin removal through the length of the dialyzer. SPAD uses a traditional hemodialysis machine. Walloon et al noted simple training

requirements for clinical staff as an advantage of SPAD (54). SPAD is commercially available in Europe (63).

Two randomized prospective crossover studies comparing SPAD and MARS have been published. The first found that MARS removed a broader set of toxins, but caused platelet loss (53). Biomarkers were worse in the SPAD group. Neither system reduced encephalopathy after a single treatment. The authors suspect that worsening biomarkers in SPAD were due to excessive citrate anticoagulation. However, many groups have successfully used citrate in liver failure patients. For instance, a small RCT in AoCLF patients with a crossover design showed that citrate was superior to no anticoagulation in MARS (47). A previous study in CRRT showed that calcium disturbances due to citrate anticoagulation are manageable and citrate anticoagulation improves filter function (46).

In the second trial, SPAD and MARS had comparable performance (54). MARS removed more creatinine. There was no significant difference in protein bound toxin removal. Bilirubin was reported as total bilirubin, conjugated bilirubin, and unbound bilirubin. Total bilirubin was described as the sum of conjugated and unbound bilirubin. This is difficult to interpret because conjugated bilirubin is typically not protein bound, while unconjugated bilirubin is typically albumin bound (65).

The two trials had different dialysate flow rates. In the first, MARS albumin dialysate flow rate was 2000 mL/hr, while SPAD flow rate was only 700 mL/hr. In the second, SPAD flow rate and MARS flow rates were both 1000 mL/hr. Higher SPAD flow rate requires either lower albumin concentrations or higher costs. RCTs without crossover would be illuminating. Both trials used MARS albumin dialysate flow rates that are significantly lower than standard MARS flow rates (Table 1-1).

SPAD requires large quantities of albumin. Today, clinical human serum albumin (HSA) can only be obtained from donor plasma. This makes it inherently scarce. There is a global shortage of HSA.

#### 1.3.2.2 Molecular Adsorbent Recirculating System (MARS):

Table 1-2: MARS RCTs. Four larger trials are highlighted in bold.

| First Author | Year | N (Treatment/ Control) | Indication | Improved Survival? |
|---|---|---|---|---|
| Mitzner (66) | 2000 | 8/5 | Hepatorenal Syndrome | Yes |
| Stange (67) | 2001 | 24 total, group assignment not reported | AoCLF + Cholestasis | Yes (Enrollment stopped. Enrolling additional placebo recipients deemed unethical) |
| Heemann (68) | 2002 | 12/12 | Acute injury in a background of cirrhosis | Yes |
| Loock (69) | 2002 | 12/4 | AoCLF | Yes |
| **Hu** (70) | **2005** | **40/42** | **Multi-Organ Failure** | **Yes** |
| El Banayosy (71) | 2007 | 20/20 | Hypoxic liver failure following cardiogenic shock | No |
| **Hassanein** (55) | **2007** | **39/31** | **AoCLF** | **No** |
| **Saliba** (72) | **2013** | **53/49** | **ALF** | **No** |
| **Bañares** (56) | **2013** | **95/94** | **AoCLF** | **No** |
| Fuhrmann (73) | 2019 | 20/19 | Hypoxic liver injury in a background of critical illness | No |

MARS recirculates albumin dialysate and regenerates HSA using sorbents. More toxin is removed per gram of HSA. The precursor to MARS was a closed loop system without regeneration, tested in uncontrolled human studies in the early 90s (74). Later versions added

regeneration to increase efficiency. The sorbent columns create a tradeoff: They remove toxins from the albumin dialysate increasing the gradient for toxin removal, but they also adsorb dialysate albumin, weakening the gradient (75). MARS is approved for a variety of indications in both the United States and Europe (10). MARS is contraindicated for patients with severe sepsis, bleeding, or coagulopathy.

MARS has been tested in numerous RCTs, summarized in Table 1-2. Many early small RCTs showed mortality reduction. These included a study of patients with hepatorenal syndrome (66), acute injury in a background of cirrhosis (68), and AoCLF (69). In one RCT of AoCLF complicated by cholestasis, MARS was deemed so effective at improving survival that the trial was stopped by an ethics committee after enrolling 24 subjects on the grounds that it was no longer ethical to enroll control group participants (67). The study has only been published as an abstract, which does not clarify how many patients were in each group.

No RCT after 2005 has shown a survival benefit from MARS. The first study that didn't show a statistically significant improvement in survival was a small early RCT of hypoxic liver failure due to cardiogenic shock following cardiac surgery (71). Controls who reached an elevated bilirubin threshold crossed over into the MARS treatment group. This meant that the control group was smaller and differed from the MARS group in clinically significant ways.

Hassanein reported a large, multicenter RCT of MARS (55). The primary endpoint, clinical improvement of hepatic encephalopathy, was met. However, 180-day survival did not improve. MARS treatment was withdrawn after 5 days. Longer treatment duration may have improved survival.

Two large RCTs in the broader liver failure population completed in the early 2010s showed symptom alleviation, but no significant improvement in survival (56,72). Improvements

in transplant organ availability may account for the difference in outcomes in the ALF RCT of Saliba et al. However, only one per-protocol patient was transplanted in the study of Bañares et al on AoCLF patients. Thus, transplantation cannot account for both unsuccessful RCTs.

The only large trial where MARS showed a statistically significant improvement in survival was the work of Hu et al in Multi-Organ Failure (MOF) patients (70). In summary, MARS produced the best results in the most severe patients and fell short in mixed cohorts.

The most recent RCT of MARS, published in 2019, focused on hypoxic liver injury secondary to critical illness (73). Its primary endpoint was a reduction in indocyanine plasma disappearance rate, a biomarker of mortality. This endpoint was met. However, survival did not significantly improve. The need for vasopressors decreased.

MARS has a blood circuit separated by a dialyzer from an albumin circuit (10). The albumin circuit is separated by another dialyzer from a bicarbonate dialysis system. In both dialyzers, flow is countercurrent. MARS uses the MARS Flux membrane, saturated with HSA based on the belief that this will remove more albumin-bound toxins from the blood. It has a cutoff of 50-60 kDa. In the albumin circuit water-soluble toxins are removed through counter-current exchange across a low flux dialyzer with traditional bicarbonate dialysate. Next, dialysate HSA that has become saturated with toxins passes through two adsorption columns. One is activated charcoal. The other is an anion exchange resin. These columns bind toxins from HSA, freeing its binding sites to enable continued toxin removal. This has the potential to lower cost. This cost savings must be weighed against the added costs of training and equipment for a specialized device. These sorbent columns also remove stabilizers present in commercial albumin formulations. The closed dialysate albumin circuit with a fixed volume limits options for excess fluid removal.

MARS is approved by U.S. and European regulators, but information on usage is limited. In the U.S., the U.S. ALF Study Group (ALFSG) registry reported 104 uses of MARS at three centers between January 2010 and December 2019 (76). We could not identify similar recent registries for Europe, but a retrospective study at the Jena University Hospital reported that from 2015 to 2021 MARS, SPAD, ADVOS, and OPAL were used 341 times (63). These systems are coded under the procedure code 8-858—liver dialysis. Approximately half of sessions were with ADVOS, with the other three systems seeing approximately even usage at this center.

#### 1.3.2.3 Extracorporeal Hepatic Support (ECHS):

The Extracorporeal Hepatic Support (EHCS) device was a MARS-like system tested in an uncontrolled human trial in 2001 (58). At the time, its greatest strength was that all components were FDA approved. Instead of the proprietary dialyzer and sorbent columns in MARS, off-the shelf dialyzers and Adsorba 300 columns were used. Even at the time, this circuit was reported to be less efficient than the MARS circuit. Now that MARS is FDA approved, ECHS has lost its primary appeal.

#### 1.3.2.4 Advanced Organ Support (ADVOS):

ADVOS, also called HepaWash or HIP1001, uses temperature and pH to regenerate albumin dialysate. Blood is pumped through a blood circuit past two dialyzers (60,61). The dialysate contains recirculating HSA. Dialysate circuit albumin carries toxins into the ADVOS multi-circuit. Instead of sorbent columns, pH gradients regenerate the albumin. Dialysate HSA passes through two dialyzers in parallel. On the dialysate side of the membrane of one dialyzer there is acid concentrate. The other receives base. This is predicted to remove toxins bound to the albumin. Toxins are discarded into a waste container along with excess fluid. The multi-circuit

temperature is 28 °C, which is thought to improve toxin release from the dialysate albumin (59). The regenerated albumin is again dialyzed against patient's blood. This conserves HSA.

Since acid and base concentrates are added independently, dialysate pH can be tuned. This can be used to correct severe metabolic acidemia (61). Improvements in biomarkers are promising, but to date no RCTs have been completed. A retrospective controlled study did not shown improved survival (59). ADVOS has been tested outside of the ICU. ADVOS is commercially available in Europe (63).

#### 1.3.2.5 Advanced Multi-Organ Replacement (AMOR):

Advanced Multi-Organ Replacement (AMOR) is an albumin dialysis system recently tested by our group (2). It was previously called the Modified Hemodialysis Machine with Added Albumin Circuit (MAHD) in an abstract describing the same study (77). It is similar to MARS, but uses a 5 L volume of low concentration (2-4%) albumin dialysate. Unlike MARS, blood then flows through a traditional renal dialysis setup, enabling the removal of excess fluid without the complication introduced by the albumin dialysis circuit being between the renal dialysate and the blood. There is only one adsorbent column (Adsorba 300, charcoal) but this column is periodically rinsed with D5NS solution to maximize toxin removal. Like SPAD, AMOR minimizes specialized training and equipment requirements, providing the potential to lower costs relative to MARS. A case series with 10 AoCLF patients has been published. All components used were FDA-approved. Patients whose clinical condition was too severe for transplant eligibility were chosen. After ELSS, all 10 were stabilized sufficiently to be transplant eligible. Five recovered or were transplanted. This system recirculates HSA and regenerates it using sorbents. AMOR stands out in its ability to safely remove excess fluid (edema). Ultrafiltration rates reported with MARS were on average 144 mL/hour (78). BioLogic-DT removed at most 2 L per treatment in an RCT (79). ADVOS reported

150 mL/hr (59). In contrast, AMOR achieved an average fluid removal of 21 liters in this case series (2). RCTs are needed to evaluate this device.

#### 1.3.2.6 Open Albumin Dialysis (OPAL):

The Open Albumin Dialysis (OPAL) system is similar to MARS, but uses a new sorbent system called Hepalbin, which provides a larger surface area. Preliminary results from an RCT at four centers with a crossover design suggest greater pruritus resolution and toxin removal than MARS (80–82). OPAL is commercially available in Europe (63).

#### 1.3.2.7 High-Efficiency Molecular Adsorbent Recirculating System (HE MARS):

The High-Efficiency Molecular Adsorbent Recirculating System (HE MARS) is a modification of MARS in which a second set of AC 250 and IE 250 sorbent columns is added to the albumin circuit (64). In the single human trial reported for this system, a mixed cohort of four patients with alcoholic liver disease and biliary cirrhosis was enrolled. The objective was to increase detoxification capacity of standard MARS. Patients crossed over from standards MARS to HE MARS. In this small cohort HE MARS had greater toxin removal. There was no ultrafiltration.

### 1.3.3 *BioLogic-DT and Related Sorbent Dialysate Systems*

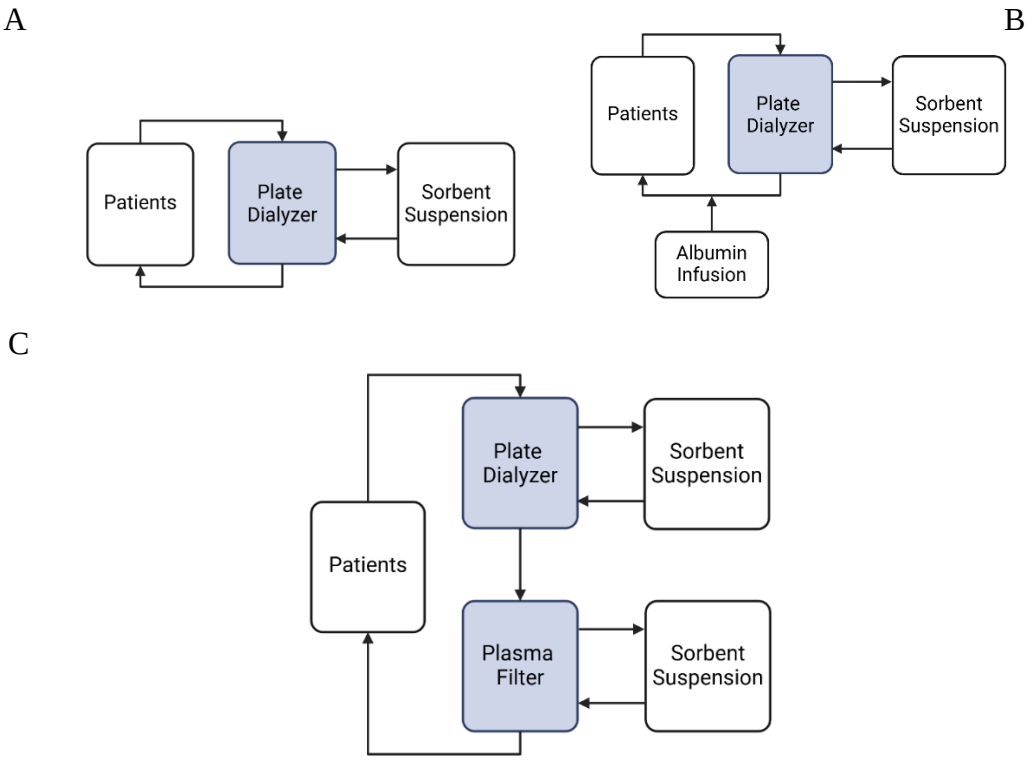


Figure 1-2: BioLogic-DT and Related Sorbent Dialysate Systems: **A**: BioLogic-DT/Liver Dialysis Unit: Charcoal and Polystyrene Sulfonate Sodium suspension is separated from blood using a dialyzer membrane. **B**: BioLogic-OSM: Similar to BioLogic-DT, but with the machine automatically infusing albumin as a volume expander to facilitate fluid removal by ultrafiltration. **C**: BioLogic-DTPF: The first circuit segment resembles BioLogic-DT. It is followed by a plasma filtration stage where plasma directly contacts suspended sorbents. Figure created with BioRender

Table 1-3: Sorbent dialysis-based liver support systems: materials, flow rates, and treatment duration.

| System | Sorbent Material | Blood Flow Rate (mL/min) | Duration (hr) |
|---|---|---|---|
| **BioLogic-DT** | 1: Charcoal<br>2: Polystyrene Sulfonate Sodium (PSS) | 200-225 (83) | 6 (79) |
| **BioLogic-OSM** | Same as above, with added lactulose | 200-225 | 8-12 (83) |
| **PF unit of the BioLogic-DTPF** | Norit A Charcoal | 80-100 | 6 (84) |

Table 1-4: Sorbent dialysis-based liver support systems, particle size, area, pore size.

| System | Particle Size (μm) | Area ($m^2$) | Pore Size (nm) |
|---|---|---|---|
| **BioLogic-DT** | Charcoal: 1-75 (79)<br>PSS: 125 (85) | Charcoal: 300,000 (79) | |
| **BioLogic-OSM** | Lactulose (342 Da), and BioLogic-DT sorbent suspension (83) | Same as BioLogic-DT | |
| **PF unit of the BioLogic-DTPF** | 1-25 (85) | 150,000 (79) | 2.5 (86) |

A family of systems used charcoal and polystyrene sulfonate sodium (PSS) in dialysate instead of albumin. In these systems, toxins crossed a dialysis membrane (sometimes driven by ultrafiltration, as in the push-pull pheresis variant) and bound to the charcoal and PSS. The BioLogic-DT, which was the most widely used of these systems, had FDA approval and a supporting RCT. However, various factors like the dependence of these systems on flat-plate dialyzers, which were phased out due to obsolescence in the much larger renal failure treatment market, contributed to this technology ceasing to be used. Given rising albumin prices, renewed interest is possible. These systems are shown in Figure 1-2. A summary is included in Table 1-3 and Table 1-4.

#### 1.3.3.1 BioLogic-DT:

The BioLogic-DT used a sorbent suspension behind a plate dialyzer. The suspension contains 70 g/L of charcoal and 40 g/L PSS (79). The sorbent can contain nutrients which diffuse into the patient. In BioLogic-DT, glucose on the charcoal is used in this way. BioLogic-DT was tested in a single multicenter trial with 31 treated patients and 25 controls (79). Individual investigators published their parts as five preliminary abstracts and publications listed in Table 2 of Ash (79). Care should be taken to avoid including the same patients twice in meta-analyses. The primary outcome was defined as survival to discharge or transplantation. Patients were divided into AoCLF (21 treated, 14 control, denoted AoC) and fulminant hepatic failure (10 treated, 11 control, denoted FHF). In the AoC group there was a significant improvement in the primary outcome. In the FHF group there was not. The FHF group had a high frequency of sepsis in both treated and control patients. Patients who had renal comorbidities greatly benefited from the ELSS.

BioLogic-DT was approved by the FDA in 1996 (87). It is also referred to as the Liver Dialysis Unit (79). As of 2007, BioLogic-DT was no longer on the market. Plate dialyzers were required because hollow fiber dialyzers would be clogged by the sorbent suspension (88). This imposed a tradeoff between unacceptably high obligate ultrafiltration rates or low dialyzer permeability (89). Low permeability prevents unconjugated bilirubin removal. The system could no longer be manufactured once plate dialyzers ceased to be available.

#### 1.3.3.2 BioLogic-OSM:

BioLogic-OSM was a modification of BioLogic-DT with the goal of addressing hypotension, ascites, and edema in liver failure patients (83). It was used in one cirrhotic patient to mitigate ascites, removing up to 0.6 L/hr of fluid and replacing it with infused albumin. 40 g of

lactulose were added to the sorbent suspension to diffuse into the blood. The system was only able to remove 0.6 L of fluid, highlighting the challenges of fluid removal.

#### 1.3.3.3 BioLogic-DTPF:

The BioLogic-DTPF system improved on BioLogic-DT by adding a plasma filter with a sorbent suspension. A plate dialyzer sorbent dialysis component identical to that used in BioLogic-DT was also present. In the plasma separation filter 100 mL/min of plasma, but not cellular components of blood, crossed into a second sorbent suspension (84). This second sorbent suspension contained 70 grams of charcoal in a 1 liter volume. Cycling positive and negative pressure facilitated plasma movement across the plasma filter. Heparin was used for anticoagulation. Glucose and branched chain amino acids were added to the sorbent to replace nutrients lost by the patient to the sorbent dialysis. To our knowledge BioLogic-DTPF has only been tested in human hepatic failure in one uncontrolled trial, making conclusions difficult to draw. As the price of HSA rises, there may be renewed interest in albumin alternatives, including sorbent suspensions.

### 1.3.4 *Perfusion-Based Systems*

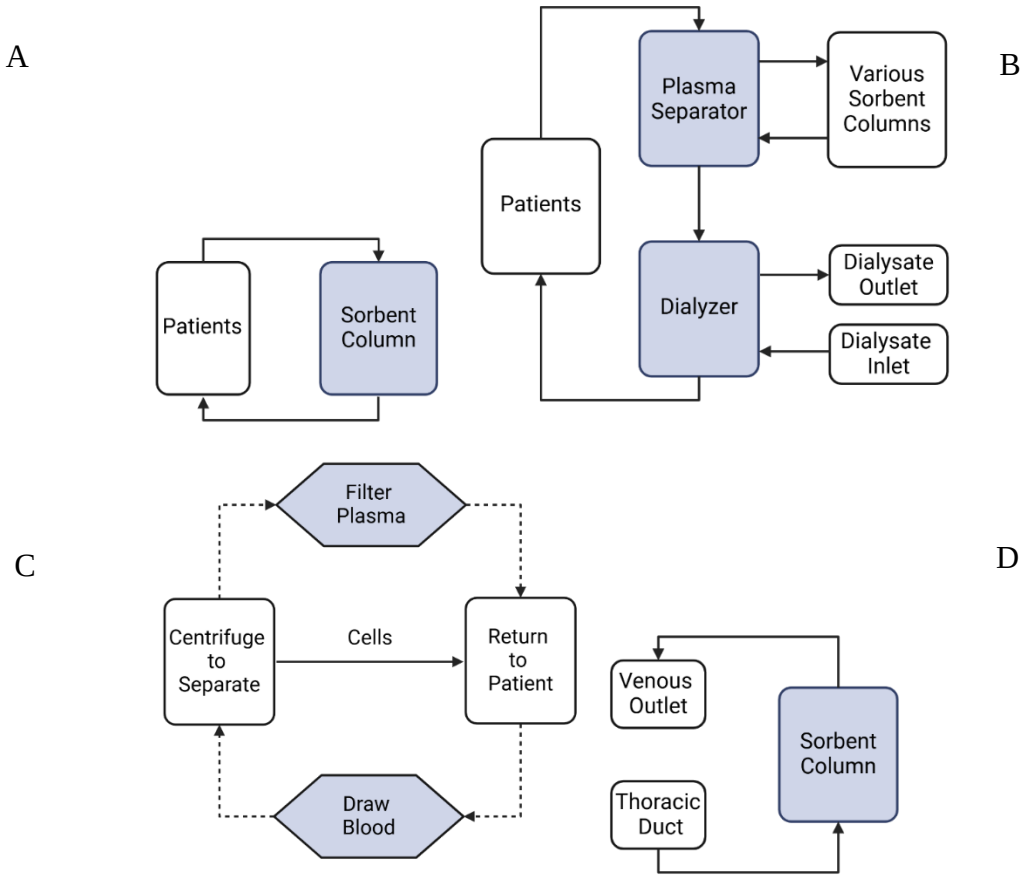


Figure 1-3: Perfusion-based systems: **A**: Hemoperfusion, such as CytoSorb. Blood directly contacts a sorbent column for detoxification. **B**: Plasmaperfusion, such as Prometheus or DPMAS. A plasma filter separates plasma from cellular components of blood. Plasma contacts sorbent columns. CRRT may be added. **C**: Gravimetric Plasmaperfusion. Instead of using a plasma filter on a connected circuit, blood is removed from the patient, separated, and then returned once the plasma has been cleaned. **D**: Lymphosorption. Lymph is perfused through an external sorbent, then returned into veins. Figure created with BioRender.

Table 1-5: Perfusion-based liver support systems: materials, flow rates, and treatment duration. * Blood flow rate for hemoperfusion, plasma flow rate for plasma perfusion. ** Zapullo, Personal Communication *** GDH is a technology for modifying activated carbons to achieve a desired porosity, rather than a single sorbent type, so other parameters are not listed.

| System | Sorbent Material | Flow Rate* (mL/min) | Duration (hr) |
|---|---|---|---|
| **Charcoal Hemo-perfusion** | Haemocol 100 | 150-200 (90) | 5-10 (90) |
| | Adsorba 300C (90) | 150-200 (90) | 5-10 (90) |
| **CytoSorb** | Polystyrene divinylbenzene (91) | 150-700 (42) | 72 (42) |
| **Prometheus** | 1: Prometh 01: Neutral styrene-divinylbenzene<br>2: Prometh 02: Anion exchange | 300 (92) | 6 (93)<br>5.7 (94) |
| **DPMAS** | 1: BS-330: Polystyrene divinylbenzene<br>2: HA330-II | 25-50 (95) | 2-3 (95) |
| **CPFA** | CG 300c: Styrene divinylbenzene | 15-36 (96) | 6-8 ** |
| **Plasorba** | BR-350: Styrene divinylbenzene anion exchange resin | 25-30 (97) | 3 (97) |
| **Medisorba** | BL-300: BPR anion exchange resin | 30 (98) | 7-18 (98) |
| **Gravimetric Plasma-perfusion** | 1: SKN-4M<br>2: SKN-2K<br>3: GDH***<br>4: BS-330 (see above) (99) | NA | NA |
| **Lympho-sorption** | 1: SKT-6A (100)<br>2: SKN<br>3: SUGS<br>4: Aktilen-I (101) | 30-40 drops/minute (100) | NA |

Table 1-6: Perfusion-based liver support systems, particle size, area, pore size. *Pore diameter was calculated from the peak value in Figure 1 in Mikhalovsky (102), obtained using DataThief III Version 1.7.

| System | Particle Size (μm) | | Area ($m^2$) | Pore Size (nm) |
|---|---|---|---|---|
| **Charcoal Hemo-perfusion** | **Haemocol 100** | 500-1000 (103) | 1,200 $m^2/g$ (103) | 1-100 (103) |
| | **Adsorba 300** | 1 mm wide, 1-8 mm long (104) | 270,000-291,000, calculated from (103–105) | 17 (102) * |
| **CytoSorb** | 400-600 (106) | | 45,000 (91) | 5.56 (107) |
| **Prometheus** | 600 for both (108) | | 120,000 for both (108) | |
| **DPMAS** | HA-330: 800 | | HA-330: 1154 $m^2/g$ (107) | HA-330: 3.5 – 9 nm (107) |
| **CPFA** | 100 (109) | | 50,000 (109) | 30 (109) |
| **Plasorba** | 400 (109) | | | 450 (110) |
| **Medisorba** | 400 (98) | | 174 $m^2/g$ (107) | 58 (98), 4.96 (107) |
| **Gravimetric Plasma-perfusion** | SKN: 500-1000 (111) | | SKN: 800-1200 $m^2/g$ (111) | SKN-4M: Wide distribution (112) |
| | | | | SKN-2K: Wide distribution (113) |
| | | | | GDH: 7.5-90 (113) |
| **Lympho-sorption** | SKT-6A: 2 mm long 0.5 mm wide | | SKT-6A: 1142 $m^2/g$ (114) | SKN: Wide distribution (112,113) |
| | SKN/SUGS: 250-800 (100) | | SKN: 800-1200 $m^2/g$ (111) | |
| | | | SUGS: 1265 $m^2/g$ (115) 100 g of sorbent (100) | |

Table 1-7: Perfusion-based liver support systems

| First Author | System | Year | N (Treatment/ Control) | Indication | Improved Survival? |
|---|---|---|---|---|---|
| O'Grady (90) | Haemocol 100 and Adsorba 300C Hemoperfusion | 1988 | 5-hour treatment: 39 10-hour treatment: 65 Control: 33 | FHF | No |
| Kribben (94) | Prometheus | 2012 | 77/68 | AoCLF | No (except in most severe subgroup) |
| Zhou (116) | DPMAS + 3 L PE | 2017 | 24/21 | ALF | Yes. No p-value given. |
| Vinay Kumar (117) | HA-330 hemoperfusion (possibly plasma-perfusion using an apheresis machine) | 2020 | 11/11 | AoCLF | No |
| Wu (118) | DPMAS + 1.4 L PE | 2022 | 62/62 | Hepatitis B AoCLF | No (except in least severe subgroup) |
| Sekandarzad (42) | CytoSorb | 2024 | 3/3 | AoCLF + AKI | No. Terminated early: Recruiting difficulties |
| Yadav (99) | BS-330 gravimetric plasmaperfusion | 2024 | 15/15 | AoCLF | No |

Movement of liquid past a fixed column of adsorbent allows the removal of toxins by binding of dissolved solutes to the adsorbent. Blood, plasma, and lymph have all been cleaned in this way. Challenges include nonspecific binding of dissolved solutes to the adsorbent and clotting and immune activation in response to the foreign substance. Nonetheless, highly specific and hemocompatible materials have been designed. Perfusion-based systems are shown in Figure 1-3 and summarized in Table 1-5, Table 1-6 and Table 1-7.

#### 1.3.4.1 Hemoperfusion:

The first use of hemoperfusion to treat liver failure was reported in 1972 (119). Sorbent columns in direct contact with blood were the first FDA-approved artificial liver support system (89). Approval was withdrawn when an RCT in the 1980s showed no benefit (90). This trial used the Haemocol 100 and Adsorba 300C sorbent columns. When sorbents directly contact blood there are concerns about particles such as charcoal dust entering the patient.

A second RCT from India studied hemoperfusion using the HA-330 adsorbent column (117). This approach was ineffective compared to PE or standard medical therapy. HA-330 is a sorbent column intended for DPMAS, which is a plasmaperfusion system (see section 1.3.4.2). Small group size (10-11 patients) is a limitation of this study. This abstract does not show the extracorporeal circuit. It is possible that this was in fact a plasmaperfusion study using an apheresis machine, instead of a study where whole blood flowed directly through the sorbent column.

Growing HSA prices and limited supply have motivated renewed interest in hemosorption. An RCT was recently conducted using the CystoSorb hemoperfusion column (42). CytoSorb was developed to treat sepsis and support patients receiving heart surgery. CytoSorb removes molecules thought to be involved in the characteristic cytokine storm pathology. In the RCT, it was combined with CRRT. The adsorption column was added prior to the dialyzer in the blood circuit. The trial was done in AoCLF patients with stage 3 AKI. Only transplant-ineligible patients were included. Sorbent columns were replaced at 12, 24, and 48 hours during the 72 hour trial to prevent saturation. Blood flow rate was set between 100 and 700 mL/min. The study aimed to have a control group with no CRRT, but those patients were permitted to cross over into the CRRT group if criteria for poor kidney function or respiratory failure were met. In practice, all patients received CRRT within 72 hours of enrollment. Patients were to be followed for 90 days, but of the 9 enrolled patients, no patients survived until this endpoint in any group. The study could not

recruit its prespecified sample size target. Only three of the nine recruited patients received CytoSorb. No statistically significant benefit was seen. An increase in vasopressor (norepenephrine) requirement was seen in CytoSorb recipients, but these patients were also on average older than the other groups.

Our group studied toxin adsorption onto solid phase sorbents using the Langmuir and BET isotherms (120). The Langmuir isotherm models monolayer adsorption of toxin onto a solid. The BET isotherm models multilayer adsorption. BET is applicable to bilirubin, because bilirubin molecules aggregate with other bilirubin molecules, including those that have already adsorbed onto the sorbent. Thus, the first layer binds to the sorbent, the second layer binds to the first layer of bilirubin, and this process continues until equilibrium is attained. The other toxins studied all fit Langmuir isotherms. This work can be used to predict and optimize sorbent column based systems.

#### 1.3.4.2 Plasmaperfusion:

Separating a fixed bed adsorbent from plasma with a membrane has a long history. In 1980, the first in-human use of an anion exchange resin (BR-601) and charcoal column to remove toxins from patient plasma was reported (121). This is plasmaperfusion. Early challenges included membrane fouling and viscosity creating high pressure, but these have been overcome. Two plasma adsorption systems have undergone RCTs. These are the Fractioned Plasma Separation and Adsorption (FPSA, Prometheus) system and the Double Plasma Molecular Adsorption System (DPMAS). These are described in their own sections below (1.3.4.3 and 1.3.4.4).

In addition, there are several plasmaperfusion devices that differ only in the sorbent column which have undergone human studies, but no RCTs. The coupled plasma filtration and adsorption (CPFA) system was developed to treat sepsis, but has been tested as a treatment for liver failure (109).

Its sorbent column is CG 300c. The anion exchange resin BR-350 has become part of routine clinical practice in some centers, but the only study demonstrating its efficacy in improving survival was retrospective (122). This device is called Plasorba. These systems all use styrene divinylbenzene in one of their columns. BL-300, using PHEMA-coated BPR anion exchange resin, is also used clinically for bilirubin removal in liver failure (98). This is the only device in this category that does not use styrene divinylbenzene. It is also known as Medisorba. Prospective RCTs are needed to test whether these systems improve survival.

#### 1.3.4.3 Prometheus:

The Prometheus system was first tested in the late 1990s (123). Prometheus is also referred to as FPSA. Blood is separated into cellular components and plasma by a filter with a 250 kDa cutoff. Plasma, albumin, and toxins flow through a neutral styrene-divinylbenzene column and an anion exchange resin. Then, clean plasma is returned to the cellular fraction of the blood. Next, traditional dialysis is performed on the blood. In the earliest study, the dialyzer was part of the plasma circuit. However, later implementations depict the dialyzer in the whole blood circuit (92). This is the depiction in Figure 1-3.

Two randomized trials compared hemodynamics and reported survival in MARS and Prometheus. Dethloff et al's study showed that Prometheus removed toxins more effectively than standard therapy, but had inferior hemodynamics to MARS and no significant impact on 6 month survival (124).

Another recent trial compared Prometheus and MARS in patients with iatrogenic MOF following cardiac surgery (93). There was no difference in 28 day survival. Both provided some physiological improvement in a group of very sick patients. Prometheus was also able to stabilize hemodynamics in this trial. Patients in the Prometheus group required up to 14 treatments, whereas

MARS patients required at most 2. Patients in the MARS group had greater improvement in mean arterial pressure.

To date, only one large RCT compared Prometheus to standard therapy. It did not show improved survival in all AoCLF patients (94). The most severe subgroup saw a survival benefit. Prometheus is approved in Europe, but a recent retrospective study of clinically used systems states it is no longer in use there (44). A center in mainland China published a retrospective study reporting 78 patients treated with FPSA between 2017 and 2022 indicating clinical usage there (125).

#### 1.3.4.4 Double Plasma Molecular Absorption System (DPMAS):

In DPMAS, plasma is separated from blood and perfused over BS 330 and HA330-II sorbents. The device is made from two connected hemoperfusion machines. DPMAS combined with PE was compared against PE alone and conservative therapy in two RCTs (116,118). A recent retrospective study reported widespread use of DPMAS coupled with PE in mainland China (126).

In Zhou et al, the DPMAS session lasted 3 hours (116). Subjects had ALF. Three liters of plasma were exchanged over 2-2.5 hours. An improvement in 24 week survival when compared to the control group was reported, but no p value was provided making determining statistical significance impossible. There was no significant difference between PE alone and PE combined with DPMAS.

In Wu et al, the duration of the DPMAS session was not reported (118). Subjects had hepatitis B virus (HBV) induced AoCLF. DPMAS recipients received 1.4 L of plasma exchanged, whereas the PE only group received 2.8 L. Despite the lower plasma volume, the DPMAS+PE group was noninferior to PE alone. However, it only improved 90 day survival above the control

group in the least severe patient subgroup (prothrombin activity percentage > 40%). No survival improvement was seen in the total study population.

#### 1.3.4.5 Gravimetric Plasmaperfusion:

Gravimetric plasmaperfusion or centrifugal-based plasmaperfusion resembles a common plasmapheresis approach, except that instead of being discarded and replaced, the toxin-laden plasma is regenerated. This technique makes more efficient use of scarce plasma. This approach allows slower plasma flow rates than membrane-based plasmapheresis because a high pressure is not required to overcome a membrane resistance, which may prevent complications (Dr. Raj Munshi, personal communication).

An RCT recently treated AoCLF patients using gravimetric plasmaperfusion with a BS 330 resin column of the same type used in DPMAS (99). The authors describe their protocol as "hemoperfusion" but the instrument they used, an Optia Spectra by Terumo BCT, does not have any standard modes in which whole blood is perfused through a secondary device. Instead, reviewing the manual for this instrument, the most likely mode is "Therapeutic Plasma Exchange with a Secondary Plasma Device" (127), making this an instance of gravimetric plasmaperfusion. Three procedures were completed on alternating days (99). Fresh frozen plasma was provided in case of hypotension after reinfusion. At the 28 day time point 2/15 patients died, compared to 3/15 in the control group and 3/15 in the plasma exchange group. The authors provide detailed metabolomics data to precisely characterize the capabilities of their sorbent, potentially enabling design improvements.

Other sorbents have been used in uncontrolled human trials (128,129). These are the activated carbons SKN-4M, SKN-2K, and GDH. GDH refers to Granulated Deliganding Hemosorbent. These carbons are designed to have a controlled pore diameter range of 7.5-90

nanometers, which is reported to increase affinity for a broad range of protein bound toxins (113). In these studies, liver damage markers declined, but nonspecific protein loss occurred. The studies do not examine mortality or directly measure toxins such as bilirubin.

#### 1.3.4.6 Lymphosorption:

Lymphosorption consists of draining lymph from the thoracic duct, passing it through an adsorbent, then reinfusing the lymph into a peripheral vein (130,131). The lymph is a promising target for extracorporeal detoxification because it often has greater toxin concentrations than plasma. Removal of lymph is also beneficial for resolving edema. Lymphosorption is often contrasted with thoracic duct drainage without reinfusion. The benefits of reinfusion are avoiding the loss of essential proteins and immune factors. However, new adverse events from reinfusion such as fever have been reported. There is significant clinical experience with this procedure in hepatic failure, particularly in Eastern Europe. Uncontrolled studies often show improvement in clinically severe patients. However, no RCT of lymphosorption in liver failure has been done. Thus, there are also no well supported guidelines for lymph flow rates and lymphosorption durations.

### 1.3.5 *Exchange Transfusion:*

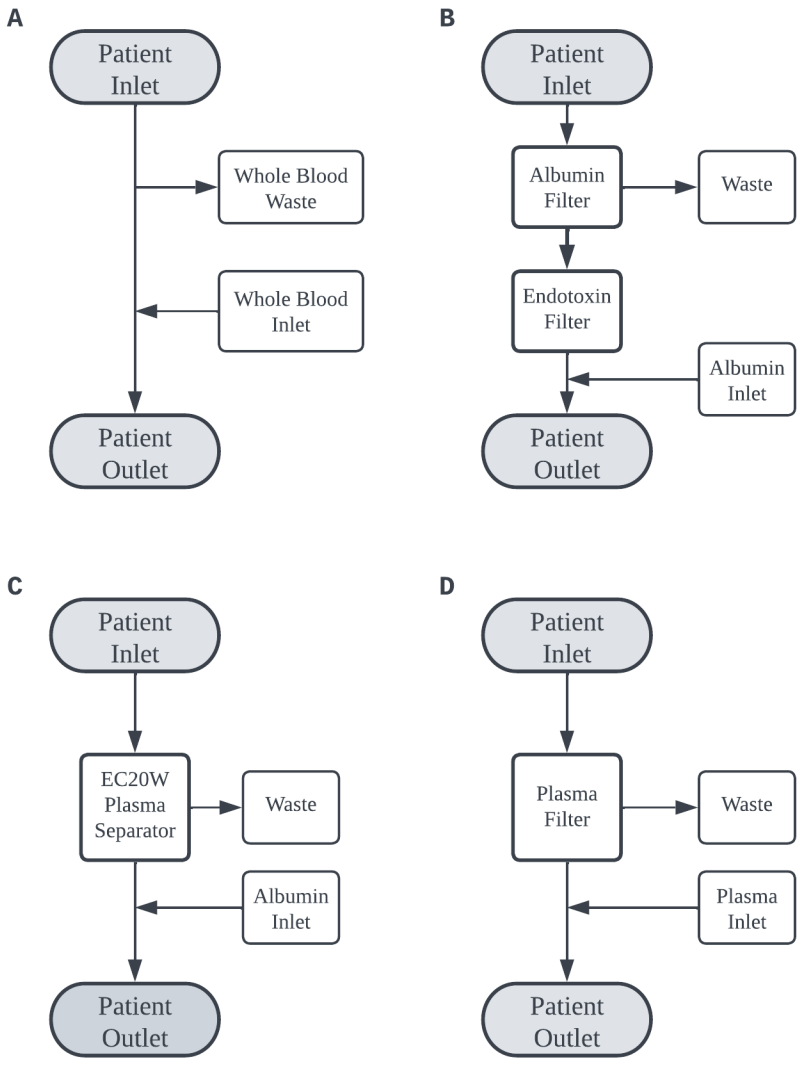


Figure 1-4: **A**: Whole Blood Exchange **B**: DIALIVE. Endotoxin removal column coupled with albumin exchange. **C**: Selective Albumin Exchange. **D**: Plasma Exchange.

Exchange transfusion is the replacement of diseased patient blood or plasma for therapeutic purposes. Plasma Exchange (PE) or plasmapheresis means replacing plasma from a liver failure patient with fresh frozen plasma (FFP) or some combination of HSA, FFP and saline. The first case report was in the 1950s (132). Exchange transfusion based systems are shown in Figure 1-4.

#### 1.3.5.1 Whole Blood Exchange:

The first RCT of exchange transfusion came less than two decades after its introduction (133). Redeker and Yamahiro exchanged 6 L of blood for heparinized whole blood over 1.5-3 hours. They did not see an improvement in survival and saw an increase in mortality in subgroup analysis.

#### 1.3.5.2 DIALIVE:

A small RCT of DIALIVE was published (134). This system combines albumin exchange with endotoxin removal. Toxin-laden and potentially damaged patient albumin is removed. It is replaced with HSA from healthy donor plasma. The sorbent column removes large harmful molecules such as endotoxins. The subjects had alcohol induced AoCLF, so they were not eligible for transplantation in the United Kingdom where the trial was conducted. Physiological state significantly improved. Survival did not. The small sample size means the trial could not determine if DIALIVE affects survival. Larger trials are ongoing. Like albumin dialysis, stabilizers in commercial HSA could make DIALIVE less effective.

#### 1.3.5.3 Selective Albumin Exchange:

Selective Albumin Exchange uses the high selectivity of the EC20W plasma separator for albumin over other plasma components (135). Instead of removing whole blood or plasma, only the albumin fraction is removed. HSA replacement fluid is infused. To date, only a short uncontrolled case series has been reported.

#### 1.3.5.4 Plasma Exchange:

At least ten RCTs comparing PE to standard medical therapy in adults have been published. They are summarized in Table 1-8. All but one were conducted in Asia, where the diagnosis of ACLF is more broad than in Europe (136). Every ALF RCT has shown a

statistically significant survival improvement. Only one of the five trials in AoCLF produced a statistically significant survival improvement in PE alone. Many found success in combining PE with another modality, but they didn't have a group which only received the second modality, so it's unclear if the PE conferred any benefit. Only one study was done in drug-induced liver injury (DILI). It did not establish a statistically significant survival improvement (137).

Table 1-8: Adult Plasma Exchange ELSS RCTs. Rows in green are trials where an improvement in transplant-free survival was seen. Rows in orange are trial where no statistically significant improvement in survival was seen. DILI stands for drug induced liver injury

| First Author | Year | Exchange Volume | Exchange Rate | Replacement Fluid | Duration | Population | Improved Survival? |
|---|---|---|---|---|---|---|---|
| Ye (138) | 2005 | 3.4-3.5 L | 24-28 mL/min | 2.9-3 L plasma + 500 mL of 4% HSA | Every 3-5 days for 10-15 days | AoCLF n = 94 | No |
| Yang (139) | 2009 | 3 | 10 mL/min | Plasma | 2 weeks | AoCLF n = 118 | No |
| Qin (16) | 2014 | 3.5 L | 25-30 mL/min | Plasma | | AoCLF n = 234 | Yes |
| Larsen (15) | 2016 | 8-12 L/day | 1-2 L/hr | Plasma | 3 days | ALF n = 182 | Yes |
| Zhou (116) | 2017 | 3 L | 3 L per 2-2.5 hr | Plasma | | ALF n = 67 | Yes. No p-value given. |
| Vinay Kumar (117) | 2020 | | | | | AoCLF n = 32 | No |
| Sinha (137) | 2020 | 0.6-2 plasma volumes | | | Mean 3 sessions every other day | DILI n = 30 | No |
| Maiwall (140) | 2022 | 5-6 L | Median 5.4 L per 4 hours | 90% plasma, 10% saline | Until response | ALF n = 40 | Yes (enrollment stopped, deemed unethical to enroll placebo) |
| Wu (118) | 2022 | 2.8 L | 25-30 mL/min | Plasma | | AoCLF n = 186 | No |
| Yadav (99) | 2024 | 1.5-2.0 plasma volumes | | 90% plasma, 10% saline | 3 sessions every other day | AoCLF n = 45 | No |

The earliest trial of Ye et al found no benefit from PE alone, but a survival benefit when PE was combined with hemofiltration (138). 3400-3500 mL of plasma were exchanged for 2900-3000 mL of fresh plasma and 500 mL of 4% HSA (138). Plasma flow rate was 25-28 mL/min. Treatments occurred every 3-5 days. In the group that only received PE, there was no improvement in survival. However, in the group that received PE and hemofiltration, survival increased significantly. The time point was not reported.

The second trial of Yang et al found similar results (139). PE alone did not improve survival, but a combination of PE and hemofiltration did. Three liters of plasma were exchanged at a rate of 10 mL/min over 5 hours (139). Survival was measured at 6 months. Plasma was replaced with fresh plasma. There was no significant difference between conducting PE and hemofiltration in series (blood passes through both before returning to the body) or in parallel (blood passes through one or the other before returning to the body).

A different large RCT showed improved 3 month and 5 year survival (16). 3.5 L of plasma were exchanged for FFP at 25-30 mL/min. Subjects had AoCLF due to HBV. They were ineligible for transplantation. Choosing transplant-ineligible patients should prevent confounding by changes in transplantation guidelines. In practice, two patients in the control group were offered transplantation shortly after assignment.

A high volume plasma exchange (HVPE) trial demonstrated improved transplant-free survival in an RCT treating ALF (15). One to two liters were exchanged hourly. 8-12 liters were replaced with FFP daily.

A fifth study saw an improvement in 24 week survival in ALF patients with PE (116). Three liters of plasma were exchanged over 2-2.5 hours. Adding DPMAS to PE yielded no further significant improvement. Plasma was replaced with fresh plasma.

A sixth study, published as an abstract, reported no survival benefit from either PE or hemoperfusion via HA-330 (117). The groups were small (10-11 patients). PE protocol details were not reported.

A seventh RCT, published as an abstract found no improvement in survival in a cohort of 30 drug induced liver injury (DILI) patients (137). 0.6-2 plasma volumes were exchanged. The average patient received 3 sessions. No information on exchange rate or replacement fluid composition is given.

A study published in 2022 saw a transplant-free survival benefit in ALF patients from exchanging 5.4 L of plasma (median) for 90% plasma and 10% saline over 242 minutes (median) (140). Exchanges were performed until patient condition improved. Cerebral edema as measured by optic nerve sheath diameter declined. Dialysis was performed in both groups as needed. Enrollment was stopped at 40 patients (20 in each group) because enrolling further control patients was deemed unethical based on the positive result obtained up to that point.

In contrast, another 2022 study saw no survival benefit from PE alone, but saw improved survival in the mild patient subgroup (prothrombin activity percentage > 40%) when PE was combined with DPMAS (118). 2.8 L of plasma were exchanged at a rate of 25-30 mL/min in AoCLF patients with HBV. In the overall patient population, there was no survival benefit from either treatment.

In Yadav and colleagues, PE did not improve survival compared to gravimetric plasmaperfusion and standard therapy in a 45-patient study (15 patients per group) (99). Patients with AoCLF were enrolled. In both the control and plasma exchange group, 28-day mortality was 3/15 (20%). 1.5-2 plasma volumes were exchanged per session. Three sessions on alternating days were conducted. Detailed metabolomics data is provided by the authors.

Studies conflict on whether PE alone improves survival in adults and whether a second system is a beneficial addition. Transplant free survival improvements have been observed, whereas improvement in populations where transplantation is common has not been seen. PE in adults may thus be most appropriate as an alternative to transplantation instead of a bridge to transplantation.

In children the literature suggests an essentially opposite conclusion. HVPE is the only artificial liver support system for which a pediatric RCT has been published (141). 48 children were randomized. Survival at 4 and 7 days improved, but there was no significant benefit at 14 and 30 days. In transplant-eligible patients even a short-term survival improvement can be greatly beneficial if it provides a bridge to transplantation. In a transplant-ineligible patient such a treatment may be futile. In this abstract no protocol details were offered, making replication impossible.

Reporting details of flow rates and replacement fluids is critical to furthering understanding. Dai et al.'s RCT of PE and HF in in critically ill COVID-19 patients did not report these parameters (142). PE improved survival, possibly by removing inflammatory cytokines. This work cannot be replicated because rate, duration of PE, and composition of replacement fluid are not available. Irreproducibility of a successful therapy in the midst of a pandemic means preventable deaths. The same can be said of the lack of protocol information in the pediatric trial discussed previously (141), though that was only reported in abstract form, so details may appear in a subsequent publication.

The success of PE has led to its inclusion in some clinical practice. Duan et al report that 2.5 - 3 liters of PE is standard therapy in the People's Republic of China (PRC) for liver failure (143). PE is recommended in the 2019 update to the AoCLF consensus recommendations of the

Asian Pacific Association for the Study of the Liver (APASL) (144). It is also recommended in the 2020 Indian National Association for the Study of Liver Consensus Statement on ALF (145). However, the 2018 European Association for the Study of the Liver (EASL) Clinical Practice Guidelines for the management of patients with decompensated cirrhosis do not recommend PE or any other ELSS (136). The 2023 ninth special issue of the "Guidelines on the Use of Therapeutic Apheresis in Clinical Practice – Evidence-Based Approach from the Writing Committee of the American Society for Apheresis" gives a strong recommendation in favor of HVPE, but not other PE protocols (146). This highlights the importance of exact PE parameters.

#### 1.3.6 *Review Conclusion:*

The need for ELSS is growing. Liver failure is becoming more common and is often fatal. Decades of research are now maturing, and new technologies are being tested in this challenging disease. Some options are clinically available. The success of PE in RCTs has brought it into clinical practice in parts of the world. Other systems have regulatory approval, but limited adoption. Figure 1-5 summarizes systems we have reviewed.

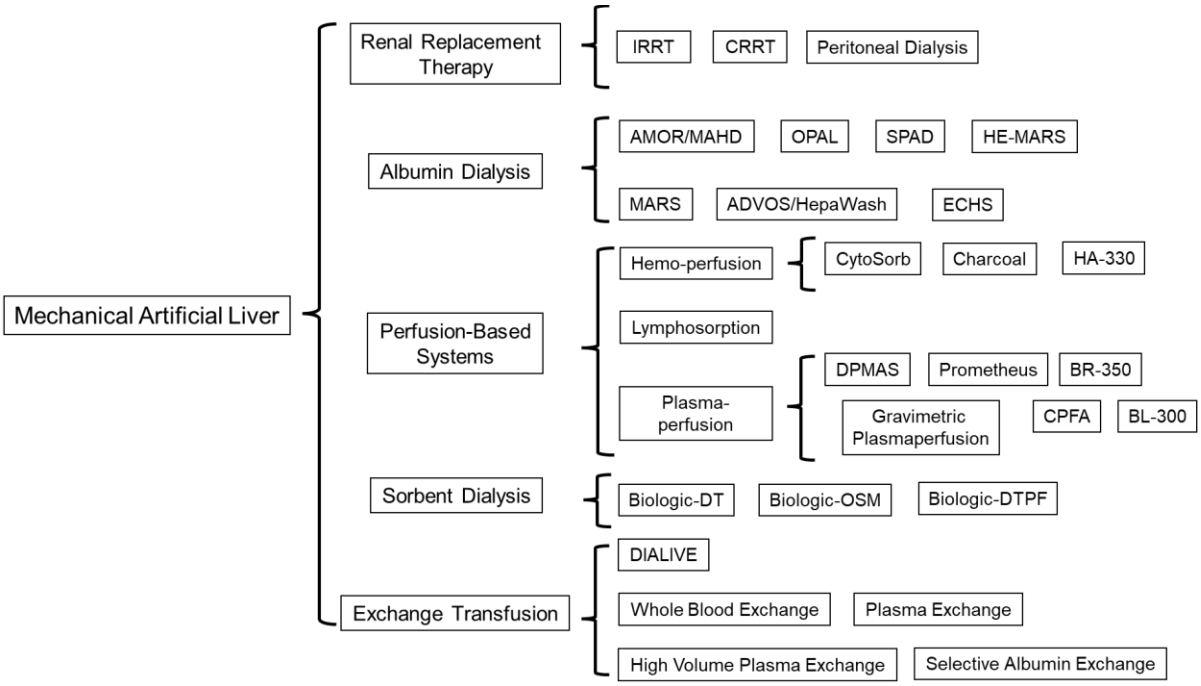


Figure 1-5: Summary of ELSS Devices

It is important for studies using exchange transfusion to report the volume, rate, duration, and replacement fluid. These parameters likely affect efficacy. If the standard of care group includes PE, that should be reported. Improvements in standard of care make it problematic to treat standard of care as a single therapy when comparing studies across different time periods in meta-analyses. Standard of care has changed significantly over the last few decades. Treating it as a single intervention to be compared against novel ELSS inflates the efficacy of newer systems by comparing them against a heterogeneous category which includes old and new standard of care. It also makes old systems appear less effective by comparing them against improved standard of care.

The purpose of ELSS should be considered carefully. If it serves as a bridge to transplantation or recovery, the ability of the patient to be a transplant candidate or to spontaneously recover must be considered. Prometheus and MARS both saw the greatest success in the most severe patient subgroups. PE in adults has only been reported to improve transplant

free survival or overall survival in cohorts where transplantation is rare. In settings where transplant organs are available, the niche of ELSS appears to be bringing transplant-ineligible patients to transplant eligibility or spontaneous recovery. In settings where transplant organs are rarely available, ELSS instead aims to improve survival in a cost-effective manner in a much larger population of patients whose clinical condition is less severe, or to improve patient quality of life by affecting other parameters such as cognitive function, lung function, edema, and ascites.

The pediatric ELSS literature is extremely scant. We only found one RCT of a pediatric liver support system. Meanwhile in 2022, 741 new children were added to the liver transplant waitlist in the United States alone (7). 3.3% of waitlisted children die on the waiting list and 15.2% of children were removed without receiving a transplant, which could indicate decompensation of liver disease.

Optimization in the ELSS space lags behind renal dialysis. No widely accepted criteria have been established for treatment dosing for any system. Theoretical study of toxin removal by binder dialysis, fixed sorbent columns, and plasma exchange can improve the use of these systems.

Innovation is needed to save liver failure patients' lives. Factors such as obesity and addiction are driving increases in liver failure, despite significant improvements in viral hepatitis control. This could create scarcities where transplant organs were previously abundant. This should motivate continued research.

# Chapter 2. COMPUTATIONAL MODEL DEVELOPMENT

## 2.1 Review of Existing Albumin Dialysis Computational Models

Computational modeling of albumin dialysis was first done in the seminal work of Patzer and colleagues, who described single pass albumin dialysis (SPAD) in three publications (51,147,148). Today, the only FDA approved albumin dialysis system is the Molecular Adsorbent Recirculating System (MARS) (11), which recirculates albumin instead of discarding it after a single pass. Three models of closed loop mode albumin dialysis have been published and are summarized in Table 2-1.

Table 2-1: Summary of Existing Models of Closed-Loop Mode Albumin Dialysis. Only assumptions regarding the albumin circuit are listed. Assumptions regarding patients (for clinical systems) and absorbent columns (for MARS) are not listed.

| Study | Transport Phenomena | Equations | Assumptions regarding albumin circuit | Boundary and Initial Conditions | Validation and fitting |
|---|---|---|---|---|---|
| Magosso, et al (78) | 1: Ultra-filtration<br>2: Diffusion<br>3: Association and dissociation | 1: Two-compartment model of patient<br>2: Equation with diffusive and convective transmembrane transport and sorbent. | 1: Well-Mixed compartments, including dialyzer<br>2: One toxin-albumin binding site<br>3: Constant ultrafiltration<br>4: Osmosis is negligible | 1: Measured concentrations at t = 0<br>2: Bound and unbound toxin at equilibrium at t = 0 | 1: Two parameters fit on one session and extended to all sessions<br>2: Three parameters set for each treatment<br>3: Eight sessions modeled |
| Annesini et al (149–154) | 1: Diffusion<br>2: Association and dissociation | 1: One-compartment model of patient<br>2: Albumin circuit described following Patzer and colleagues (51,147,148)<br>3: Linear driving force mass transfer kinetics for MARS sorbent columns | 1: Well-Mixed compartments, except dialyzer<br>2: One toxin-albumin binding site<br>3: Albumin concentration >> Toxin concentration<br>4: Osmosis is negligible | 1: Measured concentrations at t = 0<br>2: Bound and unbound toxin at equilibrium at t = 0<br>3: Dankwerts conditions for sorbent column model | Patients and *in vitro* data. Sample size not given. |
| Pei et al (155–158) | 1: Ultra-filtration<br>2: Diffusion<br>3: Association and dissociation | 1: Initial value problem describes toxin removal over time.<br>2: Boundary value problem describes toxin removal over a single pass through the dialyzer | 1: Well-mixed compartments, except dialyzer<br>2: One toxin-albumin binding site<br>3: Osmosis is negligible<br>4: Zero net ultra-filtration | 1: Measured concentrations at t = 0<br>2: Bound and unbound toxin at equilibrium at t = 0<br>3: Inlet and outlet concentration. Regula Falsi for boundary value problem. | Three *in vitro* tests which were used to fit parameters |

The first is by Magosso and colleagues (78). This model was designed using clinical data to model MARS sessions. It accounts for ultrafiltration and diffusion. However, it assumes that

the dialyzer blood and dialysate compartments and charcoal and resin columns of MARS are well mixed compartments, without modeling concentration gradients. The model has not been validated against data beyond what was used to fit its parameters.

The second is by Annesini and colleagues (149–154). This model applies chemical engineering techniques. It cannot be applied to bilirubin because it assumes albumin concentration is far greater than toxin concentration. During hyperbilirubinemia in liver failure the concentration of bilirubin may be as high as 809.8 μM while the concentration of albumin may be as low as 144 μM (13). In this case that assumption is violated. Schiesser (154) explains the implementation of this model.

The third is by Pei and colleagues, who extended the work of Patzer to include recirculation and the effect of local ultrafiltration (155–158). In this work their model could not be replicated (see Section 2.2). Since their code is not publicly available, their equation for ultrafiltration rate in the Peclet Number formula is not reported, making it difficult to identify why their data could not be reproduced. The replication attempt presented in this manuscript used Villarroel's definition of Peclet Number (159).

Our model, based on that of Pei and colleagues, and described below, addresses the gaps in the existing models and withstands external validation.

## 2.2 Effort to Replicate Model of Pei and Colleagues

### 2.2.1 *Problem Statement:*

We are interested in modeling a recirculating albumin dialysis system to optimize the removal of bilirubin. Bilirubin is a product of normal metabolism of red blood cells. It is toxic at high concentrations. This manifests as neurological symptoms, progressing to coma and death. Bilirubin cannot be removed by traditional dialysis because it is tightly bound to proteins in the

blood, most notably albumin. To model the effectiveness of this system we replicate the computational model from “Albumin Dialysis in Artificial Liver Support Systems: Open-Loop or Closed-Loop Dialysis Mode?” (158). This model modifies the traditional governing equations of dialysis to account for solute binding.

Equations are given in Section 2.2.3.3. This is a system with 6 variables described by spatial ordinary differential equations. These are: Blood and dialysate side solute amount (concentration*flow rate), blood and dialysate side pressure, and blood and dialysate side flow rate. Dialysis is counter-current, as shown in Figure 2-1. Thus, the concentration values at z = 0 for blood and at z = L for dialysate are known. Outlet dialysate pressure can be set as 0 because pressure only appears in the equations as a gradient $(P_b - P_d)$. Thus, I use gauge pressure and set the zero of pressure at the lowest value in the system, which is the dialysate outlet. The inlet blood pressure is not known but net ultrafiltration is 0, placing a constraint on inlet blood pressure. Zero ultrafiltration also means flow rate is periodic. Since inlet flow rate is a given parameter, outlet flow rate can be calculated from this information.

This can be treated as a boundary value problem. The concentration boundary conditions are not at the same z value and instead of a blood pressure boundary condition pressure is constrained by its effect on flow rate (zero net ultrafiltration). An additional requirement is computational efficiency since these spatial equations must be solved for every time step in the modeling of a full dialysis session. Pressure and flow rate equations do not change over time, but the toxin amount equations must be solved at each spatial step within the dialyzer. These spatial steps differ between time steps. Dialysis sessions may be as short as 3 hours or as long as 8 (nocturnal hemodialysis).

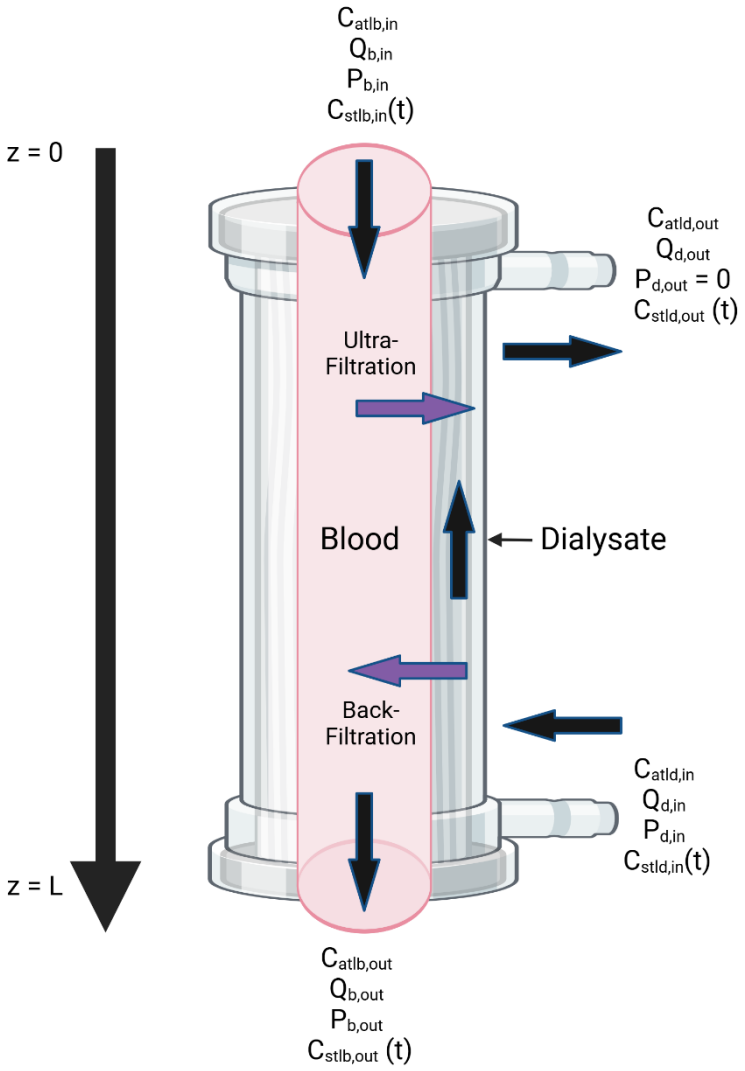


Figure 2-1: Illustration of Counter-Current Dialysis. Figure created with BioRender.

### 2.2.2 *Dialyzer Mass Transfer Area Coefficient for Free Toxin*

This model depends on the product of the dialyzer mass transfer-area coefficient for free bilirubin diffusion and area. This coefficient is analogous to $K_0A$ for toxins which are not protein bound, but there are important differences. This coefficient cannot be derived directly from the clearance of the toxin of interest by the standard relationship (160). This calculation assumes that the mean concentration difference in counter-current dialysis is the logarithmic mean of the inlet

and outlet concentration differences. For free bilirubin, this is not the case. On the blood side, as free bilirubin crosses the membrane the unbound concentration declines. This creates a thermodynamic driving force for the release of additional bilirubin from albumin. In contrast, on the dialysate side as bilirubin crosses the membrane, it binds to free binding sites on dialysate albumin. This lowers the free dialysate side bilirubin concentration. Additionally, this coefficient depends on the assumption that blood and dialysate side clearance are approximately equal. Other processes such as membrane binding of bilirubin may cause blood side clearance to exceed dialysate side clearance. Polysulfone membranes have been observed to bind small quantities of bilirubin (161). This would lead to an apparently elevated mass transfer area coefficient. Thus, we denote this value a $K_{free}A$ instead of $K_0A$ to distinguish that it is based on free toxin concentration and derived in a different way. In the manuscript of Pei and colleagues, the same parameter is denoted kA (158).

### 2.2.3 *Model Description:*

#### 2.2.3.1 Variable Names:

$P_b$ → blood pressure, $P_d$ → dialysate pressure, z → distance along dialyzer fiber from blood inlet and dialysate outlet. $\mu_b$ → viscosity of blood. $\mu_d$ → viscosity of dialysate. $Q_b$ → blood flow rate. $Q_d$ → dialysate flow rate. $r_i$ → inner dialysate fiber radius. $r_o$ → outer dialysate fiber radius. $R_m$ → inner radius of dialyzer shell (constrains the dialysate space outside the fibers). $n$ → number of fibers. $L_p$ → Membrane hydraulic permeability. $C_{stlb}$ → total blood bilirubin concentration. $C_{stld}$ → total dialysate bilirubin concentration. $C_{sb}$ → free blood bilirubin concentration. $C_{sd}$ → free dialysate bilirubin concentration. $C_{atlb}$ → total blood albumin. $C_{atld}$ → total dialysate albumin. $K_{free}A$ → diffusive mass transfer coefficient * area. $K_B$ → Albumin-bilirubin binding constant, $J_v$ → local ultrafiltration flux. f → function of Peclet

Number. $\sigma \rightarrow$ reflection coefficient of the membrane. L $\rightarrow$ dialyzer length. pe $\rightarrow$ Peclet Number, a dimensionless quantity relating convection and diffusion. $V_b \rightarrow$ blood reservoir volume. $V_d \rightarrow$ dialysate reservoir volume.

Parameter values are the same as in Pei et al for the closed loop mode albumin dialysis system unless otherwise noted (158). The number of fibers, n, is calculated from A, the total membrane area, and fiber inner radius and length because it is not explicitly given in Pei et al.

2.2.3.2 Boundary Conditions:

$$P_d(z = 0) = 0$$ (Equation 2-1: Dialysate outlet pressure)

$$C_{stlb}(z = 0, t = 0) = C_{stlb,in}$$ (Equation 2-2: Input blood side bilirubin).

$$C_{stld}(z = L, t = 0) = 0$$ (Equation 2-3: Dialysate initially has no bilirubin).

$$Q_b(z = L) = Q_b(z = 0)$$ (Equation 2-4: No net ultrafiltration).

$$Q_d(z = L) = Q_d(z = 0)$$ (Equation 2-5: No net ultrafiltration).

$$Q_b(z = 0) = Q_{b,in}$$ (Equation 2-6: Blood inlet flow rate).

$$Q_d(z = L) = Q_{d,in}$$ (Equation 2-7: Dialysate inlet flow rate).

2.2.3.3 Equations:

Change in blood pressure with respect to z: $\frac{dP_b}{dz} = -\frac{8\mu_b Q_b}{n\pi r_i^4}$ (Equation 2-8: From eq. 2 in (158))

Change in dialysate pressure with respect to z: $\frac{dP_d}{dz} = \frac{8\mu_d(R_m + nr_o)^2 Q_d}{\pi\left(R_m^2 - nr_0^2\right)^3}$ (Equation 2-9: From eq. 3 in (158))

Change in blood flow rate with respect to z: $\frac{dQ_b}{dz} = -2n\pi r_i L_p(P_b - P_d)$ (Equation 2-10: From eq. 4 and 6 in (158))

Change in dialysate flow rate with respect to z: $\frac{dQ_d}{dz} = -2n\pi r_i L_p(P_b - P_d)$ (Equation 2-11: From eq. 5 and 6 in (158))

$$\begin{bmatrix} \frac{dP_b}{dz} \\ \frac{dP_d}{dz} \\ \frac{dQ_b}{dz} \\ \frac{dQ_d}{dz} \end{bmatrix} = \begin{bmatrix} 0 & 0 & -\frac{8\mu_b}{n\pi r_i^4} & 0 \\ 0 & 0 & 0 & \frac{8\mu_d(R_m + nr_0^2)}{\pi(R_m^2 - nr_0^2)^3} \\ -2n\pi r_i L_p & 2n\pi r_i L_p & 0 & 0 \\ -2n\pi r_i L_p & 2n\pi r_i L_p & 0 & 0 \end{bmatrix} \begin{bmatrix} P_b \\ P_d \\ Q_b \\ Q_d \end{bmatrix}$$

(Equation 2-12: Ax = b representation of the linear pressure-flow subsystem)

Change in blood and dialysate total bilirubin concentration times flow rate with respect to z: $\frac{d(Q_b C_{stlb})}{dz} = \left(J_v(1-\sigma)f - \frac{K_{free}A}{L}\right) * (C_{sb} - C_{sd}) - J_v(1-\sigma)C_{sb} = \frac{d(Q_d C_{stld})}{dz}$ (Equation 2-13: From eq. 7 and 8 in (158))

Blood free bilirubin in terms of blood total bilirubin: $C_{sb} =$

$$\frac{-\left(C_{atlb} + \frac{1}{K_B} - C_{stlb}\right) + \sqrt{\left(C_{atlb} + \frac{1}{K_B} - C_{stlb}\right)^2 + \frac{4C_{stlb}}{K_B}}}{2}$$

(Equation 2-14: From eq. 9a in (158))

Dialysate free bilirubin in terms of dialysate total bilirubin: $C_{sd} =$

$$\frac{-\left(C_{atld} + \frac{1}{K_B} - C_{stld}\right) + \sqrt{\left(C_{atld} + \frac{1}{K_B} - C_{stld}\right)^2 + \frac{4C_{stld}}{K_B}}}{2}$$ (Equation 2-15: From eq. 9b in (158))

$J_v = 2n\pi r_i\, L_p(P_b - P_d)$ (Equation 2-16: Local ultrafiltration rate, eq. 6 in (158))

$f = \frac{1}{Pe} - \frac{1}{\exp(Pe) - 1}$ (Equation 2-17: From function of Peclet Number given by Pei et al. (158))

$pe = \frac{Q_f(1-\sigma)}{K_{free}A}$ (Equation 2-18: Peclet Number given by Pei et al. (158))

Unfortunately, Qf is not given in Pei et al. It is the local ultrafiltration rate, which is positive at the blood inlet (ultrafiltration) and negative at the blood outlet (back-filtration). $J_v$ is

described as the local ultrafiltration rate. It has units of $\frac{mm^2}{s}$, so it must be multiplied by dz for the units to be consistent. The area of the spatial element can be calculated as follows:

$$A_{element} = n * 2\pi r_i * dz$$ (Equation 2-19: Area of a spatial element)

The constant k is the mass transfer coefficient. Diffusive mass transfer across the individual element is:

$$K_{free}A_{local} = K_{free}A \ * \frac{A_{element}}{A_{total}}$$ (Equation 2-20: Diffusive mass transfer across individual element)

Entering these quantities into the equation for Peclet number yields:

$$p_{e,local} = \frac{J_v * dz(1-\sigma)}{K_{free}A * n * 2\pi r_i * dz * \left(\frac{1}{A_{total}}\right)} = \frac{J_v(1-\sigma)}{n * 2\pi r_i * \frac{K_{free}A}{A_{total}}}$$ (Equation 2-21: Local Peclet Number)

This formula is equivalent to that of Villarroel and colleagues (159).

Because ultrafiltration or back filtration are both possible locally, the toxin concentration equations must be modified to be a piecewise function:

$$\frac{d(Q_b C_{stlb})}{dz} = \frac{d(Q_d C_{stld})}{dz} = \begin{cases} \left(J_v(1-\sigma)f - \frac{K_{free}A}{L}\right) * (C_{sb} - C_{sd}) - J_v(1-\sigma)C_{sb} \ if \ J_v > 0 \\ \left(J_v(1-\sigma)f - \frac{K_{free}A}{L}\right) * (C_{sb} - C_{sd}) - J_v(1-\sigma)C_{sd} \ if \ J_v < 0 \end{cases}$$

(Equation 2-22: Piecewise Function Describing Toxin Concentration)

The diffusion gradient continues to favor toxin movement from blood to dialysate but the backfiltration now carries toxin into the blood, from the dialysate. Note that the sign of the ultrafiltration term doesn't change, because the sign of $J_v$ changed.

As flow rate changes, albumin concentration also changes, but since flow rate is periodic, so is albumin concentration. Thus, it doesn't change over time, only spatially.

$$C_{atlb} * Q_b(z) = C_{atlb}(z = 0) * Q_b(z = 0)$$ (Equation 2-23: From 9b in (158))

$$C_{atld} * Q_d(z) = C_{atld}(z = L) * Q_d(z = L)$$ (Equation 2-24: From 10b in (158))

Time dependence is described as follows:

$$\frac{d(C_{stlb,z=0} * V_{br})}{dt} = C_{stlb,(z=L)} * Q_{b,out} - C_{stlb,(z=0)} * Q_{bin}$$ (Equation 2-25: From 11a in (158))

$$\frac{d(C_{stld,z=0} * V_{dr})}{dt} = C_{stld,(z=0)} * Q_{d,out} - C_{stld,(z=L)} * Q_{din}$$ (Equation 2-26: From 12a in (158))

## 2.3 PERFORMANCE OPTIMIZATION

### 2.3.1 *Boundary Value Problem Solution Approaches:*

#### 2.3.1.1 Shooting Method:

The initial approach was to use the shooting method to guess the missing initial conditions to solve the spatial boundary value problem. The temporal initial value problem was then solved using a loop. The initial conditions to solve for are inlet blood pressure and dialysate bilirubin concentration at z = 0, which is the dialysate outlet in the countercurrent system. This mirrors the method using by Ding et al in an earlier paper with a very similar model (162). Because oncotic pressure is assumed to be negligible, pressure and flow rate are independent of toxin concentration. Because net ultrafiltration is 0, even though local ultrafiltration and back-filtration may occur, they are also independent of time. Thus, $P_{b,in}$ only needs to be found once. This involves a simpler, linear system of four pressure and flow rate equations with various guesses for $P_{b,in}$ until the zero-ultrafiltration criterion is met.

Once the shooting method was used to find the initial condition, a Runge-Kutta initial value problem solver with local accuracy O($dz^5$) and global accuracy O($dz^4$) was used. This is ode45 in Matlab. A 3-hour trial took 713 seconds (approximately 12 minutes) to simulate. The shooting method for the pressure-flow rate system only took 0.7291 seconds since it needs to be run only once per trial, however making this more efficient is still a concern since numerous simulations will need to be run in an optimization context.

2.3.1.2 Regula Falsi:

The next method attempted was the Regula Falsi method used by Pei et al in the paper that inspired this effort (158). Regula Falsi is a modification of the bisection method, where instead of using the midpoint of the interval, the point at which the line joining the two ends of the bisection interval crosses the x axis is used. It reduced the time the pressure-flow iteration took to 0.0426 seconds. When applied to the whole system, the 3-hour trial was simulated in 54 seconds. This is a greater than ten-fold improvement, but further improvement is desirable for parameter optimization. The Regula Falsi method is illustrated in Figure 2-2 using blood pressure as an example. Note that this method fails if the target lies outside of the region bounded by the two initial guesses.

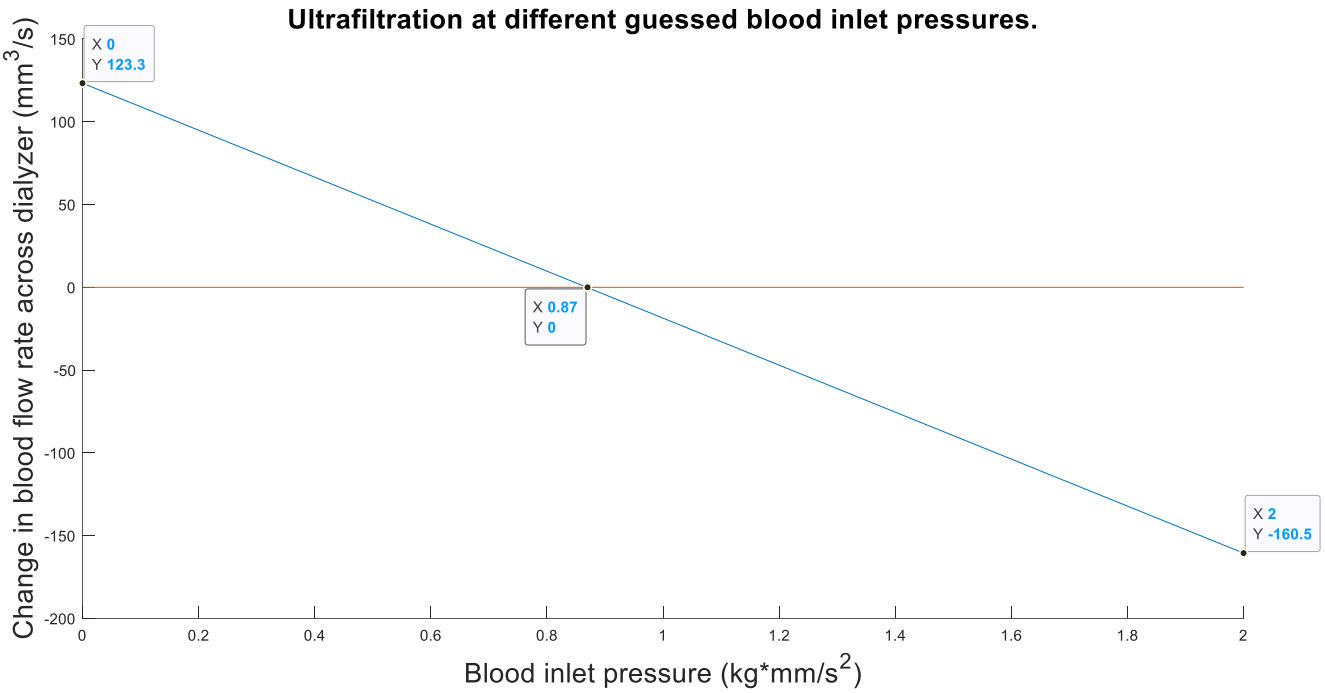


Figure 2-2: Regula Falsi with pressure. The point on the left is the low guess. The point on the right is the high guess. The point in the center will be chosen as the new guess. If the change in blood flow rate at that point is positive, it will become the new low guess. If it is negative, it will become the new high guess. If it is within tolerance of zero, it is the desired answer. The blue line is the linear interpolation between the left and right point. It is used to find the central point.

The number of iterations needed at each time step is shown in Figure 2-3. The shooting method is on the left. Regula Falsi is on the right. The Shooting Method needed 99911 iterations in total for the 3-hour trial. The Regula Falsi method needed only 3243 iterations in total for the 3-hour trial. In both, time stepping was implemented with a for loop so there was a predictable, constant number of time steps.

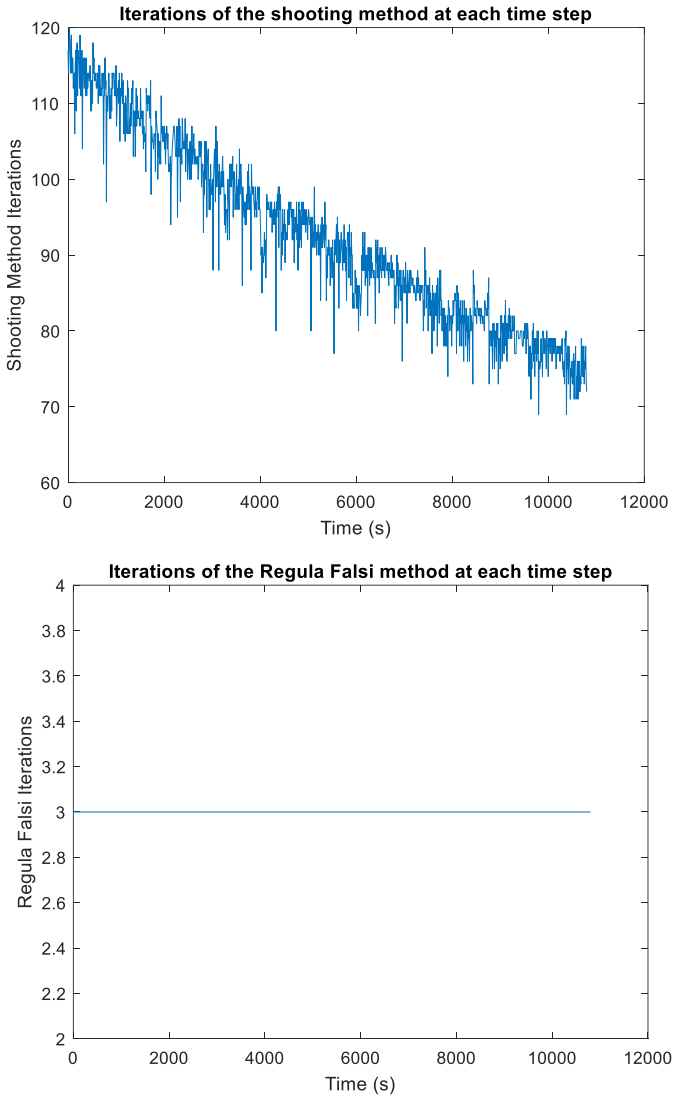


Figure 2-3: Iterations at each time step for the shooting method (top) and Regula Falsi method (bottom) with $10^{-6}$ tolerance.

Note that the Regula Falsi method only takes 3 iterations at each step. This means further improvements in efficiency through changing the boundary value problem solving method are

unlikely. A method such as Newton's method may be faster, but the advantage of Regula Falsi is that it is guaranteed to converge if the root is within the starting interval, while Newton's Method may diverge if the initial guess is far from the correct value (163). Since this method will be used for parameter sweeping and must converge in widely diverse conditions, this is a strength of Regula Falsi over Newton's Method in this context.

### 2.3.2 *"Enhanced" Efficiency Regula Falsi Method:*

At this stage, each run of the solver still took a minute, which is too long for parameter sweeps. Further improvement in efficiency can be achieved by realizing that in the Regula Falsi method, only the newly defined boundary needs to be recalculated at each step. This does not change the method, but rather eliminates redundant calculation. This reduced the time taken to as low as 28 seconds per 3-hour trial simulation. In Figure 2-5 this is labeled as "Regula Falsi Enhanced".

One unusual change can be seen in the test graph of total bilirubin over time (Figure 2-4). The sum of bilirubin in dialysis and in blood should be constant since bilirubin is neither created nor destroyed (mass conservation). However, some variation due to numerical instability is expected. With the shooting method there is a total 0.0038% increase over 3 hours (left). With the Regula Falsi method there is a 0.0303% change over 3 hours (right). The exponential pattern of the curve may cause a problem over longer simulations. The Regula Falsi method increased numerical error by an order of magnitude, but it remains <0.1%.

Due to concerns about numerical error, the order of magnitude of the change in concentration at each step was calculated. It was approximately $10^{-7}$ per spatial step. Thus, I lowered the tolerance on Regula Falsi from E-6 to E-9, to see if this changes the result. This increased the number of iterations to 4 at each step. It did not alter the final value. Numerical

error in total bilirubin concentration decreased to -1.7E-5%. Runtime did not noticeably increase (Figure 2-5, “Regula Falsi Enhanced, E-9”). Thus, this tighter tolerance was used for subsequent tests. In later tests, when $C_{alb,dial}! = C_{alb,blood}$, tolerance again needed to be reduced to E-6, because the number of iterations increased to 3000-4000 iterations needed to achieve this target.

### 2.3.3 *Runge-Kutta Time Stepping:*

A further order of magnitude gain in efficiency was achieved by replacing the for-loop time stepping approach with ode45. An implementation of ode45 that calls a boundary value problem solver at each step may be computationally expensive since adaptive time-stepping allows many small steps. However, this was not seen here. Ode45 time-stepping, along with the efficient Regula Falsi method and a tolerance of $10^{-9}$ computed the 3-hour trial in 6 seconds. This is shown in Figure 2-5 as “Regula Falsi Enhanced + ode45 for Time Stepping (E-9)”. This method also had orders of magnitude less variation in total bilirubin concentration over time than any other approach. Thus, it was chosen for parameter sweeping. The precision of these methods can be verified by comparing the blood and dialysate bilirubin concentration according to the Shooting Method with for-loop time-stepping and the Regula Falsi method with ode45 time-stepping as shown in Figure 2-6.

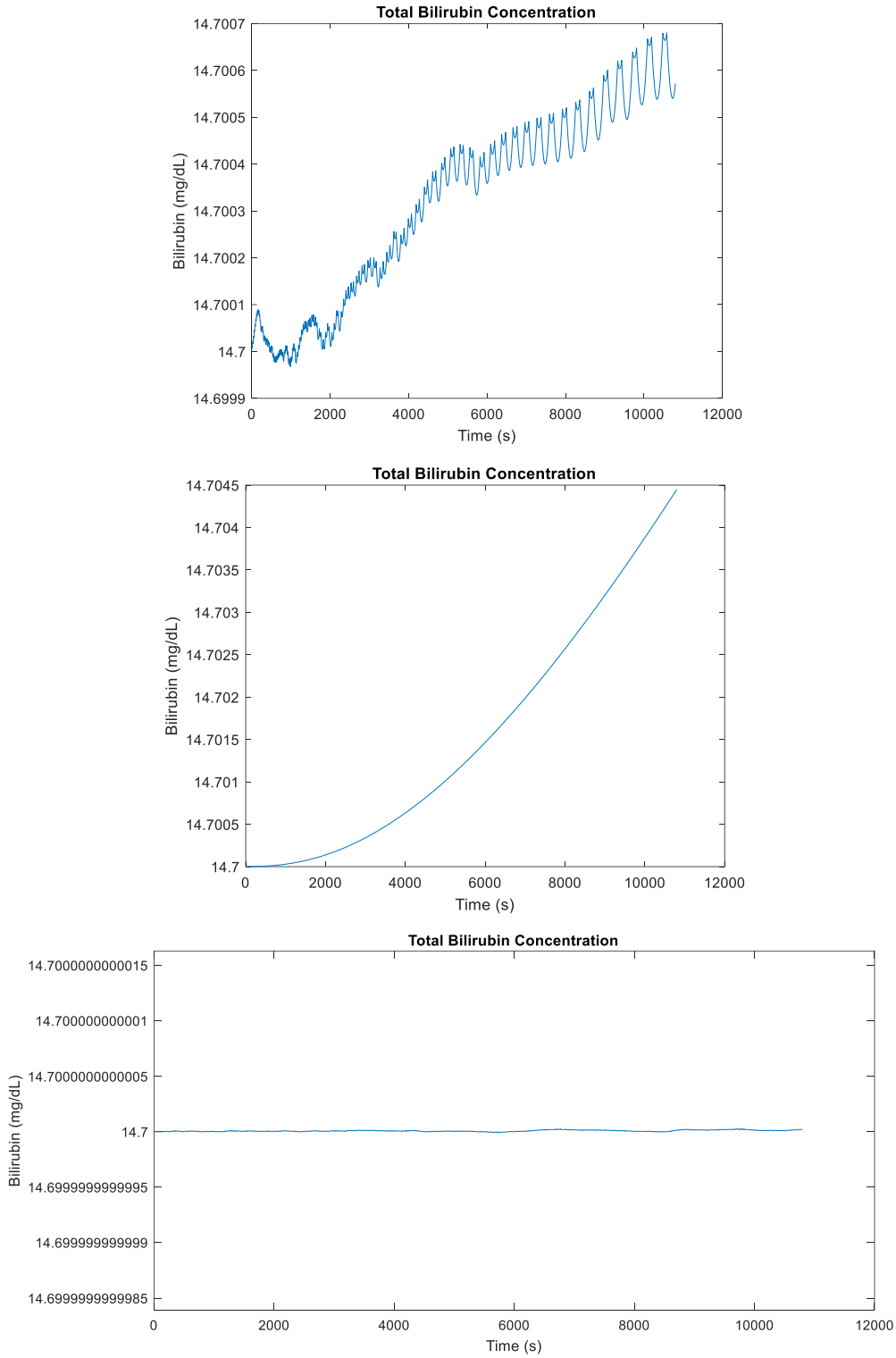


Figure 2-4: Total bilirubin concentration over time for shooting method (top), Regula Falsi (middle) and Regula Falsi + ode45 for time and space (bottom). Without numerical error, this should be constant as long as dialysate and blood volume are equal. In the Pei closed loop mode system that condition is met (158). Otherwise, bilirubin amount (concentration * volume) would be constant instead.

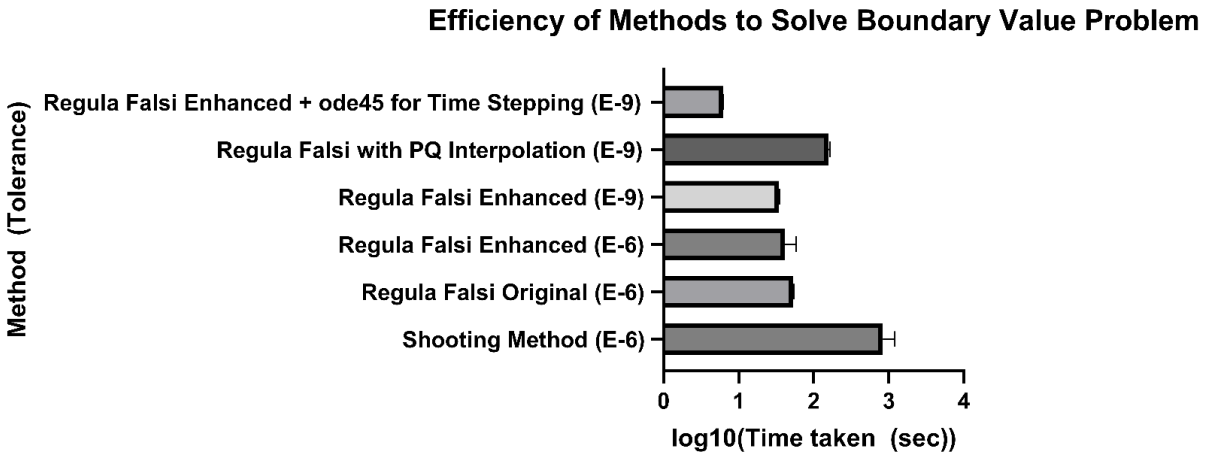


Figure 2-5: Efficiency of various methods. Time is plotted as a log scale to allow comparisons between methods with drastically different runtimes. Values are mean ± standard deviation. See text for description of methods.

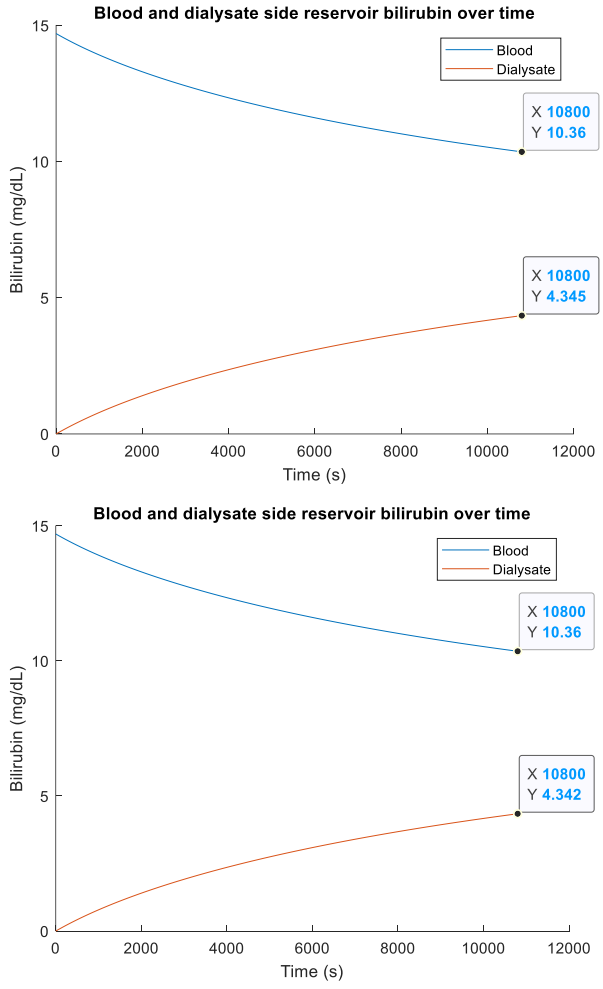


Figure 2-6: The shooting method in space with a for loop for time stepping (top) and regula falsi method in space with ode45 for time steps (bottom) predict very similar blood (blue) and dialysate (orange) bilirubin concentrations over a 3-hour trial. The endpoints are marked.

2.3.4 *Accuracy Evaluation:*

Now that the issue of efficiency and precision has been addressed, accuracy can be examined by comparing simulation results to the data in Pei et al. This comparison is not favorable. Pei provides bilirubin blood side concentration data for three initial concentrations (158). Our results do not fit theirs for any of them. Their initial blood bilirubin concentrations are: 14.7, 17.7 and 21.4 mg/dL. Their final blood bilirubin concentrations are 7.7, 9.0 and 10.8 mg/dL. Our modeled final bilirubin concentrations are 10.36, 11.08, 11.76 mg/dL.

Since our method is now precise (internally consistent) and fast, a parameter sweep is now done to accurately fit the original data. In Pei et al, $K_B$ and $K_{free}A$ were found by parameter sweeping. They report $K_B = 0.8 * 10^7 \frac{L}{M}$ and $K_{free}A = 800 \frac{mL}{min}$ (158).

2.3.5 *Parameter Sweeping Method:*

Parameter sweeping can be mathematically described as follows: Determine the values $K_{free}A$ and $K_B$ such that $\frac{\delta S}{\delta K_{free}A} = 0$ and $\frac{\delta S}{\delta K_B} = 0$ where $S = \left(C_{s,tl,b} - \overline{C_{s,tl,b}}\right)^2$ and $\overline{C_{s,tl,b}}$is the known ground truth value. Then, determine which of those values are minima. S is the square of the difference between the modeled and the true bilirubin concentration. Unfortunately, an analytical solution is not possible since it would require $\frac{\delta \overline{C_{s,tl,b}}}{\delta K_{free}A}$ while experimental data is only available for one $K_{free}A$ for a given setup. Experimental data is a dataset, not a function, so if it were collected over multiple $K_{free}A$, an approximation like the trapezoid rule would be needed. With the available data, there is no analytical approach to find minima. Instead, I iterate over a range of $K_B$ and $K_{free}A$ values. For $K_B$, this should be near $0.8 * 10^7 \frac{L}{mol}$ (from Pei et al (158)). A range for $K_{free}A$ is hard to define. Pei et al report $800 \frac{mL}{min}$, which we found was too low

(larger $K_{free}A$ means faster toxin clearance). At $K_B = 0.8 * 10^7 \frac{L}{mol}$, we found a $K_{free}A$ of 4000 $\frac{mL}{min}$ was needed for a final bilirubin concentration of 7.551 mg/dL.

Due to computational time limitations, I iterate over a narrower range of $K_B$ and $K_{free}A$ corresponding to $K_B$ near the value of Pei et al: $K_B \in [0.3: 0.05: 1.3] * 10^7 \frac{L}{mol}$ and $K_{free}A \in [500: 50: 4100]$. Next, we used datathief.jar Version 1.7 to extract the data we are fitting to from Pei et al's graphs (158). The first and last point are as given in the text. Table 2-2 lists the extracted data.

Table 2-2: Points from Figure 2 in Pei et al (158). Extracted using Datathief 1.7

| Time (min) | Trial 1 Bilirubin (mg/dL) | Trial 2 Bilirubin (mg/dL) | Trial 3 Bilirubin (mg/dL) |
|---|---|---|---|
| 0 | 14.7 | 17.7 | 21.4 |
| 15 | 12.9 | 14.7 | 17.1 |
| 30 | 11.4 | 13.3 | 15.0 |
| 45 | 10.3 | 11.6 | 13.2 |
| 60 | 9.6 | 10.8 | 12.5 |
| 80 | 8.9 | 10.2 | 11.9 |
| 100 | 8.4 | 9.7 | 11.2 |
| 120 | 8.1 | 9.6 | 11.0 |
| 140 | 7.9 | 9.3 | 11.0 |
| 160 | 7.7 | 9.2 | 10.8 |
| 180 | 7.7 | 9.0 | 10.8 |

2.3.6 *Parameter Sweep Results:*

The parameter sweep was run for $K_{free}A \in [500: 50: 4100] \frac{mL}{min}$ and $K_B \in [0.3: 0.05: 1.3] * 10^7 \frac{L}{mol}$. The initial condition was set to 14.7 $\frac{mg}{dL}$. Its results are shown in Figure 2-7. The smallest squared deviation from the experimental data is 0.2488 $\left(\frac{mg}{dL}\right)^2$, corresponding to $K_{free}A = 1500 \frac{mL}{min}$ and $K_B = 0.35 * 10^7 \frac{L}{mol}$. It took 18674 seconds to run (~5.2 hours). This is longer than would have been expected from the number of tests alone, since individual tests

were measured as taking 6 seconds and there are 1533 combinations. Thus, the expected runtime was 2.6 hours. The sweep ran twice as long as expected. With these optimal parameters, for the three initial conditions (14.7 mg/dL, 17.7 mg/dL, and 21.4 mg/dL) the model predictions were, respectively: 7.673 mg/dL, 8.966 mg/dL, 10.71 mg/dL. These parameters predict the curve for initial conditions outside of their training data. Thus, the plausibility of the proposed parameter values must be assessed.

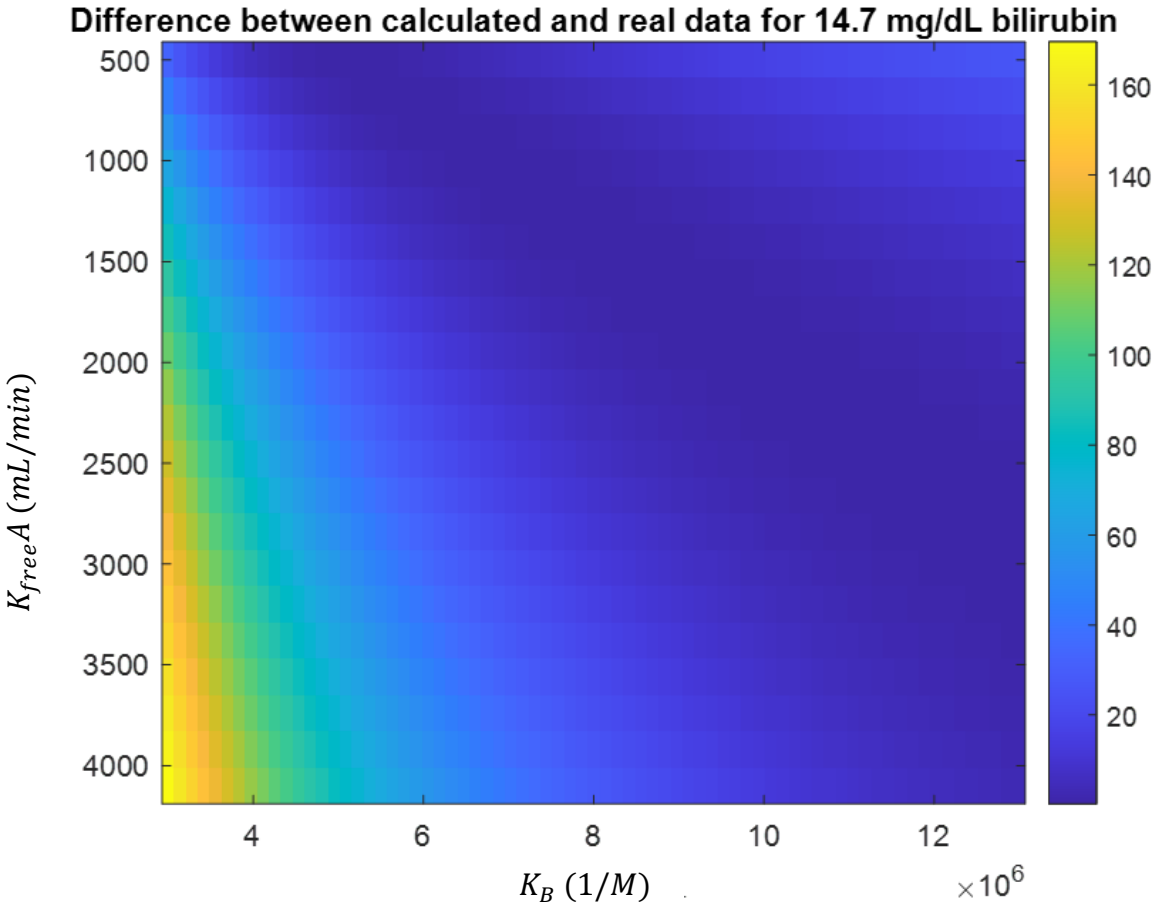


Figure 2-7: Results of the first parameter sweep (see text for range). Color key shows the sum of the squared difference between the model and the true experimental data. $K_{free}A$ is the total mass transfer coefficient of the membrane for bilirubin. $K_B$ is the binding strength of bilirubin to bovine serum albumin at the primary binding site.

### 2.3.7 *Parameter Sweep Discussion:*

Mass transfer area coefficient ($K_{free}A$) is the highest possible clearance of a solute (in this case, bilirubin) under the given conditions (164). It is the reciprocal of the resistance to solute movement in blood, dialysate, and within the membrane. This depends on the stagnant fluid layer near the surface of the membrane, the properties of the membrane itself and mixing within the dialyzer fibers. The optimal $K_{free}A$ value of 1500 $\frac{mL}{min}$ at $K_B = 0.35 * 10^7 \frac{L}{mol}$ obtained by our model is high compared to those reported in the literature for bilirubin. Pei et al used the same model, with the same parameters, and reported 800 $\frac{mL}{min}$ (158). A different paper from the same group reports 550 $\frac{mL}{min}$ as the bilirubin $K_{free}A$ under similar conditions with a different dialyzer (156). Meyer et al mention 2000 $\frac{mL}{min}$ as a plausible but extreme value of protein-binding toxin $K_{free}A$ (165).

It is plausible that a strong binder in the dialysate (as was the case in this experiment) creates a very high maximum possible clearance. If this hypothesis is correct, the binder must exert a force on the free bilirubin. This violates the model assumption that bound toxin removal is driven primarily by the diffusion of the free fraction of toxin across the membrane and the primary role of the binder (albumin) in the dialysate is to maintain this concentration gradient by binding the toxin that diffuses across. If this hypothesis is correct, $K_{free}A$ will increase as dialysate albumin concentration increases when all other parameters are equal. The model already predicts that a greater dialysate binder concentration will remove more bilirubin. This would be an additional effect, meaning if this hypothesis is true, the slope $\frac{\Delta\ bilirubin\ removed}{\Delta\ dialysate\ albumin\ concentration}$ would be greater than the model prediction for a $K_{free}A$ independent of the dialysate albumin concentration.

### 2.3.8 *Potential Reasons for Discrepancy:*

I implemented the model of Pei et al exactly and used their parameters. Thus, such a large deviation from the $K_{free}A$ they reported as providing the best fit is surprising. This may be accounted for by ambiguities in Pei et al's report. Peclet number is given in terms of $Q_f$, which is not defined (see Equation 2-18 in the model description) (158). This is the local ultrafiltration rate, therefore, I calculated it as described in "Model Description". However, this formula was chosen based on physical principles, and may not be the one used by Pei et al. For example, Yu et al recently provided another definition of Peclet number that may provide more accurate outcomes: $P_e = \frac{J_v(1-\sigma_s)}{P_s}$ (166). Here, $P_s$ is the diffusive permeability of the membrane to the toxin. Unfortunately, this value is not currently known for bilirubin, so I could not attempt to implement this definition. However, it is likely within our technical capabilities to measure, so may be used in future reports.

Pei et al also do not mention whether they corrected their bilirubin equations for backfiltration like we did in Equation 2-22. The model was also run with the un-corrected version (Equation 2-13) and this did not affect the concentration curves. Net ultrafiltration/backfiltration is 0, so backfiltration is only a local phenomenon, potentially accounting for the low sensitivity to this correction. However, it is possible that Pei et al used a different theoretical approach to backfiltration. However, if this were the case, it would be expected that they would describe it. Another ambiguity is that n, the number of dialyzer fibers was not explicitly given in Pei. I had to calculate it from membrane area and fiber geometry, which were given.

## 2.4 Optimization for Stability and Stiffness

### 2.4.1 *Background*

Once we extended the model to more conditions, we discovered that this numerical system is highly stiff. Stiffness in an ODE system means that small errors in numerical solvers are magnified, causing numerical instability (167). It occurs due to a large ratio between the real parts of eigenvalues (stiffness ratio) in the Jacobian characteristic matrix of the system at the desired input values. To be clinically useful, an albumin dialysis dosing model must accept arbitrary parameter inputs. Variables include patient volume, patient blood viscosity (dependent on hematocrit), patient albumin levels, patient toxin concentrations, desired targets, blood flow rate, dialysate flow rate, dialysate binder characteristics, and more. The model must work for any physiologically reasonable starting parameters.

We made several modifications to eliminate potential sources of instability and improve the model. First, we added a purely diffusive regime to the piecewise function representing the system to avoid division by zero errors at very low local ultrafiltration rates. Then, we solved for pressure and flow rate analytically to reduce the system to a second order system. Then we redefined the system in terms of amount of toxin removed from blood to reduce the system to a single ordinary differential equation. Then we calculated the Jacobian and Gradient of this ODE to mitigate numerical instability. Finally, we redefined the initial value problem to start at $z = L$, meaning the dialysate inlet instead of the blood inlet. This reduced the magnitude of the initial values, and ensured that the system's variable (amount of toxin removed from blood) could not increase without bound. This last modification, coupled with all the others, solved the stability/stiffness issue.

### 2.4.2 *Diffusive Transport at Low $J_v$*

Piecewise functions are frequent sources of instability in numerical ODE systems. In this case, during the transition from ultrafiltration to backfiltration $J_v = 0$ at a critical point in the dialyzer. At this point, Peclet number, which is directly proportional to $J_v$, also equals zero. This means that the function of Peclet number used to correct for the impact of fluid convection on diffusive transport of free toxin across the dialysis membrane now has unstable terms:

$$f = \frac{1}{Pe} - \frac{1}{\exp(Pe) - 1}$$ (Equation 2-27: From Equation 2-17)

Both terms approach infinity as Peclet number approaches zero. Physically, this correction ceases to be meaningful at low ultrafiltration rates. We arbitrarily define a critical value:

$$J_{v,crit} = \min(Q_b, Q_d) * 10^{-5} \frac{1}{mm}$$ (Equation 2-28)

Once $J_v$ is below this critical value, the convective transport is negligible, so the equations of toxin transport become the following:

$$\frac{d(Q_b C_{stlb})}{dz} = \frac{d(Q_d C_{stld})}{dz} = -\frac{K_{free} A}{L} * (C_{sb} - C_{sd})$$ (Equation 2-29)

On its own, this modification is not sufficient to prevent numerical instability.

### 2.4.3 *Analytical Solutions to Pressure and Flow Equations*

Second, we analytically solved the pressure and flow equations and replaced the blood and dialysate bilirubin concentrations with a single parameter representing the difference between the blood and dialysate side concentrations. This reduced the system of four ordinary differential equations to one ODE that can be solved at every time step. This derivation is shown below:

2.4.3.1 Reduction to third order system

First, consider the four ordinary differential equations for pressure and flow rate:

$$\begin{bmatrix} \frac{dP_b}{dz} \\ \frac{dP_d}{dz} \\ \frac{dQ_b}{dz} \\ \frac{dQ_d}{dz} \end{bmatrix} = \begin{bmatrix} 0 & 0 & -\frac{8\mu_b}{n\pi r_i^4} & 0 \\ 0 & 0 & 0 & \frac{8\mu_d(R_m+nr_0^2)}{\pi(R_m^2-nr_0^2)^3} \\ -2n\pi r_i L_p & 2n\pi r_i L_p & 0 & 0 \\ -2n\pi r_i L_p & 2n\pi r_i L_p & 0 & 0 \end{bmatrix} \text{ (Equation 2-30)}$$

This system can be simplified to a system of three ordinary differential equations by considering the pressure difference:

$$\Delta P = P_d - P_b \text{ (Equation 2-31)}$$

The spatial derivative of pressure difference is:

$$\frac{\delta \Delta P}{\delta z} = \frac{\delta P_b}{\delta z} - \frac{\delta P_d}{\delta z} = \frac{8\mu_d(R_m+nr_0^2)}{\pi(R_m^2-nr_0^2)^3} Q_d + \frac{8\mu_b}{n\pi r_i^4} Q_b \text{ (Equation 2-32)}$$

The system is now as follows:

$$\begin{bmatrix} \frac{\delta \Delta P}{\delta z} \\ \frac{dQ_b}{dz} \\ \frac{dQ_d}{dz} \end{bmatrix} = \begin{bmatrix} 0 & \frac{8\mu_b}{n\pi r_i^4} & \frac{8\mu_d(R_m+nr_0^2)}{\pi(R_m^2-nr_0^2)^3} \\ 2n\pi r_i L_p & 0 & 0 \\ 2n\pi r_i L_p & 0 & 0 \end{bmatrix} \begin{bmatrix} \Delta P \\ Q_b \\ Q_d \end{bmatrix} \text{ (Equation 2-33)}$$

2.4.3.2 Third order determinant and eigenvalues

The eigenvalues of this matrix can be found analytically, and they can be used to analytically solve the pressure and flow rate equations. This analytical solution proceeds as follows, from the determinant of $A - \lambda I$ where A is the matrix in Equation 2-33, $\lambda$ is the eigenvalues of this system, and I is the 3x3 identity matrix:

$$\det\left(\begin{bmatrix} -\lambda & \frac{8\mu_b}{n\pi r_i^4} & \frac{8\mu_d(R_m+nr_0^2)}{\pi\left(R_m^2-nr_0^2\right)^3} \\ 2n\pi r_i L_p & -\lambda & 0 \\ 2n\pi r_i L_p & 0 & -\lambda \end{bmatrix}\right) = -\lambda * \det\left(\begin{bmatrix} -\lambda & 0 \\ 0 & -\lambda \end{bmatrix}\right) - \frac{8\mu_b}{n\pi r_i^4} *$$

$$\det\begin{pmatrix} 2n\pi r_i L_p & 0 \\ 2n\pi r_i L_p & -\lambda \end{pmatrix} + \frac{8\mu_d(R_m+nr_0^2)}{\pi\left(R_m^2-nr_0^2\right)^3} * \det\begin{pmatrix} 2n\pi r_i L_p & -\lambda \\ 2n\pi r_i L_p & 0 \end{pmatrix} \text{ (Equation 2-34)}$$

Solving the three 2x2 determinants in Equation 2-34:

$$\det\left(\begin{bmatrix} -\lambda & 0 \\ 0 & -\lambda \end{bmatrix}\right) = \lambda^2 \text{ (Equation 2-35)}$$

$$\det\left(\begin{bmatrix} 2n\pi r_i L_p & 0 \\ 2n\pi r_i L_p & -\lambda \end{bmatrix}\right) = -\lambda * 2n\pi r_i L_p \text{ (Equation 2-36)}$$

$$\det\left(\begin{bmatrix} 2n\pi r_i L_p & -\lambda \\ 2n\pi r_i L_p & 0 \end{bmatrix}\right) = \lambda 2n\pi r_i L_p \text{ (Equation 2-37)}$$

Applying the definitions of the 2x2 determinants into Equation 2-34:

$$-\lambda^3 - \frac{8\mu_b}{n\pi r_i^4} * \left(-\lambda * 2n\pi r_i L_p\right) + \frac{8\mu_d(R_m+nr_0^2)}{\pi\left(R_m^2-nr_0^2\right)^3} * \lambda 2n\pi r_i L_p \text{ (Equation 2-38)}$$

Rearranging:

$$-\lambda^3 + \left(\frac{8\mu_b}{n\pi r_i^4}\left(2n\pi r_i L_p\right) + \frac{8\mu_d(R_m+nr_0^2)}{\pi\left(R_m^2-nr_0^2\right)^3} 2n\pi r_i L_p\right)\lambda = 0 \text{ (Equation 2-39)}$$

From this, the first eigenvalue is:

$$\lambda_1 = 0 \text{ (Equation 2-40)}$$

The two remaining eigenvalues are the roots of:

$$\lambda^2 - \left(\frac{8\mu_b}{n\pi r_i^4}\left(2n\pi r_i L_p\right) + \frac{8\mu_d(R_m+nr_0^2)}{\pi\left(R_m^2-nr_0^2\right)^3} 2n\pi r_i L_p\right) = 0 \text{ (Equation 2-41)}$$

Applying the quadratic formula:

$$\lambda_{2,3} = \frac{\pm\sqrt{4*\left(\frac{8\mu_b}{n\pi r_i^4}\left(2n\pi r_i L_p\right)+\frac{8\mu_d(R_m+nr_0^2)}{\pi\left(R_m^2-nr_0^2\right)^3}2n\pi r_i L_p\right)}}{2} = \pm\sqrt{\left(\frac{8\mu_b}{n\pi r_i^4}\left(2n\pi r_i L_p\right) + \frac{8\mu_d(R_m+nr_0^2)}{\pi\left(R_m^2-nr_0^2\right)^3} 2n\pi r_i L_p\right)}$$

(Equation 2-42)

This means that solutions to Equation 2-33 have the form:

$$y = c_1 x_1 \exp(\lambda_1 z) + c_2 x_2\, exp(\lambda_2 z) + c_3 x_3\, exp(\lambda_3 z) \text{ (Equation 2-43)}$$

z is the spatial variable corresponding to distance along the dialyzer from the blood inlet. We know that $\exp(\lambda_1 z) = 1$ from Equation 2-40. x values are derived from the eigenvectors of the A matrix (Equation 2-33).

These can be found as follows:

$$\begin{bmatrix} -\lambda & \frac{8\mu_b}{n\pi r_i^4} & \frac{8\mu_d(R_m+nr_0^2)}{\pi(R_m^2-nr_0^2)^3} \\ 2n\pi r_i L_p & -\lambda & 0 \\ 2n\pi r_i L_p & 0 & -\lambda \end{bmatrix} * \begin{bmatrix} v_1 \\ v_2 \\ v_3 \end{bmatrix} = \begin{bmatrix} 0 \\ 0 \\ 0 \end{bmatrix} \text{ (Equation 2-44)}$$

2.4.3.3 First eigenvector

The eigenvector corresponding to $\lambda_1 = 0$ is:

$$\begin{bmatrix} 0 & \frac{8\mu_b}{n\pi r_i^4} & \frac{8\mu_d(R_m+nr_0^2)}{\pi(R_m^2-nr_0^2)^3} \\ 2n\pi r_i L_p & 0 & 0 \\ 2n\pi r_i L_p & 0 & 0 \end{bmatrix} \begin{bmatrix} v_1 \\ v_2 \\ v_3 \end{bmatrix} = \begin{bmatrix} 0 \\ 0 \\ 0 \end{bmatrix} \text{ (Equation 2-45)}$$

Solving this system of equations:

$$\frac{8\mu_b}{n\pi r_i^4} v_2 + \frac{8\mu_d(R_m+nr_0^2)}{\pi(R_m^2-nr_0^2)^3} v_3 = 0 \rightarrow \frac{8\mu_d(R_m+nr_0^2)}{\pi(R_m^2-nr_0^2)^3} v_3 = -\frac{8\mu_b}{n\pi r_i^4} v_2 \rightarrow v_3 = -\frac{\pi(R_m^2-nr_0^2)^3}{8\mu_d(R_m+nr_0^2)} * \frac{8\mu_b}{n\pi r_i^4} v_2$$

(Equation 2-46)

$$2n\pi r_i L_p v_1 = 0 \rightarrow v_1 = 0 \text{ (Equation 2-47)}$$

Thus, the first eigenvector is as follows:

$$x_1 = \begin{bmatrix} 0 \\ v_2 \\ -\frac{\pi(R_m^2-nr_0^2)^3}{8\mu_d(R_m+nr_0^2)} * \frac{8\mu_b}{n\pi r_i^4} v_2 \end{bmatrix} \text{ (Equation 2-48)}$$

2.4.3.4 Second eigenvector

For the second eigenvalue $\lambda_2 = \sqrt{\left(\frac{8\mu_b}{n\pi r_i^4}(2n\pi r_i L_p) + \frac{8\mu_d(R_m+nr_0^2)}{\pi(R_m^2-nr_0^2)^3} 2n\pi r_i L_p\right)}$ (from Equation 2-42):

$$\begin{bmatrix} -\sqrt{2n\pi r_i L_p\left(\frac{8\mu_b}{n\pi r_i^4}+\frac{8\mu_d(R_m+nr_0^2)}{\pi(R_m^2-nr_0^2)^3}\right)} & \frac{8\mu_b}{n\pi r_i^4} & \frac{8\mu_d(R_m+nr_0^2)}{\pi(R_m^2-nr_0^2)^3} \\ 2n\pi r_i L_p & -\sqrt{2n\pi r_i L_p\left(\frac{8\mu_b}{n\pi r_i^4}+\frac{8\mu_d(R_m+nr_0^2)}{\pi(R_m^2-nr_0^2)^3}\right)} & 0 \\ 2n\pi r_i L_p & 0 & -\sqrt{2n\pi r_i L_p\left(\frac{8\mu_b}{n\pi r_i^4}+\frac{8\mu_d(R_m+nr_0^2)}{\pi(R_m^2-nr_0^2)^3}\right)} \end{bmatrix} * \begin{bmatrix} v_1 \\ v_2 \\ v_3 \end{bmatrix} = \begin{bmatrix} 0 \\ 0 \\ 0 \end{bmatrix}$$

(Equation 2-49)

This yields a system of three equations:

$$-\sqrt{\left(\frac{8\mu_b}{n\pi r_i^4}\left(2n\pi r_i L_p\right)+\frac{8\mu_d(R_m+nr_0^2)}{\pi\left(R_m^2-nr_0^2\right)^3}2n\pi r_i L_p\right)}v_1+\frac{8\mu_b}{n\pi r_i^4}v_2+\frac{8\mu_d(R_m+nr_0^2)}{\pi\left(R_m^2-nr_0^2\right)^3}v_3=0$$ (Equation 2-50)

$$2n\pi r_i L_p v_1-\sqrt{\left(\frac{8\mu_b}{n\pi r_i^4}\left(2n\pi r_i L_p\right)+\frac{8\mu_d(R_m+nr_0^2)}{\pi\left(R_m^2-nr_0^2\right)^3}2n\pi r_i L_p\right)}v_2=0$$ (Equation 2-51)

$$2n\pi r_i L_p v_1-\sqrt{\left(\frac{8\mu_b}{n\pi r_i^4}\left(2n\pi r_i L_p\right)+\frac{8\mu_d(R_m+nr_0^2)}{\pi\left(R_m^2-nr_0^2\right)^3}2n\pi r_i L_p\right)}v_3=0$$ (Equation 2-52)

From this:

$$2n\pi r_i L_p v_1-\sqrt{\left(\frac{8\mu_b}{n\pi r_i^4}\left(2n\pi r_i L_p\right)+\frac{8\mu_d(R_m+nr_0^2)}{\pi\left(R_m^2-nr_0^2\right)^3}2n\pi r_i L_p\right)}v_2=2n\pi r_i L_p v_1-\sqrt{\left(\frac{8\mu_b}{n\pi r_i^4}\left(2n\pi r_i L_p\right)+\frac{8\mu_d(R_m+nr_0^2)}{\pi\left(R_m^2-nr_0^2\right)^3}2n\pi r_i L_p\right)}v_3$$ (Equation 2-53: From Equation 2-51 and Equation 2-52)

Rearranging:

$$-\sqrt{\left(\frac{8\mu_b}{n\pi r_i^4}\left(2n\pi r_i L_p\right)+\frac{8\mu_d(R_m+nr_0^2)}{\pi\left(R_m^2-nr_0^2\right)^3}2n\pi r_i L_p\right)}v_2=-\sqrt{\left(\frac{8\mu_b}{n\pi r_i^4}\left(2n\pi r_i L_p\right)+\frac{8\mu_d(R_m+nr_0^2)}{\pi\left(R_m^2-nr_0^2\right)^3}2n\pi r_i L_p\right)}v_3$$ (Equation 2-54)

Therefore, for the second eigenvector:

$$v_2 = v_3$$ (Equation 2-55)

Plugging Equation 2-55 into Equation 2-52:

$$-\sqrt{\left(\frac{8\mu_b}{n\pi r_i^4}\left(2n\pi r_i L_p\right)+\frac{8\mu_d(R_m+nr_0^2)}{\pi\left(R_m^2-nr_0^2\right)^3}2n\pi r_i L_p\right)}v_1+v_2\left(\frac{8\mu_b}{n\pi r_i^4}+\frac{8\mu_d(R_m+nr_0^2)}{\pi\left(R_m^2-nr_0^2\right)^3}\right)=0$$ (Equation 2-56)

Rearranging:

$$v_2\left(\frac{8\mu_b}{n\pi r_i^4}+\frac{8\mu_d\left(R_m+nr_0^2\right)}{\pi\left(R_m^2-nr_0^2\right)^3}\right)=\sqrt{\left(\frac{8\mu_b}{n\pi r_i^4}\left(2n\pi r_i L_p\right)+\frac{8\mu_d\left(R_m+nr_0^2\right)}{\pi\left(R_m^2-nr_0^2\right)^3}2n\pi r_i L_p\right)}v_1 \text{ (Equation 2-57)}$$

Thus, solving for $v_1$ for the second eigenvector:

$$v_2=\frac{\sqrt{\left(\frac{8\mu_b}{n\pi r_i^4}\left(2n\pi r_i L_p\right)+\frac{8\mu_d\left(R_m+nr_0^2\right)}{\pi\left(R_m^2-nr_0^2\right)^3}2n\pi r_i L_p\right)}}{\left(\frac{8\mu_b}{n\pi r_i^4}+\frac{8\mu_d\left(R_m+nr_0^2\right)}{\pi\left(R_m^2-nr_0^2\right)^3}\right)}v_1 \text{ (Equation 2-58)}$$

Thus, the second eigenvector is:

$$x_2=\begin{bmatrix} v_1 \\ \frac{\sqrt{\left(\frac{8\mu_b}{n\pi r_i^4}\left(2n\pi r_i L_p\right)+\frac{8\mu_d\left(R_m+nr_0^2\right)}{\pi\left(R_m^2-nr_0^2\right)^3}2n\pi r_i L_p\right)}}{\left(\frac{8\mu_b}{n\pi r_i^4}+\frac{8\mu_d\left(R_m+nr_0^2\right)}{\pi\left(R_m^2-nr_0^2\right)^3}\right)}v_1 \\ \frac{\sqrt{\left(\frac{8\mu_b}{n\pi r_i^4}\left(2n\pi r_i L_p\right)+\frac{8\mu_d\left(R_m+nr_0^2\right)}{\pi\left(R_m^2-nr_0^2\right)^3}2n\pi r_i L_p\right)}}{\left(\frac{8\mu_b}{n\pi r_i^4}+\frac{8\mu_d\left(R_m+nr_0^2\right)}{\pi\left(R_m^2-nr_0^2\right)^3}\right)}v_1 \end{bmatrix} \text{ (Equation 2-59)}$$

2.4.3.5 Third eigenvector

For the third eigenvalue $\lambda_3=-\sqrt{\left(\frac{8\mu_b}{n\pi r_i^4}\left(2n\pi r_i L_p\right)+\frac{8\mu_d\left(R_m+nr_0^2\right)}{\pi\left(R_m^2-nr_0^2\right)^3}2n\pi r_i L_p\right)}$ (from Equation 2-42):

$$\begin{bmatrix} \left(2n\pi r_i L_p\left(\frac{8\mu_b}{n\pi r_i^4}+\frac{8\mu_d\left(R_m+nr_0^2\right)}{\pi\left(R_m^2-nr_0^2\right)^3}\right)\right)^{\frac{1}{2}} & \frac{8\mu_b}{n\pi r_i^4} & \frac{8\mu_d\left(R_m+nr_0^2\right)}{\pi\left(R_m^2-nr_0^2\right)^3} \\ 2n\pi r_i L_p & \left(2n\pi r_i L_p*\left(\frac{8\mu_b}{n\pi r_i^4}+\frac{8\mu_d\left(R_m+nr_0^2\right)}{\pi\left(R_m^2-nr_0^2\right)^3}\right)\right)^{\frac{1}{2}} & 0 \\ 2n\pi r_i L_p & 0 & \left(2n\pi r_i L_p*\left(\frac{8\mu_b}{n\pi r_i^4}+\frac{8\mu_d\left(R_m+nr_0^2\right)}{\pi\left(R_m^2-nr_0^2\right)^3}\right)\right)^{\frac{1}{2}} \end{bmatrix}*\begin{bmatrix} v_1 \\ v_2 \\ v_3 \end{bmatrix}=\begin{bmatrix} 0 \\ 0 \\ 0 \end{bmatrix}$$

(Equation 2-60)

This yields a system of three equations:

$$\sqrt{\left(\frac{8\mu_b}{n\pi r_i^4}\left(2n\pi r_i L_p\right)+\frac{8\mu_d\left(R_m+nr_0^2\right)}{\pi\left(R_m^2-nr_0^2\right)^3}2n\pi r_i L_p\right)}v_1+\frac{8\mu_b}{n\pi r_i^4}v_2+\frac{8\mu_d\left(R_m+nr_0^2\right)}{\pi\left(R_m^2-nr_0^2\right)^3}v_3=0 \text{ (Equation 2-61)}$$

$$2n\pi r_i L_p v_1 + \sqrt{\left(\frac{8\mu_b}{n\pi r_i^4}\left(2n\pi r_i L_p\right) + \frac{8\mu_d\left(R_m+nr_0^2\right)}{\pi\left(R_m^2-nr_0^2\right)^3}2n\pi r_i L_p\right)} v_2 = 0 \text{ (Equation 2-62)}$$

$$2n\pi r_i L_p v_1 + \sqrt{\left(\frac{8\mu_b}{n\pi r_i^4}\left(2n\pi r_i L_p\right) + \frac{8\mu_d\left(R_m+nr_0^2\right)}{\pi\left(R_m^2-nr_0^2\right)^3}2n\pi r_i L_p\right)} v_3 = 0 \text{ (Equation 2-63)}$$

From Equation 2-62 and Equation 2-63:

$$v_2 = v_3 \text{ (Equation 2-64)}$$

Solving Equation 2-61 for $v_1$:

$$\sqrt{\left(\frac{8\mu_b}{n\pi r_i^4}\left(2n\pi r_i L_p\right) + \frac{8\mu_d\left(R_m+nr_0^2\right)}{\pi\left(R_m^2-nr_0^2\right)^3}2n\pi r_i L_p\right)} v_1 + v_2\left(\frac{8\mu_b}{n\pi r_i^4} + \frac{8\mu_d\left(R_m+nr_0^2\right)}{\pi\left(R_m^2-nr_0^2\right)^3}\right) = 0 \text{ (Equation 2-65)}$$

Rearranging

$$-\sqrt{\left(\frac{8\mu_b}{n\pi r_i^4}\left(2n\pi r_i L_p\right) + \frac{8\mu_d\left(R_m+nr_0^2\right)}{\pi\left(R_m^2-nr_0^2\right)^3}2n\pi r_i L_p\right)} v_1 = v_2\left(\frac{8\mu_b}{n\pi r_i^4} + \frac{8\mu_d\left(R_m+nr_0^2\right)}{\pi\left(R_m^2-nr_0^2\right)^3}\right) \text{ (Equation 2-66)}$$

Thus, $v_1$ is as follows:

$$-\frac{\sqrt{\left(\frac{8\mu_b}{n\pi r_i^4}\left(2n\pi r_i L_p\right)+\frac{8\mu_d\left(R_m+nr_0^2\right)}{\pi\left(R_m^2-nr_0^2\right)^3}2n\pi r_i L_p\right)}}{\left(\frac{8\mu_b}{n\pi r_i^4}+\frac{8\mu_d\left(R_m+nr_0^2\right)}{\pi\left(R_m^2-nr_0^2\right)^3}\right)} v_1 = v_2 \text{ (Equation 2-67)}$$

The third eigenvector is as follows:

$$\begin{bmatrix} v_1 \\ -\frac{\sqrt{\left(\frac{8\mu_b}{n\pi r_i^4}\left(2n\pi r_i L_p\right)+\frac{8\mu_d\left(R_m+nr_0^2\right)}{\pi\left(R_m^2-nr_0^2\right)^3}2n\pi r_i L_p\right)}}{\left(\frac{8\mu_b}{n\pi r_i^4}+\frac{8\mu_d\left(R_m+nr_0^2\right)}{\pi\left(R_m^2-nr_0^2\right)^3}\right)} v_1 \\ -\frac{\sqrt{\left(\frac{8\mu_b}{n\pi r_i^4}\left(2n\pi r_i L_p\right)+\frac{8\mu_d\left(R_m+nr_0^2\right)}{\pi\left(R_m^2-nr_0^2\right)^3}2n\pi r_i L_p\right)}}{\left(\frac{8\mu_b}{n\pi r_i^4}+\frac{8\mu_d\left(R_m+nr_0^2\right)}{\pi\left(R_m^2-nr_0^2\right)^3}\right)} v_1 \end{bmatrix} = x_3 \text{ (Equation 2-68)}$$

2.4.3.6 Applying initial conditions to solve for constants

Plugging eigenvectors (Equation 2-48, Equation 2-59, Equation 2-68), and eigenvalues (Equation 2-40 and Equation 2-42) into the third order system (Equation 2-43) and regrouping constants produces the following formula:

$$y=\begin{bmatrix}\Delta P\\ Q_b\\ Q_d\end{bmatrix}=c_1\begin{bmatrix}0\\ 1\\ -\frac{\pi\left(R_m^2-nr_0^2\right)^3}{8\mu_d\left(R_m+nr_0^2\right)}*\frac{8\mu_b}{n\pi r_i^4}\end{bmatrix}+c_2\begin{bmatrix}1\\ \frac{\sqrt{\left(\frac{8\mu_b}{n\pi r_i^4}\left(2n\pi r_iL_p\right)+\frac{8\mu_d\left(R_m+nr_0^2\right)}{\pi\left(R_m^2-nr_0^2\right)^3}2n\pi r_iL_p\right)}}{\left(\frac{8\mu_b}{n\pi r_i^4}+\frac{8\mu_d\left(R_m+nr_0^2\right)}{\pi\left(R_m^2-nr_0^2\right)^3}\right)}\\ \frac{\sqrt{\left(\frac{8\mu_b}{n\pi r_i^4}\left(2n\pi r_iL_p\right)+\frac{8\mu_d\left(R_m+nr_0^2\right)}{\pi\left(R_m^2-nr_0^2\right)^3}2n\pi r_iL_p\right)}}{\left(\frac{8\mu_b}{n\pi r_i^4}+\frac{8\mu_d\left(R_m+nr_0^2\right)}{\pi\left(R_m^2-nr_0^2\right)^3}\right)}\end{bmatrix}*$$

$$exp\left(\sqrt{\left(\frac{8\mu_b}{n\pi r_i^4}\left(2n\pi r_iL_p\right)+\frac{8\mu_d\left(R_m+nr_0^2\right)}{\pi\left(R_m^2-nr_0^2\right)^3}2n\pi r_iL_p\right)}z\right)+$$

$$c_3\begin{bmatrix}1\\ -\frac{\sqrt{\left(\frac{8\mu_b}{n\pi r_i^4}\left(2n\pi r_iL_p\right)+\frac{8\mu_d\left(R_m+nr_0^2\right)}{\pi\left(R_m^2-nr_0^2\right)^3}2n\pi r_iL_p\right)}}{\left(\frac{8\mu_b}{n\pi r_i^4}+\frac{8\mu_d\left(R_m+nr_0^2\right)}{\pi\left(R_m^2-nr_0^2\right)^3}\right)}\\ -\frac{\sqrt{\left(\frac{8\mu_b}{n\pi r_i^4}\left(2n\pi r_iL_p\right)+\frac{8\mu_d\left(R_m+nr_0^2\right)}{\pi\left(R_m^2-nr_0^2\right)^3}2n\pi r_iL_p\right)}}{\left(\frac{8\mu_b}{n\pi r_i^4}+\frac{8\mu_d\left(R_m+nr_0^2\right)}{\pi\left(R_m^2-nr_0^2\right)^3}\right)}\end{bmatrix}*$$

$$exp\left(-\sqrt{\left(\frac{8\mu_b}{n\pi r_i^4}\left(2n\pi r_iL_p\right)+\frac{8\mu_d\left(R_m+nr_0^2\right)}{\pi\left(R_m^2-nr_0^2\right)^3}2n\pi r_iL_p\right)}z\right)$$ (Equation 2-69)

The pressure difference is as follows:

$$\Delta P=c_2\,exp\left(\sqrt{\left(\frac{8\mu_b}{n\pi r_i^4}\left(2n\pi r_iL_p\right)+\frac{8\mu_d\left(R_m+nr_0^2\right)}{\pi\left(R_m^2-nr_0^2\right)^3}2n\pi r_iL_p\right)}z\right)+$$

$$c_3\,exp\left(-\sqrt{\left(\frac{8\mu_b}{n\pi r_i^4}\left(2n\pi r_iL_p\right)+\frac{8\mu_d\left(R_m+nr_0^2\right)}{\pi\left(R_m^2-nr_0^2\right)^3}2n\pi r_iL_p\right)}z\right)$$ (Equation 2-70)

Rearranging:

$$\Delta P = c_2\, exp\left(\sqrt{\left(\frac{16\mu_b L_p}{r_i^3} + \frac{16\mu_d\left(R_m+nr_0^2\right)}{\left(R_m^2-nr_0^2\right)^3} nr_i L_p\right)} z\right) +$$

$$c_3\, exp\left(-\sqrt{\left(\frac{16\mu_b L_p}{r_i^3} + \frac{16\mu_d\left(R_m+nr_0^2\right)}{\left(R_m^2-nr_0^2\right)^3} nr_i L_p\right)} z\right) \text{ (Equation 2-71)}$$

The blood flow rate equation is as follows:

$$Q_b = c_1 + c_2 \frac{\sqrt{\left(\frac{8\mu_b}{n\pi r_i^4}\left(2n\pi r_i L_p\right)+\frac{8\mu_d\left(R_m+nr_0^2\right)}{\pi\left(R_m^2-nr_0^2\right)^3} 2n\pi r_i L_p\right)}}{\left(\frac{8\mu_b}{n\pi r_i^4}+\frac{8\mu_d\left(R_m+nr_0^2\right)}{\pi\left(R_m^2-nr_0^2\right)^3}\right)} *$$

$$exp\left(\sqrt{\left(\frac{8\mu_b}{n\pi r_i^4}\left(2n\pi r_i L_p\right) + \frac{8\mu_d\left(R_m+nr_0^2\right)}{\pi\left(R_m^2-nr_0^2\right)^3} 2n\pi r_i L_p\right)} z\right) - \frac{\sqrt{\left(\frac{8\mu_b}{n\pi r_i^4}\left(2n\pi r_i L_p\right)+\frac{8\mu_d\left(R_m+nr_0^2\right)}{\pi\left(R_m^2-nr_0^2\right)^3} 2n\pi r_i L_p\right)}}{\left(\frac{8\mu_b}{n\pi r_i^4}+\frac{8\mu_d\left(R_m+nr_0^2\right)}{\pi\left(R_m^2-nr_0^2\right)^3}\right)} c_3 *$$

$$exp\left(-\sqrt{\left(\frac{8\mu_b}{n\pi r_i^4}\left(2n\pi r_i L_p\right) + \frac{8\mu_d\left(R_m+nr_0^2\right)}{\pi\left(R_m^2-nr_0^2\right)^3} 2n\pi r_i L_p\right)} z\right) \text{ (Equation 2-72)}$$

For convenience let us define a constant:

$$K_1 = \frac{\sqrt{\left(\frac{8\mu_b}{n\pi r_i^4}\left(2n\pi r_i L_p\right)+\frac{8\mu_d\left(R_m+nr_0^2\right)}{\pi\left(R_m^2-nr_0^2\right)^3} 2n\pi r_i L_p\right)}}{\left(\frac{8\mu_b}{n\pi r_i^4}+\frac{8\mu_d\left(R_m+nr_0^2\right)}{\pi\left(R_m^2-nr_0^2\right)^3}\right)} \text{ (Equation 2-73)}$$

Plugging this constant (Equation 2-73) into Equation 2-72:

$$Q_b = c_1 + c_2 K_1\, exp\left(\sqrt{\left(\frac{16\mu_b L_p}{r_i^3} + \frac{16\mu_d\left(R_m+nr_0^2\right)}{\left(R_m^2-nr_0^2\right)^3} nr_i L_p\right)} z\right) -$$

$$K_1 c_3\, exp\left(-\sqrt{\left(\frac{16\mu_b L_p}{r_i^3} + \frac{16\mu_d\left(R_m+nr_0^2\right)}{\left(R_m^2-nr_0^2\right)^3} nr_i L_p\right)} z\right) \text{ (Equation 2-74)}$$

The dialysate flow rate equation is as follows:

$$Q_d = -\frac{\pi\left(R_m^2 - nr_0^2\right)^3}{8\mu_d\left(R_m + nr_0^2\right)}\frac{8\mu_b}{n\pi r_i^4}c_1 + c_2\frac{\sqrt{\left(\frac{8\mu_b}{n\pi r_i^4}\left(2n\pi r_i L_p\right) + \frac{8\mu_d\left(R_m + nr_0^2\right)}{\pi\left(R_m^2 - nr_0^2\right)^3}2n\pi r_i L_p\right)}}{\left(\frac{8\mu_b}{n\pi r_i^4} + \frac{8\mu_d\left(R_m + nr_0^2\right)}{\pi\left(R_m^2 - nr_0^2\right)^3}\right)} *$$

$$exp\left(\sqrt{\left(\frac{8\mu_b}{n\pi r_i^4}\left(2n\pi r_i L_p\right) + \frac{8\mu_d\left(R_m + nr_0^2\right)}{\pi\left(R_m^2 - nr_0^2\right)^3}2n\pi r_i L_p\right)}z\right) - \frac{\sqrt{\left(\frac{8\mu_b}{n\pi r_i^4}\left(2n\pi r_i L_p\right) + \frac{8\mu_d\left(R_m + nr_0^2\right)}{\pi\left(R_m^2 - nr_0^2\right)^3}2n\pi r_i L_p\right)}}{\left(\frac{8\mu_b}{n\pi r_i^4} + \frac{8\mu_d\left(R_m + nr_0^2\right)}{\pi\left(R_m^2 - nr_0^2\right)^3}\right)}c_3 *$$

$$exp\left(-\sqrt{\left(\frac{8\mu_b}{n\pi r_i^4}\left(2n\pi r_i L_p\right) + \frac{8\mu_d\left(R_m + nr_0^2\right)}{\pi\left(R_m^2 - nr_0^2\right)^3}2n\pi r_i L_p\right)}z\right) \text{ (Equation 2-75)}$$

Defining a constant $K_2$ as follows:

$$-\frac{\pi\left(R_m^2 - nr_0^2\right)^3}{8\mu_d\left(R_m + nr_0^2\right)}\frac{8\mu_b}{n\pi r_i^4} = K_2 \text{ (Equation 2-76)}$$

Plugging in $K_1$ (Equation 2-73) and $K_2$ (Equation 2-76) into Equation 2-75:

$$Q_d = -K_2 c_1 + c_2 K_1\, exp\left(\sqrt{\left(\frac{16\mu_b L_p}{r_i^3} + \frac{16\mu_d\left(R_m + nr_0^2\right)}{\left(R_m^2 - nr_0^2\right)^3}nr_i L_p\right)}z\right) -$$

$$K_1 c_3\, exp\left(-\sqrt{\left(\frac{16\mu_b L_p}{r_i^3} + \frac{16\mu_d\left(R_m + nr_0^2\right)}{\left(R_m^2 - nr_0^2\right)^3}nr_i L_p\right)}z\right) \text{ (Equation 2-77)}$$

Applying the initial condition of inlet pressure:

$$\Delta P(z = 0) = P_{dout} - P_{bin} = c_2 + c_3 \text{ (Equation 2-78)}$$

Applying the initial condition of blood flow rate:

$$Q_b(z = 0) = Q_{b,in} = c_1 + c_2\frac{\sqrt{\left(\frac{8\mu_b}{n\pi r_i^4}\left(2n\pi r_i L_p\right) + \frac{8\mu_d\left(R_m + nr_0^2\right)}{\pi\left(R_m^2 - nr_0^2\right)^3}2n\pi r_i L_p\right)}}{\left(\frac{8\mu_b}{n\pi r_i^4} + \frac{8\mu_d\left(R_m + nr_0^2\right)}{\pi\left(R_m^2 - nr_0^2\right)^3}\right)} -$$

$$\frac{\sqrt{\left(\frac{8\mu_b}{n\pi r_i^4}\left(2n\pi r_i L_p\right) + \frac{8\mu_d\left(R_m + nr_0^2\right)}{\pi\left(R_m^2 - nr_0^2\right)^3}2n\pi r_i L_p\right)}}{\left(\frac{8\mu_b}{n\pi r_i^4} + \frac{8\mu_d\left(R_m + nr_0^2\right)}{\pi\left(R_m^2 - nr_0^2\right)^3}\right)}c_3 \text{ (Equation 2-79)}$$

Applying the initial condition of dialysate inlet flow rate along with the assumption of zero net ultrafiltration:

$$Q_d(z=0) = Q_{d,out} = Q_{d,in} = -\frac{\pi\left(R_m^2 - nr_0^2\right)^3}{8\mu_d\left(R_m + nr_0^2\right)}\frac{8\mu_b}{n\pi r_i^4}c_1 +$$

$$c_2\frac{\sqrt{\left(\frac{8\mu_b}{n\pi r_i^4}\left(2n\pi r_i L_p\right) + \frac{8\mu_d\left(R_m + nr_0^2\right)}{\pi\left(R_m^2 - nr_0^2\right)^3}2n\pi r_i L_p\right)}}{\left(\frac{8\mu_b}{n\pi r_i^4} + \frac{8\mu_d\left(R_m + nr_0^2\right)}{\pi\left(R_m^2 - nr_0^2\right)^3}\right)} - \frac{\sqrt{\left(\frac{8\mu_b}{n\pi r_i^4}\left(2n\pi r_i L_p\right) + \frac{8\mu_d\left(R_m + nr_0^2\right)}{\pi\left(R_m^2 - nr_0^2\right)^3}2n\pi r_i L_p\right)}}{\left(\frac{8\mu_b}{n\pi r_i^4} + \frac{8\mu_d\left(R_m + nr_0^2\right)}{\pi\left(R_m^2 - nr_0^2\right)^3}\right)}c_3$$ (Equation 2-80)

From the pressure initial condition:

$$c_2 = P_{dout} - P_{bin} - c_3$$ (Equation 2-81)

From the blood flow rate initial condition:

$$Q_{b,in} = c_1 + (P_{dout} - P_{bin} - c_3)\frac{\sqrt{\left(\frac{8\mu_b}{n\pi r_i^4}\left(2n\pi r_i L_p\right) + \frac{8\mu_d\left(R_m + nr_0^2\right)}{\pi\left(R_m^2 - nr_0^2\right)^3}2n\pi r_i L_p\right)}}{\left(\frac{8\mu_b}{n\pi r_i^4} + \frac{8\mu_d\left(R_m + nr_0^2\right)}{\pi\left(R_m^2 - nr_0^2\right)^3}\right)} -$$

$$\frac{\sqrt{\left(\frac{8\mu_b}{n\pi r_i^4}\left(2n\pi r_i L_p\right) + \frac{8\mu_d\left(R_m + nr_0^2\right)}{\pi\left(R_m^2 - nr_0^2\right)^3}2n\pi r_i L_p\right)}}{\left(\frac{8\mu_b}{n\pi r_i^4} + \frac{8\mu_d\left(R_m + nr_0^2\right)}{\pi\left(R_m^2 - nr_0^2\right)^3}\right)}c_3$$ (Equation 2-82)

Rearranging

$$c_1 = Q_{b,in} - (P_{dout} - P_{bin} - c_3)\frac{\sqrt{\left(\frac{8\mu_b}{n\pi r_i^4}\left(2n\pi r_i L_p\right) + \frac{8\mu_d\left(R_m + nr_0^2\right)}{\pi\left(R_m^2 - nr_0^2\right)^3}2n\pi r_i L_p\right)}}{\left(\frac{8\mu_b}{n\pi r_i^4} + \frac{8\mu_d\left(R_m + nr_0^2\right)}{\pi\left(R_m^2 - nr_0^2\right)^3}\right)} +$$

$$\frac{\sqrt{\left(\frac{8\mu_b}{n\pi r_i^4}\left(2n\pi r_i L_p\right) + \frac{8\mu_d\left(R_m + nr_0^2\right)}{\pi\left(R_m^2 - nr_0^2\right)^3}2n\pi r_i L_p\right)}}{\left(\frac{8\mu_b}{n\pi r_i^4} + \frac{8\mu_d\left(R_m + nr_0^2\right)}{\pi\left(R_m^2 - nr_0^2\right)^3}\right)}c_3$$ (Equation 2-83)

Plugging in $K_1$ to Equation 2-83

$$c_1 = Q_{b,in} - (P_{dout} - P_{bin} - c_3)K_1 + K_1 c_3$$ (Equation 2-84)

Rearranging

$$c_1 = Q_{b,in} + K_1(c_3 - P_{dout} + P_{bin} + c_3) = Q_{b,in} + K_1(2c_3 - P_{dout} + P_{bin})$$ (Equation 2-85)

From the dialysate flow rate initial condition:

$$Q_{d,in} = -\frac{\pi\left(R_m^2 - nr_0^2\right)^3}{8\mu_d\left(R_m + nr_0^2\right)}\frac{8\mu_b}{n\pi r_i^4}\left(Q_{b,in} + K_1(2c_3 - P_{dout} + P_{bin})\right) + (P_{dout} - P_{bin} - c_3)\frac{\sqrt{\left(\frac{8\mu_b}{n\pi r_i^4}(2n\pi r_i L_p) + \frac{8\mu_d(R_m + nr_0^2)}{\pi\left(R_m^2 - nr_0^2\right)^3}2n\pi r_i L_p\right)}}{\left(\frac{8\mu_b}{n\pi r_i^4} + \frac{8\mu_d(R_m + nr_0^2)}{\pi\left(R_m^2 - nr_0^2\right)^3}\right)} - \frac{\sqrt{\left(\frac{8\mu_b}{n\pi r_i^4}(2n\pi r_i L_p) + \frac{8\mu_d(R_m + nr_0^2)}{\pi\left(R_m^2 - nr_0^2\right)^3}2n\pi r_i L_p\right)}}{\left(\frac{8\mu_b}{n\pi r_i^4} + \frac{8\mu_d(R_m + nr_0^2)}{\pi\left(R_m^2 - nr_0^2\right)^3}\right)}c_3$$ (Equation 2-86)

Applying $K_1$ and $K_2$ to Equation 2-86:

$$Q_{d,in} = -K_2\left(Q_{b,in} + K_1(2c_3 - P_{dout} + P_{bin})\right) + (P_{dout} - P_{bin} - c_3)K_1 - K_1c_3$$ (Equation 2-87)

Algebraically solving:

$$Q_{d,in} = -K_2\left(Q_{b,in} + 2c_3K_1 - P_{dout}K_1 + P_{bin}K_1\right) + P_{dout}K_1 - P_{bin}K_1 - c_3K_1 - K_1c_3$$ (Equation 2-88)

$$Q_{d,in} = -K_2Q_{b,in} - K_2 2c_3K_1 + K_2P_{dout}K_1 - K_2P_{bin}K_1 + P_{dout}K_1 - P_{bin}K_1 - c_3K_1 - K_1c_3$$ (Equation 2-89)

$$Q_{d,in} = -K_2Q_{b,in} + K_2P_{dout}K_1 - K_2P_{bin}K_1 + P_{dout}K_1 - P_{bin}K_1 - c_3(2K_1 + 2K_2K_1)$$ (Equation 2-90)

$$c_3(2K_1 + 2K_2K_1) = -K_2Q_{b,in} + K_2P_{dout}K_1 - K_2P_{bin}K_1 + P_{dout}K_1 - P_{bin}K_1 - Q_{d,in}$$ (Equation 2-91)

$$c_3 = \frac{\left(-K_2Q_{b,in} + K_2P_{dout}K_1 - K_2P_{bin}K_1 + P_{dout}K_1 - P_{bin}K_1 - Q_{d,in}\right)}{(2K_1 + 2K_2K_1)}$$ (Equation 2-92)

#### 2.4.3.7 Applying zero net ultrafiltration condition on blood side

Now we have defined the constants $c_1$, $c_2$, and $c_3$ (Equation 2-83, Equation 2-81, Equation 2-92 respectively) for the system (Equation 2-69) in terms of $P_{d,out} - P_{b,in} = \Delta P(z = 0)$. This initial pressure difference is determined by the constraint that $Q_{b,in} = Q_{b,out}$ meaning that:

$$Q_b(z = 0) = Q_b(z = L)$$ (Equation 2-93)

Applying the blood flow rate equation:

$$Q_b(z = 0) = c_1 + c_2K_1 - K_1c_3$$ (Equation 2-94)

$$Q_b(z=L) = c_1 + c_2K_1\, exp\left(\sqrt{\left(\frac{16\mu_b L_p}{r_i^3} + \frac{16\mu_d\left(R_m+nr_0^2\right)}{\left(R_m^2-nr_0^2\right)^3} nr_i L_p\right)} L\right) -$$

$$K_1c_3\, exp\left(-\sqrt{\left(\frac{16\mu_b L_p}{r_i^3} + \frac{16\mu_d\left(R_m+nr_0^2\right)}{\left(R_m^2-nr_0^2\right)^3} nr_i L_p\right)} L\right) \text{ (Equation 2-95)}$$

Next, we define two constants for ease of computation:

$$K_3 = exp\left(\sqrt{\left(\frac{16\mu_b L_p}{r_i^3} + \frac{16\mu_d\left(R_m+nr_0^2\right)}{\left(R_m^2-nr_0^2\right)^3} nr_i L_p\right)} L\right) \text{ and } K_4 =$$

$$exp\left(-\sqrt{\left(\frac{16\mu_b L_p}{r_i^3} + \frac{16\mu_d\left(R_m+nr_0^2\right)}{\left(R_m^2-nr_0^2\right)^3} nr_i L_p\right)} L\right) \text{ (Equation 2-96)}$$

Applying these constants to Equation 2-95:

$$Q_b(z=L) = c_1 + c_2K_1K_3 - K_1c_3K_4 \text{ (Equation 2-97)}$$

Rewriting constants in terms of $\Delta P_0(z=0) = P_{dout} - P_{bin}$

$$c_3 = \frac{\left(-K_2Q_{b,in}+K_2P_{dout}K_1-K_2P_{bin}K_1+P_{dout}K_1-P_{bin}K_1-Q_{d,in}\right)}{\left(2K_1+2K_2K_1\right)} =$$

$$\frac{\left(-K_2Q_{b,in}+K_2K_1(P_{dout}-P_{bin})+K_1(P_{dout}-P_{bin})-Q_{d,in}\right)}{\left(2K_1+2K_2K_1\right)} = \frac{\left(-K_2Q_{b,in}+K_2K_1\Delta P_0(z=0)+K_1\Delta P_0(z=0)-Q_{d,in}\right)}{\left(2K_1+2K_2K_1\right)}$$

(Equation 2-98)

$$c_1 = Q_{b,in} + K_1(2c_3 - P_{dout} + P_{bin}) = Q_{b,in} + K_1\big(2c_3 - \Delta P_0(z=0)\big) \text{ (Equation 2-99)}$$

$$c_2 = P_{dout} - P_{bin} - c_3 = \Delta P_0(z=0) - c_3 \text{ (Equation 2-100)}$$

Setting Equation 2-97 and Equation 2-94 equal per Equation 2-93:

$$c_1 + c_2K_1 - K_1c_3 = c_1 + c_2K_1K_3 - K_1c_3K_4 \text{ (Equation 2-101)}$$

Subtracting $c_1$ from both sides:

$$c_2K_1 - K_1c_3 = c_2K_1K_3 - K_1c_3K_4 \text{ (Equation 2-102)}$$

Dividing both sides by $K_1$ and rearranging:

$$c_2 - c_3 = c_2K_3 - c_3K_4 \rightarrow c_2(1-K_3) = c_3(1-K_4) \rightarrow \frac{c_2}{c_3} = \frac{1-K_3}{1-K_4} \text{ (Equation 2-103)}$$

Plugging in Equation 2-100:

$$\frac{(\Delta P_0(z=0)-c_3)}{c_3} = \frac{1-K_3}{1-K_4} \text{ (Equation 2-104)}$$

Rearranging and plugging in Equation 2-98:

$$\frac{(\Delta P_0(z=0))}{c_3} = \frac{1-K_3}{1-K_4} + 1 \rightarrow \Delta P_0(z=0) = c_3\left(\frac{1-K_3}{1-K_4}+1\right) =$$

$$\frac{\left(-K_2 Q_{b,in}+K_2K_1\Delta P_0(z=0)+K_1\Delta P_0(z=0)-Q_{d,in}\right)}{(2K_1+2K_2K_1)}\left(\frac{1-K_3}{1-K_4}+1\right) \text{ (Equation 2-105)}$$

Rearranging:

$$\Delta P_0(z=0) = \left(-K_2 Q_{b,in} + K_2K_1\Delta P_0(z=0) + K_1\Delta P_0(z=0) - Q_{d,in}\right) * \frac{\left(\frac{1-K_3}{1-K_4}+1\right)}{(2K_1+2K_2K_1)}$$

(Equation 2-106)

Defining a constant:

$$K_5 = \frac{\left(\frac{1-K_3}{1-K_4}+1\right)}{(2K_1+2K_2K_1)} \text{ (Equation 2-107)}$$

Plugging in $K_5$ to Equation 2-106:

$$\Delta P_0(z=0) = \left(-K_2 Q_{b,in} + K_2K_1\Delta P_0(z=0) + K_1\Delta P_0(z=0) - Q_{d,in}\right) * K_5 =$$

$$-K_2 Q_{b,in}K_5 + K_2K_1\Delta P_0(z=0)K_5 + K_1\Delta P_0(z=0)K_5 - Q_{d,in}K_5 \text{ (Equation 2-108)}$$

Rearranging:

$$\Delta P_0(z=0) - K_2K_1\Delta P_0(z=0)K_5 - K_1\Delta P_0(z=0)K_5 = -K_2 Q_{b,in}K_5 - Q_{d,in}K_5 \text{ (Equation 2-109)}$$

Solving for $\Delta P_0(z=0)$:

$$\Delta P_0(z=0)(1 - K_2K_1K_5 - K_1K_5) = -K_2 Q_{b,in}K_5 - Q_{d,in}K_5 \rightarrow \Delta P_0(z=0) =$$

$$\frac{\left(-K_2 Q_{b,in}K_5 - Q_{d,in}K_5\right)}{(1-K_2K_1K_5-K_1K_5)} \text{ (Equation 2-110)}$$

### 2.4.4 *Blood and Dialysate Toxin Concentration with Analytically Computed Flow Rate and Pressure Terms*

We now have explicit analytical solutions for the flow rate and pressure. In total we now have the following system of equations:

For ultrafiltration (Jv > 0):

$$\frac{dC_{stlb}}{dz} = \frac{1}{Q_b}\left(J_v(1-\sigma)f - \frac{K_{free}A}{L}\right) * (C_{sb} - C_{sd}) - \frac{J_v(1-\sigma)C_{sb}}{Q_b} - \frac{dQ_b}{dz} * \frac{C_{stlb}}{Q_b} \text{ (Equation 2-111)}$$

$$\frac{dC_{stld}}{dz} = \left(J_v(1-\sigma)f - \frac{K_{free}A}{L}\right) * \frac{(C_{sb}-C_{sd})}{Q_d} - \frac{J_v(1-\sigma)C_{sb}}{Q_d} - \frac{dQ_d}{dz} * \frac{C_{stld}}{Q_d} \text{ (Equation 2-112)}$$

For backfiltration (Jv < 0):

$$\frac{dC_{stlb}}{dz} = \left(J_v(1-\sigma)f - \frac{K_{free}A}{L}\right) * \frac{(C_{sb}-C_{sd})}{Q_b} - \frac{J_v(1-\sigma)C_{sd}}{Q_b} - \frac{dQ_b}{dz} * \frac{C_{stlb}}{Q_b} \text{ (Equation 2-113)}$$

$$\frac{dC_{stld}}{dz} = \left(J_v(1-\sigma)f - \frac{K_{free}A}{L}\right) * \frac{(C_{sb}-C_{sd})}{Q_d} - \frac{J_v(1-\sigma)C_{sd}}{Q_d} - \frac{dQ_d}{dz} * \frac{C_{stld}}{Q_d} \text{ (Equation 2-114)}$$

For both:

$$Q_b = c_1 + c_2K_1\,exp(K_3z) - K_1c_3\,exp(K_4z) \text{ (Equation 2-115)}$$

$$Q_d = -K_2c_1 + c_2K_1\,exp(K_3z) - K_1c_3\,exp(K_4z) \text{ (Equation 2-116)}$$

$$\Delta P = c_2\,exp(K_3z) + c_3\,exp(K_4z) \text{ (Equation 2-117)}$$

$$\frac{dQ_b}{dz} = \frac{dQ_d}{dz} = -2n\pi r_i L_p P_b + 2n\pi r_i L_p P_d = 2n\pi r_i L_p \Delta P \text{ (Equation 2-118)}$$

To simplify computation we define a constant

$$K_6 = 2n\pi r_i L_p \text{ (Equation 2-119)}$$

Applying this to Equation 2-118:

$$\frac{dQ_b}{dz} = \frac{dQ_d}{dz} = K_6\Delta P \text{ (Equation 2-120)}$$

The only factor affecting albumin concentrations in blood and dialysate is ultrafiltration, because albumin cannot cross the dialysis membrane. Thus, albumin follows a periodicity similar to that of flow rate:

$$C_{atld} = Q_{d0} * \frac{C_{atld0}}{Q_d} \text{ (Equation 2-121)}$$

$$C_{atlb} = Q_{b0} * \frac{C_{atlb0}}{Q_b} \text{ (Equation 2-122)}$$

Where $C_{atld}$ is dialysate albumin, and is a function of z, while $C_{atld0}$ is the fixed albumin within the dialysate reservoir. $C_{atlb}$ is blood albumin, and is a function of z, while $C_{atlb0}$ is the fixed albumin within the blood reservoir. Recalling that the free dialysate and blood side toxin concentrations are:

$$C_{sd} = \frac{-\left(C_{atld}+\frac{1}{K_B}-C_{stld}\right)+\sqrt{\left(C_{atld}+\frac{1}{K_B}-C_{stld}\right)^2+\frac{4C_{stld}}{K_B}}}{2} \text{ (Equation 2-123)}$$

$$C_{sb} = \frac{-\left(C_{atlb}+\frac{1}{K_B}-C_{stlb}\right)+\sqrt{\left(C_{atlb}+\frac{1}{K_B}-C_{stlb}\right)^2+\frac{4C_{stlb}}{K_B}}}{2} \text{ (Equation 2-124)}$$

The local ultrafiltration/backfiltration rate is:

$$J_v = -2n\pi r_i L_p \Delta P \text{ (Equation 2-125)}$$

The Peclet number and the function of Peclet number are:

$$Pe = Jv * (1-\sigma) * \frac{L}{K_{free}A} \text{ (Equation 2-126)}$$

$$\text{f} = \frac{1}{Pe} - \frac{1}{\exp(Pe)-1} \text{ (Equation 2-127)}$$

Applying Equation 2-125 to Equation 2-126 we arrive at:

$$Pe = Jv * (1-\sigma) * \frac{L}{K_{free}A} = -2n\pi r_i L_p (1-\sigma) * \frac{L}{K_{free}A} \Delta P \text{ (Equation 2-128)}$$

We define a constant $K_7$:

$$K_7 = 2n\pi r_i L_p (1-\sigma) \frac{L}{K_{free}A} = K_6 * (1-\sigma) \frac{L}{K_{free}A} \text{ (Equation 2-129)}$$

Applying Equation 2-129 to Equation 2-128:

$$Pe = -K_7 \Delta P \text{ (Equation 2-130)}$$

Applying Equation 2-130 to Equation 2-127:

$$f = \frac{1}{-K_7 \Delta P} - \frac{1}{\exp(-K_7 \Delta P)-1} \text{ (Equation 2-131)}$$

### 2.4.5 *Refining the system to a single ODE in terms of change in toxin amount*

Next, we define a function of z with the variable $\chi$ that equals the amount of toxin removed from the blood side over the course of a single pass through the dialyzer such that:

$$Q_b C_{stlb} = Q_{b0} C_{stlb0} + \chi \text{ (Equation 2-132)}$$

This means blood toxin concentration can be represented as:

$$C_{stlb} = \frac{Q_{b0} C_{stlb0} + \chi}{Q_b} \text{ (Equation 2-133)}$$

By the same reasoning on the dialysate side:

$$Q_d C_{stld} = Q_{d0} C_{stld0} + \chi \text{ (Equation 2-134)}$$

Recall that blood and dialysate flow counter-current. Hence why the sign of $\chi$ is the same in Equation 2-132 and Equation 2-134. Thus, the dialysate toxin concentration is:

$$C_{stld} = \frac{Q_{d0} C_{stld0} + \chi}{Q_d} \text{ (Equation 2-135)}$$

We impose initial condition:

$$\chi(z = 0) = 0 \text{ (Equation 2-136)}$$

During ultrafiltration the system is represented by the following single equation:

$$\frac{\delta \chi}{\delta z} = \left(J_v(1 - \sigma) f - \frac{K_{free} A}{L}\right) * (C_{sb} - C_{sd}) - J_v(1 - \sigma) C_{sb} \text{ (Equation 2-137)}$$

During backfiltration the system is represented as follows:

$$\frac{\delta \chi}{\delta z} = \left(J_v(1 - \sigma) f - \frac{K_{free} A}{L}\right) * (C_{sb} - C_{sd}) - J_v(1 - \sigma) C_{sd} \text{ (Equation 2-138)}$$

Expanding the free toxin concentration on the blood side:

$$\frac{\delta\chi}{\delta z} = \left(-2n\pi r_i L_p \Delta P(1-\sigma)\left(\frac{1}{Pe} - \frac{1}{exp(Pe)-1}\right) - \frac{K_{free}A}{L}\right) * \left(\frac{-\left(Q_{b0}*\frac{C_{atlb0}}{Q_b}+\frac{1}{K_B}-C_{stlb}\right)+\sqrt{\left(Q_{b0}*\frac{C_{atlb0}}{Q_b}+\frac{1}{K_B}-C_{stlb}\right)^2+\frac{4C_{stlb}}{K_B}}}{2} - \frac{-\left(Q_{d0}*\frac{C_{atld0}}{Q_d}+\frac{1}{K_B}-C_{stld}\right)+\sqrt{\left(Q_{d0}*\frac{C_{atld0}}{Q_d}+\frac{1}{K_B}-C_{stld}\right)^2+\frac{4C_{stld}}{K_B}}}{2}\right) + 2n\pi r_i L_p \Delta P(1-\sigma)\frac{-\left(Q_{b0}*\frac{C_{atlb0}}{Q_b}+\frac{1}{K_B}-C_{stlb}\right)+\sqrt{\left(Q_{b0}*\frac{C_{atlb0}}{Q_b}+\frac{1}{K_B}-C_{stlb}\right)^2+\frac{4C_{stlb}}{K_B}}}{2}$$ (Equation 2-139)

Defining a new constant $K_8$:

$$K_8 = 2n\pi r_i L_p(1-\sigma) = K_6 * (1-\sigma)$$ (Equation 2-140)

Applying constants to Equation 2-139:

$$\frac{\delta\chi}{\delta z} = \left(\left(\frac{-K_8\Delta P}{Pe} + \frac{K_8\Delta P}{exp(Pe)-1}\right) - \frac{K_{free}A}{L}\right) * \left(\frac{-\left(Q_{b0}*\frac{C_{atlb0}}{Q_b}+\frac{1}{K_B}-\frac{Q_{b0}C_{stlb0}+\chi}{Q_b}\right)+\sqrt{\left(Q_{b0}*\frac{C_{atlb0}}{Q_b}+\frac{1}{K_B}-\frac{Q_{b0}C_{stlb0}+\chi}{Q_b}\right)^2+\frac{4}{K_B}\left(\frac{Q_{b0}C_{stlb0}+\chi}{Q_b}\right)}}{2} - \frac{-\left(Q_{d0}*\frac{C_{atld0}}{Q_d}+\frac{1}{K_B}-\frac{Q_{d0}C_{stld0}+\chi}{Q_d}\right)+\sqrt{\left(Q_{d0}*\frac{C_{atld0}}{Q_d}+\frac{1}{K_B}-\frac{Q_{d0}C_{stld0}+\chi}{Q_d}\right)^2+\frac{4}{K_B}*\left(\frac{Q_{d0}C_{stld0}+\chi}{Q_d}\right)}}{2}\right) + K_8\Delta P\frac{-\left(Q_{b0}*\frac{C_{atlb0}}{Q_b}+\frac{1}{K_B}-\frac{Q_{b0}C_{stlb0}+\chi}{Q_b}\right)+\sqrt{\left(Q_{b0}*\frac{C_{atlb0}}{Q_b}+\frac{1}{K_B}-\frac{Q_{b0}C_{stlb0}+\chi}{Q_b}\right)^2+\frac{4}{K_B}\left(\frac{Q_{b0}C_{stlb0}+\chi}{Q_b}\right)}}{2}$$ (Equation 2-141)

Expanding blood and dialysate flow rate and pressure difference terms:

$$\frac{\delta\chi}{\delta z} = \left(\left(\frac{K_8(c_2\,exp(K_3z)+c_3\,exp(K_4z))}{K_7(c_2\,exp(K_3z)+c_3\,exp(K_4z))} + \frac{K_8(c_2\,exp(K_3z)+c_3\,exp(K_4z))}{exp\left(-K_7(c_2\,exp(K_3z)+c_3\,exp(K_4z))\right)-1}\right) - \frac{K_{free}A}{L}\right) * \frac{1}{2} *$$

$$\left(-\left(\frac{Q_{b0}C_{atlb0}}{c_1+c_2K_1\,exp(K_3z)-K_1c_3\,exp(K_4z)} + \frac{1}{K_B} - \frac{Q_{b0}C_{stlb0}+\chi}{c_1+c_2K_1\,exp(K_3z)-K_1c_3\,exp(K_4z)}\right) + \right.$$

$$\left(\left(\frac{Q_{b0}*C_{atlb0}}{c_1+c_2K_1\,exp(K_3z)-K_1c_3\,exp(K_4z)} + \frac{1}{K_B} - \frac{Q_{b0}C_{stlb0}+\chi}{c_1+c_2K_1\,exp(K_3z)-K_1c_3\,exp(K_4z)}\right)^2 + \right.$$

$$\left.\frac{\frac{4}{K_B}(Q_{b0}C_{stlb0}+\chi)}{c_1+c_2K_1\,exp(K_3z)-K_1c_3\,exp(K_4z)}\right)^{\frac{1}{2}} - \left(-\left(\frac{Q_{d0}C_{atld0}}{c_2K_1\,exp(K_3z)-K_2c_1-K_1c_3\,exp(K_4z)} + \frac{1}{K_B} - \right.\right.$$

$$\left.\frac{Q_{d0}C_{stld0}+\chi}{c_2K_1\,exp(K_3z)-K_2c_1-K_1c_3\,exp(K_4z)}\right) + \left(\left(\frac{Q_{d0}C_{atld0}}{c_2K_1\,exp(K_3z)-K_2c_1-K_1c_3\,exp(K_4z)} + \frac{1}{K_B} - \right.\right.$$

$$\left.\left.\left.\left.\frac{Q_{d0}C_{stld0}+\chi}{c_2K_1\,exp(K_3z)-K_2c_1-K_1c_3\,exp(K_4z)}\right)^2 + \frac{\frac{4}{K_B}(Q_{d0}C_{stld0}+\chi)}{c_2K_1\,exp(K_3z)-K_2c_1-K_1c_3\,exp(K_4z)}\right)^{\frac{1}{2}}\right)\right) +$$

$$\frac{K_8(c_2\,exp(K_3z)+c_3\,exp(K_4z))}{2} * \left(-\left(\frac{Q_{b0}*C_{atlb0}}{c_1+c_2K_1\,exp(K_3z)-K_1c_3\,exp(K_4z)} + \frac{1}{K_B} - \right.\right.$$

$$\left.\frac{Q_{b0}C_{stlb0}+\chi}{c_1+c_2K_1\,exp(K_3z)-K_1c_3\,exp(K_4z)}\right) + \left(\left(\frac{Q_{b0}*C_{atlb0}}{c_1+c_2K_1\,exp(K_3z)-K_1c_3\,exp(K_4z)} + \frac{1}{K_B} - \right.\right.$$

$$\left.\left.\left.\frac{Q_{b0}C_{stlb0}+\chi}{c_1+c_2K_1\,exp(K_3z)-K_1c_3\,exp(K_4z)}\right)^2 + \left(\frac{\frac{4}{K_B}*(Q_{b0}C_{stlb0}+\chi)}{c_1+c_2K_1\,exp(K_3z)-K_1c_3\,exp(K_4z)}\right)\right)^{\frac{1}{2}}\right) \quad \text{(Equation 2-142)}$$

Applying the symbolic Math Toolbox, we can verify that this form of the equation is the same as the original 4x4 system, except an anticipated sign change for $\chi$. This is shown in Figure 2-8.

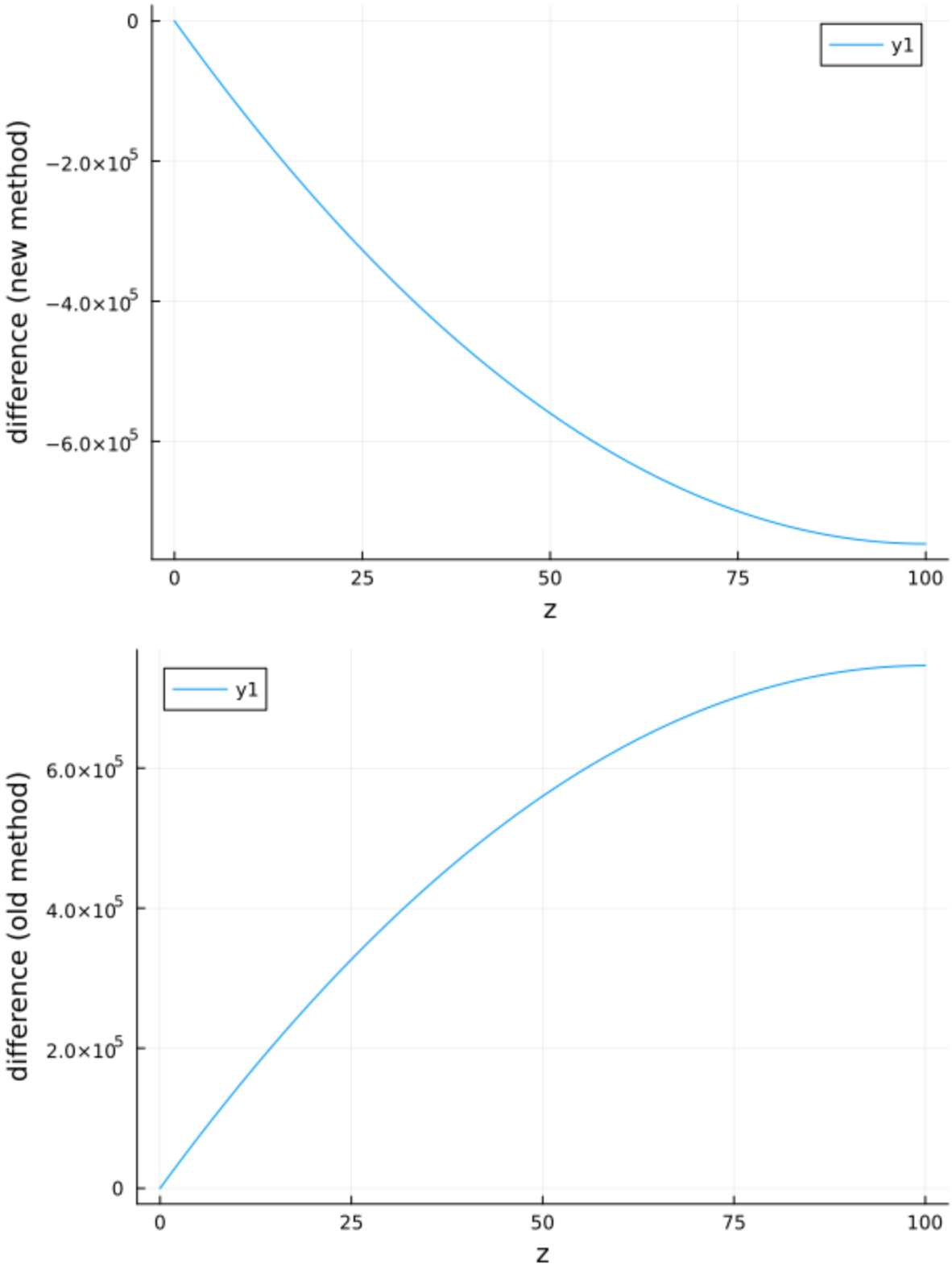


Figure 2-8: The new method (top) yields the same numerical outcome as the old method (bottom) for a stable test case.

The same reasoning applies to the backfiltration equation and to the purely diffusive equation:

$$\frac{\delta\chi}{\delta z} = \left(J_v(1-\sigma)f - \frac{K_{free}A}{L}\right) * (C_{sb} - C_{sd}) - J_v(1-\sigma)C_{sd} \text{ (Equation 2-143)}$$

$$\frac{\delta\chi}{\delta z} = -\frac{K_{free}A}{L}(C_{sb} - C_{sd}) \text{ (Equation 2-144)}$$

### 2.4.6 *Explicit Definition of the Jacobian*

#### 2.4.6.1 Ultrafiltration solution

Another method to improve stability is to provide the numerical solver with an explicitly defined Jacobian. Otherwise, numerically approximating the Jacobian may generate instability.

Now that we have reduced the system to a single equation, the Jacobian is: $\frac{\left(\frac{\delta\chi}{\delta z}\right)}{\delta\chi}$

Recall that:

$$\frac{\delta\chi}{\delta z} = \left(J_v(1-\sigma)f - \frac{K_{free}A}{L}\right) * (C_{sb} - C_{sd}) - J_v(1-\sigma)C_{sb} \text{ (Equation 2-145)}$$

Only the free toxin concentrations depend on $\chi$ so the Jacobian is as follows:

$$\frac{\left(\frac{\delta\chi}{\delta z}\right)}{\delta\chi} = \left(J_v(1-\sigma)f - \frac{K_{free}A}{L}\right) * \left(\frac{\delta C_{sb}}{\delta\chi} - \frac{\delta C_{sd}}{\delta\chi}\right) - J_v(1-\sigma) * \frac{\delta C_{sb}}{\delta\chi} \text{ (Equation 2-146)}$$

Solving for the $\frac{\delta C_{sb}}{\delta\chi}$ term:

$$\frac{\delta C_{sb}}{\delta\chi} = \frac{\delta}{\delta\chi}\left(\frac{-\left(Q_{b0} * \frac{C_{atlb0}}{Q_b} + \frac{1}{K_B} - \frac{Q_{b0}C_{stlb0}+\chi}{Q_b}\right) + \sqrt{\left(Q_{b0} * \frac{C_{atlb0}}{Q_b} + \frac{1}{K_B} - \frac{Q_{b0}C_{stlb0}+\chi}{Q_b}\right)^2 + \frac{4}{K_B}\left(\frac{Q_{b0}C_{stlb0}+\chi}{Q_b}\right)}}{2}\right) =$$

$$\frac{\delta}{\delta\chi}\left(\frac{\chi}{2Q_b}\right) + \frac{\delta}{\delta\chi}\left(\frac{1}{2}\sqrt{\left(Q_{b0} * \frac{C_{atlb0}}{Q_b} + \frac{1}{K_B} - \frac{Q_{b0}C_{stlb0}+\chi}{Q_b}\right)^2 + \frac{4}{K_B}\left(\frac{Q_{b0}C_{stlb0}+\chi}{Q_b}\right)}\right) \text{ (Equation 2-147)}$$

The solution proceeds as follows:

$$\frac{\delta C_{sb}}{\delta \chi} = \frac{1}{2Q_b} + \frac{1}{2}\left(\frac{\frac{\delta}{\delta \chi}\left(\left(Q_{b0}*\frac{C_{atlb0}}{Q_b}+\frac{1}{K_B}-\frac{Q_{b0}C_{stlb0}+\chi}{Q_b}\right)^2+\frac{4}{K_B}\left(\frac{Q_{b0}C_{stlb0}+\chi}{Q_b}\right)\right)}{2\sqrt{\left(Q_{b0}*\frac{C_{atlb0}}{Q_b}+\frac{1}{K_B}-\frac{Q_{b0}C_{stlb0}+\chi}{Q_b}\right)^2+\frac{4}{K_B}\left(\frac{Q_{b0}C_{stlb0}+\chi}{Q_b}\right)}}\right) = \frac{1}{4}*$$

$$\frac{2*\left(Q_{b0}*\frac{C_{atlb0}}{Q_b}+\frac{1}{K_B}-\frac{Q_{b0}C_{stlb0}+\chi}{Q_b}\right)*\frac{\delta}{\delta \chi}\left(\left(Q_{b0}*\frac{C_{atlb0}}{Q_b}+\frac{1}{K_B}-\frac{Q_{b0}C_{stlb0}+\chi}{Q_b}\right)\right)+\frac{4}{K_B}*\frac{\delta}{\delta \chi}\left(\frac{\chi}{Q_b}\right)}{\sqrt{\left(Q_{b0}*\frac{C_{atlb0}}{Q_b}+\frac{1}{K_B}-\frac{Q_{b0}C_{stlb0}+\chi}{Q_b}\right)^2+\frac{4}{K_B}\left(\frac{Q_{b0}C_{stlb0}+\chi}{Q_b}\right)}} \text{ (Equation 2-148)}$$

$$\frac{\delta C_{sb}}{\delta \chi} = \frac{1}{4} * \frac{2*\left(Q_{b0}*\frac{C_{atlb0}}{Q_b}+\frac{1}{K_B}-\frac{Q_{b0}C_{stlb0}+\chi}{Q_b}\right)*\frac{\delta}{\delta \chi}\left(\left(-\frac{Q_{b0}C_{stlb0}+\chi}{Q_b}\right)\right)+\frac{4}{Q_b K_B}}{\sqrt{\left(Q_{b0}*\frac{C_{atlb0}}{Q_b}+\frac{1}{K_B}-\frac{Q_{b0}C_{stlb0}+\chi}{Q_b}\right)^2+\frac{4}{K_B}\left(\frac{Q_{b0}C_{stlb0}+\chi}{Q_b}\right)}} = \frac{1}{4} *$$

$$\frac{2*\left(Q_{b0}*\frac{C_{atlb0}}{Q_b}+\frac{1}{K_B}-\frac{Q_{b0}C_{stlb0}+\chi}{Q_b}\right)*\left(-\frac{1}{Q_b}\right)+\frac{4}{Q_b K_B}}{\sqrt{\left(Q_{b0}*\frac{C_{atlb0}}{Q_b}+\frac{1}{K_B}-\frac{Q_{b0}C_{stlb0}+\chi}{Q_b}\right)^2+\frac{4}{K_B}\left(\frac{Q_{b0}C_{stlb0}+\chi}{Q_b}\right)}} \text{ (Equation 2-149)}$$

$$\frac{\delta C_{sb}}{\delta \chi} = \frac{\frac{1}{2}*\left(Q_{b0}*\frac{C_{atlb0}}{Q_b}+\frac{1}{K_B}-\frac{Q_{b0}C_{stlb0}+\chi}{Q_b}\right)*\left(-\frac{1}{Q_b}\right)+\frac{1}{Q_b K_B}}{\sqrt{\left(Q_{b0}*\frac{C_{atlb0}}{Q_b}+\frac{1}{K_B}-\frac{Q_{b0}C_{stlb0}+\chi}{Q_b}\right)^2+\frac{4}{K_B}\left(\frac{Q_{b0}C_{stlb0}+\chi}{Q_b}\right)}} \text{ (Equation 2-150)}$$

By the same reasoning we find $\frac{\delta C_{sd}}{\delta \chi}$:

$$\frac{\delta C_{sd}}{\delta \chi} = \frac{\frac{1}{2}*\left(Q_{d0}*\frac{C_{atld0}}{Q_d}+\frac{1}{K_B}-\frac{Q_{d0}C_{stld0}+\chi}{Q_d}\right)*\left(-\frac{1}{Q_d}\right)+\frac{1}{Q_d K_B}}{\sqrt{\left(Q_{d0}*\frac{C_{atld0}}{Q_d}+\frac{1}{K_B}-\frac{Q_{d0}C_{stld0}+\chi}{Q_d}\right)^2+\frac{4}{K_B}\left(\frac{Q_{d0}C_{stld0}+\chi}{Q_d}\right)}} \text{ (Equation 2-151)}$$

Thus, for the ultrafiltration system, the Jacobian is:

$$\frac{\left(\frac{\delta\chi}{\delta z}\right)}{\delta\chi} = \left(J_v(1-\sigma)f - \frac{K_{free}A}{L}\right) * \left( \frac{\frac{1}{2}*\left(Q_{b0}*\frac{C_{atlb0}}{Q_b}+\frac{1}{K_B}-\frac{Q_{b0}C_{stlb0}+\chi}{Q_b}\right)*\left(-\frac{1}{Q_b}\right)+\frac{1}{Q_bK_B}}{\sqrt{\left(Q_{b0}*\frac{C_{atlb0}}{Q_b}+\frac{1}{K_B}-\frac{Q_{b0}C_{stlb0}+\chi}{Q_b}\right)^2+\frac{4}{K_B}\left(\frac{Q_{b0}C_{stlb0}+\chi}{Q_b}\right)}} - \right.$$

$$\left. \frac{\frac{1}{2}*\left(Q_{d0}*\frac{C_{atld0}}{Q_d}+\frac{1}{K_B}-\frac{Q_{d0}C_{stld0}+\chi}{Q_d}\right)*\left(-\frac{1}{Q_d}\right)+\frac{1}{Q_dK_B}}{\sqrt{\left(Q_{d0}*\frac{C_{atld0}}{Q_d}+\frac{1}{K_B}-\frac{Q_{d0}C_{stld0}+\chi}{Q_d}\right)^2+\frac{4}{K_B}\left(\frac{Q_{d0}C_{stld0}+\chi}{Q_d}\right)}} \right) - J_v(1-\sigma) *$$

$$\frac{\frac{1}{2}*\left(Q_{b0}*\frac{C_{atlb0}}{Q_b}+\frac{1}{K_B}-\frac{Q_{b0}C_{stlb0}+\chi}{Q_b}\right)*\left(-\frac{1}{Q_b}\right)+\frac{1}{Q_bK_B}}{\sqrt{\left(Q_{b0}*\frac{C_{atlb0}}{Q_b}+\frac{1}{K_B}-\frac{Q_{b0}C_{stlb0}+\chi}{Q_b}\right)^2+\frac{4}{K_B}\left(\frac{Q_{b0}C_{stlb0}+\chi}{Q_b}\right)}} \quad \text{(Equation 2-152)}$$

Use of the symbolic math toolbox with a test parameter set confirms that this mathematical reasoning is correct. This is shown in Figure 2-9.

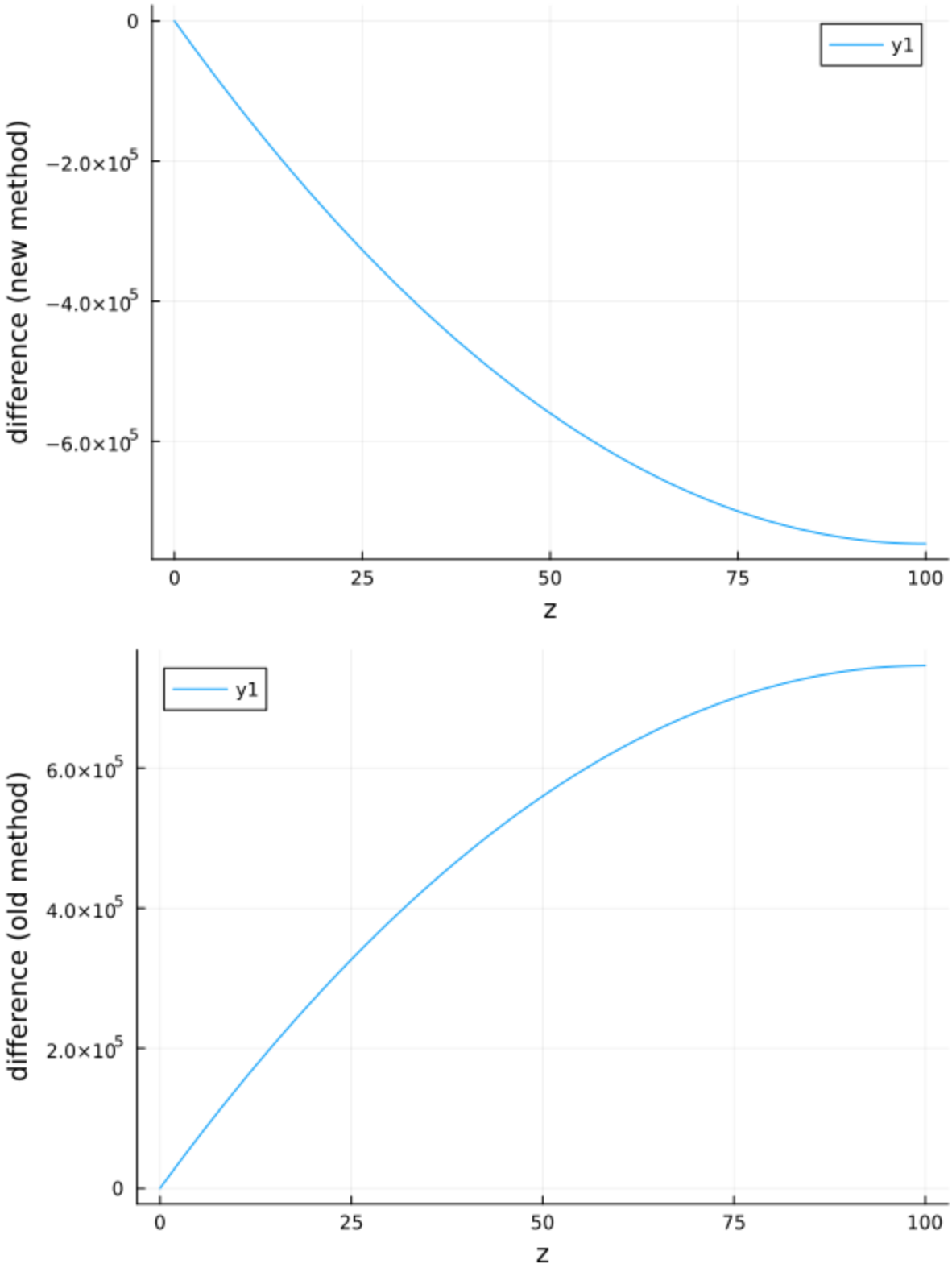


Figure 2-9: An integral solution to the Jacobian for toxin removal along a dialyzer membrane in the portion of the dialyzer where ultrafiltration takes place provides the same solution as the 4x4 system for a test parameter set.

2.4.6.2 Backfiltration solution

Applying the same reasoning to the backfiltration equation:

$$\frac{\delta\chi}{\delta z} = \left(J_v(1-\sigma)f - \frac{K_{free}A}{L}\right) * (C_{sb} - C_{sd}) - J_v(1-\sigma)C_{sd} \text{ (Equation 2-153)}$$

$$\frac{\left(\frac{\delta\chi}{\delta z}\right)}{\delta\chi} = \left(J_v(1-\sigma)f - \frac{K_{free}A}{L}\right) * \left( \frac{\frac{1}{2}*\left(Q_{b0}*\frac{C_{atlb0}}{Q_b}+\frac{1}{K_B}-\frac{Q_{b0}C_{stlb0}+\chi}{Q_b}\right)*\left(-\frac{1}{Q_b}\right)+\frac{1}{Q_bK_B}}{\sqrt{\left(Q_{b0}*\frac{C_{atlb0}}{Q_b}+\frac{1}{K_B}-\frac{Q_{b0}C_{stlb0}+\chi}{Q_b}\right)^2+\frac{4}{K_B}\left(\frac{Q_{b0}C_{stlb0}+\chi}{Q_b}\right)}} - \right.$$

$$\left. \frac{\frac{1}{2}*\left(Q_{d0}*\frac{C_{atld0}}{Q_d}+\frac{1}{K_B}-\frac{Q_{d0}C_{stld0}+\chi}{Q_d}\right)*\left(-\frac{1}{Q_d}\right)+\frac{1}{Q_dK_B}}{\sqrt{\left(Q_{d0}*\frac{C_{atld0}}{Q_d}+\frac{1}{K_B}-\frac{Q_{d0}C_{stld0}+\chi}{Q_d}\right)^2+\frac{4}{K_B}\left(\frac{Q_{d0}C_{stld0}+\chi}{Q_d}\right)}} \right) - J_v(1-\sigma) *$$

$$\frac{\frac{1}{2}*\left(Q_{d0}*\frac{C_{atld0}}{Q_d}+\frac{1}{K_B}-\frac{Q_{d0}C_{stld0}+\chi}{Q_d}\right)*\left(-\frac{1}{Q_d}\right)+\frac{1}{Q_dK_B}}{\sqrt{\left(Q_{d0}*\frac{C_{atld0}}{Q_d}+\frac{1}{K_B}-\frac{Q_{d0}C_{stld0}+\chi}{Q_d}\right)^2+\frac{4}{K_B}\left(\frac{Q_{d0}C_{stld0}+\chi}{Q_d}\right)}} \text{ (Equation 2-154)}$$

2.4.6.3 Diffusive solution

Applying the same reasoning to the purely diffusive system:

$$\frac{\left(\frac{\delta\chi}{\delta z}\right)}{\delta\chi} = -\frac{K_{free}A}{L}\left( \frac{\frac{1}{2}*\left(Q_{b0}*\frac{C_{atlb0}}{Q_b}+\frac{1}{K_B}-\frac{Q_{b0}C_{stlb0}+\chi}{Q_b}\right)*\left(-\frac{1}{Q_b}\right)+\frac{1}{Q_bK_B}}{\sqrt{\left(Q_{b0}*\frac{C_{atlb0}}{Q_b}+\frac{1}{K_B}-\frac{Q_{b0}C_{stlb0}+\chi}{Q_b}\right)^2+\frac{4}{K_B}\left(\frac{Q_{b0}C_{stlb0}+\chi}{Q_b}\right)}} - \right.$$

$$\left. \frac{\frac{1}{2}*\left(Q_{d0}*\frac{C_{atld0}}{Q_d}+\frac{1}{K_B}-\frac{Q_{d0}C_{stld0}+\chi}{Q_d}\right)*\left(-\frac{1}{Q_d}\right)+\frac{1}{Q_dK_B}}{\sqrt{\left(Q_{d0}*\frac{C_{atld0}}{Q_d}+\frac{1}{K_B}-\frac{Q_{d0}C_{stld0}+\chi}{Q_d}\right)^2+\frac{4}{K_B}\left(\frac{Q_{d0}C_{stld0}+\chi}{Q_d}\right)}} \right) \text{(Equation 2-155)}$$

The Jacobian was not sufficient to permit numerical stability for low dialysate flow rates (e.g. Qd = 5 mL/min).

## 2.4.7 *Gradient Function*

### 2.4.7.1 Ultrafiltration and backfiltration solutions

Certain numerical solvers such as Rodas5P can make use of an analytically defined gradient function $\frac{\left(\frac{\delta\chi}{\delta z}\right)}{\delta z}$ (168). Thus, we next derive an explicitly defined gradient function. For the ultrafiltration case:

$$\frac{\left(\frac{\delta\chi}{\delta z}\right)}{\delta z} = \frac{\delta}{\delta z}\left(\left(J_v(1-\sigma)f - \frac{K_{free}A}{L}\right) * (C_{sb} - C_{sd})\right) - \frac{\delta}{\delta z}(J_v(1-\sigma)C_{sb}) \text{ (Equation 2-156)}$$

Solving:

$$\frac{\left(\frac{\delta\chi}{\delta z}\right)}{\delta z} = \frac{\delta}{\delta z}\left(\left(J_v(1-\sigma)f - \frac{K_{free}A}{L}\right)\right)(C_{sb} - C_{sd}) + \left(J_v(1-\sigma)f - \frac{K_{free}A}{L}\right) * \frac{\delta}{\delta z}\big((C_{sb} - C_{sd})\big) - \left(\frac{\delta}{\delta z}\big(J_v(1-\sigma)\big)C_{sb} + J_v(1-\sigma) * \frac{\delta}{\delta z}(C_{sb})\right) \text{ (Equation 2-157)}$$

$$\frac{\delta}{\delta z}\left(\left(J_v(1-\sigma)f - \frac{K_{free}A}{L}\right)\right) = \frac{\delta}{\delta z}\left(\left(\left(\frac{-K_8(c_2\,exp(K_3z)+c_3\,exp(K_4z))}{-K_7(c_2\,exp(K_3z)+c_3\,exp(K_4z))}\right) + \frac{K_8(c_2\,exp(K_3z)+c_3\,exp(K_4z))}{exp\big(-K_7(c_2\,exp(K_3z)+c_3\,exp(K_4z))\big)-1}\right) - \frac{K_{free}A}{L}\right) \text{ (Equation 2-158)}$$

Applying the symbolic math toolbox of Matlab:

$$\frac{\delta}{\delta z}\left(\left(J_v(1-\sigma)f - \frac{K_{free}A}{L}\right)\right) = K_8 exp\big(K_7\big(c_2 exp(K_3z) + c_3 exp(K_4z)\big) + 1\big) * \big(c_2K_3 exp(K_3z) + c_3K_4 exp(K_4z)\big) + K_7K_8 exp\big(K_7\big(c_2 exp(K_3z) + c_3 exp(K_4z)\big) + 1\big) * \big(c_2K_3 exp(K_3z) + c_3K_4 exp(K_4 * z)\big)\big(c_2 exp(K_3z) + c_3 exp(K_4z)\big) \text{ (Equation 2-159)}$$

Next, considering the gradient of the free blood toxin concentration:

$$\frac{\delta}{\delta z}(C_{sb}) = \frac{\delta}{\delta z}\left(\frac{1}{2}\left(-\left(Q_{b0}\frac{C_{atlb0}}{c_1+c_2K_1\,exp(K_3z)-K_1c_3\,exp(K_4z)}+\frac{1}{K_B}-\frac{Q_{b0}C_{stlb0}+\chi}{c_1+c_2K_1\,exp(K_3z)-K_1c_3\,exp(K_4z)}\right)+\left(\left(\frac{Q_{b0}C_{atlb0}}{c_1+c_2K_1\,exp(K_3z)-K_1c_3\,exp(K_4z)}+\frac{1}{K_B}-\frac{Q_{b0}C_{stlb0}+\chi}{c_1+c_2K_1\,exp(K_3z)-K_1c_3\,exp(K_4z)}\right)^2+\frac{4}{K_B}\left(\frac{Q_{b0}C_{stlb0}+\chi}{c_1+c_2K_1\,exp(K_3z)-K_1c_3\,exp(K_4z)}\right)\right)^{\frac{1}{2}}\right)\right)$$ (Equation 2-160)

Applying the symbolic math toolbox:

$$\frac{\delta}{\delta z}(C_{sb}) = \left(2\left(\frac{\left((\chi+C_{stlb0}Q_{b0})\left(c_2K_1K_3exp(K_3z)-c_3K_1K_4exp(K_4z)\right)\right)}{\left(c_1+c_2K_1exp(K_3z)-c_3K_1exp(K_4z)\right)^2}-\frac{\left(C_{atlb0}Q_{b0}\left(c_2K_1K_3exp(K_3z)-c_3K_1K_4exp(K_4z)\right)\right)}{\left(c_1+c_2K_1exp(K_3z)-c_3K_1exp(K_4z)\right)^2}\right)*\left(\frac{1}{K_B}-\frac{(\chi+C_{stlb0}Q_{b0})}{c_1+c_2K_1exp(K_3z)-c_3K_1exp(K_4z)}+\frac{C_{atlb0}Q_{b0}}{c_1+c_2K_1exp(K_3z)-c_3K_1exp(K_4z)}\right)-\frac{\left(4(\chi+C_{stlb0}Q_{b0})\left(c_2K_1K_3exp(K_3z)-c_3K_1K_4exp(K_4z)\right)\right)}{k_B\left(c_1+c_2K_1exp(K_3z)-c_3K_1exp(K_4z)\right)^2}\right)*\frac{1}{4\left(\left(\frac{1}{K_B}-\frac{\chi+C_{stlb0}Q_{b0}}{c_1+c_2K_1exp(K_3z)-c_3K_1exp(K_4z)}+\frac{(C_{atlb0}Q_{b0})}{c_1+c_2K_1exp(K_3z)-c_3K_1exp(K_4z)}\right)^2+\frac{(4\chi+4C_{stlb0}Q_{b0})}{K_B(c_1+c_2K_1exp(K_3z)-c_3K_1exp(K_4z))}\right)^{\frac{1}{2}}}-\frac{\left((\chi+C_{stlb0}Q_{b0})\left(c_2K_1K_3exp(K_3z)-c_3K_1K_4exp(K_4z)\right)\right)}{2\left(c_1+c_2K_1exp(K_3z)-c_3K_1exp(K_4z)\right)^2}+\frac{\left(C_{atlb0}Q_{b0}\left(c_2K_1K_3exp(K_3z)-c_3K_1K_4exp(K_4z)\right)\right)}{2\left(c_1+c_2K_1exp(K_3z)-c_3K_1exp(K_4z)\right)^2}$$

(Equation 2-161)

When compared to the numeric derivative calculated by Matlab for a stable set of test values, this formula produces the correct values, as seen in Figure 2-10.

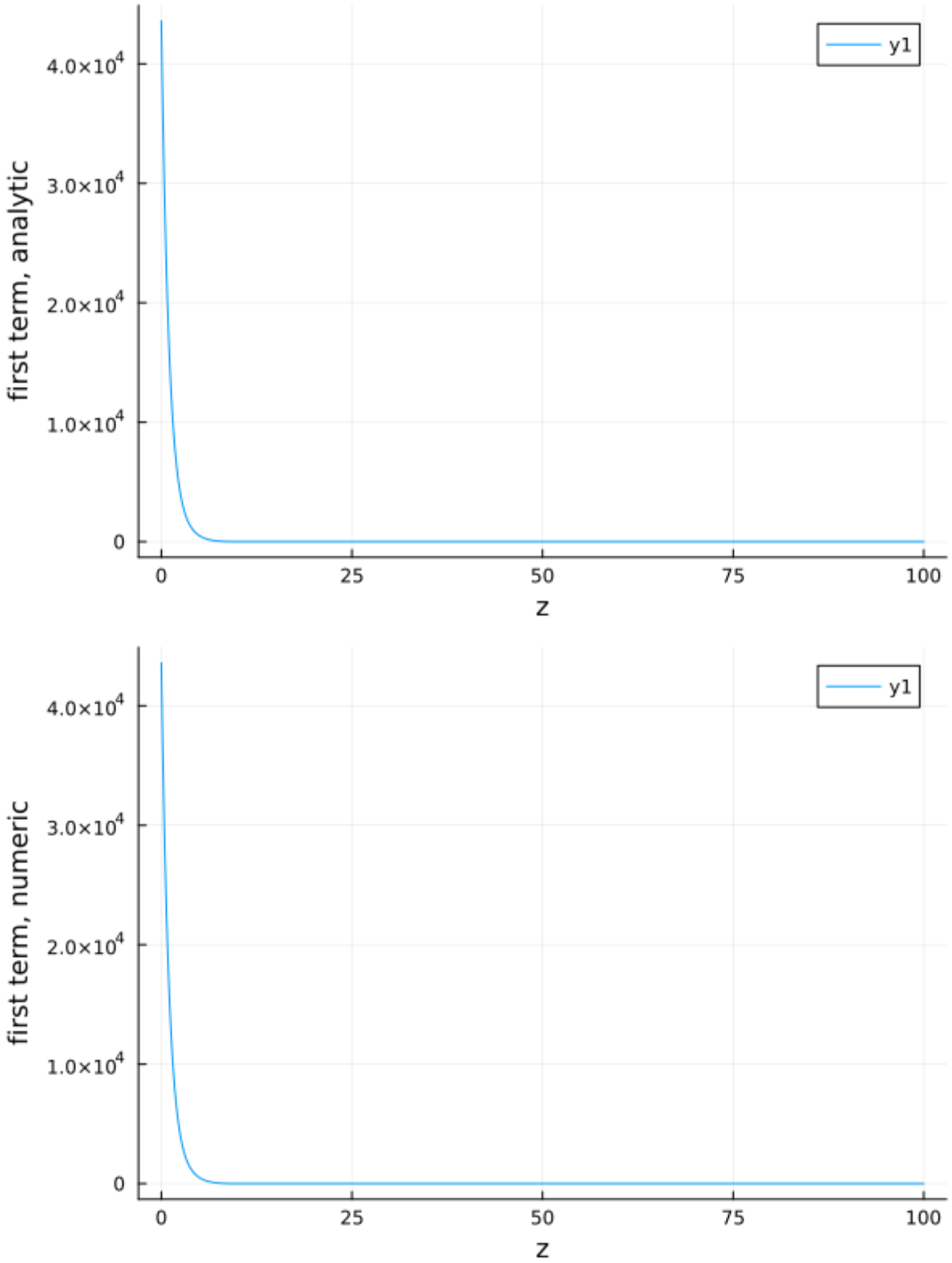


Figure 2-10: Analytic and numeric $\delta(C_{sb})/\ \delta z$ for a stable set of test values.

Next, we use the symbolic math toolbox to calculate $\frac{\delta}{\delta z}(C_{sd})$

$$\frac{\delta}{\delta z}(C_{sd}) = \frac{\delta}{\delta z}\left(\frac{1}{2} * \left(-\left(Q_{d0} * \frac{C_{atld0}}{-K_2c_1+c_2K_1\,exp(K_3z)-K_1c_3\,exp(K_4z)} + \frac{1}{K_B} - \frac{Q_{d0}C_{stld0}+\chi}{-K_2c_1+c_2K_1\,exp(K_3z)-K_1c_3\,exp(K_4z)}\right) + \left(\left(\frac{Q_{d0}C_{atld0}}{-K_2c_1+c_2K_1\,exp(K_3z)-K_1c_3\,exp(K_4z)} + \frac{1}{K_B} - \frac{Q_{d0}C_{stld0}+\chi}{-K_2c_1+c_2K_1\,exp(K_3z)-K_1c_3\,exp(K_4z)}\right)^2 + \frac{4}{K_B}\left(\frac{Q_{d0}C_{stld0}+\chi}{-K_2c_1+c_2K_1\,exp(K_3z)-K_1c_3\,exp(K_4z)}\right)\right)^{\frac{1}{2}}\right)\right)$$ (Equation 2-162)

Differentiates to:

$$\frac{\delta}{\delta z}(C_{sd}) = \left(2\left(\frac{\left((\chi + C_{stld0}Q_{d0})(c_2K_1K_3exp(K_3z)-c_3K_1K_4exp(K_4z))\right)}{(c_1K_2-c_2K_1exp(K_3z)+c_3K_1exp(K_4z))^2} - \frac{\left(C_{atld0}Q_{d0}(c_2K_1K_3exp(K_3z)-c_3K_1K_4exp(K_4z))\right)}{(c_1K_2-c_2K_1exp(K_3z)+c_3K_1exp(K_4z))^2}\right) * \left(\frac{1}{K_B} + \frac{\chi+C_{stld0}Q_{d0}}{c_1K_2-c_2K_1exp(K_3z)+c_3K_1exp(K_4z)} - \frac{C_{atld0}Q_{d0}}{c_1K_2 - c_2K_1exp(K_3z)+c_3K_1exp(K_4z)}\right) - \frac{\left(4(\chi+C_{stld0}Q_{d0})(c_2K_1K_3exp(K_3z)-c_3K_1K_4exp(K_4z))\right)}{K_B(c_1K_2-c_2\,K_1exp(K_3z)+\,c_3K_1exp(K_4z))^2}\right) * \left(4\left(\left(\frac{1}{K_B} + \frac{\chi + C_{stld0}*Q_{d0}}{c_1K_2-c_2K_1*exp(K_3z)+\,c_3K_1exp(K_4z)} - \frac{C_{atld0}Q_{d0}}{c_1K_2-c_2K_1exp(K_3z)+c_3K_1exp(K_4z)}\right)^2 - \frac{4\chi+4C_{stld0}Q_{d0}}{K_B(c_1K_2-c_2K_1exp(K_3z)+c_3K_1exp(K_4z))}\right)^{\frac{1}{2}}\right)^{-1} - \frac{\left((\chi+C_{stld0}Q_{d0})(c_2K_1K_3exp(K_3z)-c_3K_1K_4exp(K_4z))\right)}{2(c_1K_2-c_2K_1exp(K_3z)+c_3K_1exp(K_4z))^2} + \frac{\left(C_{atld0}Q_{d0}(c_2K_1K_3exp(K_3z)-c_3K_1K_4exp(K_4z))\right)}{2(c_1K_2\,-c_2K_1exp(K_3z)+c_3K_1exp(K_4z))^2}$$ (Equation 2-163)

Compared to a numeric solution for a stable test case, this analytic solution matches (Figure 2-11).

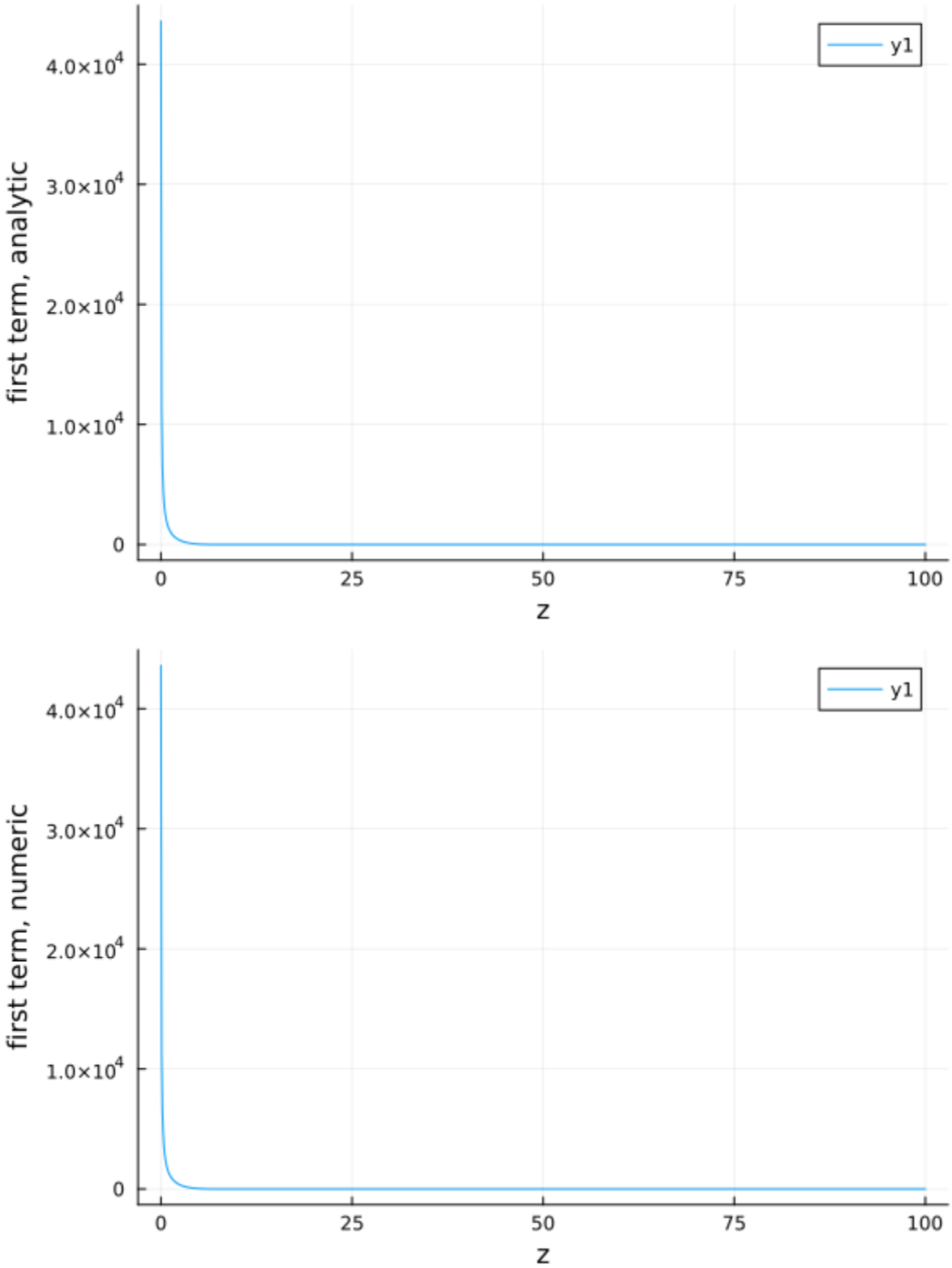


Figure 2-11: Analytic and numeric $\delta(C_{sd})/\ \delta z$ for a stable set of test values.

The final term in the gradient of the ultrafiltration solution is as follows:

$$\frac{\delta}{\delta z}(J_v(1-\sigma)C_{sb}) = \frac{\delta}{\delta z}\left(J_v(1-\sigma)\right) * C_{sb} + J_v(1-\sigma) * \frac{\delta}{\delta z}(C_{sb})$$ (Equation 2-164)

Completing the calculation for the two terms yields the following:

$$J_v(1-\sigma) = K_8(c_2\, exp(K_3 z) + c_3\, exp(K_4 z))$$ (Equation 2-165)

$$\frac{\delta(J_v(1-\sigma))}{\delta z} = K_8(c_2 K_3\, exp(K_3 z) + c_3 K_4\, exp(K_4 z))$$ (Equation 2-166)

The backfiltration solution can be solved with the same building blocks.

#### 2.4.7.2 Diffusive solution

Recall that the diffusive equation consists of:

$$\frac{\delta\chi}{\delta z} = -\frac{K_{free}A}{L}(C_{sb} - C_{sd})$$ (Equation 2-167)

Differentiating yields this formula, to which the previous building blocks can be applied.

$$\frac{\left(\frac{\delta\chi}{\delta z}\right)}{\delta z} = -\frac{K_{free}A}{L}\left(\frac{\delta C_{sb}}{\delta z} - \frac{\delta C_{sd}}{\delta z}\right)$$ (Equation 2-168)

Unfortunately, on its own, adding an explicitly defined gradient did not stabilize the system for all conditions, especially low dialysate side flow rates.

### 2.4.8 *Modified Shooting Method*

The next innovation was to replace the Regula Falsi method with a modified shooting method, in order to improve the algorithm's tolerance for instability. This algorithm is the subject of the provisional patent application "COMPUTATIONAL MODEL OF SORBENT DIALYSIS - [IP: 50020.01US1]". This work was facilitated through the use of advanced computational, storage, and networking infrastructure provided by the Hyak supercomputer system and funded by the Student Technology Fee (STF) at the University of Washington.

A shooting method solves a boundary value problem (BVP) by solving a series of initial value problems (IVPs) which are numerically tractable. One variable is known at the starting boundary. For example, this could be dialysate toxin concentration at the dialysate inlet. The

other variable (blood toxin concentration) is unknown. The variable $\chi$ (amount removed from blood) is zero at the blood inlet and unknown at the dialysate inlet. Guesses for the unknown value are made within a reasonable parameter range until the known value is obtained as the solution to the IVP. Figure 2-12 shows an example of the normal shooting method workflow. This figure was created with BioRender.

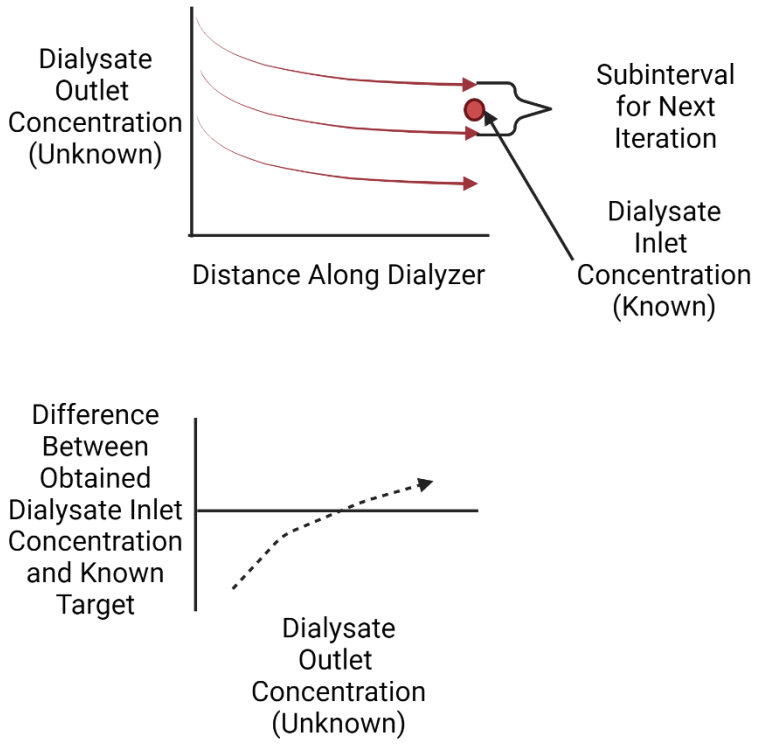


Figure 2-12: An illustration of a traditional shooting method (top) and what a search space with no instability would look like (bottom). Figure created with BioRender.

Unmodified, a shooting method is inefficient because the plausible parameter space is very large and small steps must be taken. Traditional methods of increasing efficiency such as Regula Falsi or Newton's Method cannot cope with numerical instability due to stiffness. The analytical solution should only have one value of $\chi(z = L)$ that corresponds to $\chi = 0$ at $z = 0$ (a zero-crossing). However, numerical instability causes multiple zero crossings, some of which are spurious. The modified shooting method uses predictable patterns in this system of equations to

improve efficiency. Our improvements to the shooting method make use of predictable patterns in this system of equations to allow rapid solutions, to provide clinicians with dosing recommendations in a timely manner.

Figure 2-13 shows an example of the problem we seek to solve. For individual initial conditions (e.g. dialysate outlet concentrations), the system produces final values that are below the known dialysate inlet concentration, above the known dialysate inlet concentration, within the tolerance of the known dialysate inlet concentration, or unstable (reflecting, for example, an error during the numerical solution). The analytical solution should only have one zero crossing, where a single value of dialysate outlet concentration corresponds to the target dialysate inlet concentration. However, numerical instability causes multiple zero crossings, some of which are spurious.

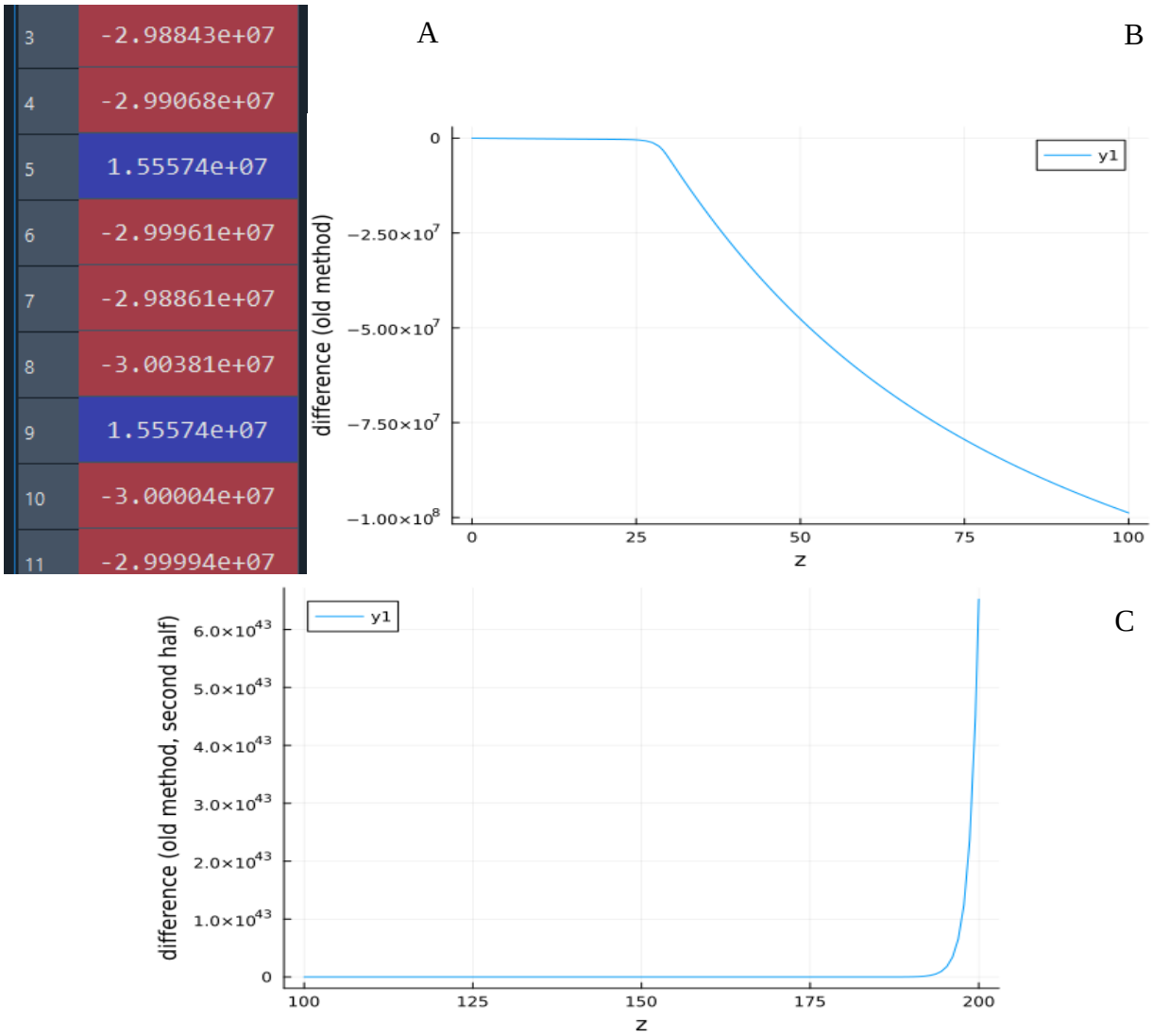


Figure 2-13: **A**: An example of the final states (predicted dialysate inlet concentrations) for a set of dialysate outlet concentrations. The solutions include multiple spurious zero crossing events and instability, meaning Newton's Method or Regula Falsi would not converge. **B**: An example of a highly unstable numerical solution for the ultrafiltration portion of the dialyzer. **C**: The same highly unstable numerical solution once it enters the backfiltration regime.

To solve this problem, we divide intervals into 9 types and prioritize them. We design the algorithm to implement a breadth first search of high priority intervals to avoid long delays from spurious zero crossings.

Table 2-3 summarizes the interval types and the associated actions. Figure 2-14 shows each of the nine interval types containing the target concentration.

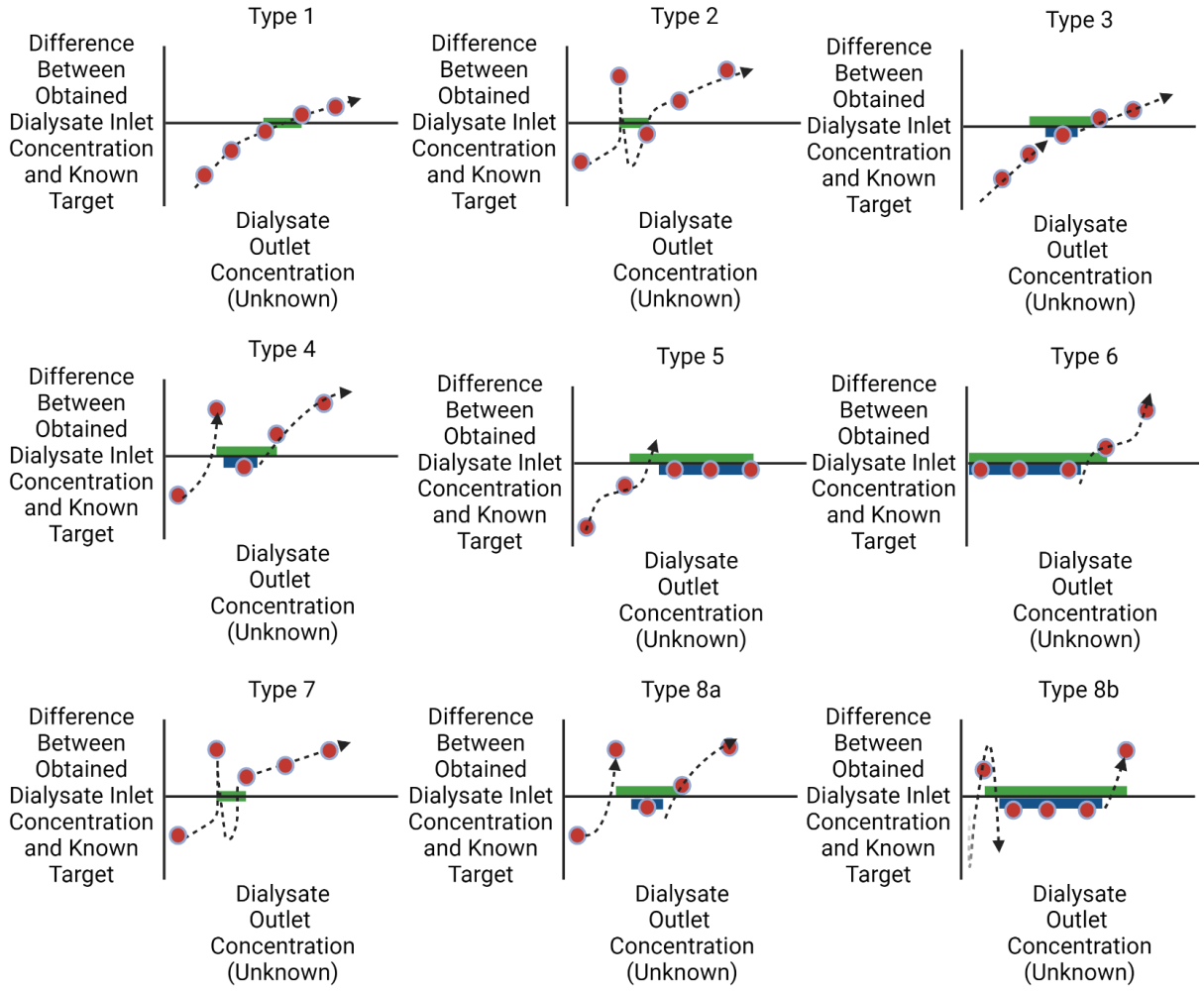


Figure 2-14: Each interval type containing the true zero. Red dots represent sampled conditions (since not all values of the dialysate outlet concentration are sampled). Blue rectangles represent unstable areas. The green rectangle represents the correct target subinterval. Figure created with BioRender.

Table 2-3: Interval types for modified shooting method

| Interval Type | Action |
|---|---|
| Type 1: Negative to Positive Transition | Consider as high priority for further searching |
| Type 2: Positive to Negative Transition | Same as Type 1 |
| Type 3: Negative to Positive with Unstable Values in Between | Consider as Low Priority. Search only after high priority intervals have been searched. Use a smaller step with more subintervals to search for stable subintervals. Once a subinterval is found, proceed as if Type 1. |
| Type 4: Positive to Negative with Unstable Values in Between | Same as Type 3 |
| Type 5: Negative to Unstable, with no Positives After It | Same as Type 3 |
| Type 6: Unstable with no Negatives Before It to Positive | Same as Type 3 |
| Type 7: Positive to Smaller Positive | Same as Type 1 (without instability, dialysate inlet concentration would increase whenever dialysate outlet concentration increases, with all other parameters held constant. Thus, this indicates instability and potentially zero crossings in the subintervals) |
| Type 8a: Positive to smaller positive with instability in between that doesn't encompass the entire interval | Same as Type 1 |
| Type 8b: Positive to smaller positive with instability in between that encompasses the entire interval | Same as Type 3 (to avoid an infinite loop) |

Once intervals in a range of initial conditions are identified they are queued. High priority intervals are processed before low priority intervals (Table 2-3). Within each category, intervals

are sorted by the distance from their bounds to the target. All initial conditions are tested, and the initial conditions whose bounds are closest to the target are selected. High priority intervals are searched with a larger step size (since they contain no or limited instability) while low priority intervals, if searched, are searched with a smaller step size to ensure small "islands of numerical stability" near the true zero are not missed. A breadth first search for the high priority intervals is implemented: Up to 13 intervals are searched sequentially before new intervals are queued. This minimizes wasted computational resources wasted on searching spurious intervals. Figure 2-15 shows an example of this process. Figure 2-16 shows a diagram.

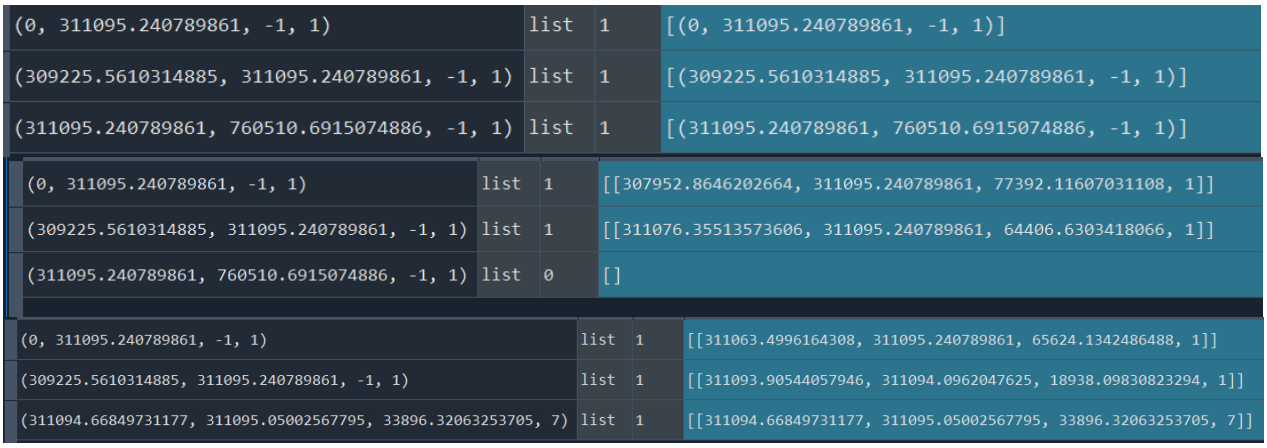


Figure 2-15: An example of the breadth first search process. On the first step, three intervals are chosen related to the predicted value of the dialysate final toxin concentration. On the second step, two of the intervals yield subintervals and one does not. On the third step, three subintervals are identified from the two intervals from step two, and the new subinterval is immediately searched.

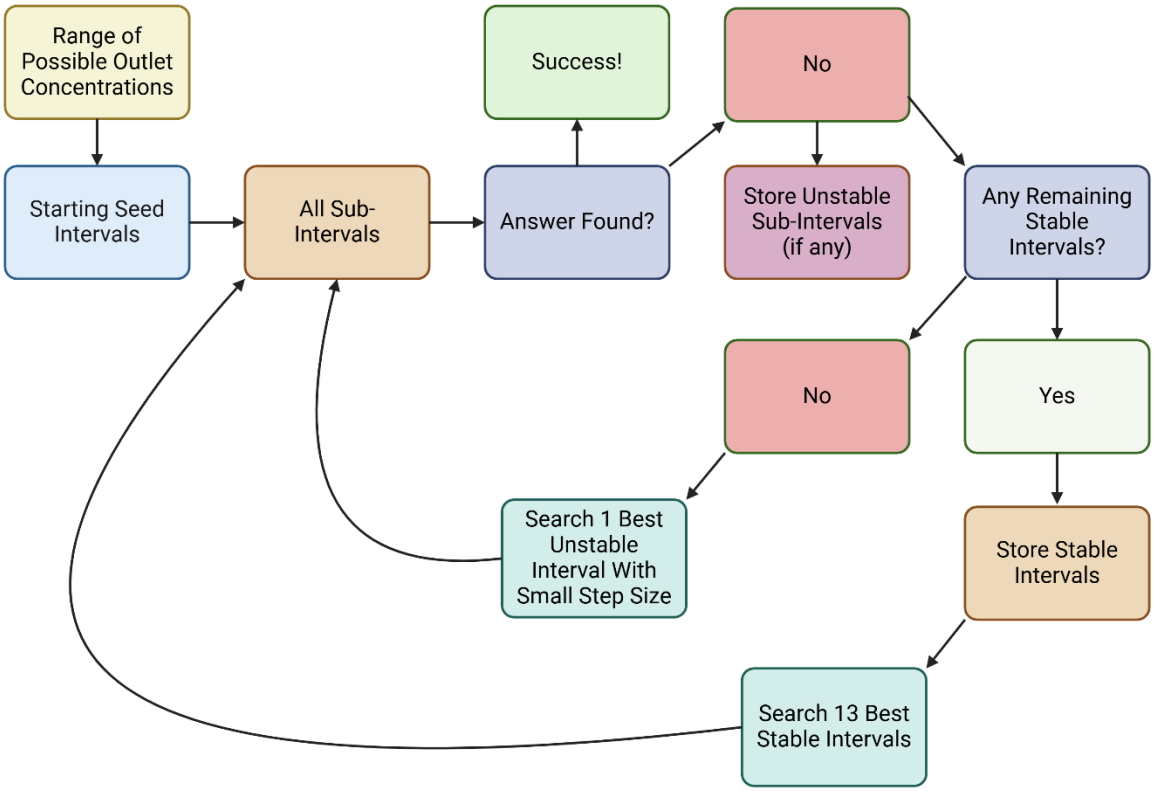


Figure 2-16: Flow Chart of the Interval Search Process. Figure created with BioRender.

This implementation allowed stable solutions for a wider range of conditions, including 5 mL/min, but the model remains unstable if the dialysate flow rate is set to 2 mL/min.

### 2.4.9 *Modification to Iterate from z = L at Dialysate Inlet/Blood Outlet Instead of z =0 at Blood Inlet/Dialysate Outlet*

The strategy which achieved convergence for $Q_d$ = 2 mL/min and lower dialysate side flow rates was to begin the iteration from z = L, at the blood outlet and dialysate inlet. This means both $C_{stlb}$ and $C_{stld}$ are smaller, leading to smaller values of the Jacobian. Stiffness is driven by large real eigenvalue components, so this proved to be the most successful stiffness minimization technique. It permitted analysis for dialysate flow rates as low as 1.5 mL/min. The dialysate toxin concentration can be redefined as:

$$C_{stld} = \frac{(Q_{d,0}C_{stld,z=L} - x_{y0} + \chi)}{Q_d} \quad \text{(Equation 2-169)}$$

$\chi$ is still the amount removed from blood at distance z across the dialyzer. $x_{y0}$ is a negative number defined as follows:

$$x_{y0} = C_{stld,z=L} * Q_{d,0} - C_{stld,0} * Q_{d,0} = C_{stlb,z=L} * Q_{b,0} - C_{stlb,0} * Q_{b,0}$$ (Equation 2-170, Amount removed in one session)

This is the difference between the blood and dialysate side toxin amounts at z = 0. This comes from the shooting method, because the guesses are different values of $C_{stld,0}$. $C_{stld,end}$ is dialysate inlet concentration, which is known. This can be contrasted with the previous definition of $C_{stld}$ as:

$$C_{stld,previous} = \frac{Q_{d0}C_{stld0}+\chi}{Q_d}$$ (Equation 2-171)

The strength of the new definition is that, if the initial value problem is started from z = L, the following initial condition becomes available:

$$\chi(z = L) = x_{y0}$$ (Equation 2-172)

As the solution proceeds towards z = 0, instead of increasing in magnitude, the absolute value of $\chi$ shrinks, reaching within tolerance of zero at the correct guess for $x_{yo}$. The modified governing equations for the system are:

For $J_v > 0$

$$\frac{\delta\chi}{\delta z} = \left(\left(\frac{K_8(c_2\,exp(K_3z)+c_3\,exp(K_4z))}{K_7(c_2\,exp(K_3z)+c_3\,exp(K_4z))} + \frac{K_8(c_2\,exp(K_3z)+c_3\,exp(K_4z))}{exp\left(-K_7(c_2\,exp(K_3z)+c_3\,exp(K_4z))\right)-1}\right) - \frac{K_{free}A}{L}\right) * \frac{1}{2} *$$

$$\left(\sqrt{\left(\frac{Q_{bo}C_{atlbo}}{c_1+c_2K_1\,exp(K_3z)-K_1c_3\,exp(K_4z)} + \frac{1}{K_B} - \frac{Q_{bo}C_{stlbo}+\chi}{c_1+c_2K_1\,exp(K_3z)-K_1c_3\,exp(K_4z)}\right)^2 + \left(\frac{\frac{4}{K_B}(Q_{bo}C_{stlbo}+\chi)}{c_1+c_2K_1\,exp(K_3z)-K_1c_3\,exp(K_4z)}\right)} - \right.$$

$$\left(\frac{Q_{bo}C_{atlbo}}{c_1+c_2K_1\,exp(K_3z)-K_1c_3\,exp(K_4z)} + \frac{1}{K_B} - \frac{Q_{bo}C_{stlbo}+\chi}{c_1+c_2K_1\,exp(K_3z)-K_1c_3\,exp(K_4z)}\right) -$$

$$\left(\sqrt{\left(\frac{Q_{do}C_{atldo}}{c_2K_1\,exp(K_3z)-K_2c_1-K_1c_3\,exp(K_4z)} + \frac{1}{K_B} - \frac{Q_{do}C_{stld,end}-x_{yo}+\chi}{c_2K_1\,exp(K_3z)-K_2c_1-K_1c_3\,exp(K_4z)}\right)^2 + \left(\frac{\frac{4}{K_B}\left(Q_{do}C_{stld,end}-x_{yo}+\chi\right)}{c_2K_1\,exp(K_3z)-K_2c_1-K_1c_3\,exp(K_4z)}\right)} - \right.$$

$$\left.\left.\left(\frac{Q_{do}C_{atldo}}{c_2K_1\,exp(K_3z)-K_2c_1-K_1c_3\,exp(K_4z)} + \frac{1}{K_B} - \frac{Q_{do}C_{stld,end}-x_{yo}+\chi}{c_2K_1\,exp(K_3z)-K_2c_1-K_1c_3\,exp(K_4z)}\right)\right)\right) + \frac{K_8(c_2\,exp(K_3z)+c_3\,exp(K_4z))}{2} *$$

$$\left(\sqrt{\left(\frac{Q_{bo}C_{atlbo}}{c_1+c_2K_1\,exp(K_3z)-K_1c_3\,exp(K_4z)} + \frac{1}{K_B} - \frac{Q_{bo}C_{stlbo}+\chi}{c_1+c_2K_1\,exp(K_3z)-K_1c_3\,exp(K_4z)}\right)^2 + \left(\frac{\frac{4}{K_B}(Q_{bo}C_{stlbo}+\chi)}{c_1+c_2K_1\,exp(K_3z)-K_1c_3\,exp(K_4z)}\right)} - \right.$$

$$\left.\left(\frac{Q_{bo}C_{atlbo}}{c_1+c_2K_1\,exp(K_3z)-K_1c_3\,exp(K_4z)} + \frac{1}{K_B} - \frac{Q_{bo}C_{stlbo}+\chi}{c_1+c_2K_1\,exp(K_3z)-K_1c_3\,exp(K_4z)}\right)\right) \quad \text{(Equation 2-173)}$$

For $J_v < 0$

$$\frac{\delta\chi}{\delta z} = \left(\left(\frac{K_8(c_2\,exp(K_3z)+c_3\,exp(K_4z))}{K_7(c_2\,exp(K_3z)+c_3\,exp(K_4z))} + \frac{K_8(c_2\,exp(K_3z)+c_3\,exp(K_4z))}{exp\left(-K_7(c_2\,exp(K_3z)+c_3\,exp(K_4z))\right)-1}\right) - \frac{K_{free}A}{L}\right) * \frac{1}{2} *$$

$$\left(\sqrt{\left(\frac{Q_{b0}C_{atlb0}}{c_1+c_2K_1\,exp(K_3z)-K_1c_3\,exp(K_4z)} + \frac{1}{K_B} - \frac{Q_{b0}C_{stlb0}+\chi}{c_1+c_2K_1\,exp(K_3z)-K_1c_3\,exp(K_4z)}\right)^2 + \frac{\frac{4}{K_B}*(Q_{b0}C_{stlb0}+\chi)}{c_1+c_2K_1\,exp(K_3z)-K_1c_3\,exp(K_4z)}} - \right.$$

$$\left(\frac{Q_{b0}C_{atlb0}}{c_1+c_2K_1\,exp(K_3z)-K_1c_3\,exp(K_4z)} + \frac{1}{K_B} - \frac{Q_{b0}C_{stlb0}+\chi}{c_1+c_2K_1\,exp(K_3z)-K_1c_3\,exp(K_4z)}\right) -$$

$$\left(\sqrt{\left(\frac{Q_{d0}C_{atld0}}{c_2K_1\,exp(K_3z)-K_2c_1-K_1c_3\,exp(K_4z)} + \frac{1}{K_B} - \frac{Q_{d0}C_{stld,end}-x_{y0}+\chi}{c_2K_1\,exp(K_3z)-K_2c_1-K_1c_3\,exp(K_4z)}\right)^2 + \left(\frac{\frac{4}{K_B}\left(Q_{d0}C_{stld,end}-x_{y0}+\chi\right)}{c_2K_1\,exp(K_3z)-K_2c_1-K_1c_3\,exp(K_4z)}\right)} - \right.$$

$$\left.\left.\left(\frac{Q_{d0}C_{atld0}}{c_2K_1\,exp(K_3z)-K_2c_1-K_1c_3\,exp(K_4z)} + \frac{1}{K_B} - \frac{Q_{d0}C_{stld,end}-x_{y0}+\chi}{c_2K_1\,exp(K_3z)-K_2c_1-K_1c_3\,exp(K_4z)}\right)\right)\right) + \frac{K_8(c_2\,exp(K_3z)+c_3\,exp(K_4z))}{2} *$$

$$\left(\sqrt{\left(\frac{Q_{d0}C_{atld0}}{c_2K_1\,exp(K_3z)-K_2c_1-K_1c_3\,exp(K_4z)} + \frac{1}{K_B} - \frac{Q_{d0}C_{stld,end}-x_{y0}+\chi}{c_2K_1\,exp(K_3z)-K_2c_1-K_1c_3\,exp(K_4z)}\right)^2 + \left(\frac{\frac{4}{K_B}\left(Q_{d0}C_{stld,end}-x_{y0}+\chi\right)}{c_2K_1\,exp(K_3z)-K_2c_1-K_1c_3\,exp(K_4z)}\right)} - \right.$$

$$\left.\left(\frac{Q_{d0}C_{atld0}}{c_2K_1\,exp(K_3z)-K_2c_1-K_1c_3\,exp(K_4z)} + \frac{1}{K_B} - \frac{Q_{d0}C_{stld,end}-x_{y0}+\chi}{c_2K_1\,exp(K_3z)-K_2c_1-K_1c_3\,exp(K_4z)}\right)\right) \text{(Equation 2-174)}$$

## 2.5 Model Implementation

The model was implemented using Julia Version 1.9.3 (169) with the packages Revise.jl, XLSX.jl, DifferentialEquations.jl (170), FileIO, JLD2, ODEInterfaceDiffEq (170), ODEInterface (170), NonlinearSolve (171), NLSolve (172), LinearAlgebra, and Roots (173). We used the Julia function linspace provided by Jonathan Bieler (174). We used the Julia remove function provided by Michael Franco (175). We used the myfind Julia function (176). The radau solver was used for the spatial solution (177). The built-in solver selection algorithm of DifferentialEquations.jl was used for the temporal differential equation solution (178). Parameter sweeps were conducted on the University of Washington's Hyak Supercomputer. This computer uses the Rocky 8 operating system and the slurm scheduler. Individual nodes have 28 threads and 192 GB of memory.

# Chapter 3. TOXIN SELECTION AND ASSAY DEVELOPMENT

## 3.1 Selection of Toxins of Interest

We selected five representative protein bound toxins for benchtop testing: bilirubin, cholic acid, indoxyl sulfate, copper, and manganese. Each of these toxins binds to albumin at different binding sites and is involved in one or more human diseases. Creatinine was also included in the test solution, initially intended as a fully water soluble toxin control. Our investigation and further literature search identified that it was also albumin-bound.

Bilirubin is a yellow pigment produced as the result of the breakdown of hemoglobin heme groups during the recycling of old red blood cells or the cycling of heme-containing proteins (179). Bilirubin binds to albumin at three binding sites that are distinct from the binding sites of other toxins (180). The primary binding site has an affinity two orders of magnitude greater than the

secondary binding sites. Most bilirubin in blood is carried on albumin, though some binds to lipoproteins. Bilirubin is taken up by hepatocytes in the liver through passive diffusion and active transport. In hepatocytes, bilirubin is conjugated with glucuronic acid. This increases solubility, forming the soluble “direct bilirubin”. In liver failure, the unconjugated bilirubin is significant because it cannot be removed via urinary excretion. Bilirubin is an easily measurable marker for liver function. It is also toxic, leading to white matter damage, edema and coma at very high concentrations (181). In healthy people bilirubin levels are 0.1-1.2 mg/dL (182). In liver failure concentrations can reach 20 mg/dL or greater (183,184).

Cholic acid is a bile salt synthesized from cholesterol in the liver (185). In health, bile salts have an important function in the formation of micelles in bile, which allow the excretion of lipid waste. Bile acids, including cholic acid, are then conjugated with sugars by gut bacteria, and reabsorbed into the blood (186,187). Cholic acid levels become elevated during bile duct blockage (cholestasis) and intestinal blockage (stagnant loop syndrome). Elevated bile acid concentrations lead to liver cell death and are associated with pruritus (23). Cholic acid binds to Sudlow Site I on albumin (188). In health unconjugated cholic acid concentrations are approximately 0.04 µM (189). The highest disease concentration reported in the literature we identified was 19.3 µM in stagnant loop syndrome (190).

Indoxyl sulfate is a product of tryptophan metabolism. It is elevated in renal failure, and predicts vascular pathology and death in dialysis patients (19). Some (24), but not all (25), studies link it to pruritus in dialysis patients. It binds to Sudlow Site II on albumin (191). In healthy patients the concentration is approximately 0.113 mg/dL, but in disease it can rise as high as 4 mg/dL (19).

Copper, acquired from food or environmental exposure, is elevated in some (192), but not all (193), liver failure patients, and in inborn errors of metabolism like Wilson’s disease (30).

Excess copper causes inflammation, liver toxicity, iron deficiency, and ulcers (194). In healthy individuals, copper in the blood is 80% bound to ceruloplasmin, with the rest binding to albumin and free histidine (192,195). It binds to the N-terminal zinc binding site on albumin (196). ATPase ATP7B transports copper onto blood ceruloplasmin and enables secretion into bile (29). In healthy individuals, copper plasma concentrations are approximately 13.09 μM (197). In liver failure plasma concentrations can rise to 21.56 μM. In Wilson's disease total blood copper can be lower than in healthy individuals. Copper accumulates in tissues, but more of this copper is exchangeable and loosely bound to albumin, instead of being sequestered on ceruloplasmin (30). The lack of ceruloplasmin-bound copper may lead to lower overall blood copper, while at the same time a greater fraction of exchangeable copper is present.

Manganese, also acquired from environmental or dietary pathways, is elevated in liver failure (197), occupational exposures (194), and inborn errors of metabolism (33). It is transported in blood on Cadmium Site B of Human Serum Albumin (196). The SLC30A10 (solute carrier family 30, member 10) transporter enables its removal (34). If manganese accumulates in excess, neurological symptoms ensue (33,198). In healthy people plasma concentration is 0.02 μM (197). In liver failure concentration can rise to 2.5 μM.

Creatinine is a water-soluble toxin, which is a product of protein metabolism, derived from creatine (199). It is a common marker for renal failure. In healthy people, creatinine levels are 0.5-1.2 mg/dL (200). In disease, creatinine concentration can reach 15 mg/dL or greater (201). Despite being commonly cited as a water-soluble toxin and readily dialyzable, creatinine binds to human serum albumin at Sudlow Site I with a binding affinity of 8.92E4 (1/M) at pH 7 (202). This may confound analysis for cholic acid.

## 3.2 Analysis Strategy Overview

Bilirubin, albumin, and creatinine were measured using standard spectrophotometric reagents on the AU680 clinical chemistry analyzer (Beckman Coulter). Cholic Acid and Indoxyl Sulfate were measured using mass spectrometry on a 1525u LC-Quattro Micro quadrupole tandem mass spectrometer (MS), manufactured by Waters Corp, Milford, MA. Manganese and copper were measured using inductively coupled plasma mass spectrometry (ICP-MS) on an iCap RQ Quadrupole ICP-MS (Thermo-Fisher Scientific).

## 3.3 Reagents

97% pure bilirubin (Alfa Aeser, A17522). 98% pure Bovine Serum Albumin (BSA) from Millipore Sigma (A7906). 98% pure indoxyl sulfate from Millipore Sigma (I3875). 98% pure cholic acid from Millipore Sigma (C1129). 99.99% pure manganese chloride (Millipore Sigma, 203734). 99.0% pure copper chloride (Millipore Sigma, 307483). 98% pure creatinine (Millipore Sigma, C4255). 1 Norm hydrochloric acid (Fisher Chemical, SA48). 1 Norm sodium hydroxide (Titristar, SX0607H-6). 99.9% Anhydrous sodium carbonate (Millipore Sigma, 1063920500). 99.9% pure Dimethylsulfoxide (DMSO) (Millipore Sigma, MX1458-6).

Dialysate was made by mixing the Bicarbonate Concentrate (Centrisol MB-330-L, Minntech) with Acid Concentrate (NaturaLyte 08-3301-2, Fresenius) according to the instructions on the packaging. Bilirubin measurement reagent was from Beckman Coulter (OSR6112). Albumin measurement reagent was from Beckman Coulter (OSR6102). Creatinine measurement reagent was from Beckman Coulter (OSR6178). Bicarbonate measurement reagent was from Beckman Coulter (OSR6237). Dextrose was from Fisher Scientific (D16-3). Saline was from

Baxter (2B1324). Glutaraldehyde was from Sigma-Aldrich (G6403-500ML). Sodium hypochlorite was from Sigma-Aldrich (239305-500ML).

## 3.4 AU680 BILIRUBIN

The AU680 spectrophotometric assay for bilirubin is designed for serum, so we needed to verify that the assay is effective in dialysate with BSA. It is based on the diazonium salt method. 3,5-dichlorophenyldizonium tetrafluoroborate (DPD) reacts with bilirubin, forming azobilirubin. The assay detects the wavelengths 570/660 nm. Our range of concentrations of interest is between 20 mg/dL (a clinically relevant toxic concentration (183)) and 1.2 mg/dL (the maximum normal adult bilirubin concentration (182)). As designed, the assay has a blank and a color reagent. We modified the assay so the blank is not used. This produces better results for low concentrations in dialysate (Figure 3-1). The 0 mg/dL negative control samples are excluded from standard curve calculations because the first standard (0.75 mg/dL) cannot be reliably distinguished from the negative control, meaning that in dialysate, 0 mg/dL is outside the linear range of this assay.

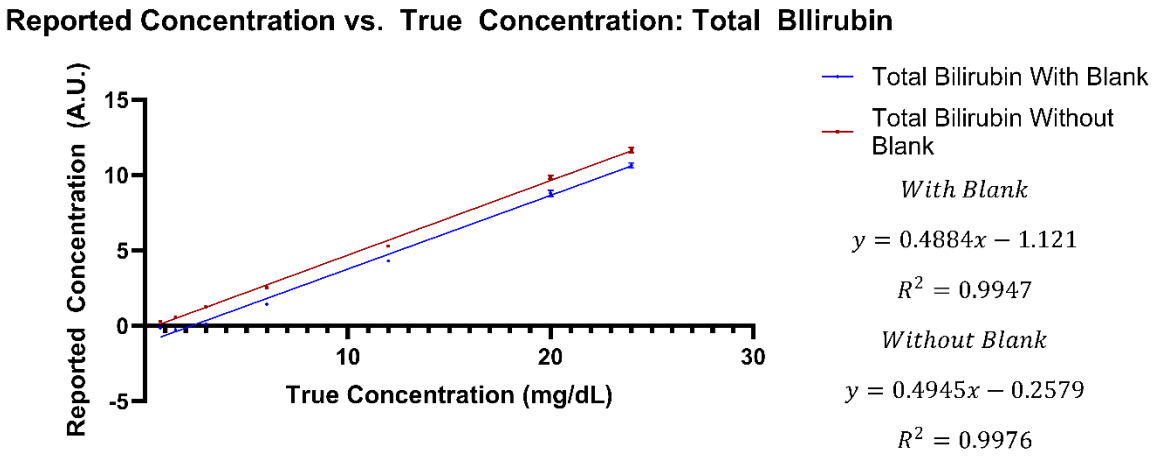


Figure 3-1. Bilirubin assay setup with varying concentrations of bilirubin dissolved in deionized water with $Na_2CO_3$ and DMSO as previously described (183). Without the blank, the assay produced an $R^2 = 0.9976$ over the range of interest. A.U. refers to arbitrary units, reflecting unadjusted concentration given by the AU680.

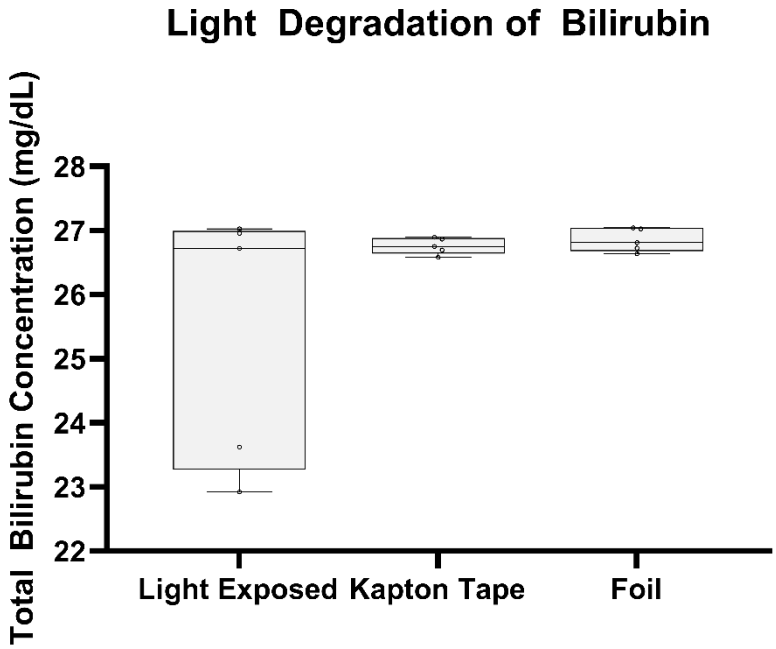


Figure 3-2. Degradation of bilirubin by light in clear, Kapton tape coated, and foil coated tube.

We next tested light sensitivity and methods to prevent light degradation of bilirubin. There were five bilirubin aliquots in clear tubes, five aliquots in tubes covered in Kapton tape, and five aliquots in foil-coated tubes. Kapton tape is an electrical isolation tape with an amber color that is visually similar to the glass bottles that bilirubin is shipped and stored in. While the average of the

light exposed tubes was approximately 1 mg/dL lower than the foil-coated or Kapton-coated tubes, the effect did not reach statistical significance (Figure 3-2).

### 3.4.1 *Dissolving Bilirubin for Stock Creation*

Next, we tested different methods to dissolve bilirubin. Past work describes a protocol using 4 mL of DMSO and 6 mL of 0.25 M $Na_2CO_3$ (183). We were concerned about outgassing of $Na_2CO_3$ so we created pH-matched NaOH solutions with the same DMSO contents (Figure 3-3). It could not dissolve the bilirubin (Figure 3-4). Thus, we continued using the $Na_2CO_3$, ensuring the solutions we used were made on the same day as the bilirubin dissolution.

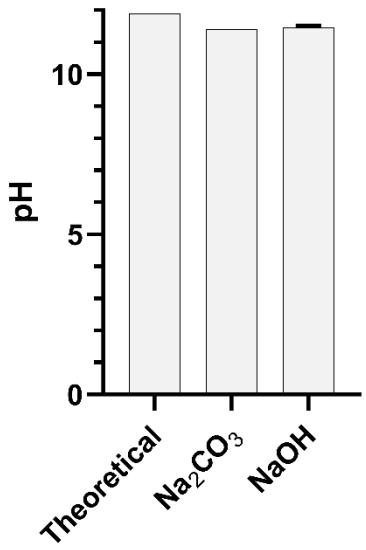


Figure 3-3. pH of base solutions. Each bar is the average of 3 measurements, except the theoretical value. Error bars are standard deviation. For $Na_2CO_3$, all values were identical. pH was measured by a pHoenix XL meter from MesaLabs.

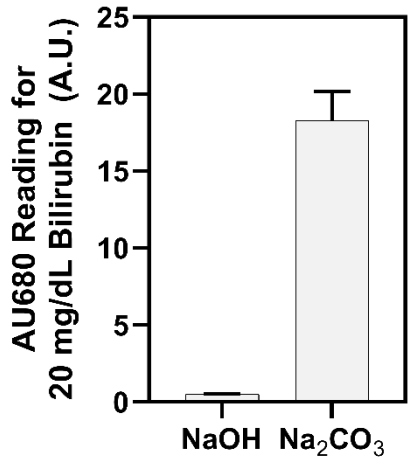


Figure 3-4. pH-matched NaOH + DMSO solutions dissolve much less of a 20 mg/dL bilirubin powder solution than matching $Na_2CO_3$ + DMSO solutions. Each bar is the average of 3 trials. Each sample is the average of three technical replicates. A. U. stands for "arbitrary units" and refers to an AU680 output that has not been converted to a final concentration using a standard curve.

## 3.5 AU680 ALBUMIN

The Beckman Coulter AU680 Albumin reagent designed for serum is a bromocresol green (BCG) based test. The 600/800 nm wavelength is used to measure the concentration of Albumin-BCG complex. Most of our solutions are intended to have approximately 2 g/dL albumin. The unmodified assay produces a highly linear output from 0 to 6 g/dL for BSA (Figure 3-5).

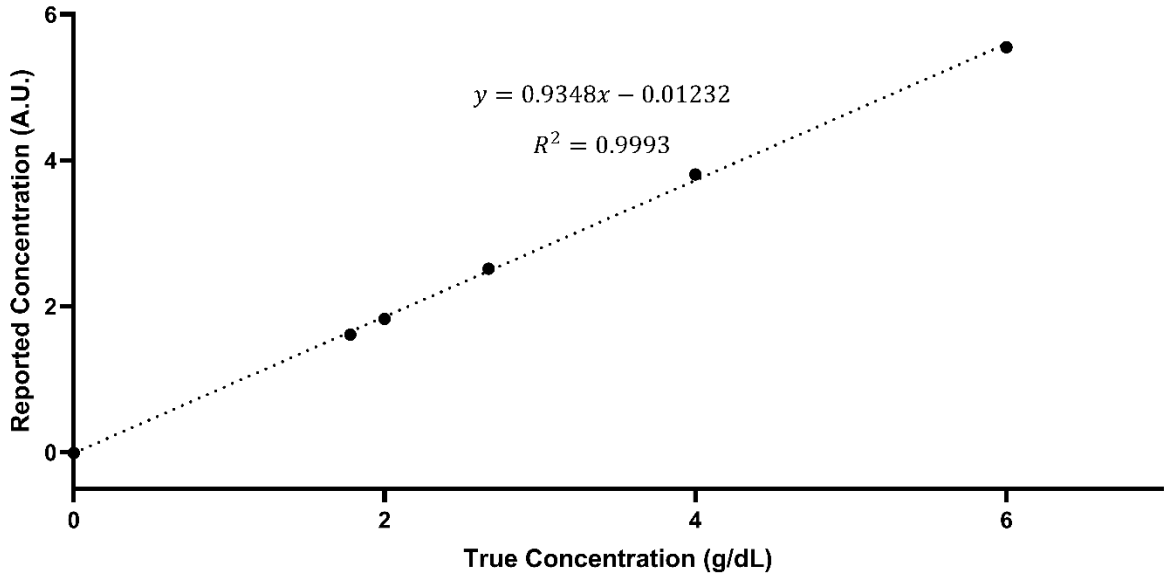


Figure 3-5. Albumin assay setup with varying concentrations of BSA dissolved in deionized water. $R^2 = 0.9993$. Points are the average of three technical replicates. Error bars are not shown because they would not be visible due to being blocked by the data point.

We found that simultaneously testing albumin and bilirubin in dialysate samples significantly altered the albumin measurement (Figure 3-6). Thus, one assay must be run first (usually bilirubin). The second assay must be run afterwards.

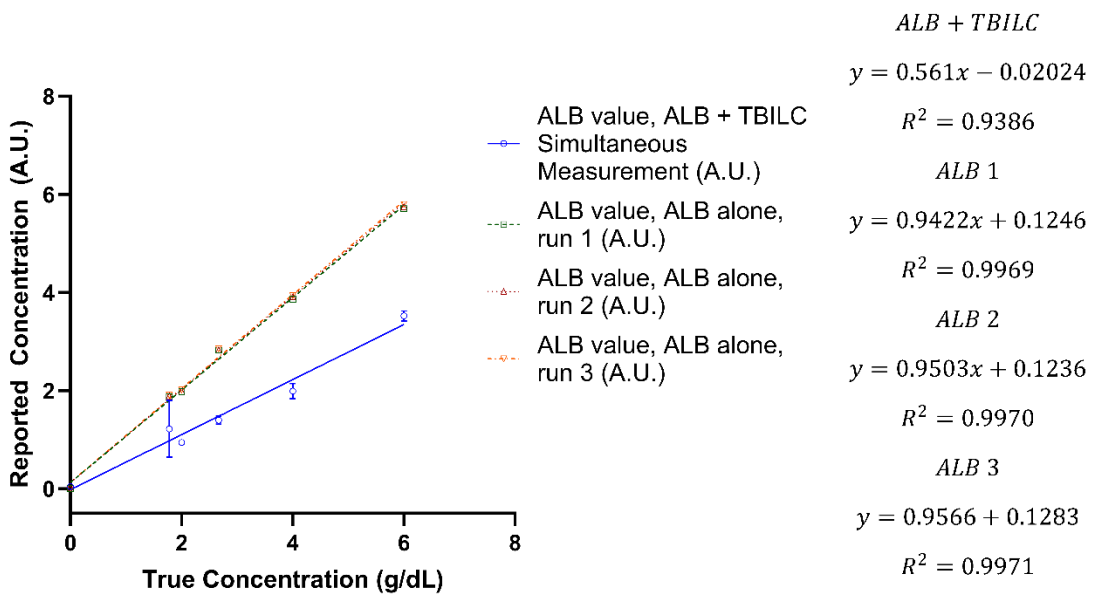


Figure 3-6. The reported concentration of BSA is altered when the bilirubin concentration test is run at the same time. ALB stands for the albumin reagent. TBILC stands for the total bilirubin color reagent. The same ALB samples were tested three times to demonstrate low variation between trials. Values are mean ± standard deviation. Where error bars are not shown, they would not be visible due to being blocked by the data point.

Albumins from different animal species produce linear outputs, the slopes appear compatible, but the intercept is significantly different. This means that each albumin requires a standard curve made from albumin from the same species (Figure 3-7).

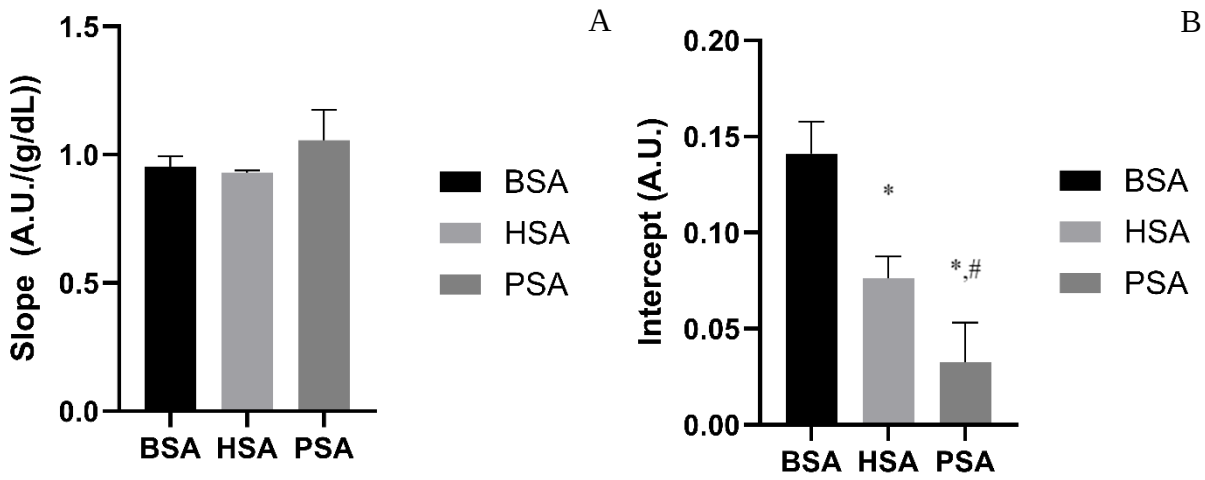


Figure 3-7. Slopes (Panel A) and intercepts (Panel B) of standard curves of albumins of various species. The slope is the ratio of the change in measured concentration, in arbitrary units (A.U.) to the change in true concentration in g/dL. The intercept is a measure of the reported concentration (in A.U.) for a true concentration of 0 g/dL. Each slope/intercept is the average of n = 3 independently created standard curves. Each sample is the average of n = 3 technical replicates. * indicates a significant difference from BSA. # indicates a significant difference from HSA. Significance is set at $p < 0.05$. Statistics were done in Microsoft Excel.

## 3.6 AU680 CREATININE

The Beckman Coulter AU680 Creatinine Reagent designed for serum is a version of the Jaffe reaction. Creatinine reacts with picric acid at an alkaline pH to form a compound that fluoresces at 520/800 nm. Our concentration range of interest is from 1.2 mg/dL to 15 mg/dL. The lower bound is the upper limit of the healthy adult range (203). The upper bound is relevant to renal failure (201). We found that high bilirubin levels interfere with this reaction and 1:6 dilution is needed (see 3.7: AU680 interference tests). Figure 3-8 shows that the assay is linear throughout the desired range both for undiluted and 1:6 diluted standards.

A B

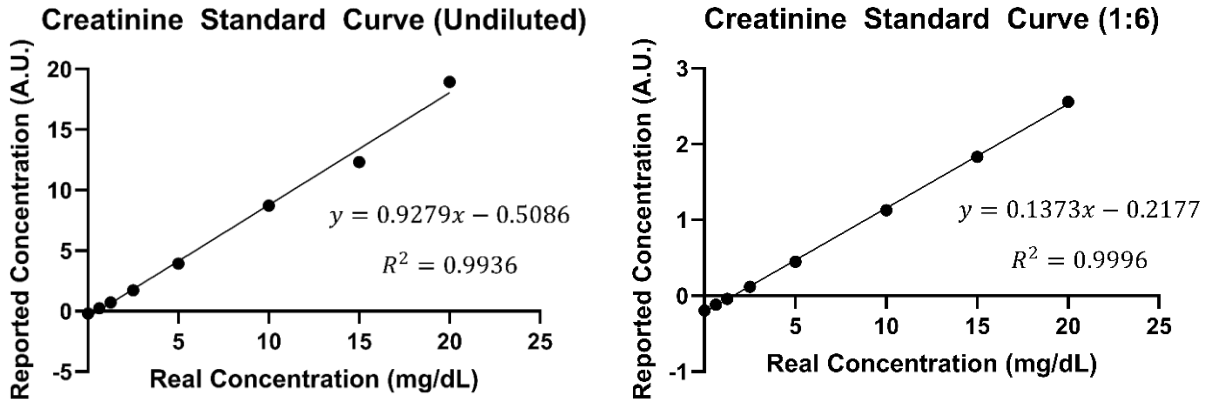


Figure 3-8. Creatinine assay setup with varying concentrations of creatinine dissolved in deionized water. Panel A: Undiluted $R^2$ = 0.9936. Panel B: Diluted $R^2$ = 0.9996. Values are mean ± standard deviation. Error bars are not shown, because they would not be visible due to being blocked by the data point.

## 3.7 AU680 Interference Tests

We tested to verify that varying concentrations of substances found in our blood analog solution did not interfere with the AU680 assays. The blood analog solution is made from dialysate concentrates prepared following clinical protocols. 2 g/dL albumin is added, followed by our toxins of interest (bilirubin, indoxyl sulfate, cholic acid, creatinine, copper, manganese). pH is balanced using NaOH or HCl. As shown in Figure 3-9 none of the substances of interest interfered with bilirubin or albumin measurement. As shown in Figure 3-10, indoxyl sulfate and bilirubin interfered with creatinine measurements. We also confirmed that cholic acid does not interfere with bilirubin measurements in a second test. As shown in Figure 3-11, we confirmed that bilirubin and not the substances used to dissolve it, interfere with the undiluted creatinine measurement. As shown in Figure 3-12, 1:6 dilution reduces or eliminates the impact of bilirubin and indoxyl sulfate on creatinine measurements. In all panels in these figures, each value is the result of n = 3 independent tests. Each measurement is the result of n = 3 technical replicates.

Sham tubes had the starting concentrate diluted with deionized water. IS → indoxyl sulfate. CA → cholic acid. Cu → Copper. Mn → Manganese. Bili → Bilirubin. Cre → Creatinine.

We next tested whether a high concentration of dextran interferes with AU680 spectrophotometry measurements. A dextran concentration of 1263.15 µM is chosen because this corresponds to 8.84 g/dL 70 kDa Dextran and 12.6 g/dL 100 kDa dextran. The maximum solubility of these dextrans is 15 g/dL (204). As shown in Figure 3-13, Dextran 100, but not Dextran 70, significantly interfered with measured albumin concentration using the AU680. 1:6 dilution caused this interference to become worse, with both Dextran 70 and Dextran 100 interfering. Figure 3-14 shows that Dextran 100, but not Dextran 70 at 1263.15 µM significantly interfered with bilirubin measurements. Dilution caused there to be no significant interference, but a large standard deviation was seen between independent tests. As shown in Figure 3-15, both dextrans interfered with creatinine, but 1:6 dilution rendered the Dextran 70 interference no longer statistically significant, while Dextran 100 interference remained significant.

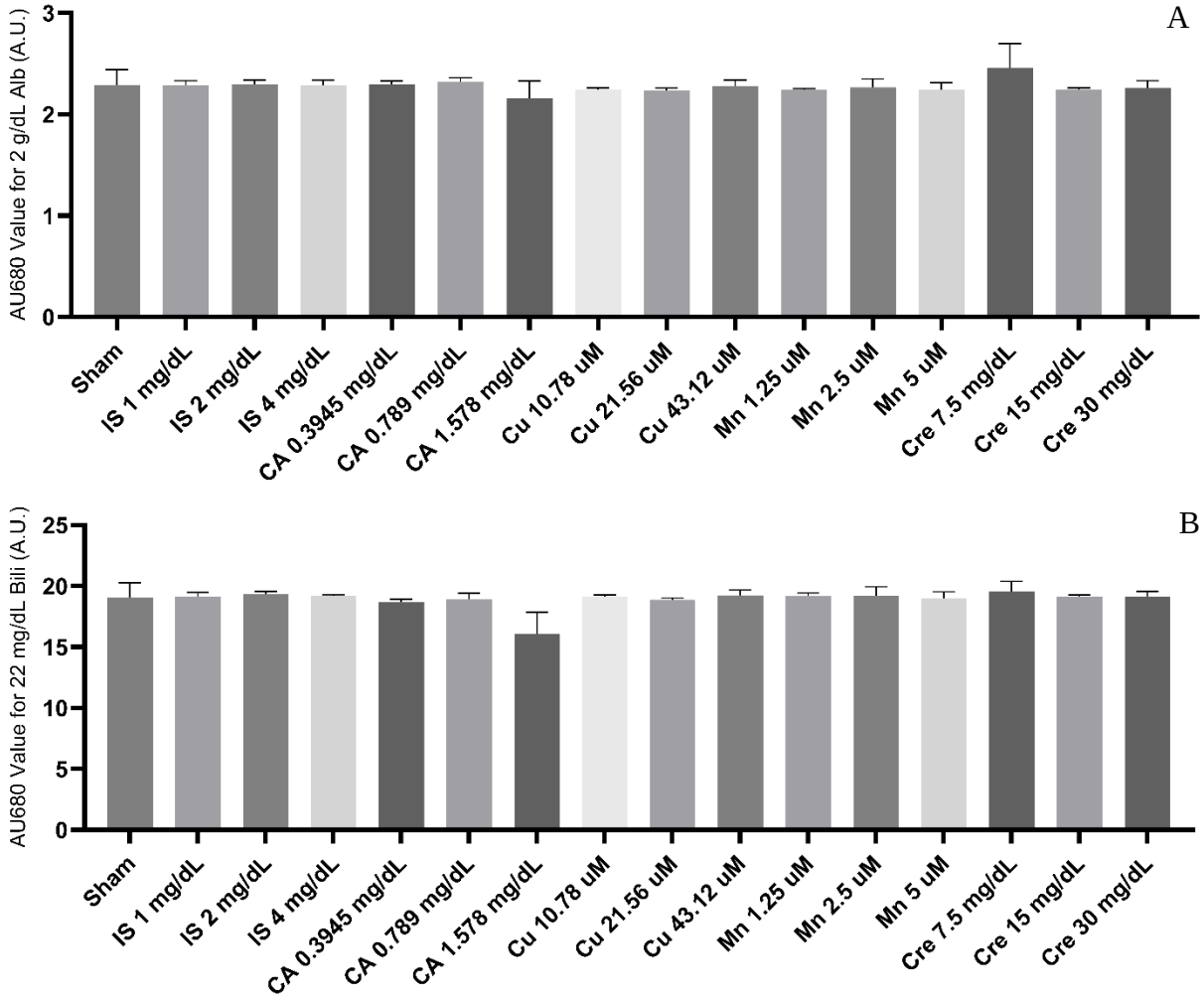


Figure 3-9. **A**: AU680 readout for 2 g/dL albumin combined with various concentrations of substances present in our blood analog solution. **B**: AU680 readout for 22 mg/dL bilirubin. Error bars are standard deviation in all panels.

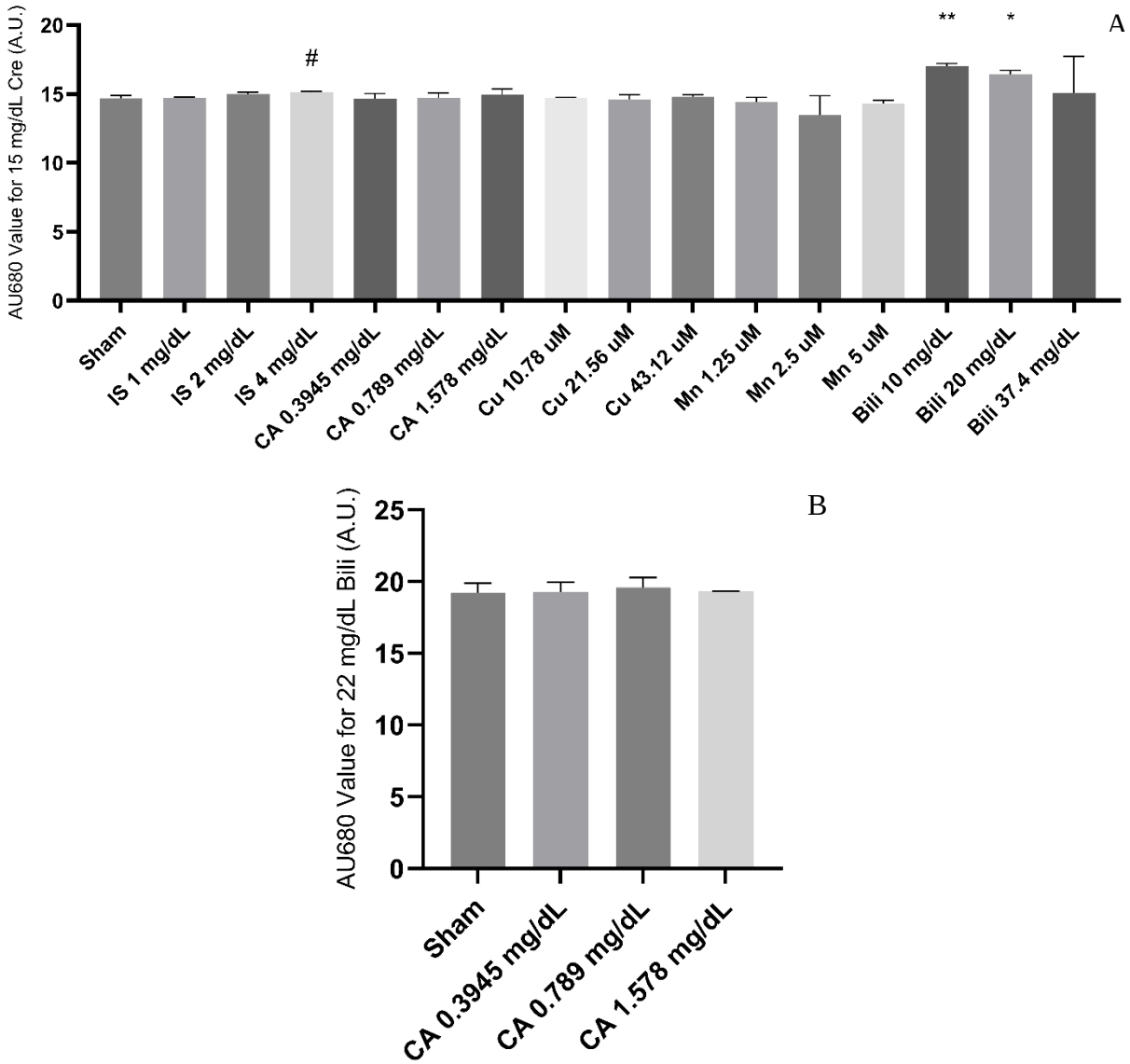


Figure 3-10. **A**: AU680 value for 15 mg/dL creatinine. Note significant interference from 4 mg/dL indoxyl sulfate and 10 and 20 mg/dL bilirubin. **B**: AU680 value for 22 mg/dL bilirubin and various cholic acid concentrations. # → $p < 0.05$. * → $p < 0.002632$ (adjusted for 19 comparisons). ** → $p < 0.0002632$. Error bars are standard deviation in all panels.

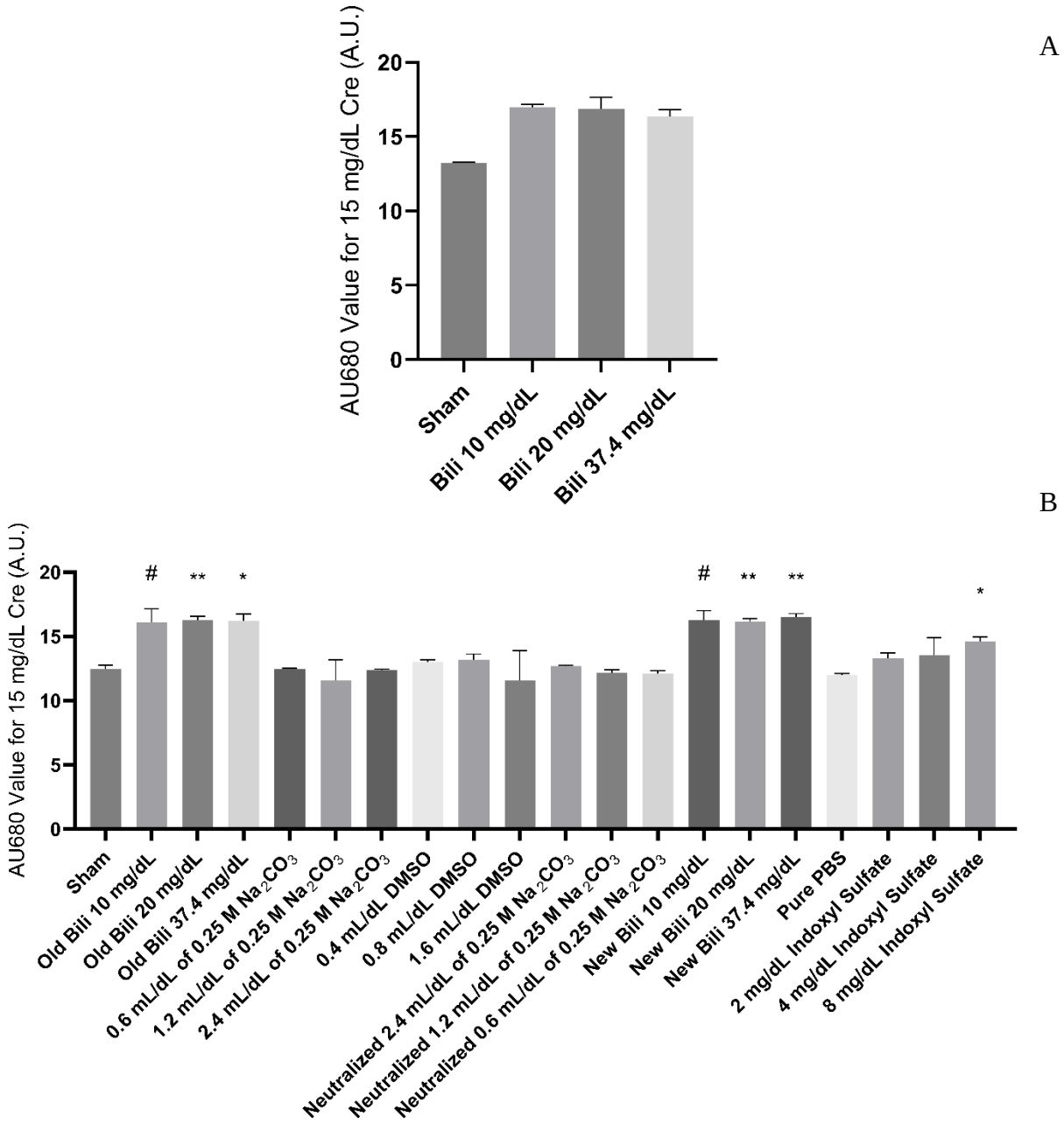


Figure 3-11. **A**: AU680 value for 15 mg/dL creatinine. Significant interference from all bilirubin concentrations. **B**: AU680 value for 15 mg/dL creatinine. Significant interference from two independent bilirubin stocks ("Old Bili" and "New Bili"). Could not replicate significant interference from 4 mg/dL indoxyl sulfate, although 8 mg/dL indoxyl sulfate interfered significantly. # → $p < 0.05$. * → $p < 0.002632$ (adjusted for 19 comparisons). ** → $p < 0.0002632$. Error bars are standard deviation in all panels.

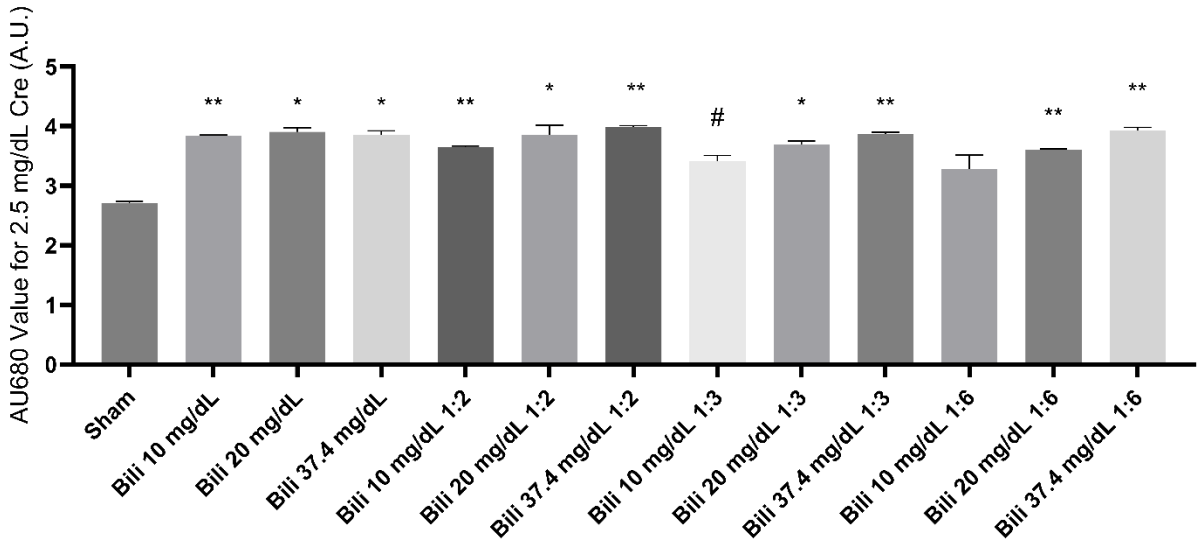


Figure 3-12. AU680 value for 15 mg/dL creatinine. 1:6 Dilution eliminates significant interference from 10 mg/dL bilirubin but not higher concentrations. # → $p < 0.05$. * → $p < 0.002632$ (adjusted for 19 comparisons). ** → $p < 0.0002632$. Error bars are standard deviation in all panels.

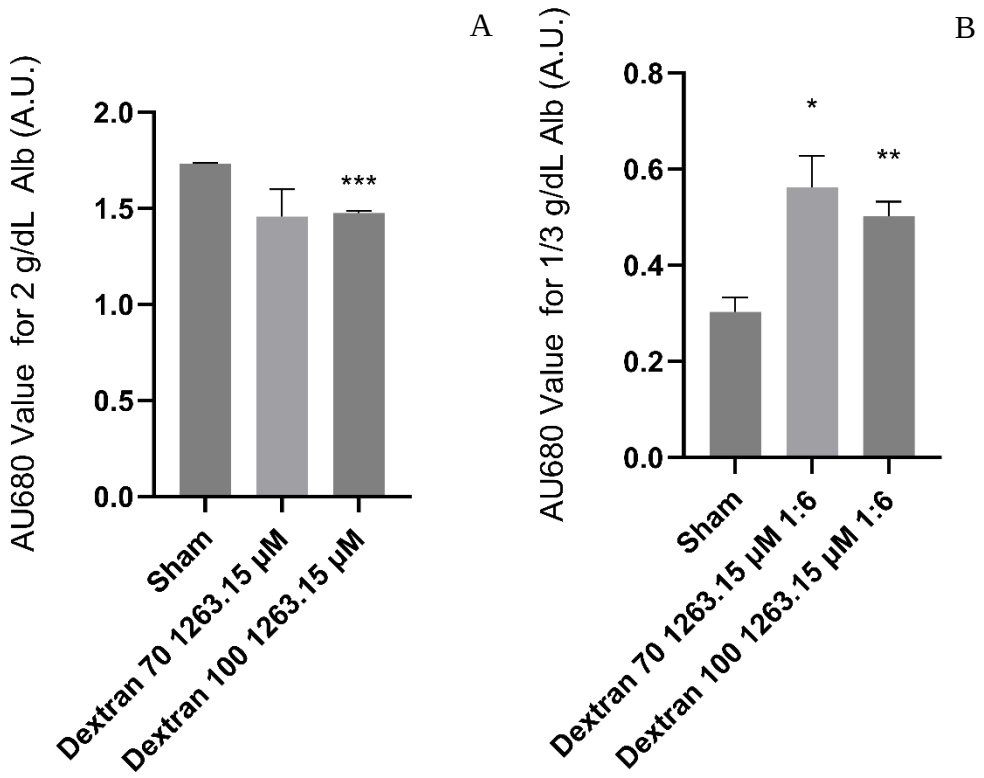


Figure 3-13. **A**: AU680 value for 2 g/dL bovine serum albumin in Dextran solutions. 70 kDa dextran does not interfere significantly with albumin measurement. 100 kDa dextran does interfere. *** represents $p < 10E\text{-}4$. **B**: 1:6 dilution does not eliminate Dextran 100 interference with 2 g/dL albumin measurement using spectrophotometry. Post-dilution, 70 kDa dextran also interfered with the measurement. * → $p < 0.05$. ** → $p < 0.005$. Error bars are standard deviation in all panels.

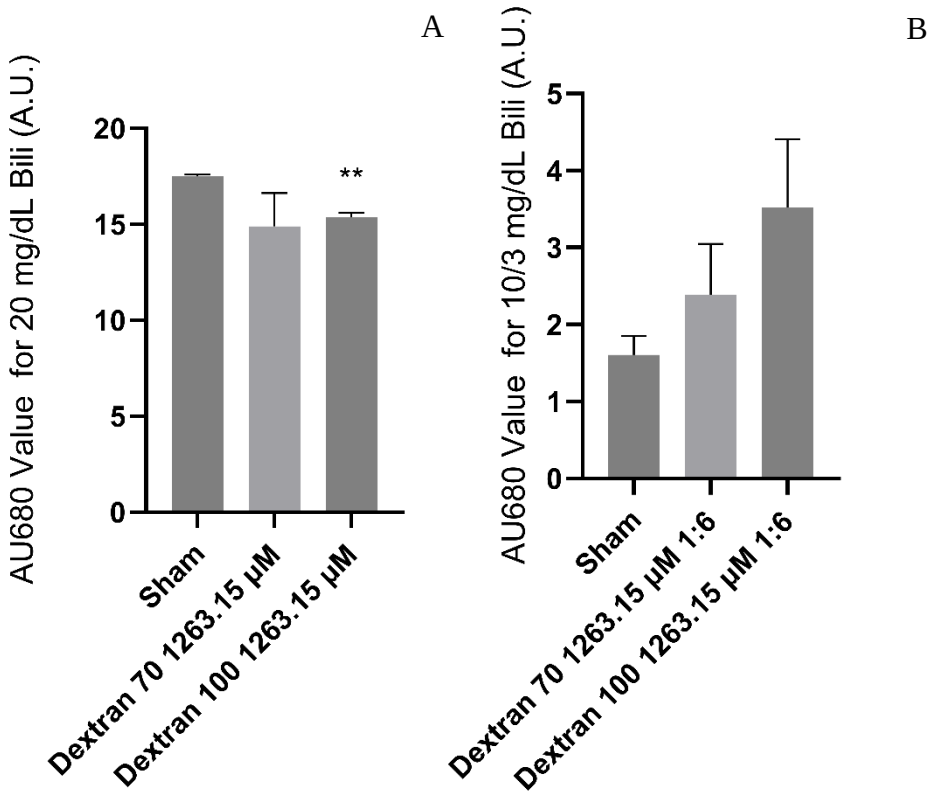


Figure 3-14. **A**: AU680 value for 20 mg/dL bilirubin in Dextran solution. 70 kDa dextran does not interfere significantly with bilirubin measurement. 100 kDa dextran does interfere. ** indicates $p < 0.005$. **B**: After 1:6 dilution, no statistically significant interference is observed because of wide variance in the assay. Error bars are standard deviation in all panels.

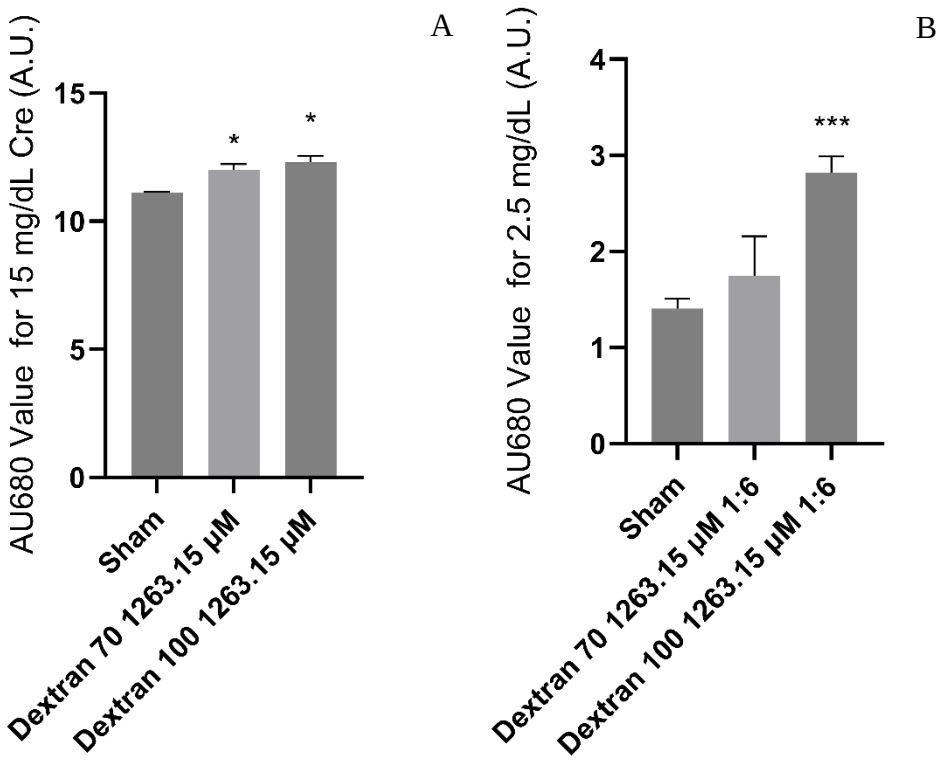


Figure 3-15. **A**: AU680 value for 15 mg/dL creatinine in dextran solution. Both 70 kDa and 100 kDa dextran interfere with creatinine measurements. * indicates $p < 0.05$. **B**: AU680 value for 15 mg/dL creatinine in dextran solution after 1:6 dilution. Dextran 70 did not significantly interfere, while Dextran 100 interference was highly significant. *** indicates $p < 1E-3$

## 3.8 Bilirubin Standard Curves in Dextran

There was significant variation between measurements of independent samples of bilirubin dissolved in dextran solution, even when there was no statistically significant difference observed (Figure 3-14). Thus, to verify that bilirubin in concentrated dextran solutions can be measured accurately using the AU680 and standard bilirubin reagent, we conducted standard dilutions of 40 mg/dL bilirubin stock dissolved in 2 g/dL BSA. The diluent was 1263.15 µM Dextran 70 and Dextran 100, with dialysate diluent serving as a control. Each experiment was replicated three times, and each point was the average of n = 3 technical replicates. The coefficient of variation of the slope and intercept were then calculated (average/standard deviation). Further consistency was ensured by applying Standard Curve 1 to calculate the concentrations of the solutions in Standard

Curves 2 and 3 and comparing them to the true concentrations. The 0 mg/dL negative control samples are excluded from standard curve calculations because the first standard (0.75 mg/dL) cannot be reliably distinguished from the negative control, meaning that in dextran, 0 mg/dL is outside the linear range of this assay. The resulting standard curves are highly linear (Figure 3-16) and predict values near the correct concentrations when one is used to adjust the others (Figure 3-17). The slope and intercept differ from the normal bilirubin assay, but the coefficient of variation is not higher than normal dialysate.

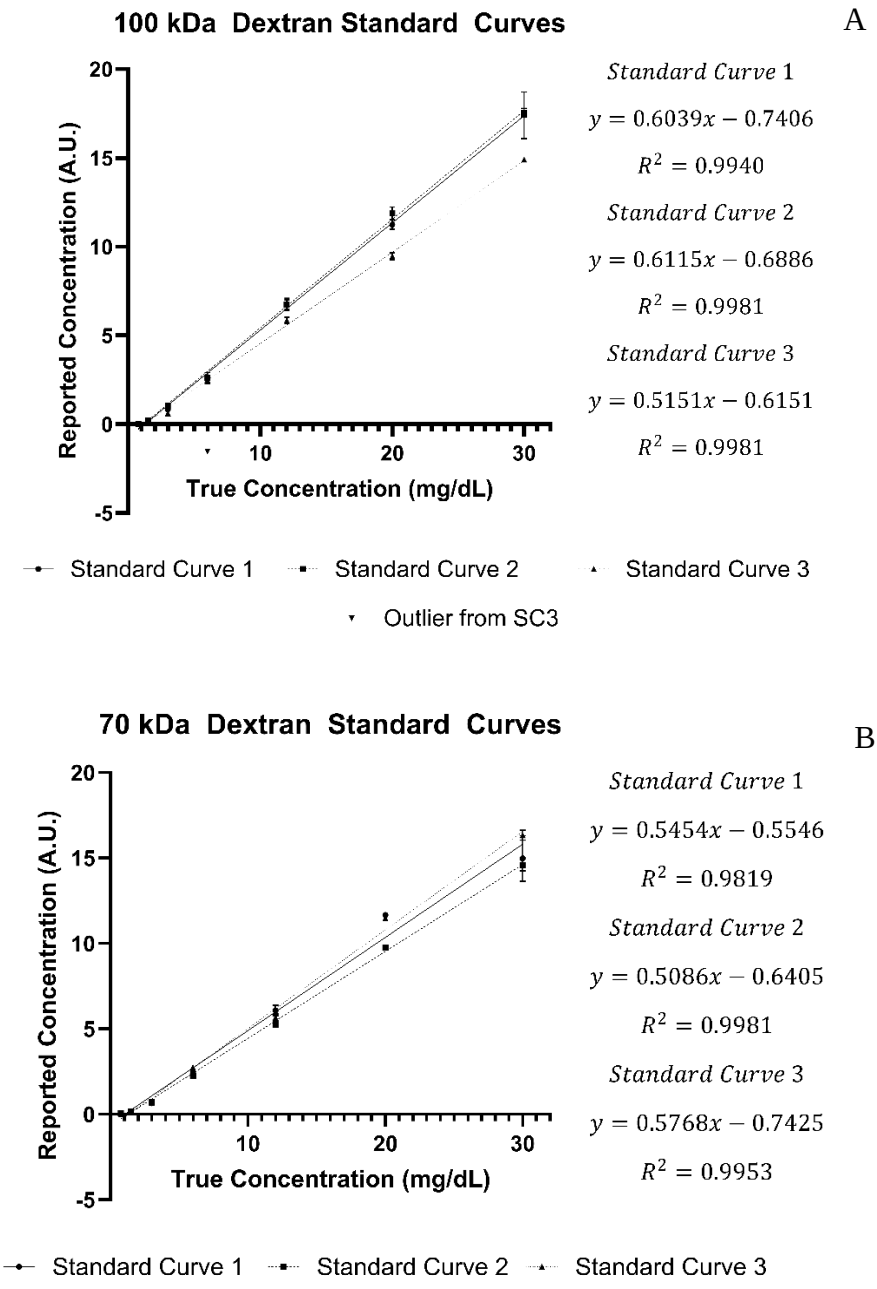


Figure 3-16. Bilirubin standard curves in 1263.15 µM 100 kDa (A) and 70 kDa (B) Dextran demonstrate a high degree of linearity and repeatability. Points are average values of three technical replicates. Error bars are standard deviation. They are not shown when the bar would be less than the size of the graphed data point. One outlier was removed from the 100 kDa Dextran data (A) and is graphed as a separate category.

A

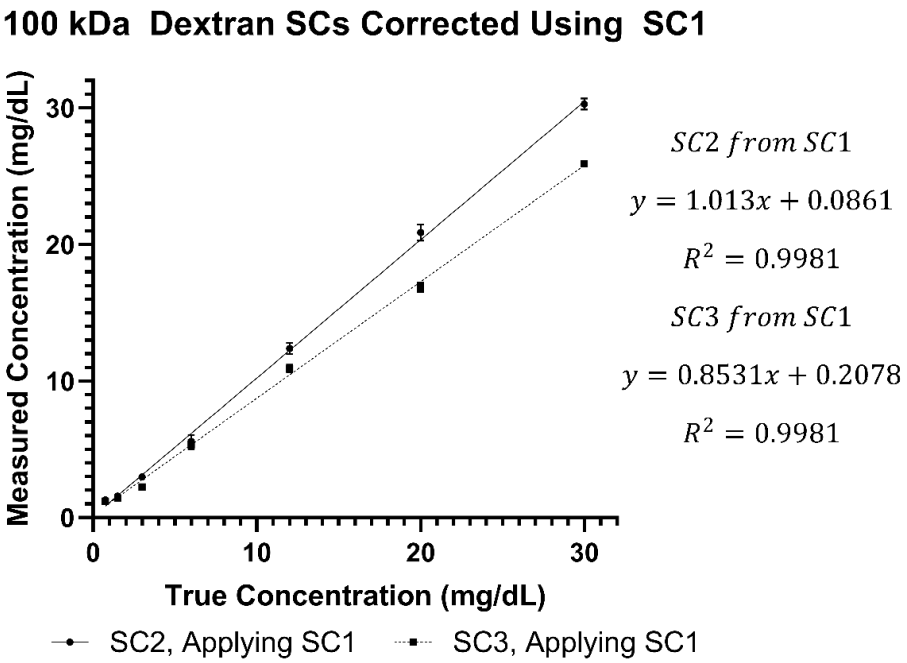


B

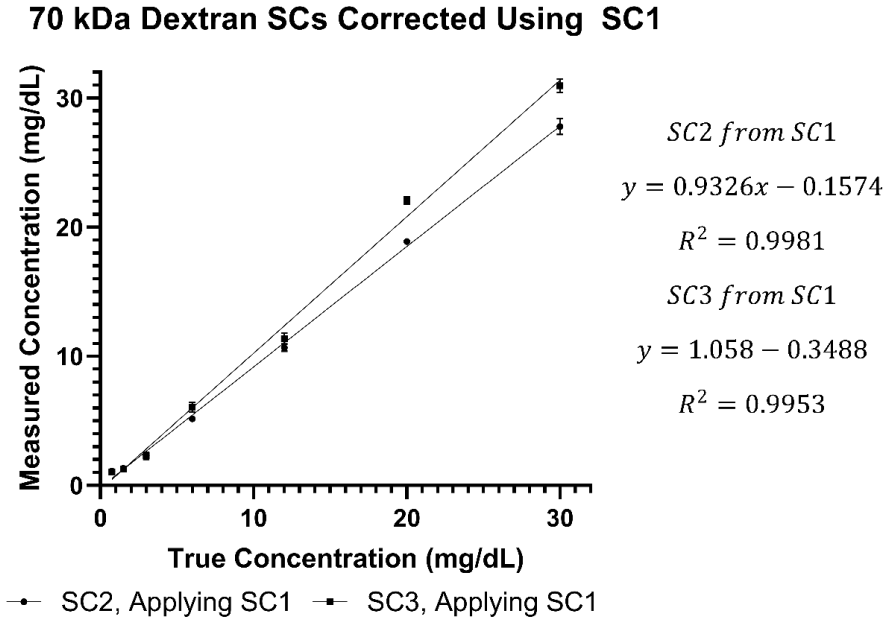


Figure 3-17. The first independent standard curve is used to derive the concentrations in the other two standard curves measured on the same day. The resulting slopes are near 1, and concentrations are near 0 for both 100 kDa (A) and 70 kDa (B) dextran, confirming linearity and repeatability. Points are average values of three technical replicates. Error bars are standard deviation. They are not shown when the bar would be less than the size of the graphed data point.

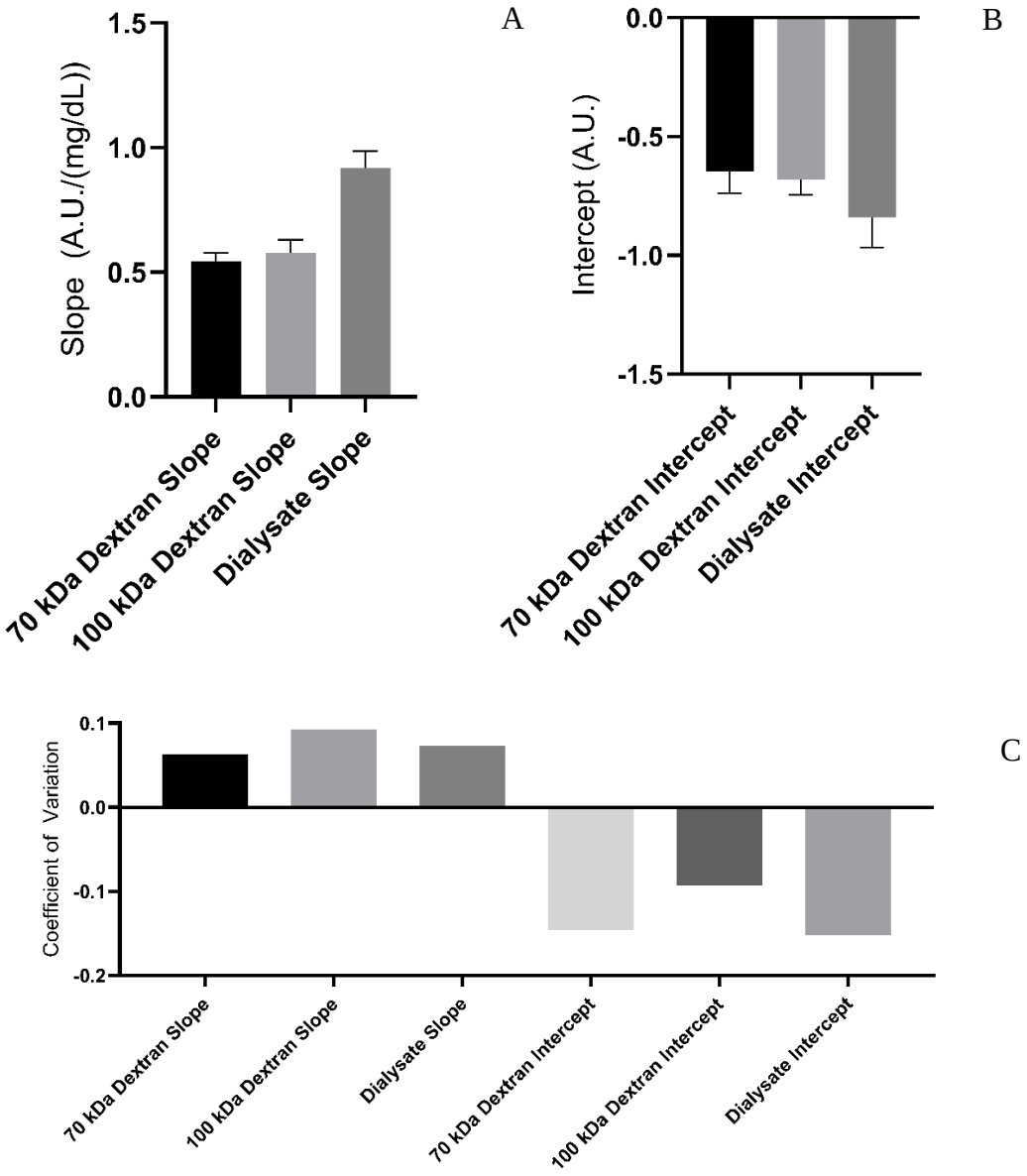


Figure 3-18. **A**: In both dextran solutions, the slope of the reported bilirubin concentration compared to the true concentration is lower than in a dialysate control. Error bars in A and B are standard deviation. Points are the average of 3 technical replicates. **B**: In both dextran solutions the intercept is less negative than a dialysate control. **C**: Same-day coefficient of variance (COV) for all slopes does not exceed 0.1, and for all intercepts does not exceed -0.2. Adding dextran does not increase COV for this assay.

## 3.9 INDOXYL SULFATE AND CHOLIC ACID ASSAY SETUP

Indoxyl sulfate and cholic acid were tested on the Waters Quattro Micro Liquid Chromatograph & Direct Infusion Mass Spectrometer. The HPLC column was the Zorbax Eclipse

XDB-C18, 2.1 x 50 mm, 5-micron, Agilent. Particles were modified with 18 carbon chains by the manufacturer. Both analyses were MS/MS. This means the original ions were analyzed by MS, then they were fragmented. The fragments underwent a second round of analysis (MS/MS). This prevents other molecules with the same mass to charge ratio (m/z) from confounding the measurement. The assay was set up with help from Dr. Martin Sadilek of the mass spectrometry facility. Capillary voltage was 2.5 kV. Cone voltage is 32 V. Extractor voltage is 2 V. RF lens voltage is 0.2 V. Source temperature is set to 100 °C. Desolvation temperature is set to 350 °C. Desolvation gas flows at 500 L/hr. Cone gas speed is in L/hr. LM (low mass) and HM (high mass) Resolutions were both 13. Ion energy was 0.5. Entrance voltage was 15 V. Collision voltage was 16 V. Exit voltage was 16 V. Multiplier was set to 650. Syringe pump flow rate was 5 µL/min. Figure 3-19 shows the percentage of mobile phase A over the course of one sample run.

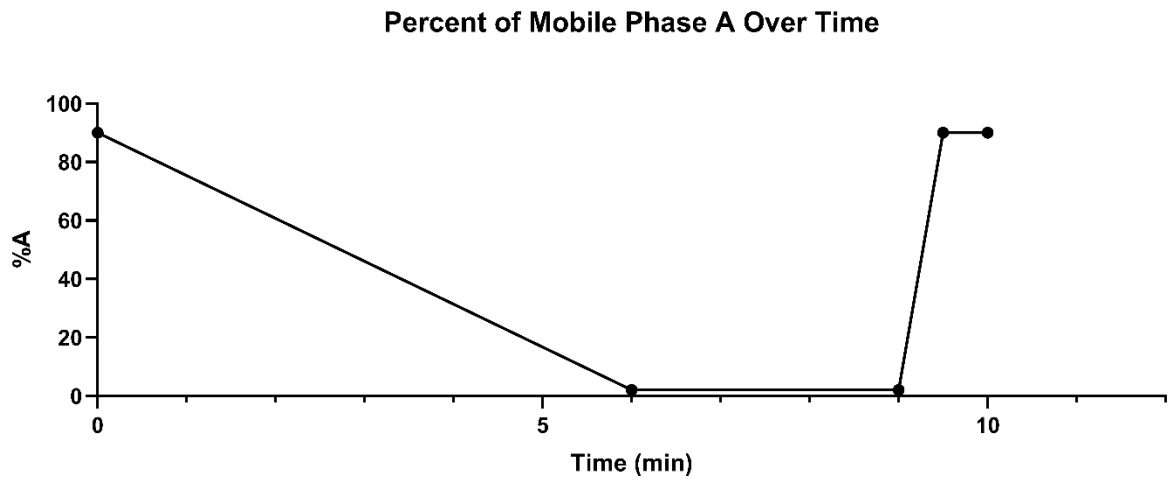


Figure 3-19. Percent of mobile phase A over time

For indoxyl sulfate, the chosen fragments were the 80.95 and 79.95 Da fragments of a 213 Da molecular ion. As shown in Figure 3-20, they yield very linear standard curves. For cholic acid, the 407 Da and 343 Da fragments were chosen. 407 corresponds to the molecular ion. As shown in Figure 3-21, the resulting standard curves are highly linear. Internal standard was added to samples prior to sample preparation at a concentration of 1 mg/dL for indoxyl sulfate and 0.00682

mg/dL for cholic acid. The indoxyl sulfate internal standard was 13C6 labeled, with the chemical formula C2*C6H6KNO4S. The product number was CLM-9565 from Cambridge Isotope Labs (Tewksbury, MA, USA). The standard was 95% labeled and 99% chemically pure. Cholic acid internal standard was labeled with 4 deuterium atoms, with the chemical name 5β-Cholanic Acid-3α, 7α, 12α-triol-2,2,4,4-d4. It was item number C1900-015 from Steraloids (Newport, R.I., USA). The standard was Indoxyl sulfate internal standard fragments were 80.95 and 79.95 Da fragments of a 218 Da molecular ion. Cholic acid internal standard fragments were 411.4 Da (molecular ion) and 347.5 Da. Samples were prepared for analysis following an established protocol (205), with a few modifications. Guided by Stokes formula (206), the centrifuge was adjusted for 3801 x g for 54 minutes, equivalent to the previously reported 21,000 x g for 10 minutes. The injection volume was increased to 90 uL because this reduced variance between technical replicates. When lots of internal standard were changed, a correction factor was applied to account for variability between internal standard lots. Additionally, when the blood side solution at t = 0 minutes reading was greater than 2 mg/dL off from the expected concentration consistently in a single instrument run, some samples were re-run. If re-run samples displayed expected concentration readings and had a consistent ratio with the anomalous values, a correction factor was applied to the entire run based on this ratio.

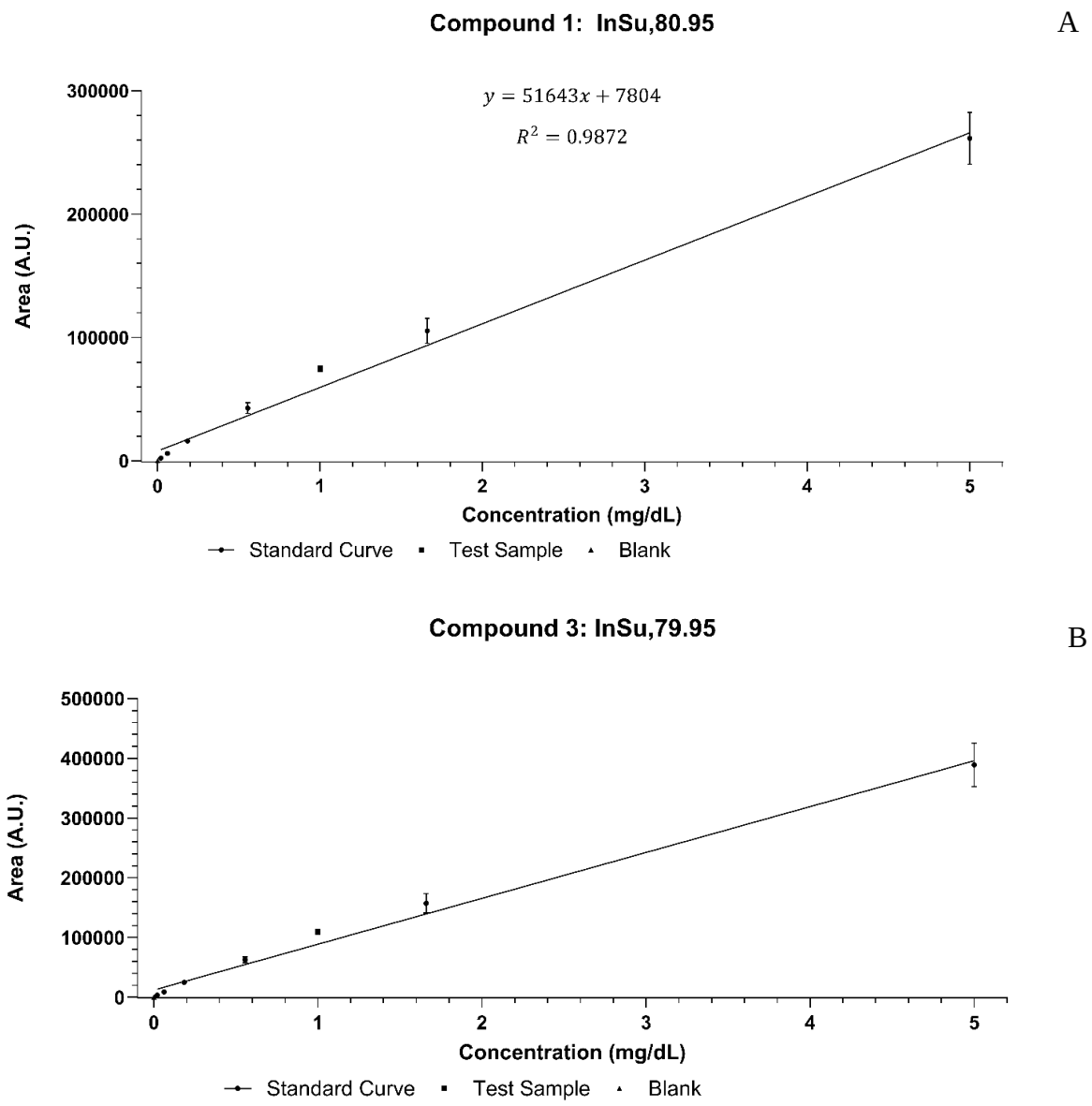


Figure 3-20. Indoxyl sulfate standard curves (circles) and individual samples of known concentration (squares) that verify the standard curves. All measurements are the average of N = 3 technical replicates. The blank is shown as a triangle. Error bars are standard deviation. Where error bars are not shown, the error bars would be smaller than the symbol showing the data point. Panels A and B show the 80.95 Da and 79.95 Da fragments, respectively.

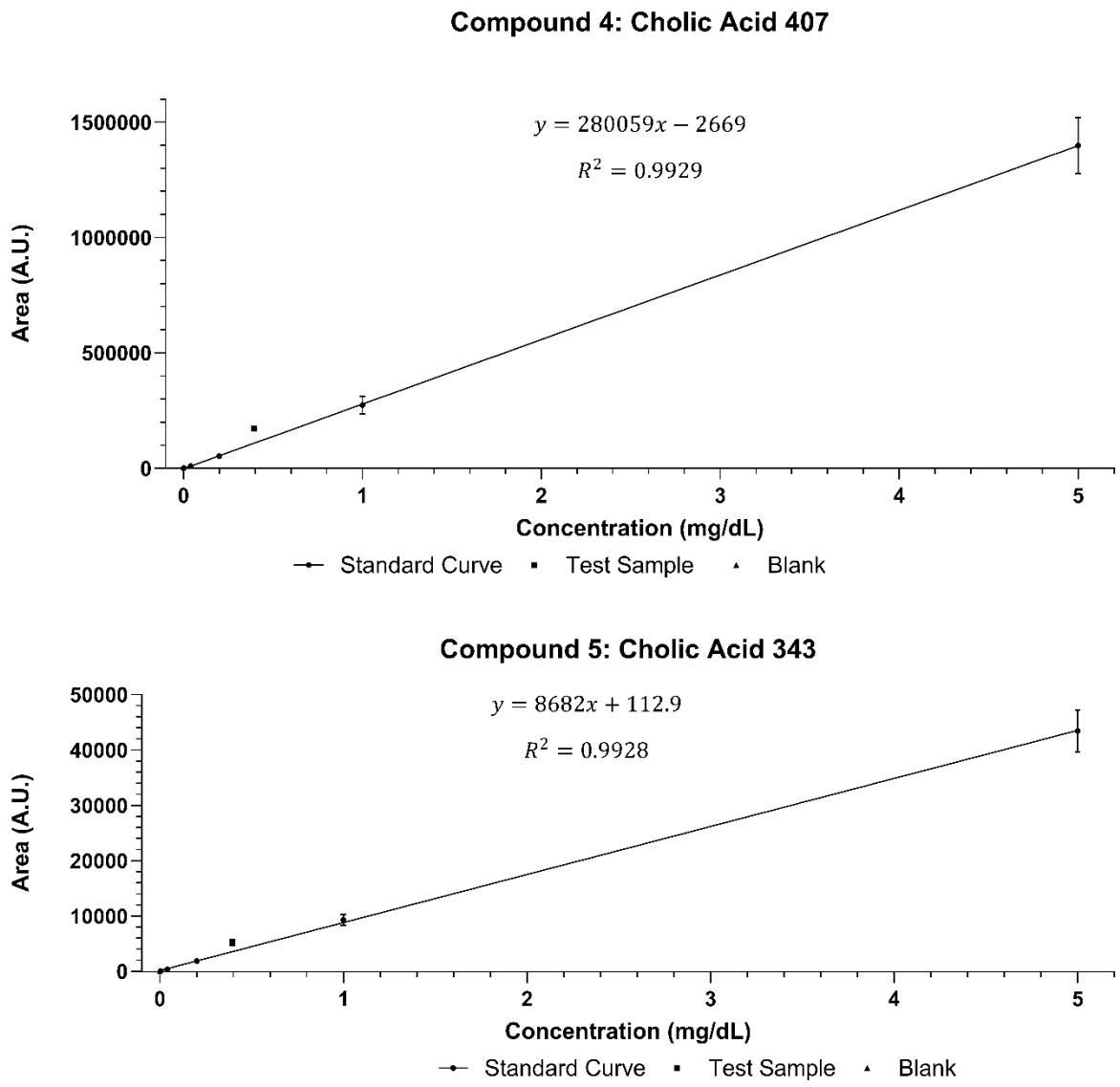


Figure 3-21. Cholic acid standard curves (circles) and test samples of known concentration (squares). All measurements are the average of N = 3 technical replicates. The blank is a triangle. Error bars are standard deviation. Where error bars are not shown, the error bars would be smaller than the symbol showing the data point. Panels A and B show the 407 Da and 343 Da fragments, respectively.

### 3.9.1 *Dissolving Cholic Acid for Stock Creation*

To create cholic acid stocks and standards we followed the protocol of Weiping Ding (183). 1 gram of the appropriate albumin (BSA, HSA, or PSA) was dissolved in 48 mL of diH2O. Then, 10 mg of cholic acid were weighed out in a glass beaker. 2 mL of glacial acetic acid were added

to the glass beaker (Sigma Aldrich, Reagent Plus grade, 99% purity, A6283-100ML). The cholic acid was fully dissolved in the acetic acid. Then the mixture was added to the albumin solution. The final stock concentration was 20 mg/dL.

## 3.10 Copper and Manganese

Copper and manganese were measured using an iCAP™ RQ ICP-MS. Assays were run by Dr. Jakub Sliwinski of the Tracelab. Yttrium, scandium, and rhodium were used as internal standards. Yttrium was used to control for sample loss during digestion and dilution. Scandium and rhodium were used to control for instrument error and variation. Samples were digested using 350 µL of 50% nitric acid and 150 µL of 30% hydrogen peroxide for every 350 µL of sample. This digestion solution contained the yttrium internal standard at 10 ppb. Digestion occurred at 75 ºC on a Drybath Standard 4 block 100-120V hotplate (Thermo Scientific, Waltham, MA, USA) overnight. If undigested aggregates were seen, an additional 300 µL of 30% $H_2O_2$ was added. If three more additions of 30% $H_2O_2$ were insufficient, then another 350 µL of 50% nitric acid and 150 µL of 30% $H_2O_2$ was added. This additional digestion solution did not contain any yttrium. Samples were then diluted in 2% nitric acid to a final volume of 7 mL (20 x dilution) to minimize damage to the ICP-MS from high dialysate salt concentrations. Scandium or rhodium internal standard at 10 ppb was added at the last step, right before measurement.

Standards were created via the standard addition method (207). Dialysate containing 2 g/dL bovine serum albumin was selected as the matrix for the standard. Externally validated standard solution (Spex CertiPrep CLMS-2 Claritas PPT® Grade ICP-MS Multi-Element Solution 2 with Mercury, 10 µg/mL (10 ppm) in 5% HNO3, Cole-Parmer, Vernon Hills, IL, USA) was added to

achieve the following concentrations: 0, 2, 20, 200, and 2000 ppb. Because none of the samples exceeded 2000 ppb, only the first four points of the standard curve were used.

To minimize trace metal contamination, digestions were done in cleaned Teflon vials (15 mL Standard Vial, Rounded Interior, Savillex, Eden Prairie, MN, USA) and dilution was done in cleaned polypropylene tubes (Environmental Express Digestion Tubes, Natural Screw-Top Caps, PP, 15 mL, Cole-Parmer, Vernon Hills, IL, USA). Cleaning was done as follows: Isopropyl alcohol was used to remove tube labels. Then tubes were soaked overnight in 2% citranox (Alconox Critical Cleaning Experts, White Plains, NY, USA). Then, tubes were rinsed three times with milli-Q water. Rinsed tubes were brought into a dedicated cleanroom. Tubes were loaded into a Teflon vessel and soaked in 50% nitric acid and heated to 105 °C for at least four hours. Then, nitric acid was decanted, and tubes were rinsed three times with milli-Q water. Next, tubes were soaked in 50% hydrochloric acid and heated to 105 °C for at least four hours. Hydrochloric acid was decanted, tubes were rinsed 3x with milli-Q water, and left to dry overnight in a laminar flow hood in the cleanroom.

Figure 3-22 shows the scandium and yttrium measurement over the course of one trial. Variations were used to correct concentration measurement errors. Figure 3-23 shows the copper and manganese standard curves, verifying the linearity of this assay on the desired range. Standard curves were made based on the ratio of copper and manganese to scandium or rhodium, to account for variation in machine parameters.

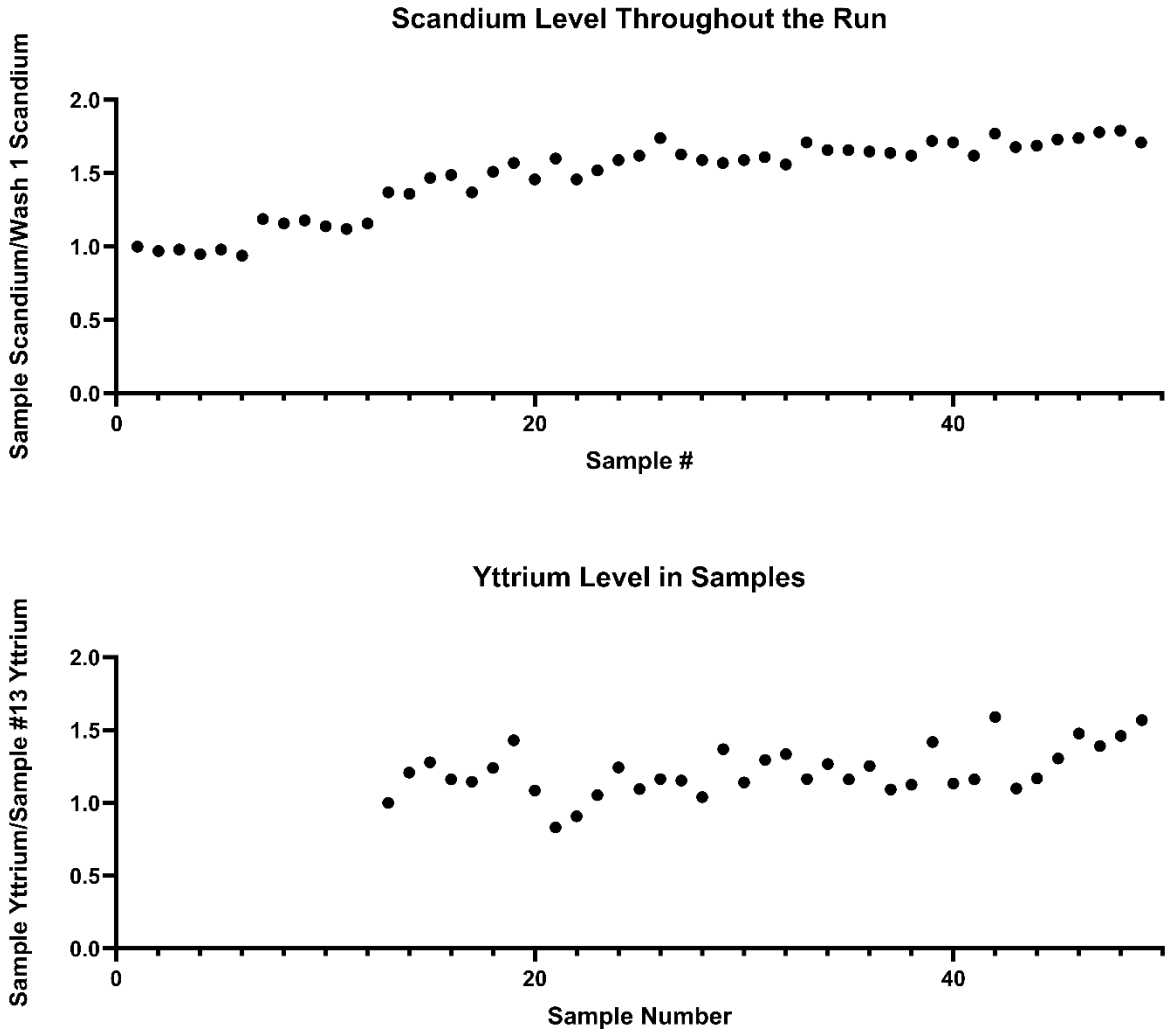


Figure 3-22: **A**: Scandium measurement variation across 49 samples. **B**: Yttrium measurement variation across 49 samples. Sample 13 is the baseline because it is the first test sample (rather than standards, blanks, and conditioning washes).

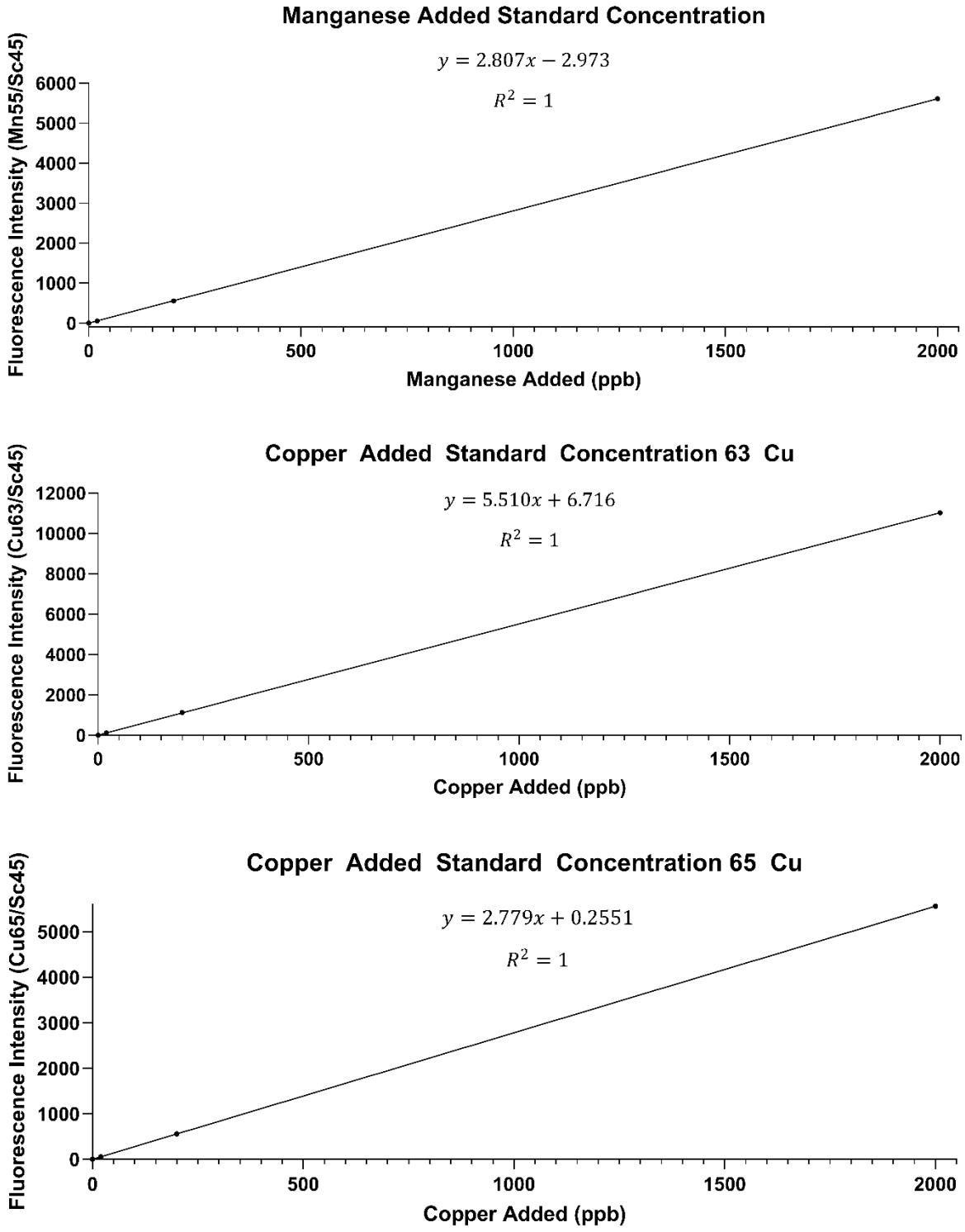


Figure 3-23: Standard curves for both stable copper isotopes and the only stable manganese isotope. Intensities are reported as the ratio of the target ion to the scandium internal standard.

Data analysis was performed as follows: First, copper, manganese, and yttrium values were divided by the scandium or rhodium measurement intensity to account for variation in the instrument. Second, the % of yttrium loss during digestion was calculated for all samples, relative to the sample with the greatest yttrium concentration. Third, the standard curve was applied. Results for the two copper isotopes were averaged. The standard reduction formula is as follows (Equation 3-1)

$$\left(\frac{\left(100\% * \frac{X}{[Sc_{45}\ or\ Rh_{103}]}\right)}{100\% - \%Loss, Y_{89}} * Slope + Intercept\right) * DF = [X](ppb) \text{ (Equation 3-1)}$$

Here, X is instrument reported value for the test analyte. $Sc_{45}$ is the instrument intensity for scandium internal standard. $Rh_{103}$ is the instrument intensity for rhodium internal standard. $\%Loss, Y_{89}$ is the % loss of yttrium, calculated by Equation 3-2 in the absence of an internal standard reference procedure, or Equation 3-3 for later plates, where an internal standard reference was added. "Slope" and "Intercept" are obtained from the standard curve. DF is the dilution factor. [X] is the concentration of test analyte in ppb.

$$\%Loss, Y_{89} = \frac{\left(\max\left(\left\{\frac{Y_{89,i}}{[Sc_{45,i,Ref}\ or\ Rh_{103,i,Ref}]} : i = 1,\ldots,n\right\}\right) - \frac{Y_{89}}{[Sc_{45}\ or\ Rh_{103}]}\right) * 100\%}{\max\left(\left\{\frac{Y_{89,i}}{[Sc_{45,i,Ref}\ or\ Rh_{103,i,Ref}]} : i = 1,\ldots,n\right\}\right)} \text{ (Equation 3-2)}$$

Here $Y_{89}$ is the instrument intensity for yttrium internal standard. i is an index signifying sample number. n is the number of samples. Thus, $\max\left(\left\{\frac{Y_{89,i}}{[Sc_{45,i,Ref}\ or\ Rh_{103,i,Ref}]} : i = 1, \ldots, n\right\}\right)$ is the maximum scandium or rhodium-normalized yttrium intensity among samples 1 through n.

A potential weakness of this method is that it underestimates the sample loss during digestion. The yttrium correction is only applied up to the sample that lost the least yttrium (the

sample with the highest yttrium reading). This is because introducing an undigested sample would damage the instrument, and introducing a sample with a known yttrium concentration with no dialysate matrix would not account for matrix effects.

Thus, we created a yttrium internal standard reference (Inorganic Ventures, Christiansburg, VA, USA) using a dialysate sample digested without yttrium in the digestion solution. 1000 ppb yttrium was added to the solution to achieve a final concentration of 10 ppb, matching the pre-digestion yttrium concentration in the samples. This prevented yttrium loss during digestion in the reference sample. Thus, the concentration could be calculated as follows:

$$\%Loss, Y_{89} = \frac{\left(\frac{Y_{89,ref}}{\left[Sc_{45,ref}\ or\ Rh_{103,ref}\right]} - \frac{Y_{89}}{\left[Sc_{45}\ or\ Rh_{103}\right]}\right) * 100\%}{\frac{Y_{89,ref}}{\left[Sc_{45,ref}\ or\ Rh_{103,ref}\right]}} \quad \text{(Equation 3-3)}$$

$Y_{89,ref}$ is the yttrium reference standard concentration of yttrium. $Sc_{45,ref}$ is the yttrium reference standard concentration of scandium. $Rh_{103,ref}$ is the yttrium reference standard concentration of rhodium.

## 3.11 Susceptibility to Freeze-Thaw

Among our analytes of interest only bilirubin has been reported to significantly decrease after one freeze-thaw cycle (208). A 3.5% decline in bilirubin concentration was reported after one freeze-thaw cycle. Thus, care was taken to ensure that samples used for bilirubin analysis were frozen and thawed no more than once. Other analytes including albumin, creatinine, bile acids, indoxyl sulfate, and copper have been verified to be stable when frozen and thawed (208–211). Freeze-thaw stability has not been reported for manganese, but like copper, it is a pure element and there is no reason to anticipate it would degrade when frozen and thawed.

### 3.11.1 *Dialysate Bicarbonate Concentrate*

In our experiments it was valuable to freeze and thaw a dialysate bicarbonate concentrate stock to efficiently make dialysate solutions. Bicarbonate concentrate may outgas as carbon dioxide, creating the risk that concentrate would lose potency from refrigerated storage or repeated freeze-thaw cycles. We researched this subject and our data has been published as a conference abstract (212). It is reported here.

#### 3.11.1.1 Previous work

Dialysate bicarbonate concentrate has a concentration of 967.2 mEq/L. Previous studies on bicarbonate stability under cold storage conditions have focused on lower concentrations. Past work on bicarbonate stability is summarized in the following tables.

Table 3-1: Previous work on Bicarbonate Stability

| Paper | Container | Definition of instability |
|---|---|---|
| Wear, 2010 (213) | Polyolefin bags | pH < 7.0 or > 8.5 |
| Naorungroj, 2020 (214) | Polyolefin bags | Significantly Negative Slope |
| Hicks, 1972 (215) | Capped poly-propylene syringes | pH < 8 |
| Sayre, 2012 (216) | Polyolefin bags | pH < 7.0 or > 8.5<br>Concentration < 95% or > 105% of starting value |

Table 3-2: Previous work on bicarbonate stability at -20 ºC

| Paper | mEq/L | Stability |
|---|---|---|
| Sayre, 2012 (216) | 100 | 21 days |
| Sayre, 2012 (216) | 150 | 21 days |

Table 3-3: Previous work on bicarbonate stability at 4 ºC

| Paper | mEq/L | Stability |
|---|---|---|
| Wear, 2010 (213) | 50 | ≥ 7 days |
| Wear, 2010 (213) | 100 | ≥ 7 days |
| Sayre, 2012 (216) | 100 | 21 days |
| Wear, 2010 (213) | 150 | ≥ 7 days |
| Sayre, 2012 (216) | 150 | 21 days |

Table 3-4: Previous work on bicarbonate stability at room temperature

| Paper | mEq/L | Stability |
|---|---|---|
| Hicks, 1972 (215) | 44.5 | 45 days |
| Wear, 2010 (213) | 50 | 48 hours |
| Wear, 2010 (213) | 100 | 30 hours |
| Sayre, 2012 (216) | 100 | 7 days |
| Wear, 2010 (213) | 150 | 30 hours |
| Sayre, 2012 (216) | 150 | 7 days |
| Naorungroj, 2020 (214) | 350-400 | < 48 hours |

#### 3.11.1.2 Methods

We froze 967.2 mEq/L sodium bicarbonate (Centrisol MB-330-L, Minntech) in its original one gallon container at -20 °C. It was thawed while capped, weekly, overnight by air convection. Then it was stirred until fully dissolved. We measured bicarbonate pH for 8 weeks and concentration for 7 weeks (our reagent failed the standard curve test on week 8). Instability was defined as statistically significant ($p < 0.05$) difference from Week 0 measured by a two-sided t-test. pH Measurement was done using the MesaLabs pHoenix XL pH Meter, verified by standard calibration solutions (MesaLabs). Concentration Measurement was done using the Beckman Coulter AU680 spectrophotometer, OSR6237 bicarbonate reagent. Concentration measurement

was verified by a standard curve made from fresh bicarbonate frozen in liquid nitrogen and thawed once directly before measurement. Standard concentrations were 0, 3.71, 6.92, 12.9, 24.1, and 45 mEq/L. Figure 3-24 shows an example standard curve. For concentration measurement, bicarbonate concentrate was diluted 69.8:1500 to ensure that sample concentration was in the chemistry analyzer's linear range. We performed N = 3 technical replicates at each time point.

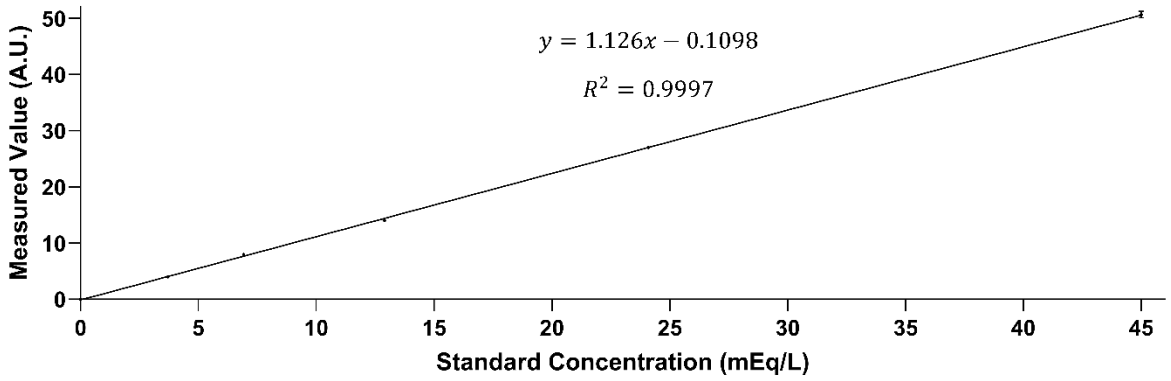


Figure 3-24: Example Bicarbonate Standard Curve. A.U. refers to arbitrary units. Error bars are standard deviation of n = 3 technical replicates. Where error bars are not shown, they would be smaller than the data point on the graph.

#### 3.11.1.3 Results

Bicarbonate concentration and pH were stable across the 8-week study as shown in Figure 3-25 and Figure 3-26. Therefore, we proceeded with storing, freezing, and thawing bicarbonate according to this protocol for our experiments. We switched the freezing temperature to -80 ºC to ensure consistency. Care must be taken to ensure all precipitates dissolve fully before use.

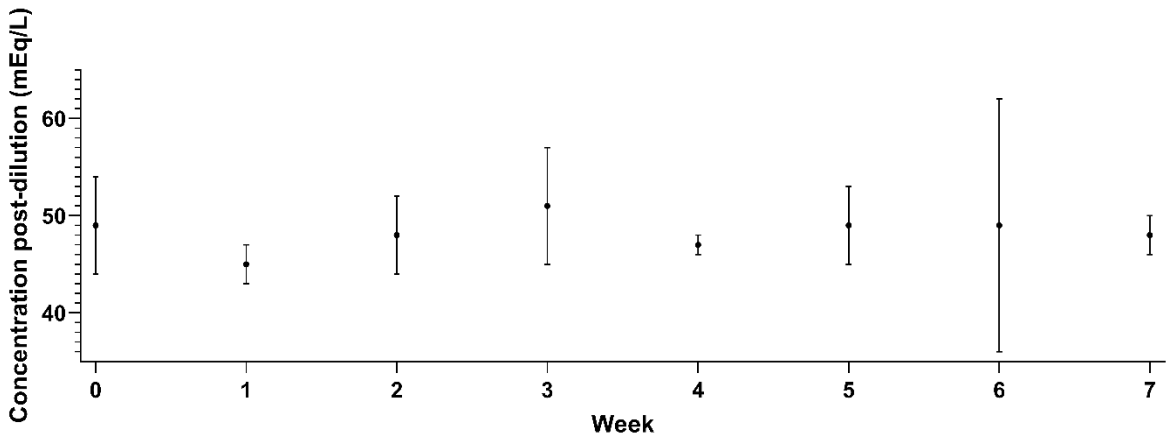


Figure 3-25: Bicarbonate concentration does not undergo a statistically significant change over 7 weeks storage at -20 ºC and 7 freeze-thaw cycles. Error bars are standard deviation.

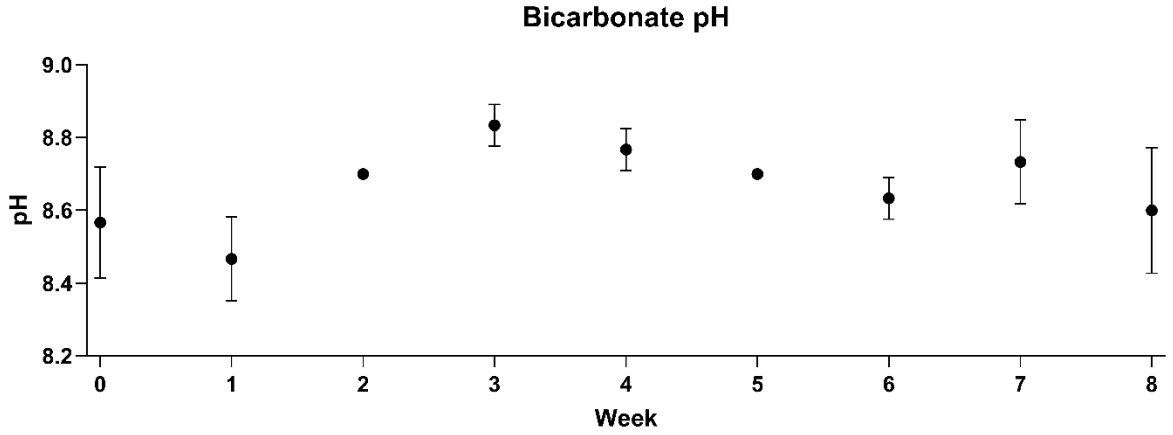


Figure 3-26: Bicarbonate concentrate pH does not undergo a statistically significant change over 8 weeks storage at -20 ºC and 8 freeze-thaw cycles. Error bars are standard deviation. Where error bars are not shown, all three pH replicates were identical.

# Chapter 4. HYDRAULIC PERMEABILITY MEASUREMENT

## 4.1 INTRODUCTION

Hydraulic permeability relates the volume flux density across the dialysis membrane to the pressure differential across the membrane (217). Volume flux density measures the volume of fluid transported across the membrane per unit area, per unit time. Hydraulic permeability has been used to characterize dialyzer membranes since the early history of renal dialysis innovation.

It depends on the material the membrane is made from, but also on the membrane thickness, porosity, and pore radius. It could also be influenced by factors such as temperature. Hydraulic permeability appears in the equations characterizing protein bound toxin removal by dialysate with added binder described in Chapter 2. Thus, measuring it in relevant conditions is a prerequisite for making testable predictions of protein bound toxin removal.

## 4.2 METHODS

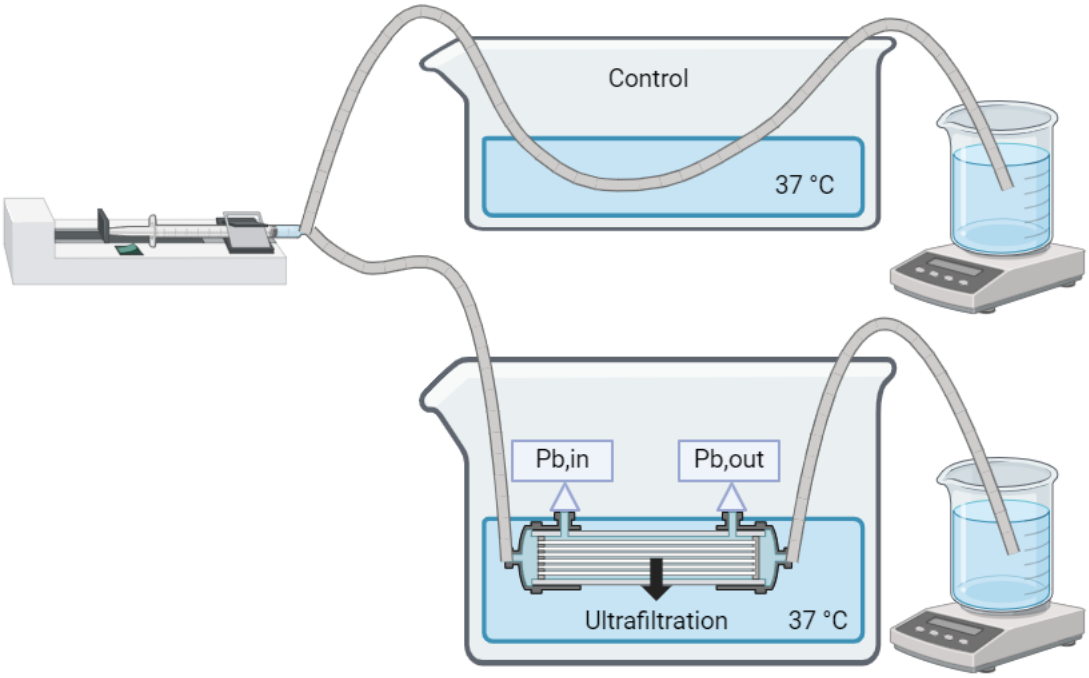


Figure 4-1: Hydraulic Permeability Test Setup. Figure created with BioRender.

Polysulfone membrane hydraulic permeability was measured by a method based on the work of Liao et al (218), with some modification. A small dialyzer, called a "mini-module" was created out of individual F6HPS dialyzer fibers in a custom-made casing. Figure 4-1 shows the test setup. The formula for hydraulic permeability was:

$$L_p = \frac{\Delta V/\Delta t}{P*A}$$ (Equation 4-1)

$\Delta V$ refers to the ultrafiltration volume. $\Delta t$ is the time. A is the total area of the dialysis membrane in the mini-module. Here, pressure is calculated as:

$$P = \frac{P_{b,in}+P_{b,out}}{2} - \frac{P_{d,in}+P_{d,out}}{2}$$ (Equation 4-2)

In this formula, $P_{b,in}$ is the inlet blood pressure and $P_{b,out}$ is the outlet blood pressure. $P_{d,in}$ and $P_{d,out}$ are the corresponding dialysate pressures. Since the module is near the surface of a stirred water bath (Figure 4-1), these pressures are equal and negligible.

Mini-modules were constructed out of F6HPS dialyzer polysulfone fibers. Fibers were carefully selected to be straight, to avoid any damage or kinking. Two mini-modules were constructed (designated F6HPS and F6HPS2). They were then bundled together in a fitting using Gorilla Epoxy (Gorilla Glue, Cincinnati, OH, USA). Each mini-module used 10 fibers. Its total area was 9.42 $cm^2$. Fibers were 0.15 m long, with a 100 µm inner radius and a 140 µm outer radius.

A neMESYS Low Pressure Syringe Pump (Cetoni, Korbussen, Germany) was used to set precise flow rate. Pressure on the inlet and outlet of the mini-module was measured using PX409-USBH sensors (Omega Engineering, Norwalk, CT, USA). Mini-modules were immersed in a 37 °C water bath. Heating, stirring, and temperature control was provided using hotplates, K-type thermocouples, and a data acquisition unit (DAQ). Hot plates were from Corning (Glendale, AZ, USA), with model numbers PC-420, and PC-420D. K-type thermocouples were from MN Measurement Instruments (St. Paul, MN, USA). The DAQ was from Measurement Computing (Norton, MA, USA). Flow through the mini-module was compared to flow through a control tube. The difference was the ultrafiltration rate $\Delta V$. Following Liao et al (218), flow rates of 1910 $\frac{\mu L}{min}$, 764 $\frac{\mu L}{min}$, and 191 $\frac{\mu L}{min}$ were tested for both mini-modules. One of the 191 $\frac{\mu L}{min}$ tests was an extreme outlier, so it was repeated, and 382 $\frac{\mu L}{min}$ was also tested for that mini-module. These additional tests did not replicate the outlier value, so the outlier value was then discarded.

## 4.3 RESULTS

Hydraulic permeability was measured as $8.61*10^{-11}$ m/(s*Pa) ± 2.14 * $10^{-11}$ m/(s*Pa) (average ± standard deviation). This measurement was used for subsequent modeling. This is much lower than the value obtained by Liao et al for polysulfone of $1.628*10^{-9}$ m/(s*Pa) (218). However, it is comparable to the value obtained by Benavente and Jonsson of $10^{-10}$ m/(s*Pa) (219). Hydraulic permeability test raw data is reported in Table 4-1. The discarded outlier test is highlighted in yellow. Averages and standard deviations are reported in Table 4-2.

Table 4-1: Hydraulic Permeability Measurements from Individual Trials. Lp refers to hydraulic permeability. $P_{b,in}$ refers to blood side (luminal) inlet pressure. $P_{b,out}$ refers to blood side outlet pressure. Delta V refers to the change in volume.

| Lp (m/s*Pa) | Mini-Module | Flow Rate (uL/min) | $P_{b,in}$ (cm H2O) | $P_{b,out}$ (cm H2O) | Delta V (mL) | Time (min) |
|---|---|---|---|---|---|---|
| 1.013E-10 | F6HPS2 | 1910 | 209.7 | 3.94 | 0.628 | 10.5 |
| 1.020E-10 | F6HPS2 | 764 | 65.139 | 2.615 | 0.383 | 20 |
| 9.601E-11 | F6HPS2 | 382 | 35.828 | 2.58 | 0.409 | 40 |
| 2.768E-11 | F6HPS2 | 191 | 19.76 | 4.162 | 0.11 | 60 |
| 8.851E-11 | F6HPS2 | 191 | 21.127 | 2.904 | 0.473 | 80 |
| 9.750E-11 | F6HPS | 1910 | 531.57 | 3.726 | 1.45 | 10 |
| 7.463E-11 | F6HPS | 764 | 269.35 | 1.955 | 1.122 | 20 |
| 4.257E-11 | F6HPS | 191 | 50.8 | 4.507 | 0.522 | 80 |

Table 4-2: Average and standard deviation hydraulic permeability values for both mini-modules and overall.

| Mini-Module | Average Lp (m/s*Pa) | Standard Deviation (m/s*Pa) |
|---|---|---|
| F6HPS | 7.157E-11 | 2.75928E-11 |
| F6HPS2 | 9.696E-11 | 6.233E-12 |
| Total | 8.61E-11 | 2.14E-11 |

# Chapter 5. OPTIMIZING ALBUMIN DIALYSIS PART 1: PREDICTING IMPACT OF POLYSULFONE DIALYZER SELECTION AND DIALYSATE FLOW RATE

## 5.1 THEORY

Patient size and dialysis disequilibrium syndrome constrain dialyzer size. A larger dialyzer provides a greater membrane surface area, increasing toxin removal. However, for patients who cannot tolerate a large increase in blood volume, smaller dialyzers are needed (164). This is particularly common in children, hence why such dialyzers are often termed “pediatric dialyzers”. In addition, smaller dialyzers may be used to prevent dialysis disequilibrium syndrome (220). Dialysis disequilibrium syndrome is believed to occur when blood concentration of urea and other solutes drops significantly below the concentration in cerebro-spinal fluid (CSF). This causes an osmotic pressure gradient favoring water movement into the central nervous system, raising intracranial pressure. This causes symptoms that range from restlessness and headaches to coma and death. Thus, in some patients, slower initial toxin removal with a smaller dialyzer is preferred.

Similar tradeoffs typically govern flow rate. Higher blood flow rates allow a greater fraction of the blood to contact the membrane, but vascular access, blood volume, and cardiac output limit acceptable blood flow rates. Higher dialysate flow rates may improve the concentration gradient for toxin removal. In dialysis without recirculation, the cost of increasing dialysate flow rate is that a larger dialysate volume is used. When recirculation is used, such as in MARS or AMOR, increasing dialysate flow rate increases dialyzer inlet pressure. Pressure in the extracorporeal circuit must be managed in recirculating dialysis.

These considerations make it valuable to predict the impact of dialyzer selection and flow rate on toxin removal in binder dialysis. This will enable the selection of optimal conditions for individual patients and optimal device designs and uniform clinical trial parameters.

## 5.2 Modeling Flow Rate Effects

Two hypotheses were considered. First, the model described in Chapter 2 was implemented. Under this hypothesis, dialysate side flow rate impacts the residence time of toxin and binder (albumin) within the dialyzer, and thus the amount removed in a single pass through the dialyzer. It also impacts ultrafiltration and backfiltration. However, other parameters, such as the membrane transfer coefficient for free toxin are assumed to be independent of flow rate. Second, a model was implemented that simulated a linear decline in membrane transfer coefficient as dialysate flow rate declined. This was based on previous work on urea, which demonstrated that $K_0A_{urea}$ declined with flow rate, because urea removal at low flow rates was lower than would be predicted based on fluid mechanics alone (221). This is predicted to occur because slower flow rates increase the resistance of the boundary layer which forms on the dialysate side due to fluid viscosity. This process was described by the following formula:

$$K_{free}A = K_{free}A_{Qd=500}\left(1 + \beta_{Q_d} * \frac{Q_{d,0}-500*UCF}{300*UCF}\right)$$ (Equation 5-1, Hypothetical impact of flow rate on membrane transfer coefficient, based on Equation 4 in (221))

Here, $K_{free}A_{Qd=500}$ is the theoretical mass transfer-area coefficient of unbound biirubin diffusive transport at 500 mL/min. $\beta_{Q_d}$ is the percentage change in this coefficient from 800 to 500 mL/min. It was set to 0.05544 during parameter fitting following past work on urea (221). UCF is a unit conversion factor. As an approximation, the adjustment is performed using the dialysate inlet and outlet flow rate $Q_{d,0}$ instead of the local dialysate flow rate $Q_d$. Modifying this equation

and the governing equations of the model to account for the impact of local ultrafiltration on local $K_{free}A$ is planned in future work. To recover the model in Chapter 2, we simulated $\beta_{Q_d} = 0$.

### 5.2.1 *Step Size Sensitivity Test*

To verify that the model used a sufficiently fine mesh, tests were performed in which the maximum step size was decreased. The maximum step size along the z axis had been set to 1 mm for all modeling. A step size of 0.1 mm was tested, and the results were compared. In time, a maximum step size of 100 seconds was set for all modeling. A maximum step size of 10 seconds was tested for comparison.

### 5.2.2 *Parameter Sweep Protocol*

Parameter sweeps were conducted on the University of Washington's Hyak Supercomputer. Goodness of fit was analyzed by minimizing the sum of squares (goodness of fit to the entire solution) or by minimizing the percent error at the end of the trial (goodness of fit to the equilibrium toxin concentration). The two criteria are shown in Equation 5-2 and Equation 5-3 respectively. Here, t is time during the trial. $t_{end}$ is the time at the end of the trial. $C_{true}$ is the measured concentration. $C_{model}$ is the concentration predicted by the model. i is an index that varies from 1 to n where n is the number of time points.

$$Error = \sum_{i=1}^{n}\left(C_{model}(t = t_i) - C_{true}(t = t_i)\right)^2$$ (Equation 5-2, Sum of Squares Goodness of Fit Criterion)

$$Error = \frac{\left(C_{model}(t=t_{end}) - C_{true}(t=t_{end})\right) * 100\%}{C_{true}(t=t_{end})}$$ (Equation 5-3, Percent Error Goodness of Fit Criterion)

Three parameters were fit computationally rather than being determined from the literature. The first two were fit based only on F6HPS data at a single flow rate and used to predict the results

for other conditions. These were $K_B$ and $K_{free}A_{Qd=500}$. The last parameter was initially set based on prior work, then updated once data for the F3 dialyzer at all dialysate flow rates was collected. This was $\beta_{Q_d}$. The first parameter is the primary binding constant for a particular toxin to BSA. The second is the hypothetical membrane area mass transfer coefficient at a 500 mL/min dialysate flow rate. Thie final parameter is the dependency, if any, of membrane area mass transfer coefficient on dialysate side flow rate.

We conducted a literature search regarding bilirubin-BSA binding. This parameter depends on conditions such as salt concentration, temperature, and pH (222,223). No existing measurement of this parameter was conducted in dialysate at 37 °C so the best available option is to approximate based on reported values under similar conditions and fitting to a test condition. All values for this parameter fall within a narrow range (Table 5-1). The primary binding site of bilirubin on BSA has approximately an order of magnitude greater affinity than the secondary binding site (224). Thus, the secondary binding site was neglected for this analysis. The constant for the primary binding site was fit. The lower bound of the search space was set to 0.5E7 (1/M). The upper bound was set to 7.5E7 (1/M). The space was searched in steps of 1E7 (1/M).

Table 5-1: Reported values of bilirubin-BSA binding constant

| Study | Primary Bilirubin-BSA Binding Constant (1/M) | Temperature (ºC) | Solution | pH |
|---|---|---|---|---|
| Chen, 1973 (224) | 2.2E7 | 25 | 0.1 M potassium phosphate buffer | 7.4 |
| Faerch and Jacobsen, 1974 (225) | 2.7E7 | 37 | 67 mM phosphate buffer | 7.4 |
| Rubaltelli and Jori, 1979 (226) | 2.16E7 | 19 | 0.5 M $KH_2PO4$-$Na_2HPO4$ buffer | 7.4 |
| Muzaffar et al, 1991 (227) | 1.05E7 | 30 | Tris-HCl buffer | 8.0 |
| Williams et al, 2002 (228) | 1.2E7 | Room Temperature | 0.125 M phosphate buffer | 7.4 |
| Chen et al, 2007 (229) by fluorescence enhancement | 6.57E7 | Not given | Double-distilled water | Not given |
| Chen et al, 2007 (229) by fluorescence quenching | 4.34E7 | Not given | Double-distilled water | Not given |

The second fit parameter was the product of the dialyzer mass transfer-area coefficient for free bilirubin diffusion and area at a dialysate flow rate of 500 mL/min ($K_{free}A_{Qd=500,Bilirubin}$). This parameter varies between different dialyzers, different toxins, and different flow conditions (221). Thus, it must be fit to experimental data for the specific toxin-dialyzer combination The highest value of this coefficient reported in the literature is 2000 mL/min, discussed by Meyer et al (165). Thus, this parameter was optimized over the range from 100 to 2500 mL/min in steps of 100 mL/min. This range is chosen because it encompasses the range typically reported for dialyzer membranes (230).

Afterwards, $K_{free}A_{Qd=500}$was adjusted to account for a new dialyzer following Equation 5-4. Because the F3 and F6HPS dialyzers are both polysulfone, it was assumed that area was the only adjustment needed, meaning the two dialyzers had the same value of $K_{free}$.

$$K_{free}A_{New,Qd=500} = K_{free}A_{Old,Qd=500} * \frac{A_{new}}{A_{old}} \text{ (Equation 5-4)}$$

The final fit parameter was the difference in $K_{free}A$ between 500 and 800 mL/min ($\beta_{Q_d}$). This parameter was initially set to 0.05544 based on past work on urea (221). This variation is proposed to occur because of boundary layer effects. Once the results for different flow conditions were found, a parameter sweep of this value was conducted. The lower bound of this parameter sweep was 0, which represents the assumption that $K_{free}A$ is independent of dialysate side flow rate. The upper value was calculated as 0.6, since this is the value at which $K_{free}A(Q_d = 0) = 0$ mL/min. Values greater than this are not physically meaningful since $K_{free}A$ cannot be negative.

The binding constant of cholic acid to BSA was also fit using a parameter sweep. The cholic acid-BSA binding constant is reported to range from 0.9E4 to 6.8E4 (Table 5-2). Thus, we searched parameter values from 0.5E4 (1/M) to 7.5E4 (1/M) in steps of 0.5E4 (1/M).

Table 5-2: Reported values of cholic acid-BSA binding constant

| Study | Primary Cholic Acid-BSA Binding Constant (1/M) | Temperature (ºC) | Solution | pH |
|---|---|---|---|---|
| Pico and Houssier, 1989 (231) | 6.8E4 | 20 ºC | 20 mM phosphate buffer | 7.4 |
| Pico, 1990 (232) | 1.6E4 | 20 ºC | 20 mM phosphate buffer | 7.4 |
| Farrugia and Pico, 1992 (233) | 6.4E4 | 20 ºC | 20 mM phosphate buffer | 7.4 |
| Farrugia and Pico, 1992 (234) | 1.2E4 | 20 ºC | 15 mM phosphate buffer | 5 |
| Farrugia and Pico, 1992 (234) | 9.3E3 | 20 ºC | 15 mM phosphate buffer | 6 |
| Farrugia and Pico, 1992 (234) | 9.5E3 | 20 ºC | 15 mM phosphate buffer | 7 |
| Farrugia and Pico, 1992 (234) | 1.0E4 | 20 ºC | 15 mM phosphate buffer | 8 |
| Farrugia and Pico, 1992 (234) | 1.3E4 | 20 ºC | 15 mM phosphate buffer | 9 |
| Farrugia and Pico, 1992 (234) | 1.9E4 | 20 ºC | 15 mM phosphate buffer | 10 |

The dialyzer diffusive mass transfer area coefficient for free cholic acid is denoted $K_{free}A_{Qd=500,Cholic\ Acid}$. It was varied from 10 to 250 mL/min in steps of 10 mL/min. Larger values were tested, but did not produce good fits to the experimental results (data not shown).

The binding constant of indoxyl sulfate to BSA was also fit using a parameter sweep. Literature values are listed in Table 5-3. We searched a range from 1E3 (1/M) to 1E5.7 (1/M) in equally spaced logarithmic steps. This means we searched a range of 10^(3:0.1:5.7).

Table 5-3: Reported values of indoxyl sulfate-BSA binding constant

| Study | Primary Indoxyl Sulfate-BSA Binding Constant (1/M) | Temperature (ºC) | Solution | pH |
|---|---|---|---|---|
| Davilas, 2006 (235) | 3125 | 25 | 100 mM sodium phosphate buffer | 7.4 |
| Moschen, 2016 (236) | 3.33E5 | 25 | 50 mM potassium phosphate buffer | 5.8 |

The dialyzer diffusive mass transfer area coefficient for free indoxyl sulfate was denoted $K_{free}A_{Qd=500,indoxyl\ sulfate}$. It was varied from 100 to 1500 mL/min in steps of 100 mL/min.

The binding constant of $Cu^{2+}$ to BSA was studied. Cu binding to BSA depends on the reduction/oxidation state of Cysteine 34 on the BSA protein (237). Reported values are shown in Table 5-4. The range of reported copper-BSA binding constants spans fifteen orders of magnitude, from E3 (1/M) to E17 (1/M). We searched this parameter space in equally spaced logarithmic steps. This means we searched a range of 10^(3:0.5:17). The dialyzer diffusive mass transfer area coefficient for free copper was denoted $K_{free}A_{Qd=500,Copper}$.

Table 5-4: Reported values of $Cu^{2+}$-BSA binding constant

| Study | Primary Copper-BSA Binding Constant (1/M) | Temperature (ºC) | Solution | pH |
|---|---|---|---|---|
| Singh, 2017 (238) | 5.76E5 | 26.85 | 20 mM Tris | 7.4 |
| Singh, 2017 (238) | 2.34E4 | 64.85 | 20 mM Tris | 7.4 |
| Arnquist, 2012 (239) | 3.98E17 | 4 | 100 mM Tris | 9.53 |
| Arnquist, 2012 (239) | 3.98E14 | 4 | 100 mM Tris | 7.93 |
| Zhang, 2002 (237), reduced BSA | 3.89E14 | 25 | 100 mM borate and 100 mM Tris buffer with 20 mM NaCl | 9.2 |
| Zhang, 2002 (237), oxidized BSA | 2.75E15 | 25 | 100 mM borate and 100 mM Tris buffer with 20 mM NaCl | 9.2 |
| Zhang, 2000 (240) | 1.06E7 | 25 | 100 mM Tris | 9.1 |
| Liang, 1998 (241) | 2.35E4 | 20 ± 0.5 | 0.1 M NaCl, 0.1 M Tris-HCl | 7.43 |
| Sommer-Knudsen, 1997 (242) | 3.6E15 | N/A | MES-Buffer | 6.0 |
| Masuoka, 1993 (243) | 1.32E11 | 4 | 250 mM NaCl, 30 mM Hepes Buffer | 7 |
| Zgirski, 1990 | 1E12-1E13 | 25 ± 2 | 30 mM barbital buffer, 150 mM NaCl (244) | 7.4 |
| Syvertsen, 1986 (245) | 3.98E12 | 23 | 20-50 mM Bistris, 0.1 $KNO_3$ | 7.3 |
| Syvertsen, 1986 (245) | 1.58E13 | 23 | 20-50 mM Hepes, 0.1 $KNO_3$ | 7.3 |
| Syvertsen, 1986 (245) | 1.58E11 | 23 | 20-50 mM acetate, 0.1 $KNO_3$ | 5.9 |
| Giroux and Schoun, 1981 (246) | 1.58E13 | N/A | 4 mg/mL of 0.05 M morpho-linoproane sulfonic acid | 7.5 |
| Ryall, 1974 (247) | 1.1E12 | 37 | 0.1 M Potassium Nitrate, 0.05 M Hepes | 7.4 |
| Rao and Lal, 1958 (248) | 7.59E4 | 25 | Acetate buffer, ionic strength 0.2 | 6.5 |
| Tanford, 1952 (249) | 5.01E3 | 25 | 0.15 Potassium Chloride | 4.96 |
| Klotz and Curme, 1948 (250), calculated in Masuoka, 1993 (243) | 2.00E4 | 25 | 0.0357 M acetic acid. 0.0643 M sodium acetate. | 4.83 |

## 5.3 Albumin Dialysis Setup

### 5.3.1 *Experimental Setups*

Six sets of experiments were done in total:

- Condition 1: A pilot study (n = 3) using Bovine Serum Albumin (BSA) on both sides of an F6HPS dialyzer (Fresenius, Waltham, MA, USA) with blood and dialysate flow rates of $Q_b = 180$ mL/min and $Q_d = 90$ mL/min. This was used to fit two parameters:
    - 1: The dialyzer mass transfer coefficient for free toxin moving through polysulfone ($K_{free}A_{Qd=500}$)
    - 2: The toxin binding equilibrium constant for the primary binding site on BSA (kB,BSA)
- Condition 2: A validation data set (n = 3) using BSA on both sides of an F3 dialyzer (Fresenius, Waltham, MA, USA) with blood and dialysate flow rates of 150 mL/min
- Condition 3: A test data set (n = 3), like condition 2, but with the dialysate flow rate set to 20 mL/min, as previously described in a pilot study of AMOR (2)
- Condition 4: A test data set (n = 3), like condition 2, but with the dialysate flow rate set at 800 mL/min, which is the highest flow rate identified in clinical practice (251)
- Condition 5: A test data set (n = 3), like condition 2, but with the dialysate flow rate set at 2 mL/min, which is relevant in some neonatal dialysis applications (252)
    - The parameter $\beta_{Q_d}$ which measures the dependence of transmembrane toxin transport on flow rate was fit once all five conditions were analyzed.
- Condition 6: A negative control (n = 3), like condition 2, but with no albumin on the dialysate side.

The setups are summarized in Table 5-5. The F6HPS trials (setup 1) was used to set model parameters. These were the toxin binding affinity for albumin, and the dialyzer mass transfer-area coefficient for free bilirubin diffusion at 500 mL/min dialysate flow rate ($K_{free}A_{Qd=500}$). The F3 trials were used to independently validate model predictions. The $K_{free}A$ value was adjusted between the two dialyzers (see Section 5.4.1.5). Flow rate was set using Masterflex Pumps with model numbers 07551-20 and 77521-40, using Easy-Load II Rotors with Model Number 772990-62 (Cole-Parmer, East Bunker, CT, USA) except for the 2 mL/min trial, in which an Ismatec 78017-10 (IDEX Corporation, Northbrook, IL, USA) pump was used on the dialysate side. Pressure was controlled using four RSCDRRE015PGSE3 pressure sensors (Honeywell International Inc, Charlotte, NC, USA) to prevent ultrafiltration, except in the 800 mL/min trial, where more robust PS04-G100KP-A4W pressure sensors (CUI Devices, Lake Oswego, OR, USA) were used. Data from Honeywell pressure sensors were obtained using a Raspberry Pi 3B (Raspberry Pi, Cambridge, England, UK). CUI Devices pressure sensor readings were processed using an HX711 (Sparkfun, Niwot, CO, USA) connected to an Arduino Uno (Arduino SA, Chiasso, Switzerland). Pressure was adjusted using c-clamps. The blood and dialysate reservoirs were immersed in a 37 °C water bath (Benchmark, Sayreville, NJ), except in Setup 1. There, temperature was measured by K type thermocouples connected to a Measurement Advantage DAQ and maintained between 35 and 40 °C on both sides using hotplates. Hotplates were from Corning (Glendale, AZ, USA), with model numbers PC-420, and PC-420D. K-type thermocouples were from MN Measurement Instruments (St. Paul, MN, USA). The DAQ was from Measurement Computing (Norton, MA, USA). Figure 5-1 shows diagrams of the circuits for each setup.

Table 5-5: Albumin Dialysis Setups Used in This Study

| | Setup 1 | Setups 2-5 | Setup 6 |
|---|---|---|---|
| Duration (hr) | 3 | 5 | 5 |
| Blood Analog Solution Volume (mL) | 628.33 | 200 | 200 |
| Dialysate Volume (mL) | 626.67 | 200 | 200 |
| Blood flow rate (mL/min) | 180 | 150 | 150 |
| Dialysate flow rate (mL/min) | 90 | 2, 20, 150, 800 | 150 |
| Ultrafiltration rate (mL/min) | 0 | 0 | 0 |
| Blood Albumin Concentration (g/dL) | 2 | 2 | 2 |
| Dialysate Albumin Concentration (g/dL) | 2 | 2 | 0 |
| Blood Albumin | BSA | BSA | BSA |
| Dialysate Albumin | BSA | BSA | NA |
| Dialyzer | F6HPS | F3 | F3 |
| Material | Polysulfone | Polysulfone | Polysulfone |
| Number of Fibers | 8400 (253) | 2304 (253) | 2304 (253) |
| Hollow Fiber Inner Radius (μm) | 100 (254) | 100 (255) | 100 (255) |
| Hollow Fiber Outer Radius (μm) | 140 (254) | 140 (256) | 140 (256) |
| Hollow Fiber Length (cm) | 21 (257) | 20 (255) | 20 (255) |
| Area ($m^2$) | 1.3 (254) | 0.4 (255) | 0.4 (255) |
| Housing Inner Radius (mm) | 20 (254) | 11 (measured) | 11 (measured) |
| Bilirubin Reflection Coefficient (assumed (158)) | 0 | 0 | 0 |
| Reflection Coefficients for Other Toxins (Assumed) | 0 | 0 | 0 |

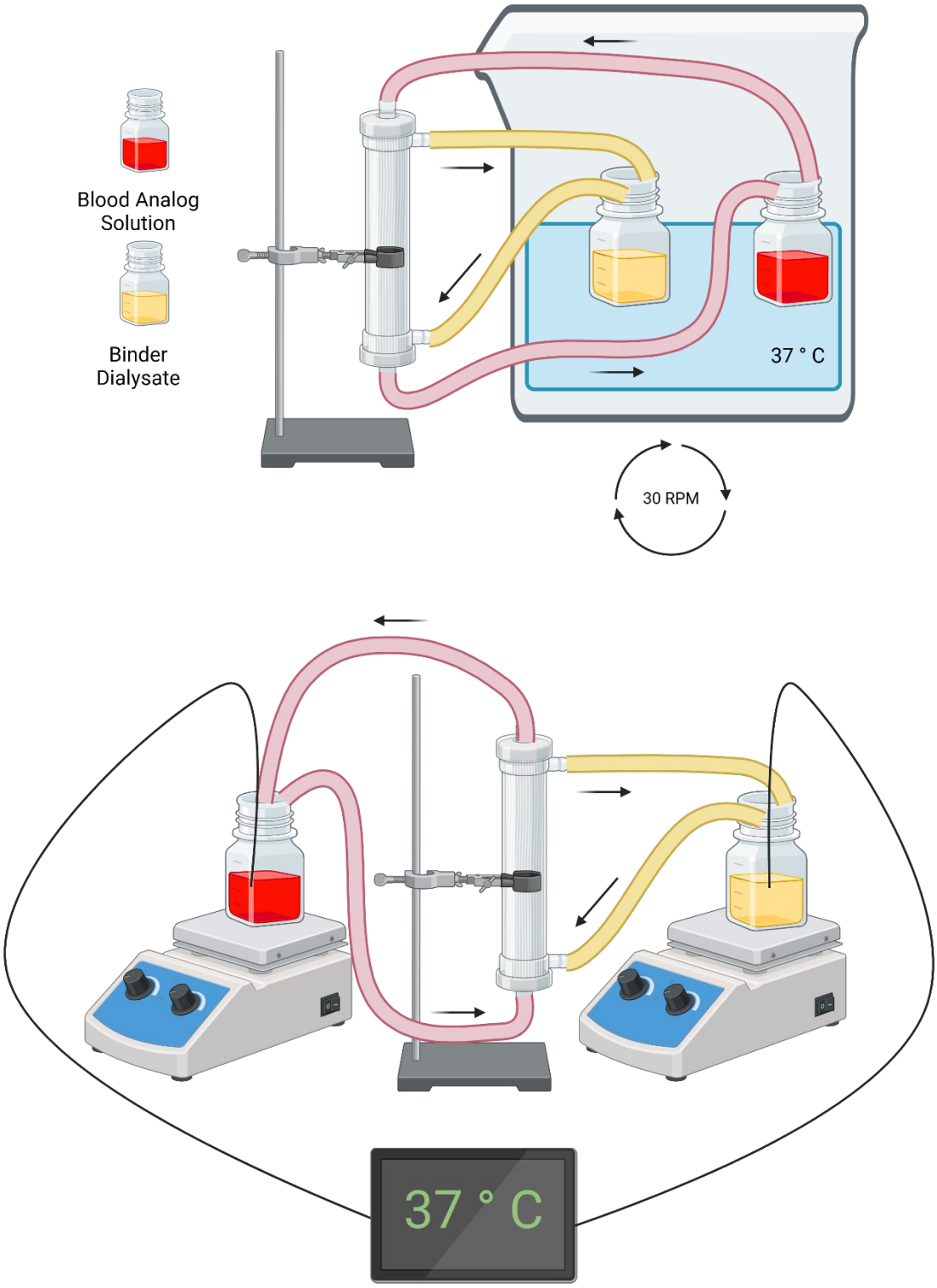


Figure 5-1: Experimental setup for conditions 2-6 (top) and condition 1 (bottom). Figure created in BioRender.

### 5.3.2 *Blood analog solution*

Blood side solution contained BSA, bilirubin, cholic acid, creatinine, indoxyl sulfate, copper, and manganese dissolved in dialysate. Solute concentrations, along with references supporting their clinical relevance, are listed in Table 5-6. pH on the blood and dialysate side was maintained between 7.35 and 7.45 using a pH Meter (OrionStar A211, Thermo Scientific, Waltham, MA), except in Setup 1, where the pH was maintained between 7.2 and 7.5 using the less precise pHoenix XL meter from MesaLabs. For Setup 1, pH in this was initially set at 7.2 ± 0.1 following previous work on protein bound toxin removal (158). Acidosis is common in CKD patients (258,259). However, pH values below 7.3 are unusual. Acknowledging this, later trials used a pH set point for Setup 1 of 7.4 ± 0.1. In all setups, pH adjustment was done using 1 N HCl and NaOH. In all setups care was taken to protect the setup from light to minimize photodegradation of bilirubin. For Setup 1, dialyzers were reused after being cleaned according to established clinical protocols (260,261).

Table 5-6: Toxin concentrations in blood analog solution. *: Except Setup 1 (see Table 5-5), where it was 2 mg/dL.

| Solute | Concentration |
|---|---|
| BSA | 2 g/dL (13) |
| Bilirubin | 20 mg/dL (183,184) |
| Cholic Acid | 19.3 µM (190) |
| Creatinine | 15 mg/dL (201) |
| Indoxyl Sulfate | 4 mg/dL (19)* |
| Copper | 21.56 µM (197) |
| Manganese | 2.5 µM (197) |

### 5.3.3 *Statistical Method for Comparison with Negative Control*

Unless otherwise noted, comparisons were done using the unpaired two-tailed Student's t-test without assuming equal variance. Calculations were done in Microsoft Excel. A $p < 0.05$ was

considered statistically significant. For albumin dialysis trials, percent of solute removed was calculated as follows (Equation 5-5):

$$\%\ Removed(t) = 100\% * \frac{C_i - C(t=5)}{C_i} \text{ (Equation 5-5)}$$

$C_i$ is the solute concentration at time 0. C (t = 5) is the solute concentration at time t = 5 hours. The concentration at the dialyzer inlet is used. Unlike in our past publication (2), the concentration is reported as toxin per albumin (mg/g) instead of toxin per deciliter (mg/dL) to enable consistency with other analysis and the computational model described in Chapter 2.

## 5.4 Bilirubin Removal

### 5.4.1 *Results*

#### 5.4.1.1 Initial Values for Modeling

Table 5-7 summarizes measured average starting bilirubin and albumin concentrations for all six setups. These values were used for modeling to avoid error caused by variations in the initial solution composition.

Table 5-7: Average Initial Bilirubin and Albumin Concentration. N = 3 for all conditions. Values are shown as mean ± standard deviation.

| Condition | Starting Blood Bilirubin (mg/dL) | Starting Blood Albumin (g/dL) | Starting Dialysate Albumin (g/dL) |
|---|---|---|---|
| 1 (F6HPS, *Qb* = 180 mL/min, *Qd* = 90 mL/min) | 15.37 ± 3.06 | 2.24 ± 0.37 | 1.77 ± 0.41 |
| 2 (F3, *Qb* = *Qd* = 150 mL/min) | 18.81 ± 2.84 | 1.90 ± 0.07 | 1.94 ± 0.23 |
| 3 (F3, *Qb* = 150 mL/min, *Qd* = 20 mL/min) | 16.76 ± 2.35 | 2.13 ± 0.12 | 2.29 ± 0.13 |
| 4 (F3, *Qb* = 150 mL/min, *Qd* = 800 mL/min) | 18.28 ± 0.43 | 2.03 ± 0.02 | 2.10 ± 0.04 |
| 5 (F3, *Qb* = 150 mL/min, *Qd* = 2 mL/min) | 17.36 ± 1.94 | 2.15 ± 0.22 | 2.21 ± 0.14 |
| 6 (F3, Negative Control, *Qb* = *Qd* = 150 mL/min) | 15.27 ± 1.14 | 1.97 ± 0.09 | 0 |

#### 5.4.1.2 Step Size Sensitivity Test

The impact of reducing the maximum spatial step on bilirubin modeling was minimal. We compared results for all five conditions when the step size was set to 1 mm or 0.1 mm or when the maximum time step was decreased from 100 seconds to 10 seconds. The largest difference was a 0.032% change for condition 4, when the spatial step size was decreased. This demonstrates that the mesh applied was sufficiently fine to prevent errors due to discretization. For subsequent cholic acid, indoxyl sulfate, and copper modeling, step sizes were reduced to 0.1 mm and 10 seconds, respectively, due to greater numerical instability (model non-convergence) than was seen with bilirubin.

#### 5.4.1.3 Comparison with Negative Control

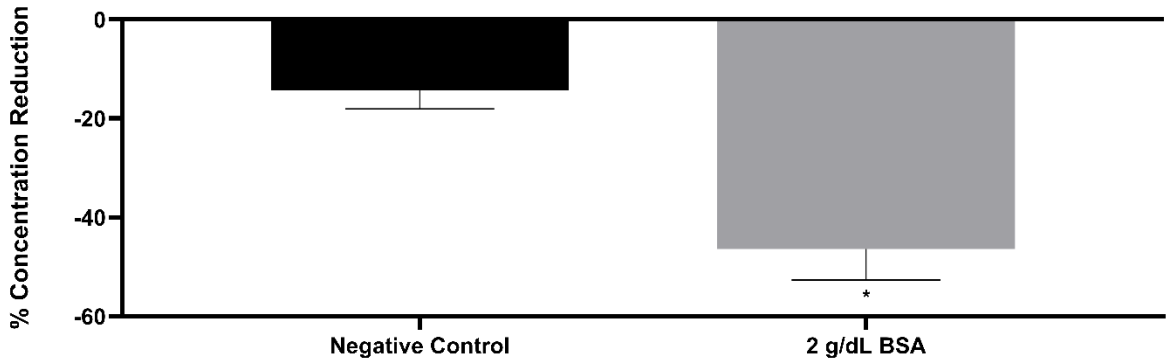


Figure 5-2: Percentage of bilirubin removed from blood side to dialysate over 5 hours. The negative control is dialysate without BSA. N = 3. The * indicates BSA dialysis removed significantly more bilirubin than dialysate without BSA ($p = 0.003$). Values are mean ± standard deviation.

*In vitro* testing showed that albumin dialysate successfully removes bilirubin. Figure 5-2 shows that bilirubin removal was significantly greater in condition 2 than in the control ($p = 0.003$, $n = 3$). In the negative control, the bilirubin concentration (mg/g) declined on average 14.0% while in condition 2, the average concentration decline was 46.4%.

5.4.1.4 $K_{free}A$ and kB Parameter Sweep:

The optimal values of kB,BSA and $K_{free}A_{Qd=500}$ for bilirubin removal Setup 1 were found to be kB,BSA = 0.5E7 (1/M) and $K_{free}A_{Qd=500}$ = 2500 mL/min. This result was not sensitive to changing the number of fibers from n = 8400 provided by Fresenius to n = 9200 from the work of Eloot et al (254). The impact of this change was -0.018%. The results are shown in Figure 5-3. Panel A shows the parameter sweep results for the sum of squares criterion. Panel B shows the parameter sweep results for the percent error criterion. Figure 5-4 shows the model prediction compared to the true measurements.

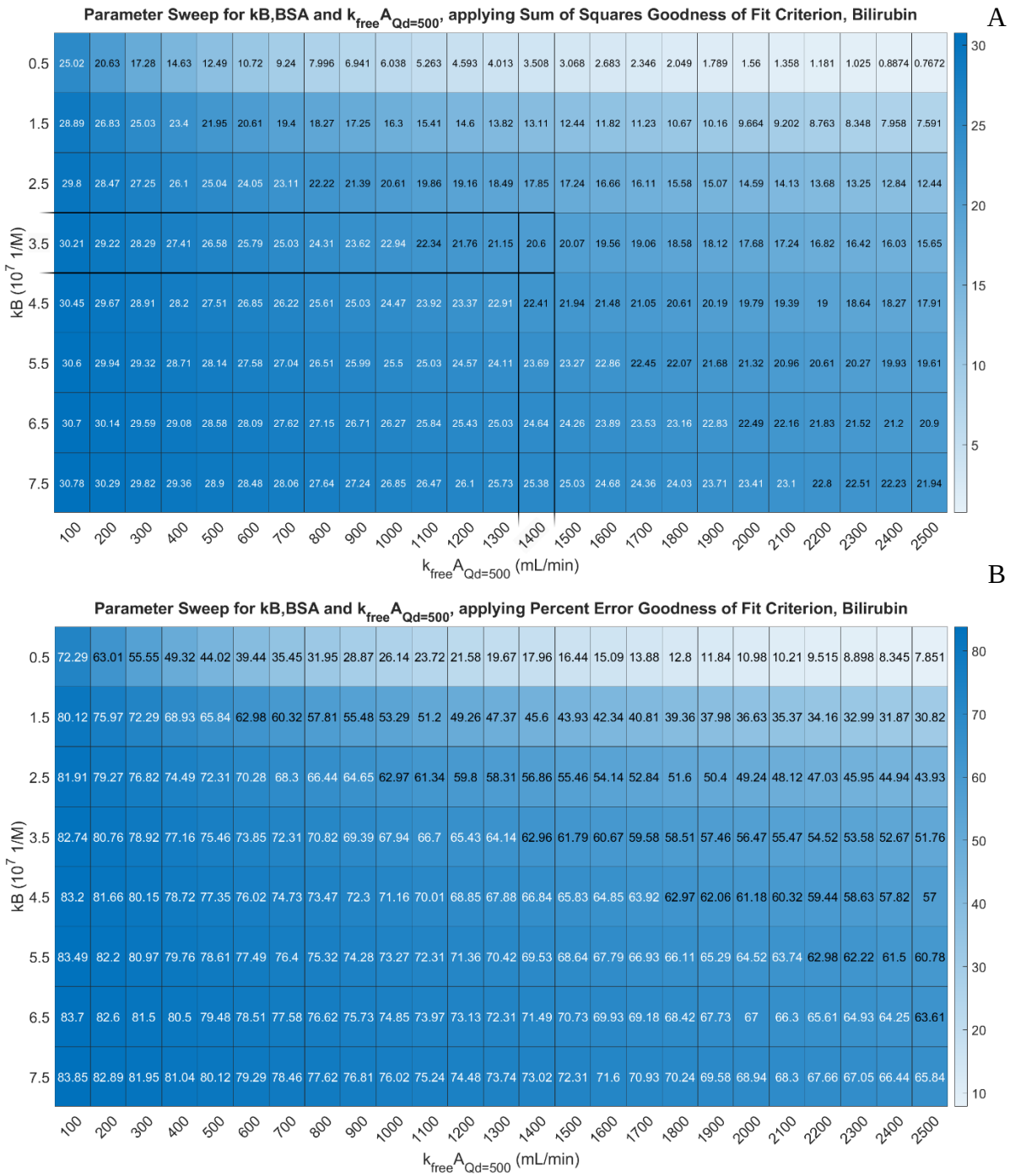


Figure 5-3: **A**: Parameter sweep results for kB,BSA for bilirubin and $K_{free}A_{Qd=500}$, measuring best fit by the sum of squares criterion. **B**: Parameter sweep results for kB,BSA for bilirubin and $K_{free}A_{Qd=500}$ measuring best fit by the percent error criterion.

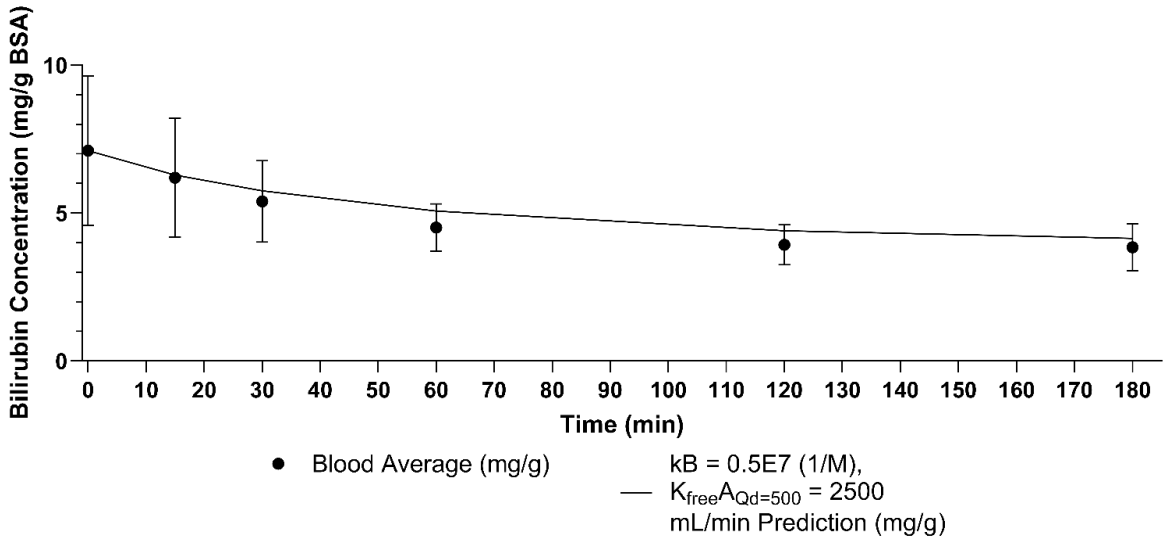


Figure 5-4: Blood side reservoir bilirubin over time for F6HPS with kB = 0.5E7 (1/M) and $K_{free}A_{Qd=500}$ = 2500 mL/min and n = 8400 compared to experimental data. Error bars are standard deviation. Final percent error 7.85%. Sum of squares error 0.77.

5.4.1.5 Model Validation for F3 Dialyzer and Flow Rates

The model was validated using Condition 2, then tested against the other three flow rates for the F3 polysulfone dialyzer. Applying Equation 5-4, the new $K_{free}A_{Qd=500}$ for this dialyzer was 769.23 mL/min. Figure 5-5 shows the model prediction for different values of $\beta_{Q_d}$. All values of the parameter fit the data for 150 mL/min and 800 mL/min dialysate side flow rates. This validates the $K_B$ and $K_{free}A_{Qd=500}$ values obtained from the F6HPS dialyzer. However, for lower flow rates, models with $\beta_{Qd}$ values of 0.3 and less predict a less than 5% change in bilirubin removal across the entire range of flow rates tested. This deviates from our observation. Applying the sum of squares goodness of fit criterion, $\beta_{Qd} = 0.45$ fits the data best. This is shown in Figure 5-5, panel B. This means a 45% decline in $K_{free}A_{Qd=500}$ when dialysate side flow rate declines by 300 mL. Individual conditions are shown in Figure 5-6, along with model predictions for $\beta_{Qd}$ = 0 (no dependency on flow rate), $\beta_{Qd}$ = 0.05544 (literature value), and $\beta_{Qd}$ = 0.45 (best fit for bilirubin data).

Table 5-8 summarizes the accuracy of the model in predicting the outcomes in these conditions. For all flow rates, the model predicted the final blood bilirubin concentration within 7%. Further study of whether $\beta_{Qd}$ varies between dialyzers is warranted, since applying the $\beta_{Qd} = 0.45$ model to the original F6HPS condition increased the error.

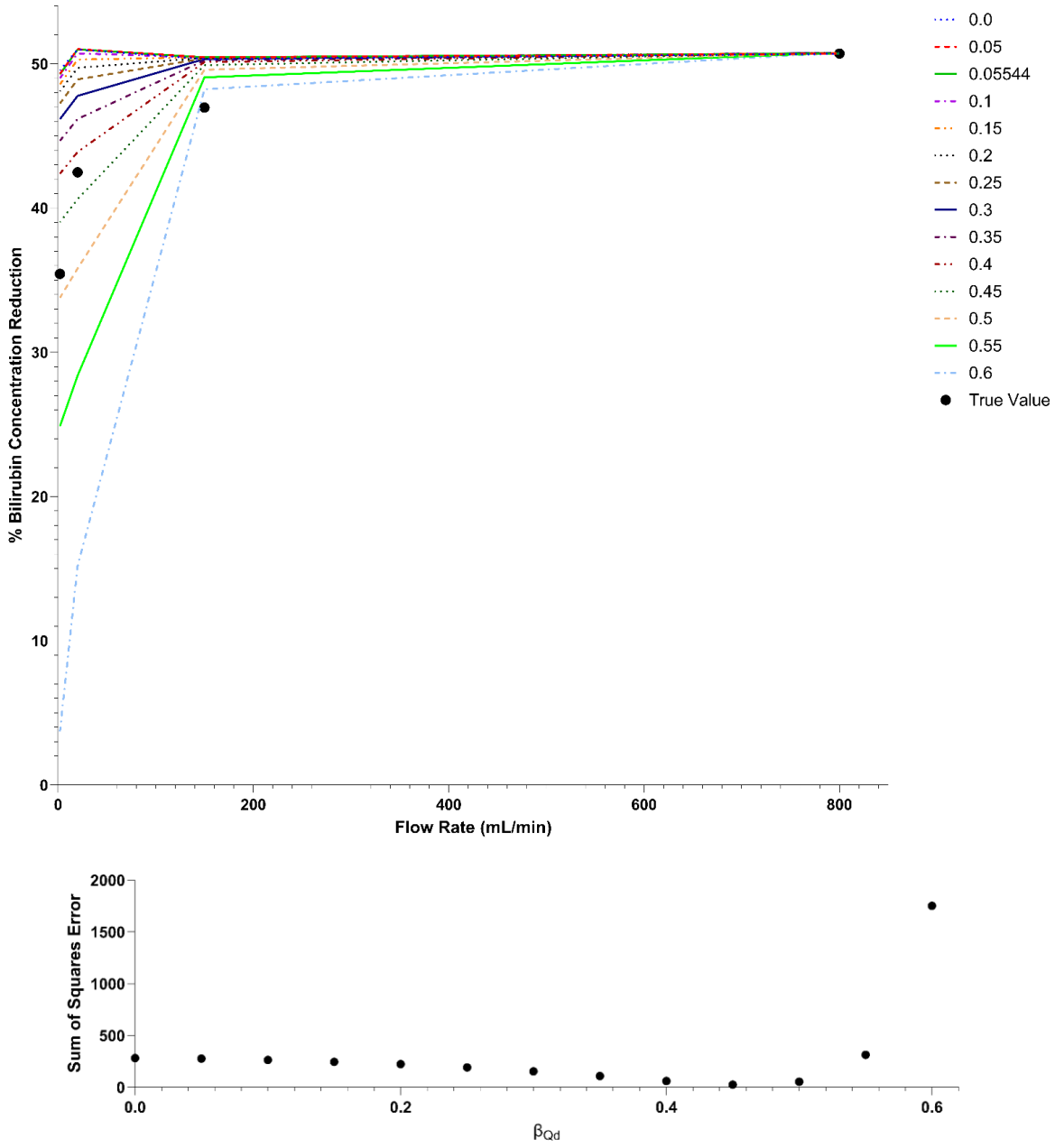


Figure 5-5: **A:** Model predictions for bilirubin removal with varying $K_{free}A$ dialysate side flow rate dependency parameters. **B:** Sum of squares error for fitting the observed relationship between percentage concentration decline and dialysate side flow rate.

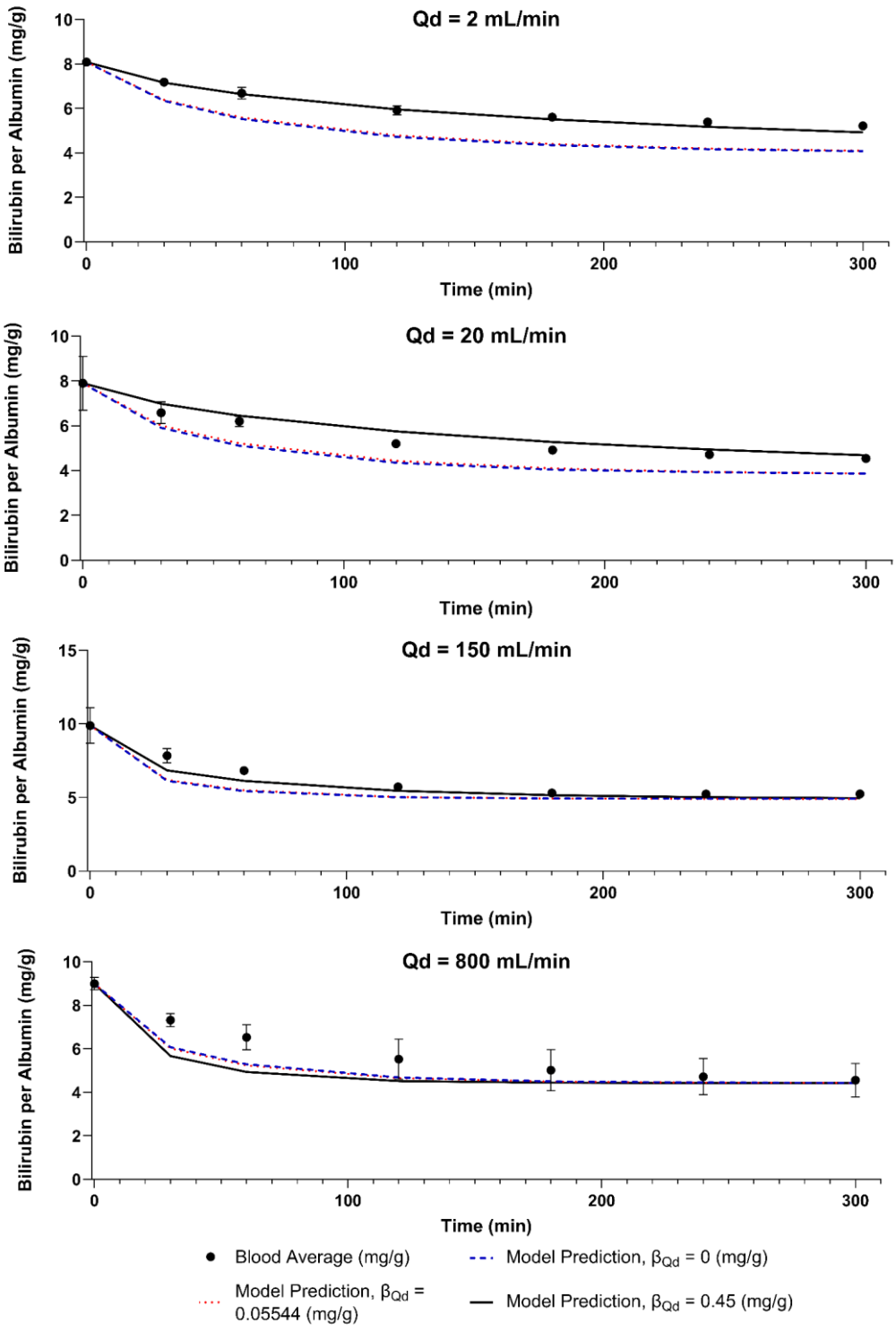


Figure 5-6: Results and model predictions for dialysate flow rates of 2 mL/min (Panel A), 20 mL/min (Panel B), 150 mL/min (Panel C), and 800 mL/min (Panel D). Errors bars are standard deviation. Where error bars are not shown, it is because they would be smaller than the data point depicted on the graph. Points are experimental data and the lines are the model predictions.

Table 5-8: Goodness of Fit for Different Conditions by Sum of Squares and Percent Error of Final Value Criteria.

| Condition | Sum of Squares, $\beta_{Qd} = 0$ | Percent Error of Final Value, $\beta_{Qd} = 0$ | Sum of Squares, $\beta_{Qd} = 0.05544$ | Percent Error of Final Value, $\beta_{Qd} = 0.05544$ | Sum of Squares, $\beta_{Qd} = 0.45$ | Percent Error of Final Value, $\beta_{Qd} = 0.45$ |
|---|---|---|---|---|---|---|
| 1 (F6HPS, *Qb* = 180 mL/min, *Qd* = 90 mL/min, training) | 0.566 | 6.99 | 0.767 | 7.85 | 5.70 | 25.1 |
| 2 (F3, *Qb* = *Qd* = 150 mL/min, validation) | 5.69 | -6.35 | 5.31 | -6.58 | 1.69 | -5.55 |
| 3 (F3, *Qb* = 150 mL/min, *Qd* = 20 mL/min, test) | 4.21 | -14.8 | 3.61 | -14.8 | 0.719 | 3.23 |
| 4 (F3, *Qb* = 150 mL/min, *Qd* = 800 mL/min, test) | 4.12 | -2.79 | 4.48 | -2.82 | 6.67 | -2.94 |
| 5 (F3, *Qb* = 150 mL/min, *Qd* = 2 mL/min, test) | 7.86 | -21.9 | 7.24 | -21.4 | 0.147 | -5.58 |

### 5.4.2 *Discussion*

We have developed a thermodynamically-based computational model that can be used to rationally design albumin dialysis. This paves the way for optimization of an albumin dialysis system for protein bound toxin removal. It also creates the potential for personalized dialysis regiments, where patients are given flow rate conditions and dialysate compositions tailored to their body volume and toxin concentrations. This would play a similar role to the NxStage Dosing Calculator in home dialysis (262). This work will guide us in optimizing AMOR treatment prescriptions.

This model differs from previous models since it accounts for both ultrafiltration and backfiltration, in addition to diffusive transport and protein binding. It considers differences in toxin transport throughout the length of the dialyzer, rather than treating it as a well-mixed

compartment or averaging ultrafiltration across the entire membrane. It does not make any assumptions about the albumin and toxin concentration. It also incorporates the dependence of membrane permeability on flow rate. A novel algorithm was used to improve its numerical stability over a wide range of test conditions.

This work analyzed the model's ability to predict the impact of changes in dialyzer and dialysate flow rate. demonstrate that there is a pronounced effect of dialysate flow rate on bilirubin removal at low flow rates (2 mL/min – 20 mL/min) which becomes insignificant at greater flow rates (150 mL/min and 800 mL/min). When flow rate changes by 300 mL/min, the membrane transfer coefficient for free bilirubin changes by 45%. We estimate this effect using a linear approximation based on prior work on urea (221). This effect may be due to the formation of a boundary layer on the dialysate side. Further work using computational models that explicitly model the boundary layer, such as that of Snisarenko and colleagues (263), would test this proposed mechanism.

With high flow rate conditions (150 mL/min and 800 mL/min), our model has been validated against conditions which were not used to set its parameters. This is strong evidence of its predictive power. For lower flow rates (2 mL/min and 20 mL/min) the flow rate adjustment is necessary. Additional independent validation is needed to confirm the value of the flow rate adjustment parameter. In their original work on the subject, Depner and colleagues noted a small but statistically significant variability of $\beta_{Qd}$ between dialyzers (221). Other dialyzers, or other flow rates may provide independent verification of our $\beta_{Qd}$ value. When we applied the best-fit model for the F3 dialyzer to the F6HPS data, error increased. This may indicate this parameter varies between dialyzers.

A limitation of this work is that it is "post-blind" (264). Our pre-blind analysis is available in the form of a preprint (265). A numerical error in that version of the model caused us to underestimate the deviation at 20 mL/min. Additional external validation in which the version of the model presented here is the "pre-blind" version will increase confidence in this modeling approach.

Further work is in progress to predict the impact of changes in blood flow rate and other parameters. Another limitation was small scale. In the test conditions used to validate the model, blood volume was 200-630 mL. In a patient the plasma volume is approximately 3 L (266). A larger scale *in vitro* test is needed to validate the model's predictive ability in patients.

The model correctly predicts the equilibrium outcomes of albumin dialysis, but it overestimates the kinetics of bilirubin transport across the membrane at high dialysate flow rates. This appears mathematically in an implausibly high $K_{free}A_{Qd=500}$ value. For example, it predicts a $K_{free}A_{Qd=500}$ value for bilirubin of 2500 mL/min for the F6HPS dialyzer, whose kA for urea is only 746 mL/min under similar flow conditions (267). Pei and colleagues previously reported a bilirubin kA value of 800 mL/min for a Gambro 6LR dialyzer using a similar model (158). The KoA for urea for the Gambro 6LR dialyzer is 736 mL/min (230). We could not replicate their result with an 800 mL/min $K_{free}A$ using their model and Villarroel's definition of Peclet Number (159). A higher $K_{free}A$ value would be needed. In their original work on the subject, Patzer and Bane noted that the dialyzer mass transfer coefficient of their membranes increased after 180 minutes (3 hours) of dialysis (147). They suggested that bilirubin and albumin binding to membrane pores accounts for this phenomenon. It would be very useful to accurately predict bilirubin kinetics in our model so that it can be coupled with models of bilirubin absorption onto activated charcoal to predict the behavior of a combined dialysis/absorption system like MARS.

Thus, we will extend the model to incorporate bilirubin binding to the dialysis membrane. Snisarenko and colleagues have presented a theoretical framework for this in their proposed dialysis membrane design (263).

Another potential extension of the model is to incorporate non-Newtonian blood rheology (268). For this work, a blood analog solution consisting of albumin and toxins dissolved in dialysate was used. However, if plasma or whole blood were used instead, the impact of non-Newtonian rheology would need to be considered. The model's equations can be modified to incorporate a different definition of viscosity.

## 5.5 Cholic Acid Removal

### 5.5.1 *Results*

#### 5.5.1.1 Initial Values for Modeling

Table 5-9 summarizes measured average starting cholic acid and albumin concentrations for all six setups. These values were used for modeling to avoid error caused by variations in the initial solution.

Table 5-9: Average Initial Cholic Acid and Albumin Concentration. N = 3 for all conditions. Values are shown as mean ± standard deviation.

| Condition | Starting Blood Cholic Acid (mg/dL) | Starting Blood Albumin (g/dL) | Starting Dialysate Albumin (g/dL) |
|---|---|---|---|
| 1 (F6HPS, *Qb* = 180 mL/min, Qd = 90 mL/min) | 0.92 ± 0.38 | 2.24 ± 0.37 | 1.77 ± 0.41 |
| 2 (F3, *Qb* = *Qd* = 150 mL/min) | 0.86 ± 0.07 | 1.90 ± 0.07 | 1.94 ± 0.23 |
| 3 (F3, *Qb* = 150 mL/min, *Qd* = 20 mL/min) | 0.43 ± 0.04 | 2.13 ± 0.12 | 2.29 ± 0.13 |
| 4 (F3, *Qb* = 150 mL/min, *Qd* = 800 mL/min) | 0.52 ± 0.11 | 2.03 ± 0.02 | 2.10 ± 0.04 |
| 5 (F3, *Qb* = 150 mL/min, *Qd* = 2 mL/min) | 0.49 ± 0.05 | 2.15 ± 0.22 | 2.21 ± 0.14 |
| 6 (F3, Negative Control, *Qb* = *Qd* = 150 mL/min) | 0.54 ± 0.15 | 1.97 ± 0.09 | 0 |

5.5.1.2 Comparison with Negative Control

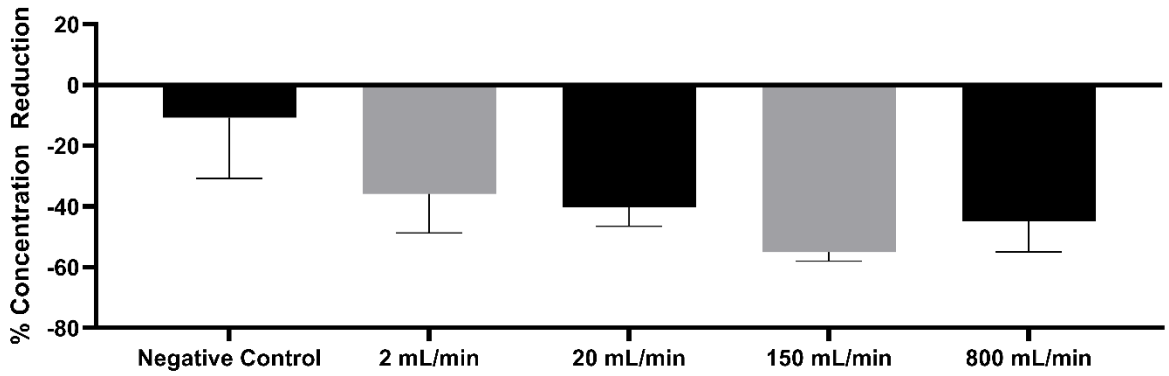


Figure 5-7: Percentage of cholic acid removed from blood side to dialysate over 5 hours. The negative control is dialysate without BSA. N = 3. No F3 condition reached the prespecified p = 0.05 threshold for statistical significance compared to the negative control. The lowest p value was 0.055 for the comparison between the 150 mL/min condition and the negative control. Values are mean ± standard deviation.

*In vitro* testing showed that additional trials are needed to test the impact of 2 g/dL bovine serum albumin on cholic acid removal from dialysate. Figure 5-7 shows cholic acid removal by condition. The smallest p value was 0.055 for the 150 mL/min condition. In the negative control, the cholic acid concentration (mg/g) declined on average 10.7% while in condition 2, the average concentration decline was 55.0%. A statistical power calculation will be performed to prospectively constrain the sample size of a confirmatory study that would test whether this difference occurred by chance or represents a genuine improvement in cholic acid removal from adding BSA to dialysate.

5.5.1.3 $K_{free}A$ and kB Parameter Sweep:

The optimal kB,BSA and $K_{free}A_{Qd=500}$ value that fit the data was kB = 3.5E4 (1/M), $K_{free}A_{Qd=500}$= 40 (mL/min). The results are shown in Figure 5-8. Panel A shows the parameter sweep results for the sum of squares criterion. Panel B shows the parameter sweep results for the percent error criterion. Figure 5-9 shows the model prediction compared to the true measurements.

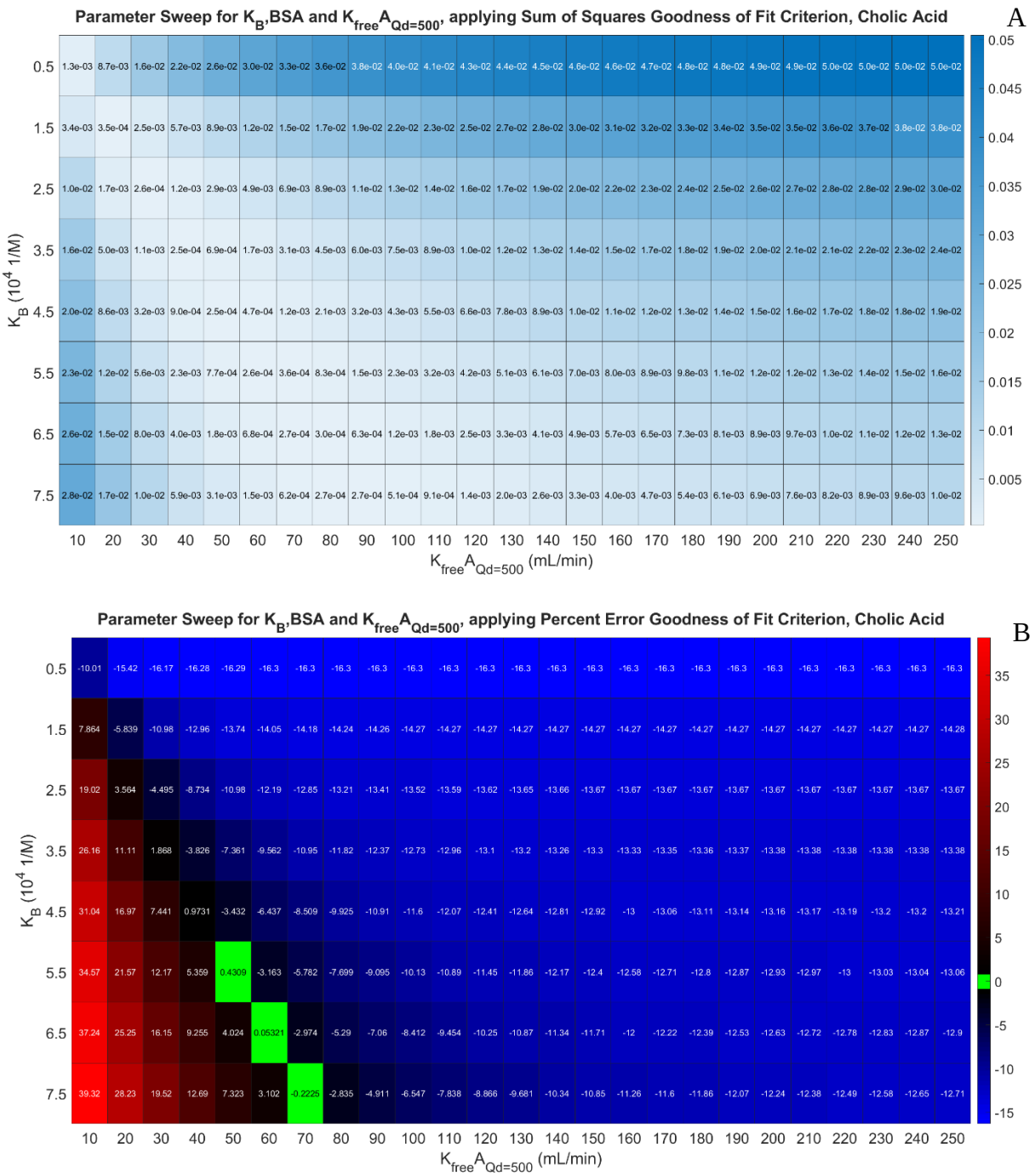


Figure 5-8: **A**: Parameter sweep results for kB,BSA for cholic acid and $K_{free}A_{Qd=500}$, measuring best fit by the sum of squares criterion. **B**: Parameter sweep results for kB,BSA for cholic acid and $K_{free}A_{Qd=500}$, measuring best fit by the percent error criterion.

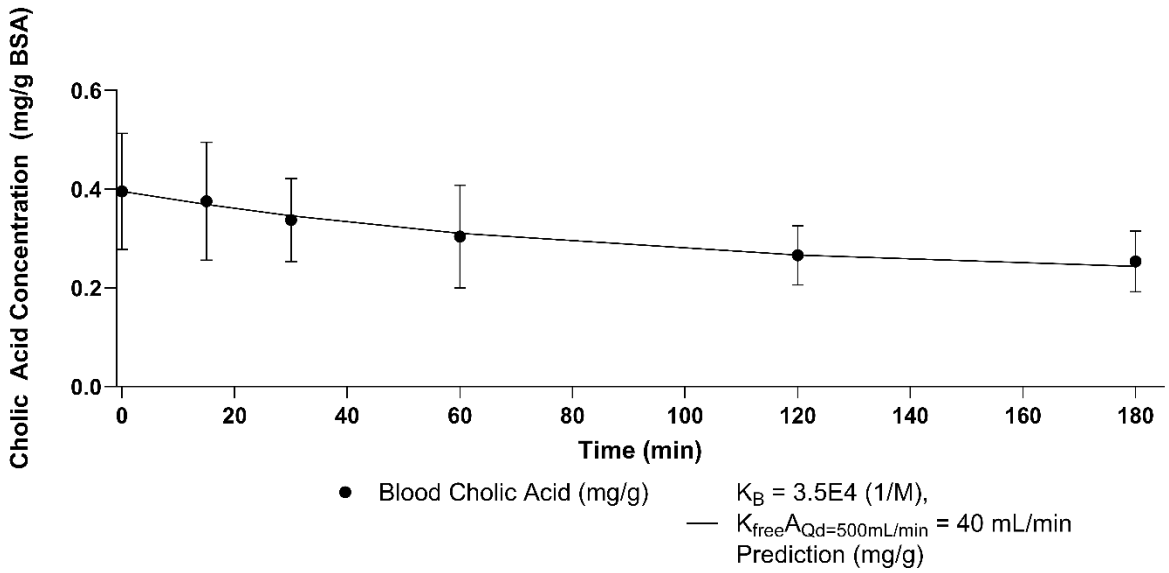


Figure 5-9: Blood side reservoir cholic acid over time for F6HPS with the identified optimal conditions and n = 8400 compared to experimental data. Error bars show standard deviation. Percent Error -3.83%. Sum of Squares Error 2.5E-4.

#### 5.5.1.4 Model Validation for F3 Dialyzer and Flow Rates

The model was validated using Condition 2, then tested against the other three flow rates for the F3 polysulfone dialyzer. Applying Equation 5-4, the new $K_{free}A_{Qd=500}$ for this dialyzer was 12.31 mL/min.

Figure 5-10 shows the model prediction for different values of $\beta_{Q_d}$. A value of 0.35 best fit the data. The simulation at $\beta_{Q_d} = 0.6$ encountered numerical errors. Figure 5-11 shows results for individual conditions. Table 5-10 summarizes goodness of fit results for the analyzed models.

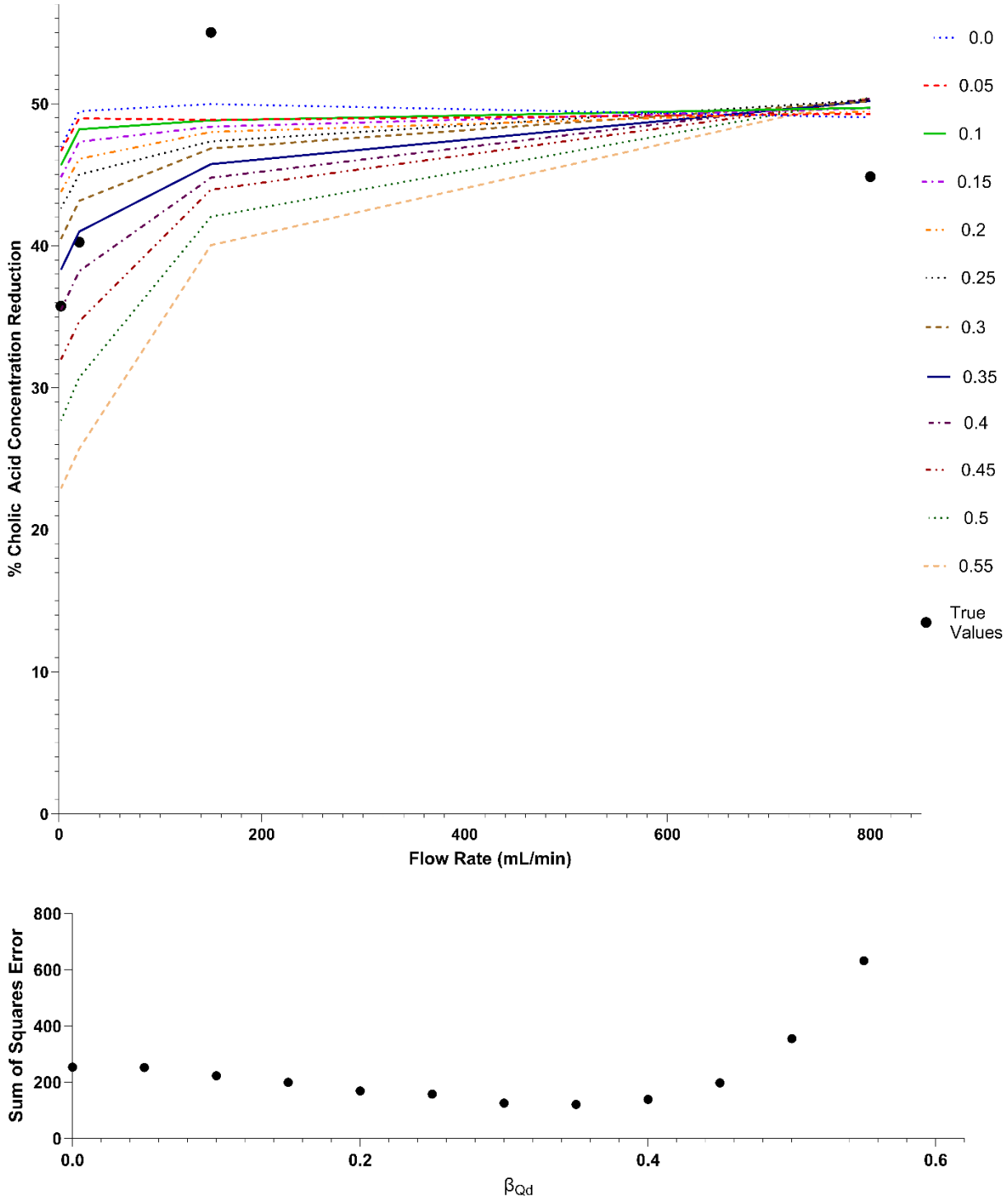


Figure 5-10: **A:** Model predictions for cholic acid removal with varying $K_{free}A$ dialysate side flow rate dependency parameters. **B:** Sum of squares error for fitting the observed relationship between percentage concentration decline and dialysate side flow rate.

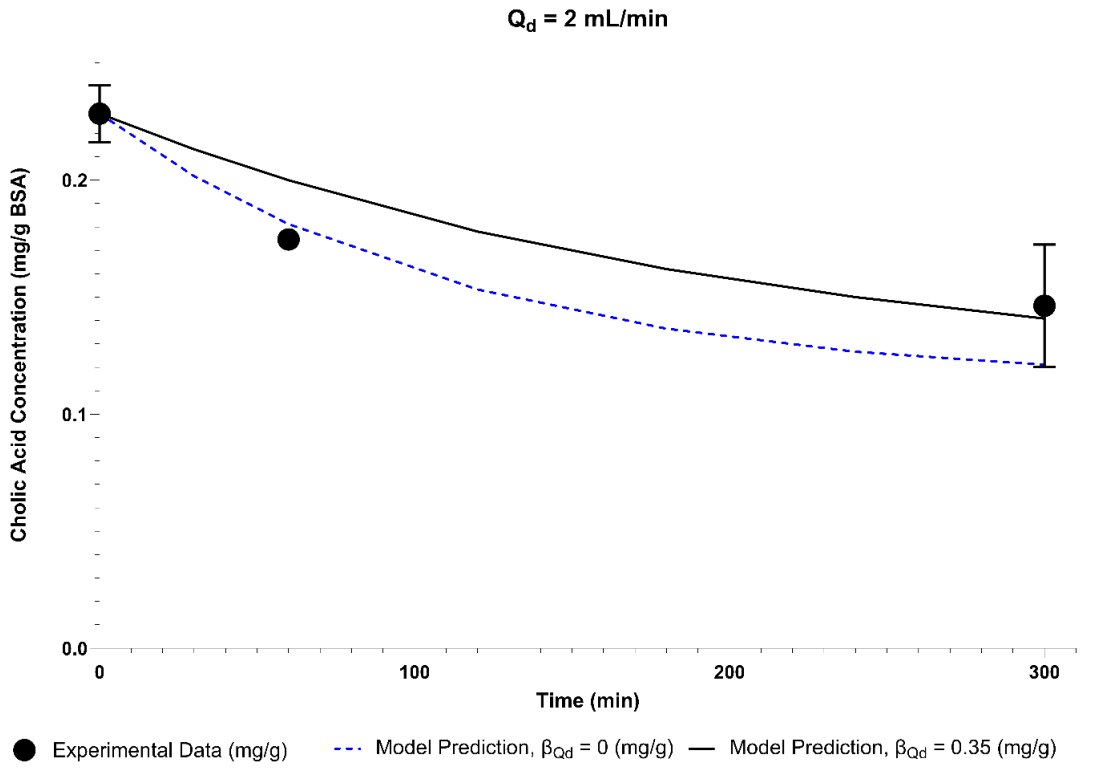
$Q_d$ = 2 mL/min
Cholic Acid Concentration (mg/g BSA)
0.0
0.1
0.2
0
100
200
300
Time (min)
Experimental Data (mg/g)
Model Prediction, $\beta_{Qd}$ = 0 (mg/g)
Model Prediction, $\beta_{Qd}$ = 0.35 (mg/g)

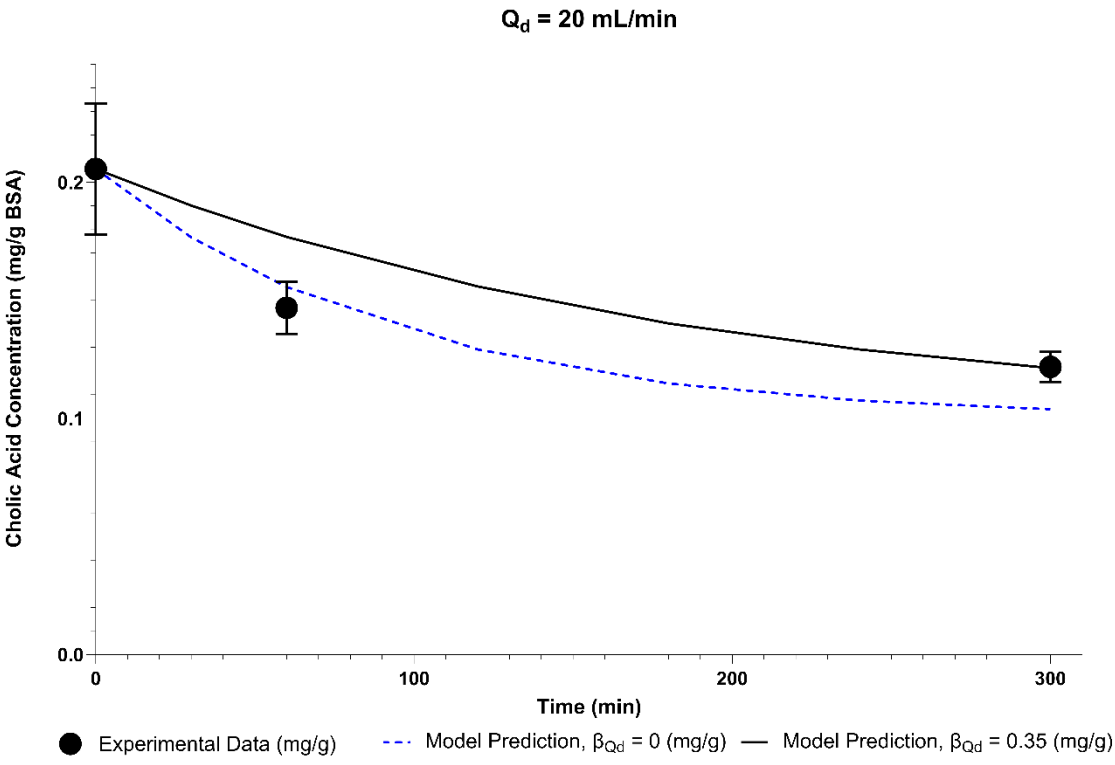
$Q_d$ = 20 mL/min
Cholic Acid Concentration (mg/g BSA)
0.0
0.1
0.2
0
100
200
300
Time (min)
Experimental Data (mg/g)
Model Prediction, $\beta_{Qd}$ = 0 (mg/g)
Model Prediction, $\beta_{Qd}$ = 0.35 (mg/g)

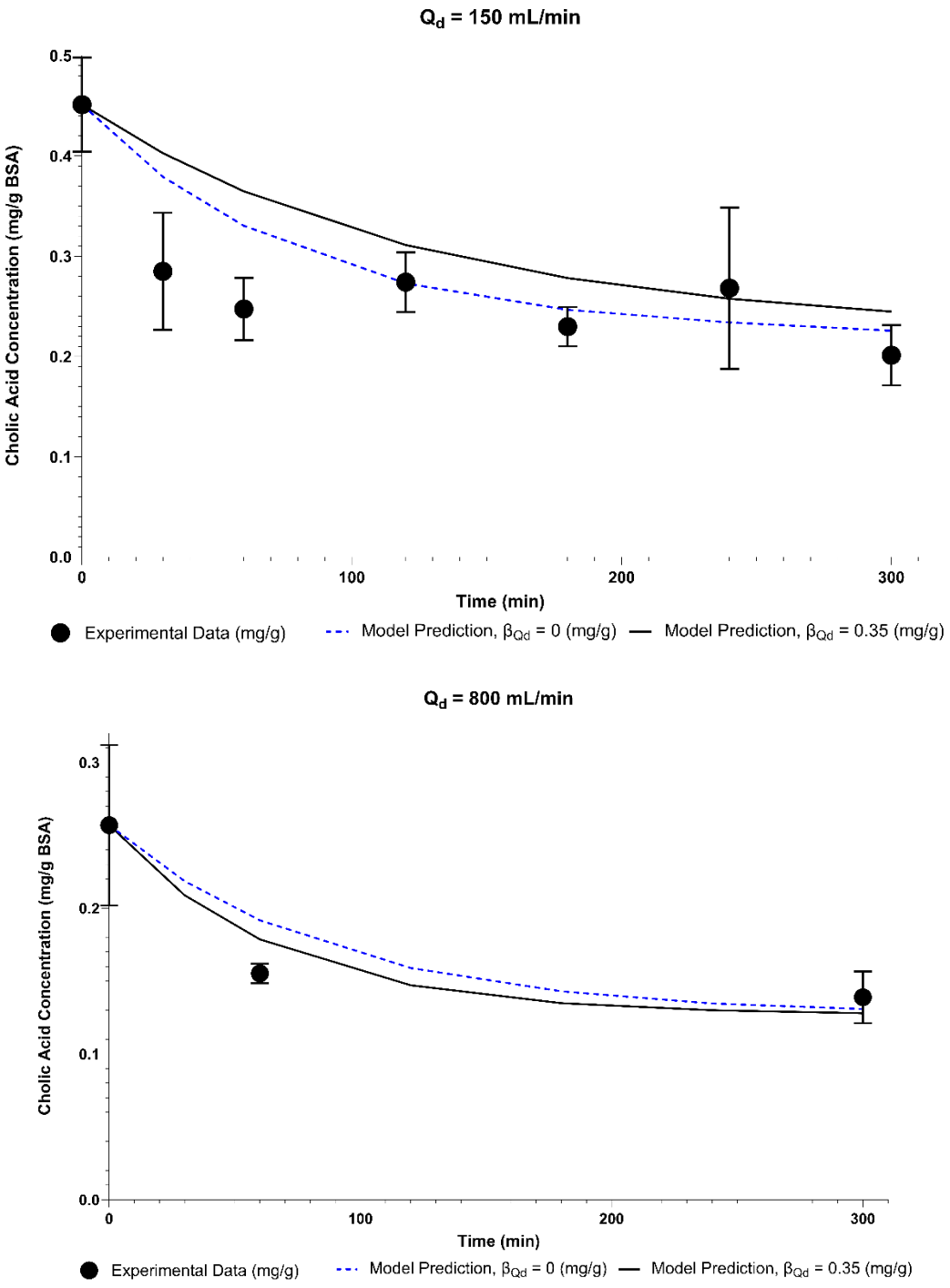


Figure 5-11: Results and model predictions for dialysate flow rates of 2 mL/min (Panel A), 20 mL/min (Panel B), 150 mL/min (Panel C), and 800 mL/min (Panel D). Errors bars are standard deviation. Where error bars are not shown, it is because they would be smaller than the data point depicted on the graph. Points are experimental data and the lines are the model predictions.

Table 5-10: Goodness of Fit for Different Conditions by Sum of Squares and Percent Error of Final Value Criteria.

| **Condition** | **Sum of Squares, $\beta_{Qd} = 0$** | **Percent Error of Final Value, $\beta_{Qd} = 0$** | **Sum of Squares, $\beta_{Qd} = 0.35$** | **Percent Error of Final Value, $\beta_{Qd} = 0.35$** |
|---|---|---|---|---|
| 2 (F3, *Qb* = *Qd* = 150 mL/min, validation) | 0.018 | 12.19 | 0.033 | 21.66 |
| 3 (F3, *Qb* = 150 mL/min, *Qd* = 20 mL/min, test) | 0.00040 | -14.70 | 0.00090 | -0.40 |
| 4 (F3, *Qb* = 150 mL/min, *Qd* = 800 mL/min, test) | 0.0014 | -5.71 | 0.00066 | -7.83 |
| 5 (F3, *Qb* = 150 mL/min, *Qd* = 2 mL/min, test) | 0.00067 | -17.19 | 0.00067 | -3.68 |

### 5.5.2 *Discussion*

The cholic acid model predicted the outcomes of three of the four tested flow rate conditions with low percent error. Sum of squares error was low for all predictions. A larger sample size is needed, as demonstrated by the lack of statistical significance in the comparison with the negative control. Prospectively constraining the sample size will be important to prevent overfitting. Analysis of additional time points will confirm whether the $\beta_{Qd} = 0.35$ model produces a better fit to the entire solution, and not merely the final concentration compared to the $\beta_{Qd} = 0$ model.

## 5.6 INDOXYL SULFATE REMOVAL

### 5.6.1 *Results*

#### 5.6.1.1 Initial Values for Modeling

Table 5-11 summarizes measured average starting indoxyl sulfate and albumin concentrations for all six setups. These values were used for modeling to avoid error caused by variations in the initial solution.

Table 5-11: Average Initial Indoxyl Sulfate and Albumin Concentration. N = 3 for all conditions. Values are shown as mean ± standard deviation.

| Condition | Starting Blood Indoxyl Sulfate (mg/dL) | Starting Blood Albumin (g/dL) | Starting Dialysate Albumin (g/dL) |
|---|---|---|---|
| 1 (F6HPS, *Qb* = 180 mL/min, *Qd* = 90 mL/min) | 2.27 ± 0.67 | 2.24 ± 0.37 | 1.77 ± 0.41 |
| 2 (F3, *Qb* = *Qd* = 150 mL/min) | 3.87 ± 0.54 | 1.90 ± 0.07 | 1.94 ± 0.23 |
| 3 (F3, *Qb* = 150 mL/min, *Qd* = 20 mL/min) | 2.69 ± 0.10 | 2.13 ± 0.12 | 2.29 ± 0.13 |
| 4 (F3, *Qb* = 150 mL/min, *Qd* = 800 mL/min) | 2.88 ± 0.29 | 2.03 ± 0.02 | 2.10 ± 0.04 |
| 5 (F3, *Qb* = 150 mL/min, *Qd* = 2 mL/min) | 2.57 ± 0.18 | 2.15 ± 0.22 | 2.21 ± 0.14 |
| 6 (F3, Negative Control, *Qb* = *Qd* = 150 mL/min) | 2.78 ± 0.31 | 1.97 ± 0.09 | 0 |

#### 5.6.1.2 Comparison to Negative Control

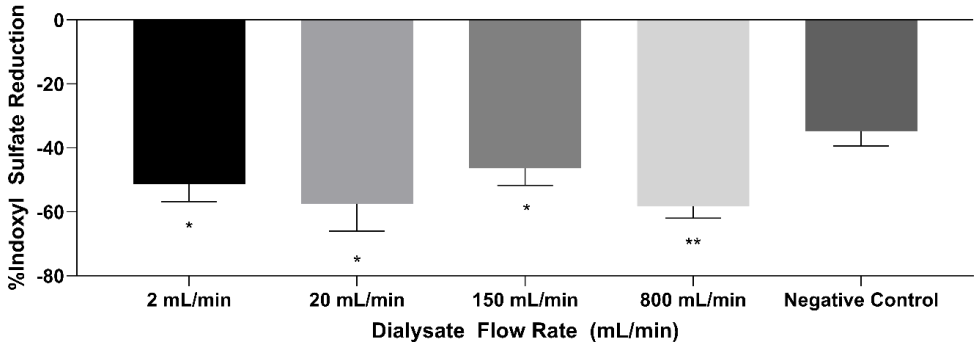


Figure 5-12: Percentage of indoxyl sulfate removed from blood side to dialysate over 5 hours by F3 dialyzer conditions (Conditions 2-6). The negative control is dialysate without BSA. N = 3. The symbol * indicates $p < 0.05$. The ** symbol indicates $p < 0.005$. Values are mean ± standard deviation.

5.6.1.3 $K_{free}A$ and kB Parameter Sweep:

Applying the sum of squares goodness of fit criterion, the best fit was obtained with a $K_{free}A_{Qd=500}$ value of 1500 mL/min and a log10(kB,BSA) value of 4.9, where units of kB,BSA are 1/M. The results are shown in Figure 5-13. Panel A shows the parameter sweep results for the sum of squares criterion. Panel B shows the parameter sweep results for the percent error criterion. Figure 5-14 shows the model prediction and experimental data for the identified optimal parameter values.

A

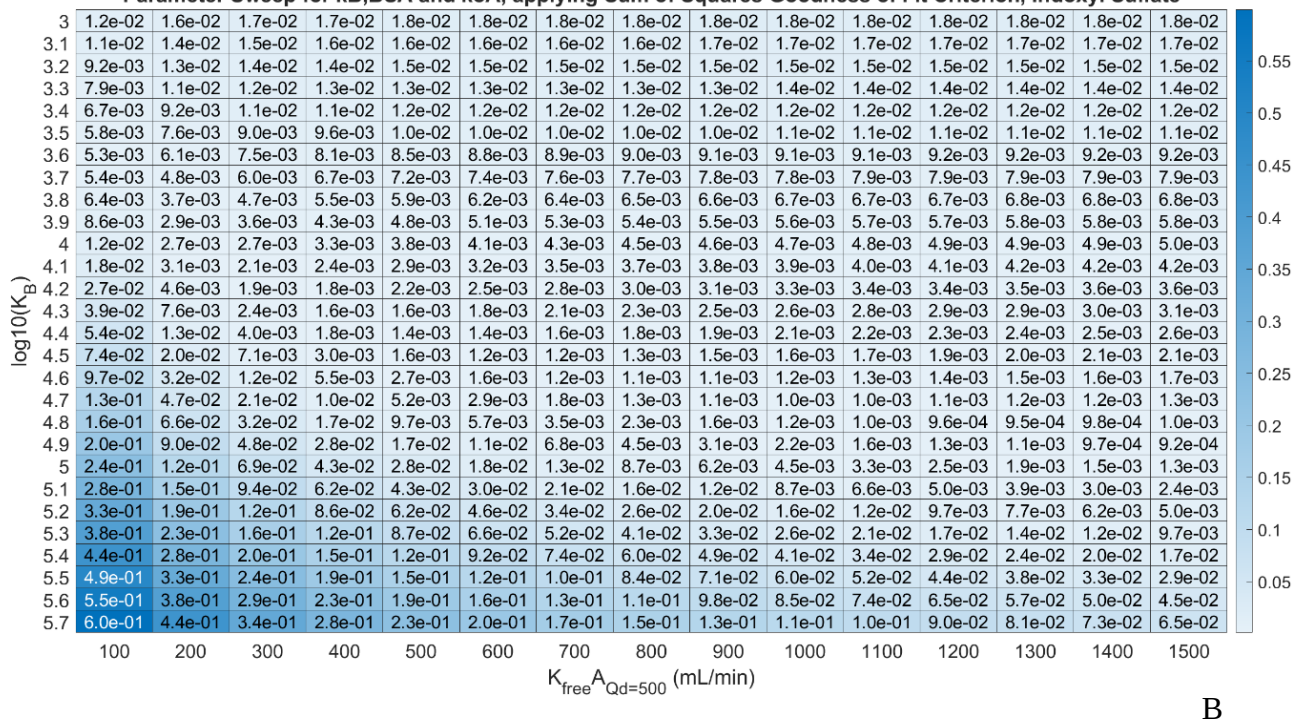


B

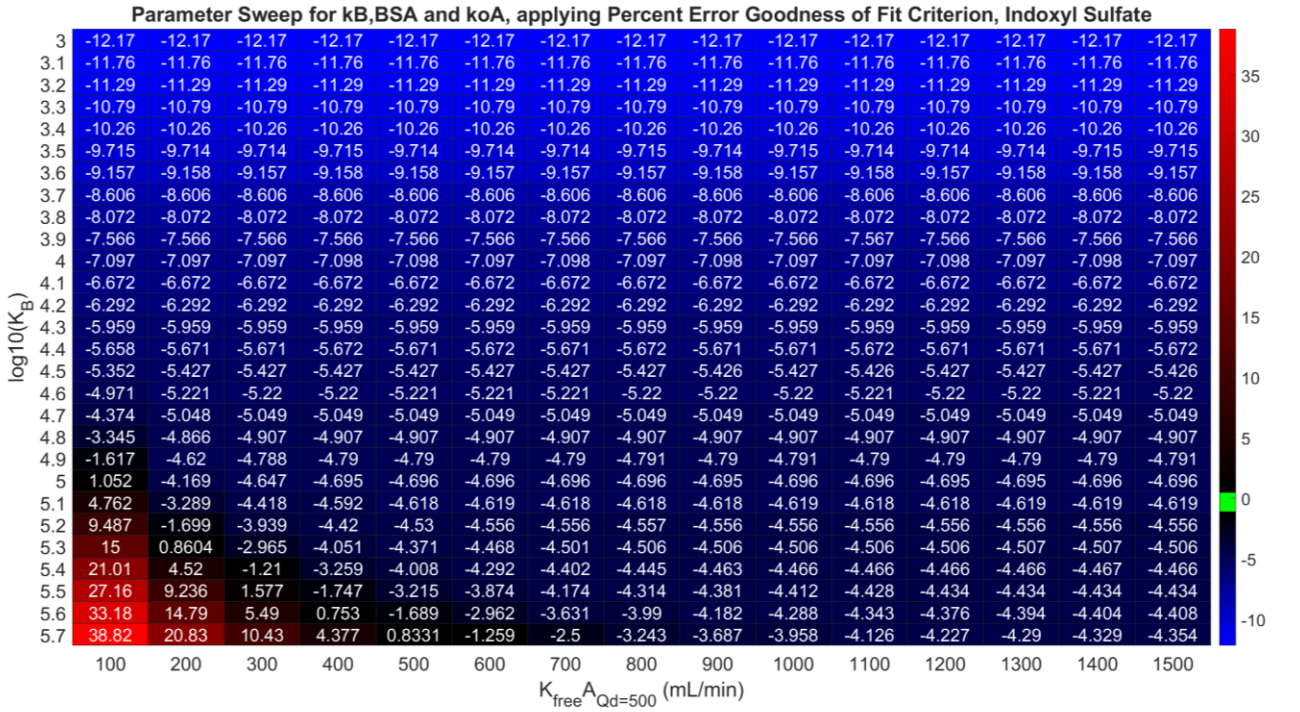


Figure 5-13: **A:** Parameter sweep results for kB,BSA for indoxyl sulfate and $K_{free}A_{Qd=500}$, measuring best fit by the sum of squares criterion. **B:** Parameter sweep results for kB,BSA for indoxyl sulfate and $K_{free}A_{Qd=500}$, measuring best fit by the percent error criterion.

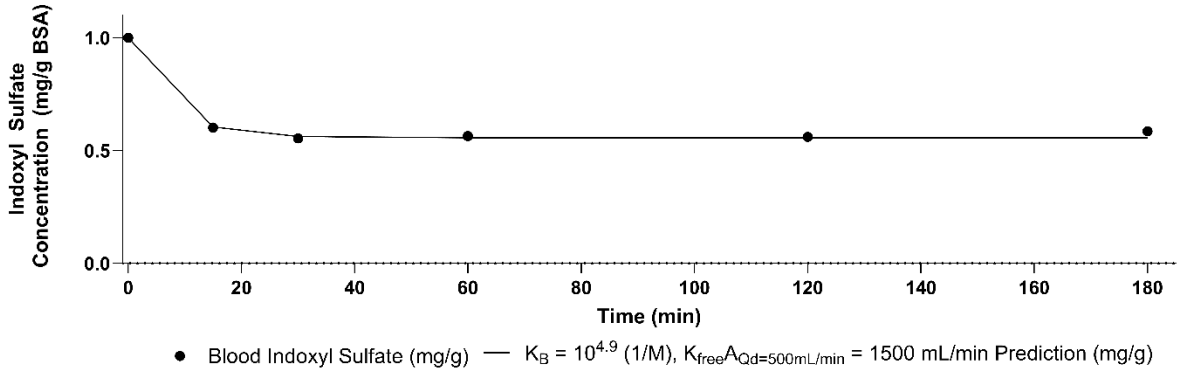


Figure 5-14: Blood side reservoir indoxyl sulfate over time for F6HPS with the identified optimal conditions and n = 8400 compared to experimental data. Error bars show standard deviation. Percent Error -4.791%. Sum of Squares Error 9.2E-4.

5.6.1.4 Model Validation for F3 Dialyzer and Flow Rates

The model was validated using Condition 2, then tested against the other three flow rates for the F3 polysulfone dialyzer. Applying Equation 5-4, the new $K_{free}A_{Qd=500}$ for this dialyzer was 461.54 mL/min. Figure 5-15 shows the model prediction for different values of $\beta_{Q_d}$. No significant increase in predictive power is derived from flow rate adjustment, so $\beta_{Q_d} = 0.0$ was used for further modeling. Goodness of fit results are summarized in Table 5-12. Individual conditions are graphed in Figure 5-16.

Table 5-12: Goodness of Fit for Different Conditions by Sum of Squares and Percent Error of Final Value Criteria.

| **Condition** | **Sum of Squares, $\beta_{Qd} = 0$** | **Percent Error of Final Value, $\beta_{Qd} = 0$** |
|---|---|---|
| 2 (F3, *Qb* = *Qd* = 150 mL/min, validation) | 0.035 | 1.50 |
| 3 (F3, *Qb* = 150 mL/min, *Qd* = 20 mL/min, test) | 0.015 | 14.9 |
| 4 (F3, *Qb* = 150 mL/min, *Qd* = 800 mL/min, test) | 0.057 | 8.08 |
| 5 (F3, *Qb* = 150 mL/min, *Qd* = 2 mL/min, test) | 0.036 | 18.7 |

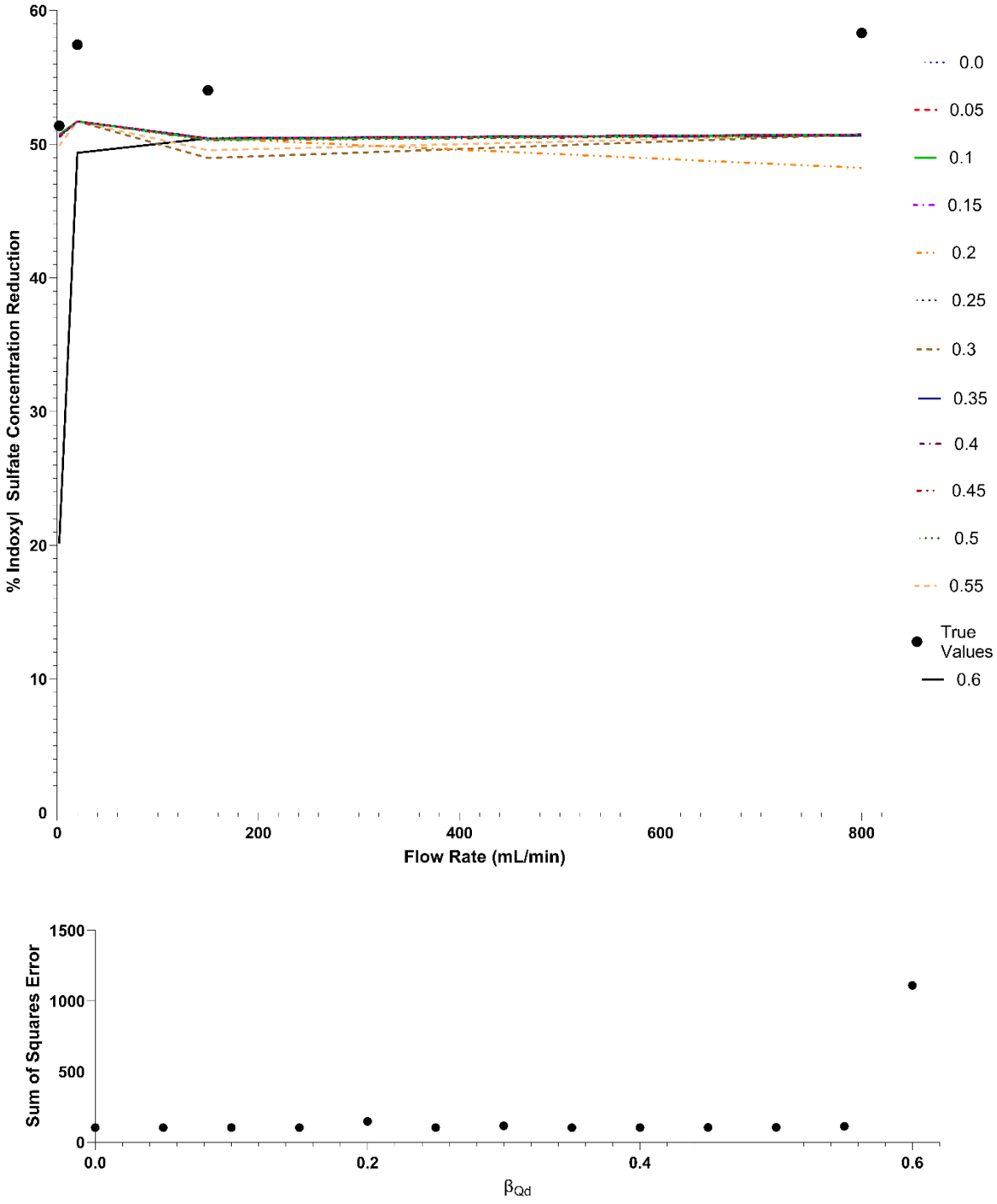


Figure 5-15: **A**: Model predictions for indoxyl sulfate removal with varying $K_{free}A$ dialysate side flow rate dependency parameters. **B**: Sum of squares error for fitting the observed relationship between percentage concentration decline and dialysate side flow rate.

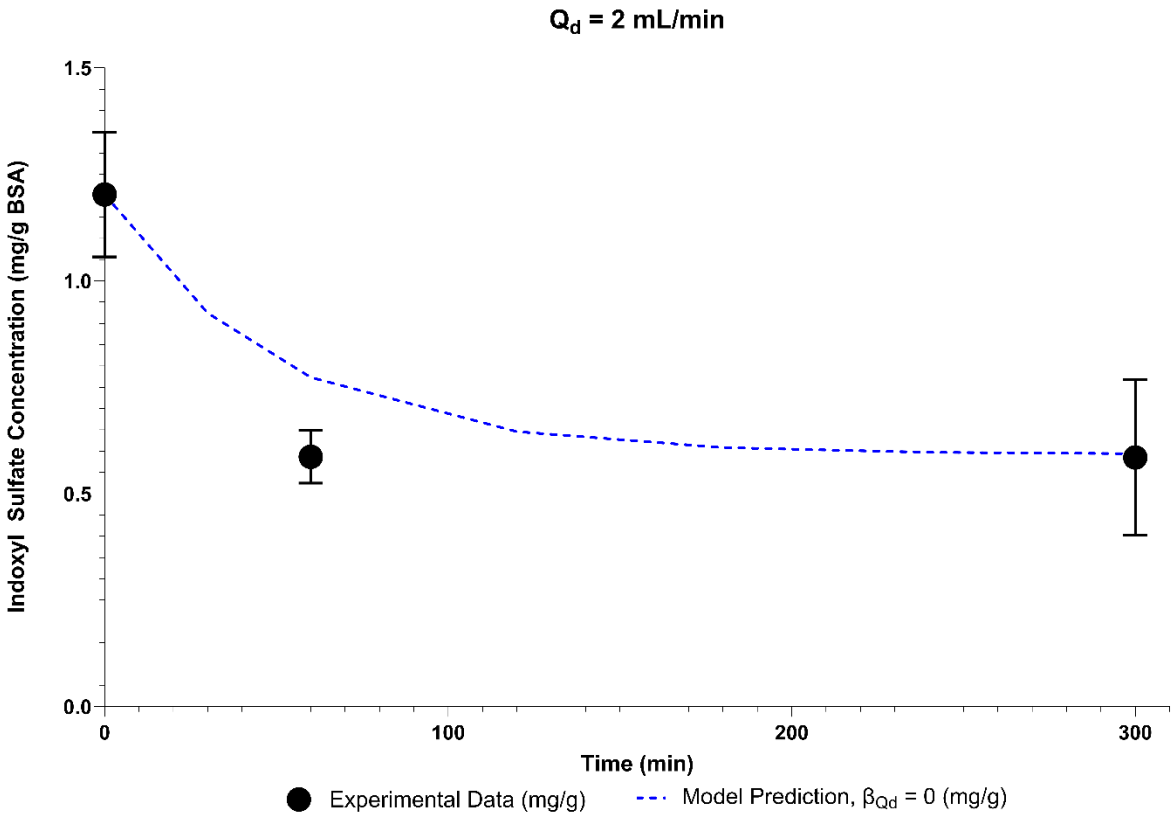
$Q_d$ = 2 mL/min
Indoxyl Sulfate Concentration (mg/g BSA)
1.5
1.0
0.5
0.0
0
100
200
300
Time (min)
Experimental Data (mg/g)
Model Prediction, $\beta_{Qd}$ = 0 (mg/g)

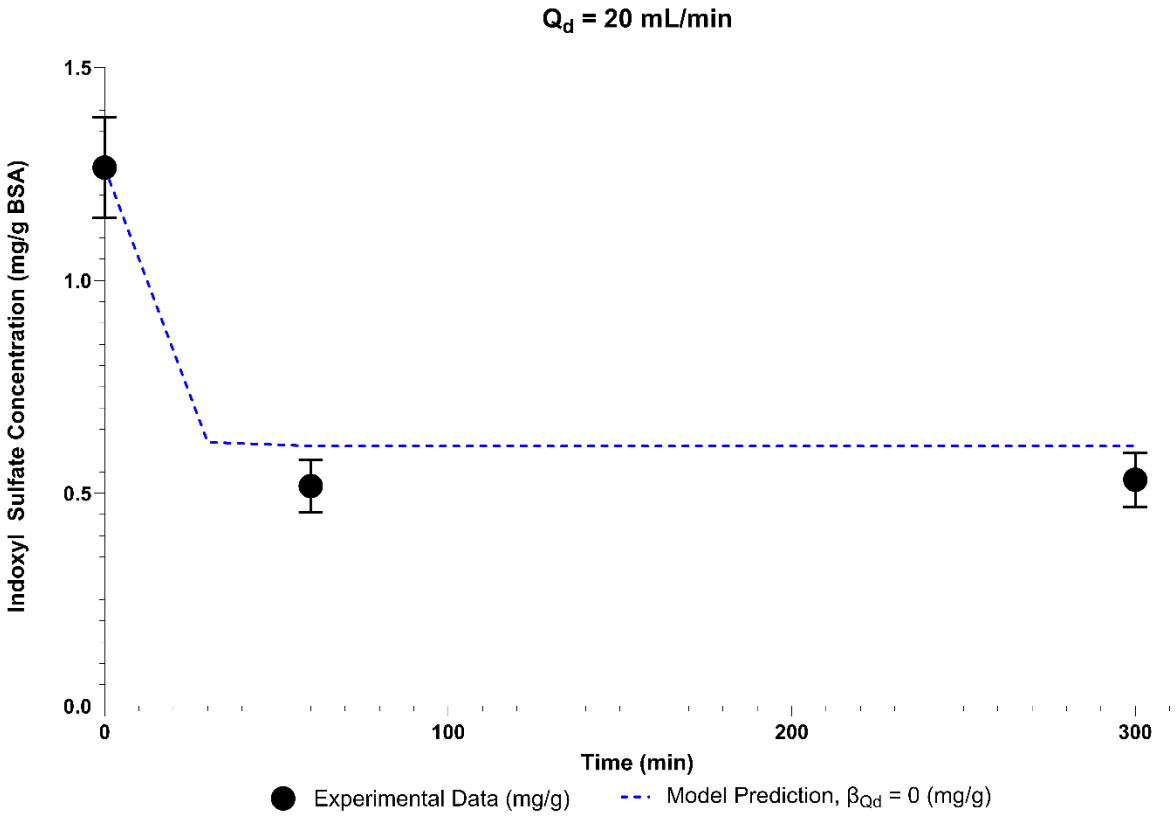
$Q_d$ = 20 mL/min
Indoxyl Sulfate Concentration (mg/g BSA)
1.5
1.0
0.5
0.0
0
100
200
300
Time (min)
Experimental Data (mg/g)
Model Prediction, $\beta_{Qd}$ = 0 (mg/g)

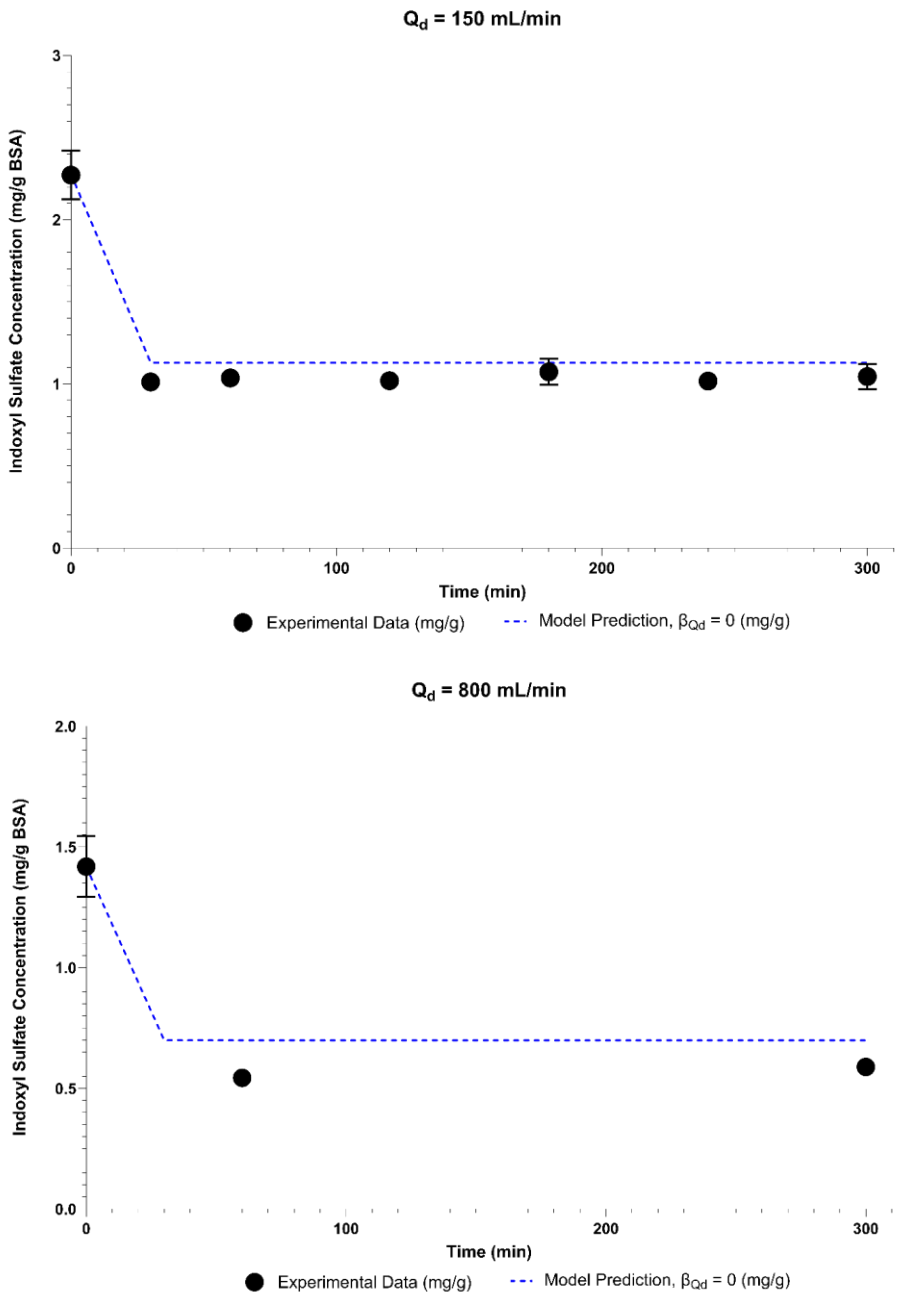


Figure 5-16: Results and model predictions for dialysate flow rates of 2 mL/min (Panel A), 20 mL/min (Panel B), 150 mL/min (Panel C), and 800 mL/min (Panel D). Errors bars are standard deviation. Where error bars are not shown, it is because they would be smaller than the data point depicted on the graph. Points are experimental data and the lines are the model predictions.

### 5.6.2 *Discussion*

All albumin dialysis conditions removed a significantly greater indoxyl sulfate amount than the negative control. No significant impact of dialysate flow rate on indoxyl sulfate removal could be observed. The model slightly underestimated indoxyl sulfate removal, but sum of squares error was low for all conditions.

## 5.7 COPPER REMOVAL

### 5.7.1 *Results*

#### 5.7.1.1 Initial Values for Modeling

Table 5-13 summarizes measured average starting copper and albumin concentrations for all six setups. These values were used for modeling to avoid error caused by variations in the initial solution.

Table 5-13: Average Initial Copper and Albumin Concentration. N = 3 for all conditions. Values are shown as mean ± standard deviation.

| Condition | Starting Blood Copper (mg/dL) | Starting Blood Albumin (g/dL) | Starting Dialysate Albumin (g/dL) |
|---|---|---|---|
| 1 (F6HPS, *Qb* = 180 mL/min, *Qd* = 90 mL/min) | 0.24 ± 0.12 | 2.24 ± 0.37 | 1.77 ± 0.41 |
| 2 (F3, *Qb* = *Qd* = 150 mL/min) | 0.18 ± 0.018 | 1.90 ± 0.07 | 1.94 ± 0.23 |
| 3 (F3, *Qb* = 150 mL/min, *Qd* = 20 mL/min) | 0.18 ± 0.011 | 2.13 ± 0.12 | 2.29 ± 0.13 |
| 4 (F3, *Qb* = 150 mL/min, *Qd* = 800 mL/min) | 0.13 ± 0.043 | 2.03 ± 0.02 | 2.10 ± 0.04 |
| 5 (F3, *Qb* = 150 mL/min, *Qd* = 2 mL/min) | 0.23 ± 0.12 | 2.15 ± 0.22 | 2.21 ± 0.14 |
| 6 (F3, Negative Control, *Qb* = *Qd* = 150 mL/min) | 0.17 ± 0.013 | 1.97 ± 0.09 | 0 |

5.7.1.2 Comparison to Negative Control

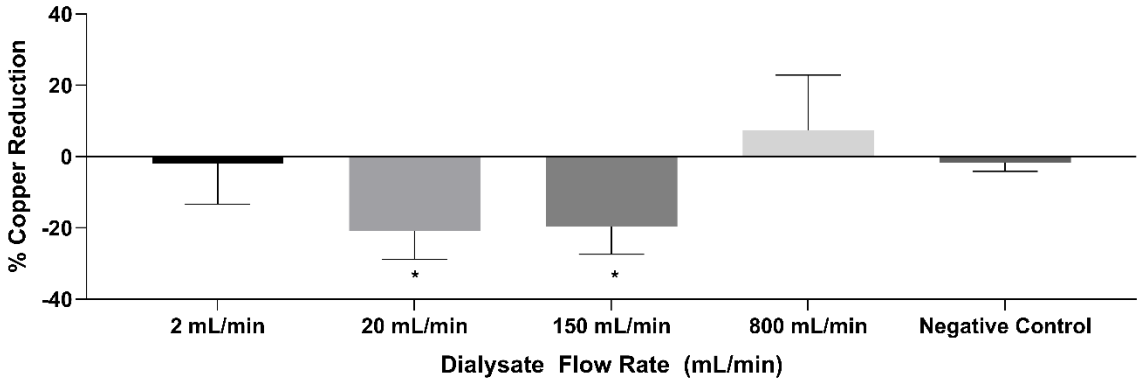


Figure 5-17: Percent Copper Reduction in Different Test Conditions. * indicates $p < 0.05$ compared to the negative control.

As shown in Figure 5-17, albumin dialysis appeared to increase copper removal over the negative control. The 20 mL/min and 150 mL/min flow rates attained statistical significance in improving copper removal ($p = 0.043$ and 0.048 respectively). The 800 mL/min flow rate saw an elevation in blood copper. This may be due to copper leaching from the connectors used to attach the high pressure tolerant pressure sensors. The 20 mL/min and 150 mL/min flow rates appeared to significantly outperform the 2 mL/min flow rate, but excessive variation and small sample size prevent a definitive conclusion from being drawn ($p = 0.085$ and 0.101 respectively).

5.7.1.3 $K_{free}A$ and kB Parameter Sweep:

Since only the initial and final copper was measured, we applied only the percent error goodness of fit criterion to the copper parameter sweep. The best fit was obtained with a $K_{free}A_{Qd=500}$ value of 600 mL/min and a $\log_{10}(K_{B,BSA})$ value of 6. The parameter sweep results are shown in Figure 5-18. The modeled and actual concentration is shown in Figure 5-19.

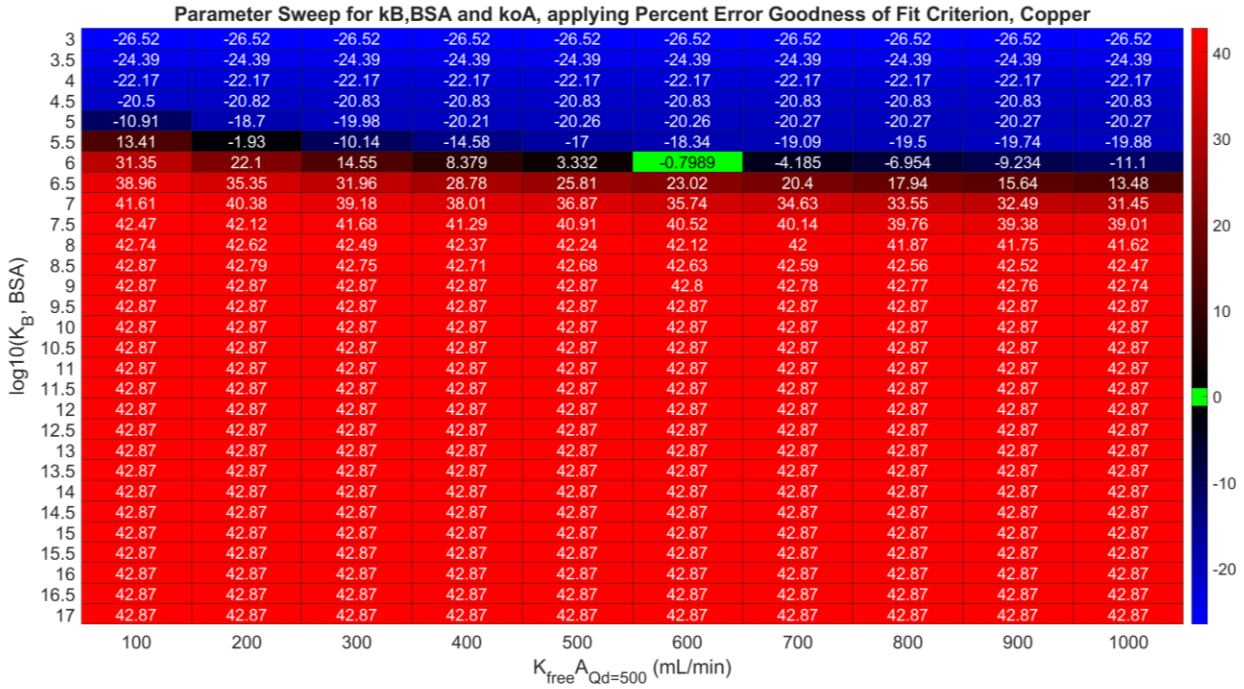


Figure 5-18: Parameter sweep results for kB,BSA for copper and $K_{free}A_{Qd=500}$, measuring best fit by the percent error criterion.

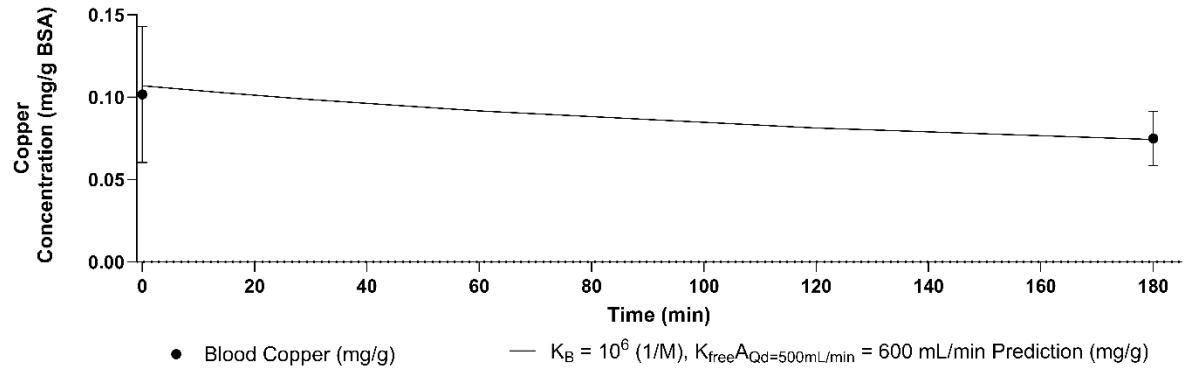


Figure 5-19: Blood side reservoir copper over time for F6HPS with the identified optimal conditions and n = 8400 compared to experimental data. Error bars show standard deviation. Percent Error -0.80%.

5.7.1.4 Model Validation for F3 Dialyzer and Flow Rates

The model was validated against the 2 mL/min, 20 mL/min, and 150 mL/min flow rates. The 800 mL/min flow rate was disregarded due to the possibility of copper contamination from the pressure sensors. Applying Equation 5-4, the new $K_{free}A_{Qd=500}$ for this dialyzer was 184.62

mL/min. Figure 5-20 shows the model prediction for different values of $\beta_{Q_d}$. A value of 0.55 best fit the data. Figure 5-21 shows results for individual conditions. Table 5-14 summarizes goodness of fit results for the analyzed models.

Table 5-14: Goodness of Fit for Different Conditions by Sum of Squares and Percent Error of Final Value Criteria.

| **Condition** | **Percent Error of Final Value, $\boldsymbol{\beta_{Qd} = 0}$** | **Percent Error of Final Value, $\boldsymbol{\beta_{Qd} = 0.55}$** |
|---|---|---|
| 2 (F3, *Qb* = *Qd* = 150 mL/min, validation) | -30.49 | -8.93 |
| 3 (F3, *Qb* = 150 mL/min, *Qd* = 20 mL/min, test) | -28.44 | 12.66 |
| 5 (F3, *Qb* = 150 mL/min, *Qd* = 2 mL/min, test) | -37.69 | -2.96 |

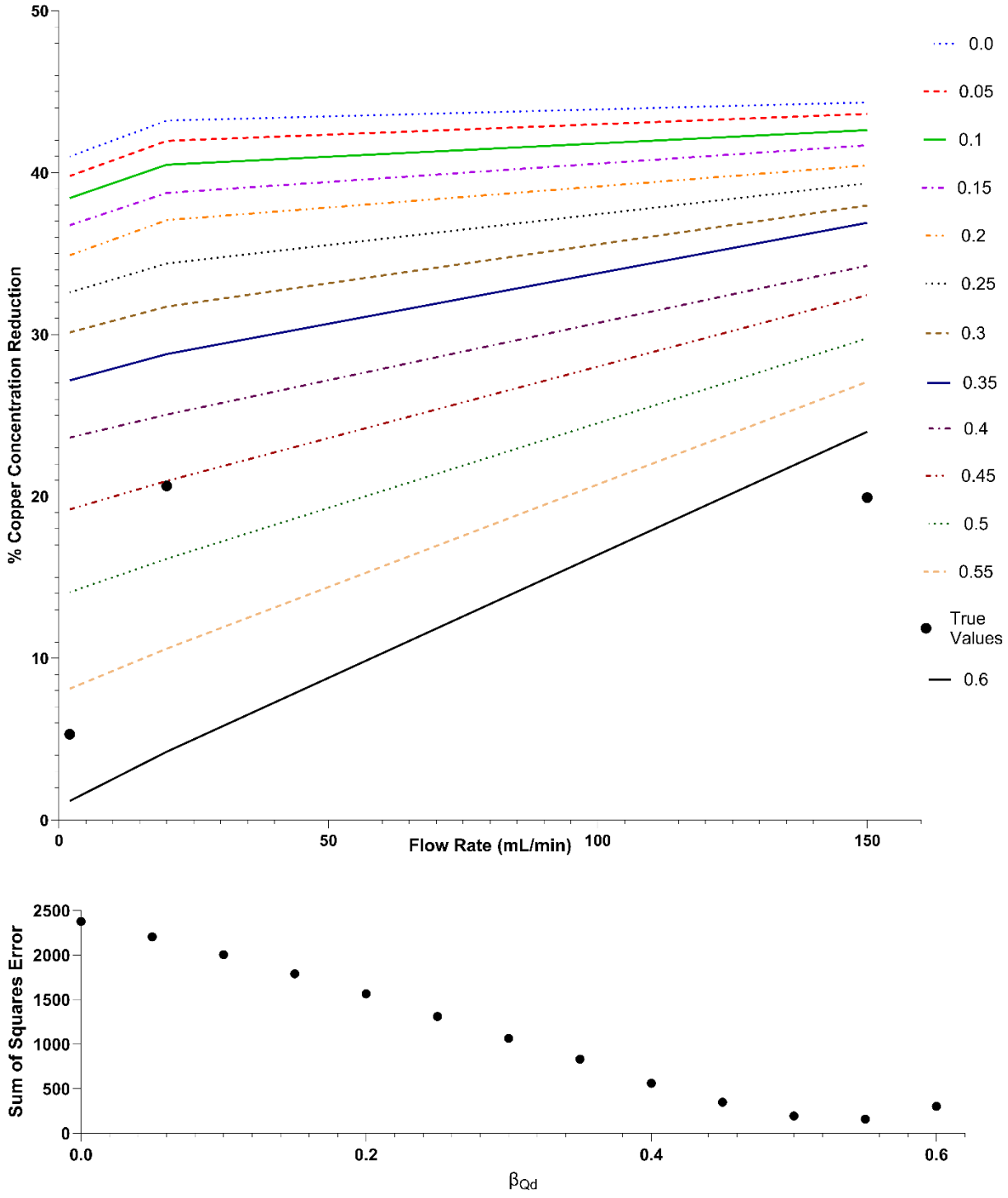


Figure 5-20: **A:** Model predictions for copper removal with varying $K_{free}A$ dialysate side flow rate dependency parameters. **B:** Sum of squares error for fitting the observed relationship between percentage concentration decline and dialysate side flow rate.

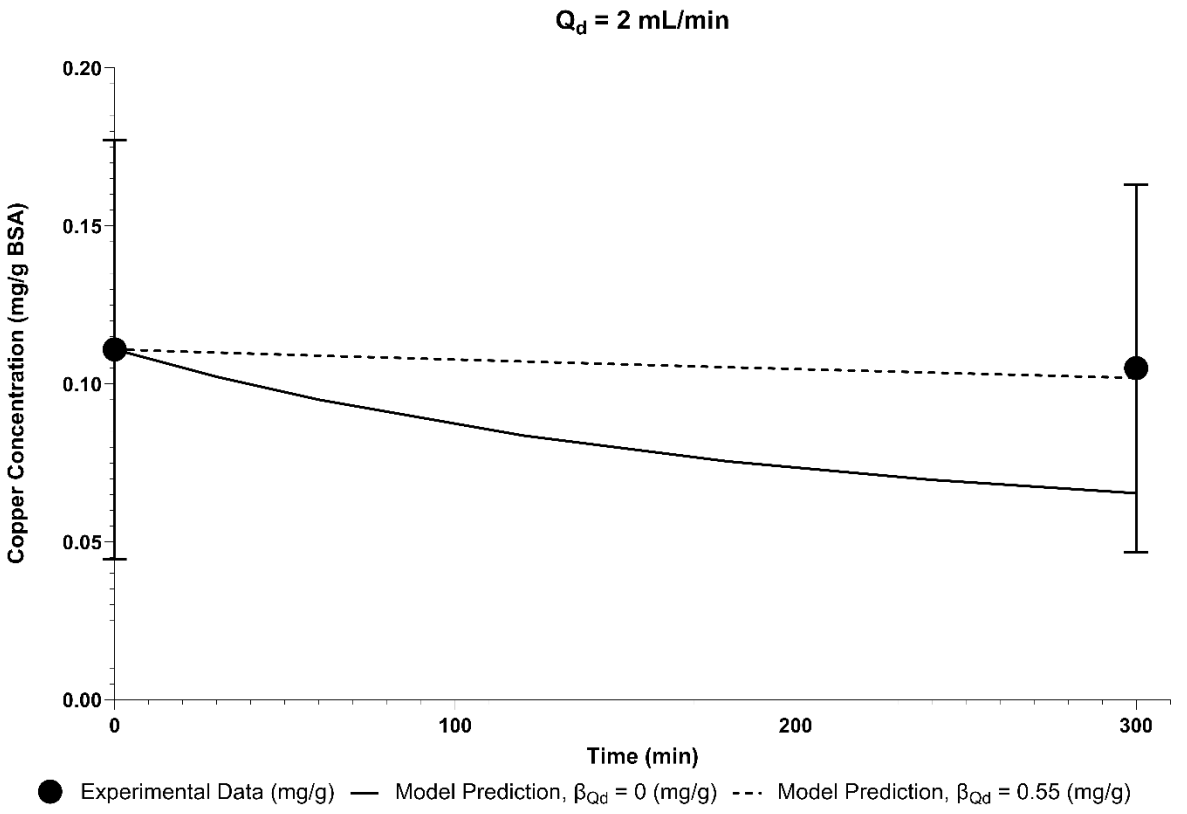
$Q_d$ = 2 mL/min
Copper Concentration (mg/g BSA)
0.20
0.15
0.10
0.05
0.00
0
100
200
300
Time (min)
Experimental Data (mg/g)
Model Prediction, $\beta_{Qd}$ = 0 (mg/g)
Model Prediction, $\beta_{Qd}$ = 0.55 (mg/g)

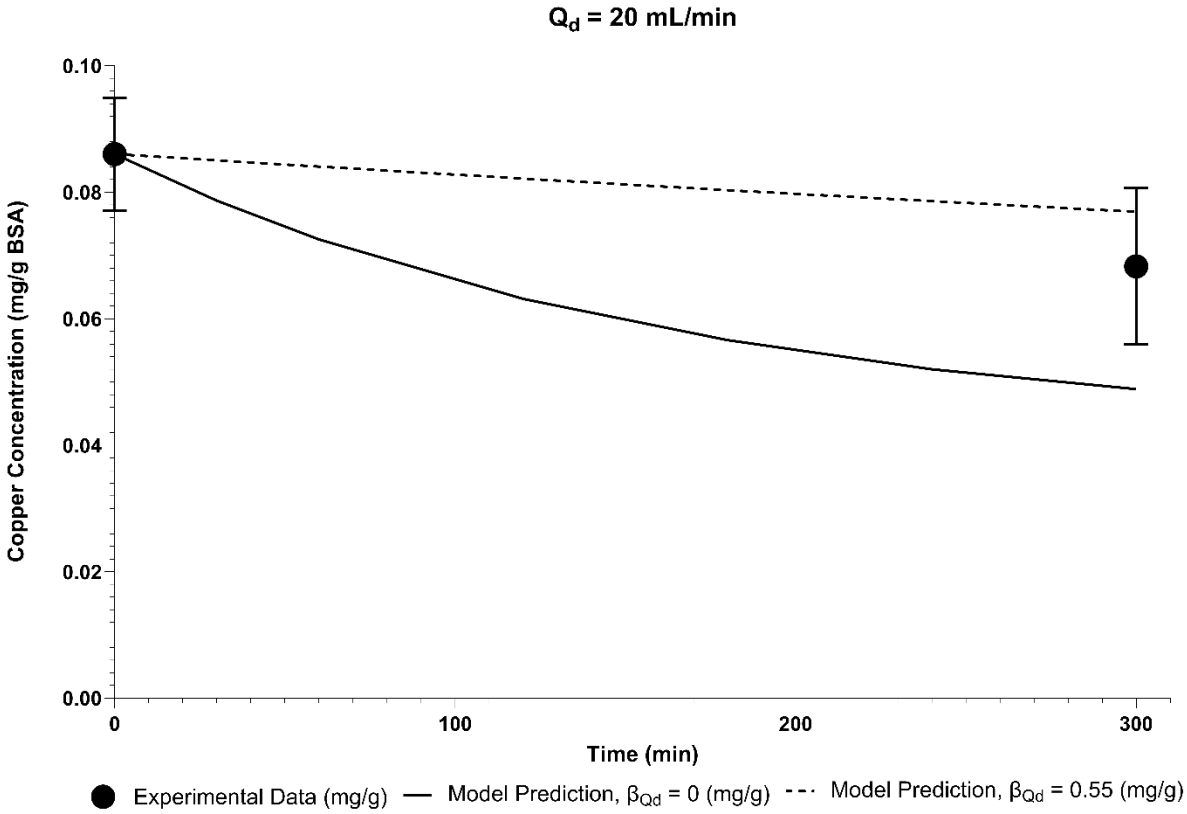
$Q_d$ = 20 mL/min
Copper Concentration (mg/g BSA)
0.10
0.08
0.06
0.04
0.02
0.00
0
100
200
300
Time (min)
Experimental Data (mg/g)
Model Prediction, $\beta_{Qd}$ = 0 (mg/g)
Model Prediction, $\beta_{Qd}$ = 0.55 (mg/g)

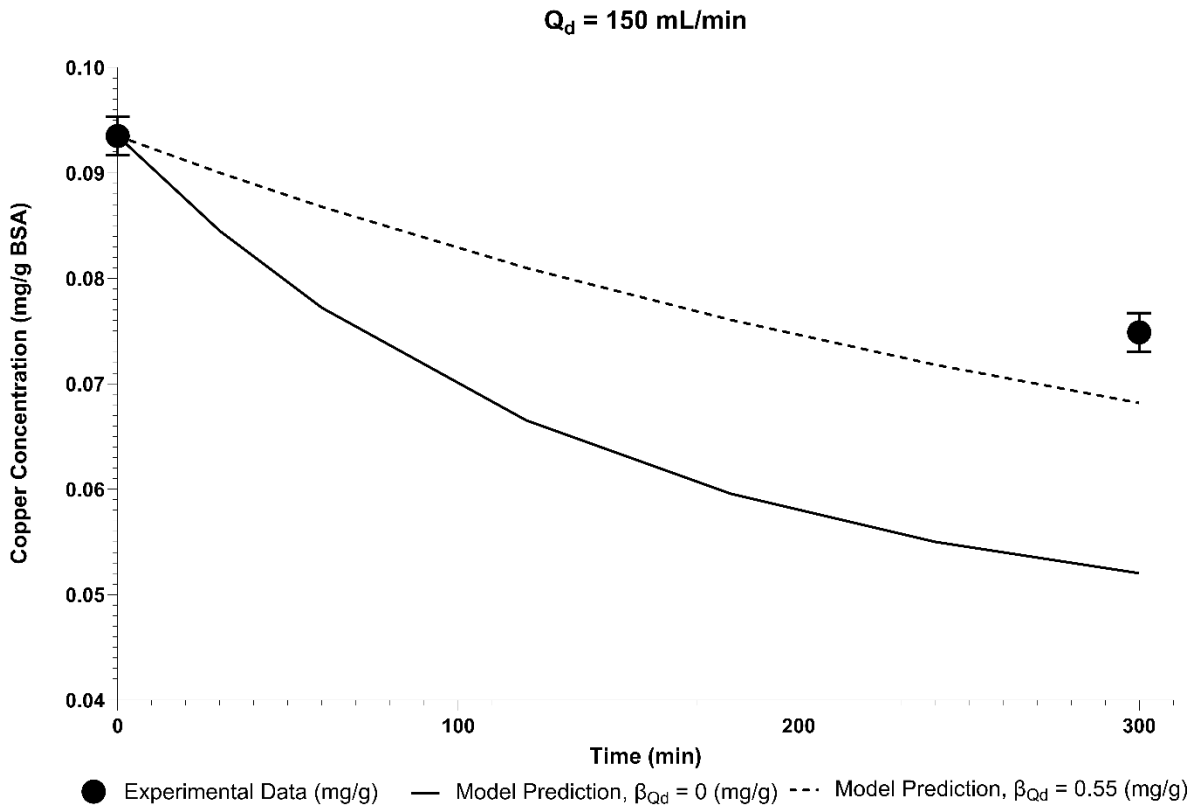


Figure 5-21: Results and model predictions for dialysate flow rates of 2 mL/min (Panel A), 20 mL/min (Panel B), 150 mL/min (Panel C). Errors bars are standard deviation. Where error bars are not shown, it is because they would be smaller than the data point depicted on the graph. Points are experimental data and the lines are the model predictions.

### 5.7.2 *Discussion*

The statistically significant improvement in copper removal for albumin dialysis conditions compared to the negative control confirms our hypothesis that albumin dialysis is promising for the treatment of Wilson's disease and the removal of copper in liver failure. The removal of copper appears to be strongly flow rate dependent, with the highest value of flow rate dependence out of all toxins analyzed. The new, high-pressure tolerant sensors used for the 800 mL/min trial may have leached copped into the solution because of the use of brass plumbing connectors to attach them, confounding that test.

## 5.8 MANGANESE REMOVAL

### 5.8.1 *Results*

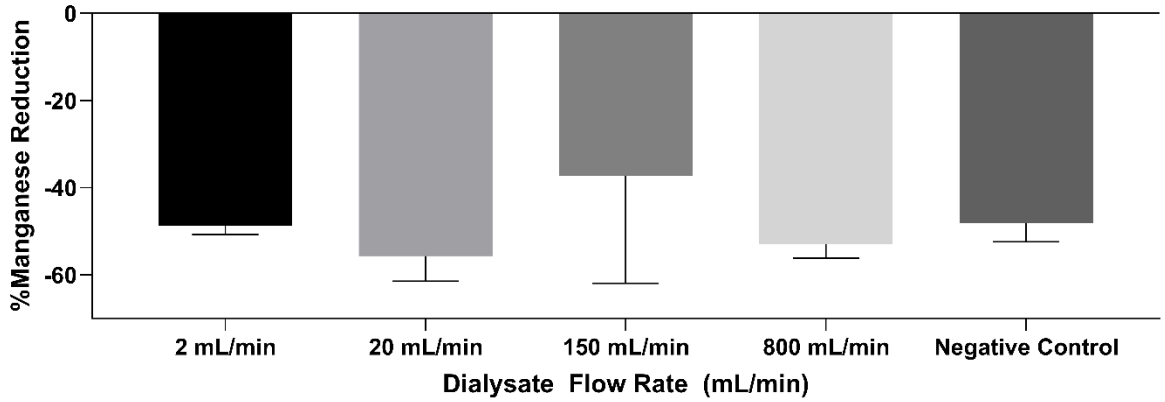


Figure 5-22: Percent Manganese Reduction in Different Test Conditions.

As shown in Figure 5-22, we could not demonstrate any benefit of albumin dialysis in manganese removal. The pure dialysate negative control removed approximately 50% of blood manganese, as would be expected from a purely water-soluble toxin. Thus, we did not apply the protein bound toxin removal model to manganese.

### 5.8.2 *Discussion*

Despite the known albumin binding of manganese (196), we saw nearly 50% manganese concentration reduction in the binder-free dialysis test. This is potentially corroborated by an early report in which chronic kidney disease patients who were not undergoing dialysis had elevated manganese, but dialysis patients had normal manganese (269). Some more recent work supports this conclusion (270). However, a recent study found manganese buildup in the brains of dialysis patients despite normal blood levels (271). Another recent study found elevated blood manganese in hemodialysis patients (272). One study reported lower blood manganese in dialysis patients compared to healthy controls (273). Many population-specific factors such as dietary and environmental exposure or dialysis water quality could influence these varying conclusions. Thus,

more research is needed into whether dialysis alone can remove manganese, both in genetic hypermanganesemia, and environmental exposure or disease-induced hypermanganesemia. It is possible that an error in our blood analog solution preparation, such as the absence of a necessary binding cofactor, caused the manganese to fail to achieve the same binding to our albumin as in a patient.

# Chapter 6. OPTIMIZING ALBUMIN DIALYSIS PART 2: BOVINE SERUM ALBUMIN REMOVES TOXINS FROM HUMAN SERUM ALBUMIN BLOOD-ANALOG SOLUTION

## 6.1 BACKGROUND

Today, all albumin dialysis systems use human serum albumin (HSA). Currently, this HSA is only derived from blood donor plasma. Recombinant HSA is studied, but lacks regulatory approval because of immunogenicity concerns (274). Being the only clinically used agent, HSA remains in short supply and is very expensive. In traditional open-loop dialysis, dialysate passes through the dialyzer once and is discarded. In closed-loop albumin dialysis, the dialysate is returned to the dialysate reservoir and recirculated. The goal of recirculation is reducing costs (158). The closed-loop system increases efficiency, maximizing toxin removal for each dialysate albumin molecule. In MARS, adsorbent columns on the dialysate side prevent albumin saturation by removing toxins from the dialysate albumin. Still the total cost of MARS treatment remains high: One study reported that in 2020, one MARS session cost $2673 United States Dollars (54).

Bovine serum albumin (BSA) is a well characterized, inexpensive alternative to HSA. Thus, BSA is an ideal test molecule to validate the use of a computational model to appropriately

dose an HSA alternative. It is promising for use in extracorporeal circuits because it is part of Fetal Bovine Serum, an ingredient in more than 80% of mesenchymal stem cell-based therapies in clinical trials as of 2014 (275). In the vast majority of cases, these therapies have been safe, indicating that BSA is well tolerated by most patients. While some patients have allergic responses to BSA (276), in albumin dialysis the membrane separates the patient from this potential hazard. Dialysate is not sterile, and usually is not implicated in immune issues because of the membrane.

In this work, we validate the ability of our model of albumin dialysis to accurately predict the impact of changing BSA and HSA concentrations on bilirubin removal from an HSA-based blood analog solution.

## 6.2 METHODS

### 6.2.1 *Experimental Setup*

Five sets of experiments were done in total:

- Condition 1: A pilot study (n = 3) using BSA on both sides of an F6HPS dialyzer (Fresenius, Waltham, MA, USA). This data is the same as in Chapter 5. This was used to fit three parameters:
    - 1: Dialyzer diffusive mass transfer coefficient for free bilirubin moving through polysulfone at a 500 mL/min dialysate side flow rate ($K_{free}A_{Qd=500}$)
    - 2: Bilirubin binding equilibrium constant for the primary binding site on BSA ($K_B$,BSA)
    - 3: The rate at which diffusive mass transfer coefficient for free bilirubin declines with declining dialysate side flow rate for the F3 dialyzer ($\beta_{Q_d}$)

- Condition 2: A pilot study (n = 1) using HSA on the blood side and BSA on the dialysate side using an F6HPS dialyzer. This was used to fit the bilirubin binding equilibrium constant for the primary binding site on HSA (kB,HSA)
- Condition 3: A series of trials (n = 6) with HSA on both sides using an F3 dialyzer (Fresenius, Waltham, MA, USA). This was a positive control, since data from MARS demonstrates bilirubin removal by HSA-containing dialysate from HSA blood solution. The sample size was determined prospectively by a statistical power calculation using the first three trials (see below).
- Condition 4: A series of trials (n = 6) with HSA on the blood side and an equal BSA concentration on the dialysate side using an F3 dialyzer. Conditions 4-5 tested predictions about BSA removing toxins from HSA.
- Condition 5: A series of trials with HSA on the blood side and BSA at a tenfold greater concentration on the dialysate side (n = 6).

The precise values for the five setups are summarized in Table 6-1. The F6HPS trials (setups 1 and 2) were used to set model parameters (binding affinity, dialyzer mass transfer-area coefficient, and flow rate dependence). The F3 trials were used to independently validate the model predictions. The dialyzer mass transfer-area coefficient was adjusted according to the area of the dialyzer as previously described (Section 5.4.1.5). Setups 1 and 2 had the same albumin dialysis circuit design as in Chapter 5, Setup 1. Setups 3-5 had the same albumin dialysis circuit design as in Chapter 5, Setups 2-6. Blood analog solution was the same as in Chapter 5. In all setups care was taken to minimize light exposure. For setups 1 and 2, dialyzers were reused after being cleaned according to established clinical protocols (260,261).

Table 6-1: Albumin Dialysis Setups Used in This Study

| | Setup 1 | Setup 2 | Setup 3 | Setup 4 | Setup 5 |
|---|---|---|---|---|---|
| Duration (hr) | 3 | 3 | 5 | 5 | 5 |
| Blood Analog Solution Volume (mL) | 628.33 | 610 | 200 | 200 | 200 |
| Dialysate Volume (mL) | 626.67 | 637 | 200 | 200 | 200 |
| Blood flow rate (mL/min) | 180 | 180 | 150 | 150 | 150 |
| Dialysate flow rate (mL/min) | 90 | 90 | 150 | 150 | 150 |
| Ultrafiltration rate (mL/min) | 0 | 0 | 0 | 0 | 0 |
| Blood Albumin Concentration (g/dL) | 2 | 2 | 2 | 2 | 2 |
| Dialysate Albumin Concentration (g/dL) | 2 | 2 | 2 | 2 | 20 |
| Blood Albumin | BSA | HSA | HSA | HSA | HSA |
| Dialysate Albumin | BSA | BSA | HSA | BSA | BSA |
| Dialyzer | F6HPS | F6HPS | F3 | F3 | F3 |
| Material | Poly-sulfone | Poly-sulfone | Poly-sulfone | Poly-sulfone | Poly-sulfone |
| Number of Fibers | 8400 (253) | 8400 (253) | 2304 (253) | 2304 (253) | 2304 (253) |
| Hollow Fiber Inner Radius (μm) | 100 (254) | 100 (254) | 100 (255) | 100 (255) | 100 (255) |
| Hollow Fiber Outer Radius (μm) | 140 (254) | 140 (254) | 140 (256) | 140 (256) | 140 (256) |
| Hollow Fiber Length (cm) | 21 (257) | 21 (257) | 20 (255) | 20 (255) | 20 (255) |
| Area ($m^2$) | 1.3 (254) | 1.3 (254) | 0.4 (255) | 0.4 (255) | 0.4 (255) |
| Housing Inner Radius (mm) | 20 (254) | 20 (254) | 11 (measured) | 11 (measured) | 11 (measured) |
| Bilirubin Reflection Coefficient (assumed (158)) | 0 | 0 | 0 | 0 | 0 |
| Reflection Coefficients for Other Toxins (Assumed) | 0 | 0 | 0 | 0 | 0 |

### 6.2.2 *Statistical Power Calculation*

After 3 tests of conditions 4 and 5 were done, a statistical power calculation was performed to predict the sample size needed for statistical significance. This was done to prospectively

constrain the sample size, to avoid spurious significance. The following formula was used (Equation 6-1).

$$n = \left(Z_{1-\frac{\alpha}{2}} + Z_{1-\beta}\right)^2 * \frac{V}{\Delta^2}$$ (Equation 6-1, Sample Size Calculation)

Here, n is the target sample size. $Z_{1-\frac{\alpha}{2}}$ is the z score corresponding to the desired significance level. $\alpha$ is 0.05. $Z_{1-\beta}$ is the z score corresponding to the desired statistical power. $\beta = 0.2$ for a power of 80%. V is the variance of the difference between the sample means of Conditions 4 and 5. Δ is the difference. This calculation determined our final sample size of 6 trials.

### 6.2.3 *Parameter Sweep Ranges*

Six parameters were fit computationally rather than being determined from the literature. These were the primary binding constant for toxin to BSA, the free toxin dialyzer mass transfer area coefficient at a 500 mL/min dialysate side flow rate ($K_{free}A_{Qd=500}$), the rate of change of the toxin dialyzer mass transfer area coefficient with changing dialysate side flow rate for the F3 dialyzer, and the primary binding constant for bilirubin-HSA binding, cholic acid-HSA binding, and indoxyl sulfate HSA binding. The first three were the same as in Chapter 5 for all three toxins.

The primary binding constant for HSA-bilirubin binding was fit as follows: The primary binding site of bilirubin on HSA has approximately an order of magnitude greater affinity than the secondary binding site (224). Thus, the secondary binding site was neglected for this analysis. The constant for the primary binding site was fit. Table 6-2 summarizes past research regarding this parameter. The value of Gray and Stroupe of 4E9 (1/M) was collected at 4° C, which likely increased the binding affinity (277). Thus, we excluded it. A range from 5E6 (1/M) to 4.15E8 (1/M) covers all other reported values. Goodness of fit criteria were the same as in Chapter 5.

Table 6-2: Reported values of bilirubin-HSA binding constant. * Values obtained using DataThief.jar Version 1.7.

| Study | Primary Bilirubin-HSA Binding Constant (1/M) | Temperature (ºC) | Solution | pH |
|---|---|---|---|---|
| Jacobsen, 1969 (278) | 1E8 | | | |
| Beaven, 1973 (279) | 6.7E6 | 24 | 0.5 M NaCl | 8.5 |
| Chen, 1973 (224) | 7.0E7 | 25 | 0.1 M $K_3PO_4$ buffer | 7.4 |
| Gray and Stroupe, 1977 (277) | 4E9 | 4 | 0.1 M $Na_3PO_4$ buffer, 1 mM EDTA | 7.4 |
| Blauer, 1977 (280) | 2E8 | 26.5 | Tris-HCl buffer, 0.02 M, 0.1 M NaCl | 7.4 |
| Jacobsen 1977 (222) | 5.4E7-4E8 depending on conditions* | 20-37 | 0.0067 M Phosphate buffer. Added NaCl or phosphates | 7.4 |
| Rubaltelli and Jori, 1979 (226) | 2.07E8 | 19 | 0.5 M $KH_2PO_4$-$Na_2HPO_4$ buffer | 7.4 |
| Berde et al, 1979 (281) | 1.3E8 | 5 | 122 nM NaCl, 4.7 nM KCl, 1.2 nM $MgSO_4$, 16 mM $Na_2HPO_4$ | 7.4 |
| Berde et al, 1979 (281) | 1.2E7 | 23 | 122 nM NaCl, 4.7 nM KCl, 1.2 nM $MgSO_4$, 16 mM $Na_2HPO_4$ | 7.4 |
| Berde et al, 1979 (281) | 6.4E7 | 37 | 122 nM NaCl, 4.7 nM KCl, 1.2 nM $MgSO_4$, 16 mM $Na_2HPO_4$ | 7.4 |
| Athar, 1999 (282) | 1.31E7 | 28 | Tris-HCl buffer, ionic strength 0.15 | 8 |
| Khan, 2000 (283) | 1.5E7 | 25 | 0.06 M $Na_3PO_4$ buffer, ionic strength 0.15 | 8 |
| Weisiger, et al 2001 (223) | 0.65E7-5.37E7 depending on HSA concentration | 23-25 | 0.25 M Sucrose, 20 mM hepes, tris for pH adjustment | 7.4 |
| Weisiger, et al 2001 (223) | 0.28E7–1.70 E7 depending on HSA concentration | 23-25 | 50 mM KCl, 20 mM hepes, tris for pH adjustment | 7.4 |
| Khan, 2002 (284) | 2.2E7 | 25 | 0.06 M $Na_3PO_4$ buffer | 8 |
| Tayyab et al, 2003 (285) | 1.5E7 | 25 | 0.06 M Phosphate buffer | 8.0 |

The primary binding constant for HSA-cholic acid binding was fit as follows: Table 6-3 summarizes literature values for the HSA-cholic acid binding constant. We excluded Rudman and Kendall, 1957 because the temperature was 5 °C (286). We excluded the value obtained by

Mandeep and colleagues in 2023 for molten-globule HSA because the denatured HSA under study, differed greatly from the form present in our solution (287). Among the remaining range, we tested values of $10^{\alpha}$ (1/M) where α is the exponent of the binding constant, ranging from 2.55 to 4.75 in steps of 0.5.

Table 6-3: Reported values of cholic acid-HSA binding constant

| Study | Primary Cholic Acid-HSA Binding Constant (1/M) | Temperature (ºC) | Solution | pH |
|---|---|---|---|---|
| Mandeep, 2023, native HSA (287) | 3.87E2 | 24-25 °C | Sodium citrate and sodium monophosphate buffer | 7 |
| Mandeep, 2023, molten-globule HSA (287) | 2.34E2 | 24-25 °C | Sodium citrate and sodium monophosphate buffer | 3 |
| Rohacova, 2010, UV (188) | 2.23E4 | Room temperature | 0.01 M PBS | 7.4 |
| Rohacova, 2010, NBD fluorescence (188) | 2.47E4 | Room temperature | 0.01 M PBS | 7.4 |
| Rohacova, 2010, quenching, (188) | 5.18E4 | Room temperature | 0.01 M PBS | 7.4 |
| Scagnolari, 1984 (288) | 3.3E3 | 25 °C | 0.1 M Na-Phosphate | 7.2 |
| Roda, 1982 (289) | 3E3 | 37 °C ± 0.2 °C | 0.1 M Phosphate | 7.2 |
| Burke, 1971 (290) | 2.8E4 | 37 °C | Fasting Serum | 7.4 |
| Burke, 1971 (290) | 3.12E4 | 37 °C | 0.15 M phosphate | 7.4 |
| Rudman and Kendall, 1957 (286) | 1.43E3 | 5 °C | 0.15 M NaCl, 0.01 M Na-phosphate | 7.6 |

The primary binding constant for HSA-indoxyl sulfate binding was fit as follows: Table 6-4 summarizes literature values for the HSA-indoxyl sulfate binding constant. We excluded the value obtained by Deltombe and colleagues in 2017 for blank hemodialysis serum (cleaned of uremic toxins) because this matrix differed greatly from ours (291). Among the remaining values, Sakai, 1995 (292) was the largest value, at 1.61E6 (1/M) and Bergé-Lefranc, 2013 (293) at 37°C

was the smallest at 1.22E3 (1/M). Thus, we considered values of $10^{\alpha}$ (1/M) where $\alpha$ is the exponent of the binding constant, ranging from 3 to 6.3 in steps of 0.1.

Table 6-4: Reported values of Indoxyl Sulfate-HSA binding constant. PBS is an abbreviation for Phosphate-Buffered Saline. Based on the work of Niestanak and Unsworth (294) and Deltombe and colleagues (291)

| Study | Primary Indoxyl Sulfate-HSA Binding Constant (1/M) | Temperature (ºC) | Solution | pH |
|---|---|---|---|---|
| Li, 2021 (295), isothermal titration calorimetry | 1.006E4 | 24.85 °C | 0.1 M PBS | 7.2 |
| Li, 2021 (295), fluorescence | 5.75E4 | 24.85 °C | 0.1 M PBS | 7.2 |
| Li, 2021 (295), fluorescence | 4.63E4 | 29.85 °C | 0.1 M PBS | 7.2 |
| Li, 2021 (295), fluorescence | 3.79E4 | 36.85 °C | 0.1 M PBS | 7.2 |
| Yamamoto, 2021 (296) | 1.27E5 | 37 °C | Phosphate buffer | 7.1 |
| Kato, 2020 (297) | 6.16E4 | 25 °C | 50 mM Tris-HCl buffer, 0.15 M ionic strength | 7.4 |
| Kato, 2020 (297) | 5.53E4 | 30 °C | 50 mM Tris-HCl buffer, 0.15 M ionic strength | 7.4 |
| Kato, 2020 (297) | 3.91E4 | 37 °C | 50 mM Tris-HCl buffer, 0.15 M ionic strength | 7.4 |
| Zaidi, 2019 (298) | 1.04E6 | 25 °C | Sodium Phosphate buffer | 7.4 |
| Deltombe, 2017 (291) | 3.23E4 | 40 °C (299) | Healthy serum | 7.4 |
| Deltombe, 2017 (291) | 9.9E2 | 40 °C (299) | Blank hemodialysis serum (cleaned of uremic toxins) | 7.4 |
| Deltombe, 2017 (291) | 1.515E3 | 40 °C (299) | Non-treated hemodialysis serum | 7.4 |
| Yu, 2017 (300), Native HSA | 3.43E5 | 25 °C | 10 mM MOPS, 10 mM NaCl | 7.4 |
| Yu, 2017 (300), Native HSA | 2.79E5 | 30 °C | 10 mM MOPS, 10 mM NaCl | 7.4 |
| Yu, 2017 (300), Native HSA | 1.36E5 | 37 °C | 10 mM MOPS, 10 mM NaCl | 7.4 |
| Yu, 2017 (300), Native HSA | 1.22E5 | 25 °C | 10 mM MOPS, 140 mM NaCl | 7.4 |
| Yu, 2017 (300), Native HSA | 8.3E4 | 30 °C | 10 mM MOPS, 140 mM NaCl | 7.4 |

| | | | | |
|---|---|---|---|---|
| Yu, 2017 (300), Native HSA | 5.5E4 | 37 °C | 10 mM MOPS, 140 mM NaCl | 7.4 |
| Yu, 2017 (300), 10 mM urea HSA | 3.49E5 | 25 °C | 10 mM MOPS, 10 mM urea | 7.4 |
| Yu, 2017 (300), 10 mM urea HSA | 2.37E5 | 30 °C | 10 mM MOPS, 10 mM urea | 7.4 |
| Yu, 2017 (300), 10 mM urea HSA | 1.34E5 | 37 °C | 10 mM MOPS, 10 mM urea | 7.4 |
| Yu, 2017 (300), 10 mM urea HSA | 1.3E5 | 25 °C | 10 mM MOPS, 10 mM urea, 130 mM NaCl | 7.4 |
| Yu, 2017 (300), 10 mM urea HSA | 1.03E5 | 30 °C | 10 mM MOPS, 10 mM urea, 130 mM NaCl | 7.4 |
| Yu, 2017 (300), 10 mM urea HSA | 5.9E4 | 37 °C | 10 mM MOPS, 10 mM urea, 130 mM NaCl | 7.4 |
| Rueth, 2015 (301) | 3.69E5 | Room temperature | HSA from CKD in PBS | 7.4 |
| Rueth, 2015 (301) | 1.64E5 | Room temperature | HSA from healthy person in PBS | 7.4 |
| Ascenzi, 2015 (302) | 8.14E5 - 9.09E5 | 22 °C | 0.1 M Bis-tris propane buffer | 7.5 |
| Devine, 2014 (303) | 3.66E4 | Room temperature | Uremic plasma, 1:2 dilution by PBS with 0.15 M NaCl (physiological) | 7.4 |
| Devine, 2014 (303) | 1.79E4 | Room temperature | Uremic plasma, 1:2 dilution by PBS with 0.75 M NaCl | 7.4 |
| Devine, 2014 (303) | 3.66E4 | Room temperature | Uremic plasma, 1:2 dilution by PBS with 0.15 M NaCl (physiological) | 7.4 |
| Devine, 2014 (303) | 2.70E4 | Room temperature | Uremic plasma, 1:2 dilution by PBS with 0.3 M NaCl | 7.4 |
| Devine, 2014 (303) | 2.15E4 | Room temperature | Uremic plasma, 1:2 dilution by PBS with 0.5 M NaCl | 7.4 |
| Devine, 2014 (303) | 1.79E4 | Room temperature | Uremic plasma, 1:2 dilution by PBS with 0.75 M NaCl | 7.4 |
| Devine, 2014 (303) | 9.17E4 | Room temperature | Normal plasma, 1:2 dilution by PBS with 0.15 M NaCl (physiological) | 7.4 |
| Devine, 2014 (303) | 7.46E4 | Room temperature | Normal plasma, 1:2 dilution by PBS with 0.15 M NaCl (physiological) | 7.4 |

| | | | | |
|---|---|---|---|---|
| Devine, 2014 (303) | 4.52E4 | Room temperature | Normal plasma, 1:2 dilution by PBS with 0.30 M NaCl | 7.4 |
| Devine, 2014 (303) | 2.52E4 | Room temperature | Normal plasma, 1:2 dilution by PBS with 0.50 M NaCl | 7.4 |
| Devine, 2014 (303) | 1.82E4 | Room temperature | Normal plasma, 1:2 dilution by PBS with 0.75 M NaCl | 7.4 |
| Devine, 2014 (303) | 1.78E4 | Room temperature | Normal plasma, 1:2 dilution by PBS with 0.75 M NaCl | 7.4 |
| Devine, 2014 (303) | 7.46E4 | Room temperature | Normal plasma, 1:2 dilution by PBS with 0.15 M NaCl (physiological) | 7.4 |
| Devine, 2014 (303) | 2.49E4 | Room temperature | Normal plasma, 1:2 dilution by PBS with 0.5 M NaCl | 7.4 |
| Devine, 2014 (303) | 1.12E5 | Room temperature | Normal plasma, 1:10 dilution by PBS with 0.15 M NaCl (physiological) | 7.4 |
| Devine, 2014 (303) | 2.24E4 | Room temperature | Normal plasma, 1:10 dilution by PBS with 0.50 M NaCl (physiological) | 7.4 |
| Viaene, 2013 (304) | 1.98E5 | 37 °C | PBS | |
| Viaene, 2013 (304) | 6.51E4 | 37 °C | Normal serum | |
| Viaene, 2013 (304) | 3.99E4 | 37 °C | Uremic serum | |
| Bergé-Lefranc, 2013 (293) | 3.03E3 | 15 °C | 25 mM 2-(N-morpholino)ethanesulfonic acid in NaCl solution, 0.15 M ionic strength | 7.4 |
| Bergé-Lefranc, 2013 (293) | 2.55E3 | 20 °C | 25 mM 2-(N-morpholino)ethanesulfonic acid in NaCl solution, 0.15 M ionic strength | 7.4 |
| Bergé-Lefranc, 2013 (293) | 1.75E3 | 25 °C | 25 mM 2-(N-morpholino)ethanesulfonic acid in NaCl solution, 0.15 M ionic strength | 7.4 |
| Bergé-Lefranc, 2013 (293) | 1.22E3 | 37 °C | 25 mM 2-(N-morpholino)ethanesulfonic acid in NaCl solution, 0.15 M ionic strength | 7.4 |

| | | | | |
|---|---|---|---|---|
| Zsila, 2013 (305) | 1E6 | 25 °C | Ringer buffer solution | 7.35 |
| Watanabe, 2012 (191) | 9.8E4 | 25 °C | PBS | 7.4 |
| Sakai, 2001 (306) | 1.01E6 | 25 °C | 67 mM sodium phosphate buffer | 6.5 |
| Sakai, 2001 (306) | 9.1E5 | 25 °C | 67 mM sodium phosphate buffer | 7.4 |
| Sakai, 2001 (306) | 8.1E5 | 25 °C | 67 mM sodium phosphate buffer | 8.5 |
| Sakai, 1995 (292) | 1.61E6 | 25 °C | 67 mM sodium phosphate buffer | 7.4 |

## 6.3 RESULTS

### 6.3.1 *Initial Conditions for Modeling (Bilirubin):*

Table 6-5 summarizes measured average starting bilirubin and albumin concentrations for all five setups. These values were used for modeling to avoid error caused by variations in the initial solution.

Table 6-5: Average Initial Bilirubin and Albumin Concentration. $C_{atlb}$ is initial albumin concentration in blood. $C_{atld}$ is initial albumin concentration in dialysate. For Condition 1, n = 3. For Condition 2, n = 1. For Conditions 3-5, n = 6. Values are shown as mean ± standard deviation, except for condition 2.

| Condition | Starting Blood Bilirubin (mg/dL) | Starting Blood Albumin (g/dL) | Starting Dialysate Albumin (g/dL) |
|---|---|---|---|
| 1 (F6HPS, $C_{atlb}$ = 2 g/dL (BSA), $C_{atld}$ = 2 g/dL (BSA)) | 15.37 ± 3.06 | 2.24 ± 0.37 | 1.77 ± 0.41 |
| 2 (F6HPS, $C_{atlb}$ = 2 g/dL (HSA), $C_{atld}$ = 2 g/dL (BSA)) | 20.20 | 1.76 | 1.84 |
| 3 (F3, $C_{atlb}$ = 2 g/dL (HSA), $C_{atld}$ = 2 g/dL (HSA)) | 19.41 ± 3.08 | 2.07 ± 0.07 | 2.12 ± 0.11 |
| 4 (F3, $C_{atlb}$ = 2 g/dL (HSA), $C_{atld}$ = 2 g/dL (BSA)) | 19.93 ± 1.96 | 2.10 ± 0.21 | 2.19 ± 0.14 |
| 5 (F3, $C_{atlb}$ = 2 g/dL (HSA), $C_{atld}$ = 20 g/dL (BSA)) | 20.33 ± 3.26 | 1.99 ± 0.09 | 21.84 ± 3.10 |

### 6.3.2 *$K_{free}A$ and kB Parameter Sweep (Bilirubin):*

The optimal values of kB,BSA, $K_{free}A_{Qd=500}$, and $\beta_{Q_d}$ for bilirubin removal in Setup 1 were found to be kB,BSA = 0.5E7 (1/M) and $K_{free}A_{Qd=500}$= 2500 mL/min for the F6HPS, and

$\beta_{Q_d} = 0.45$ for the F3 dialyzer and 0.05544 for the F6HPS. The F6HPS parameter is based on the literature value obtained for a similar parameter for urea (221). Parameter sweeps are reported in Chapter 5.

Next, we conducted a pilot study (Setup 2) to determine the optimal value of kB,HSA. Because of limited HSA, this was only done once. BSA was used on the dialysate side, while blood side solution was prepared with HSA. Results are shown in Figure 6-1.

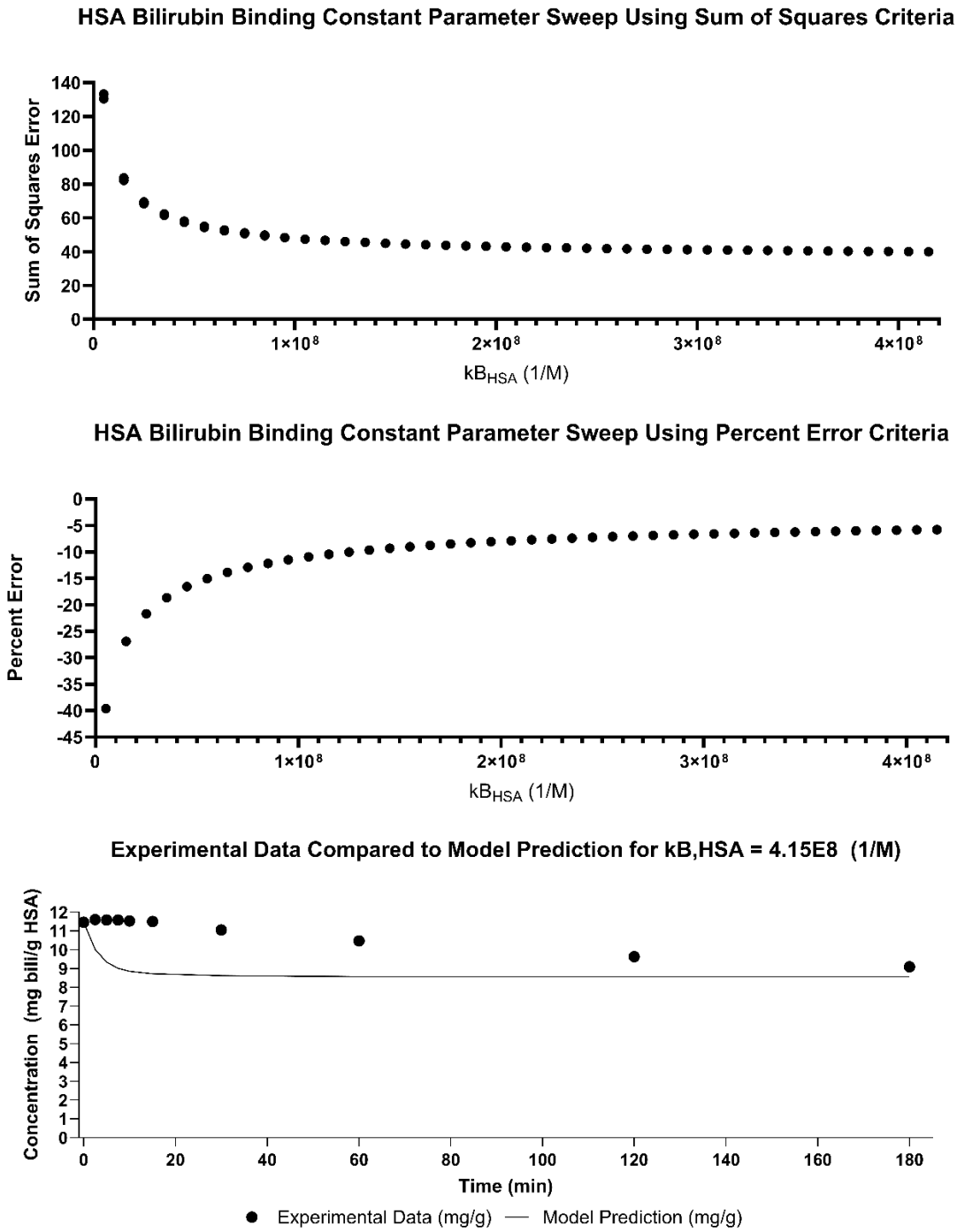


Figure 6-1: **A:** Parameter sweep of HSA-Bilirubin binding constant from 0.5E7 to 4.15E8 1/M evaluated by least squares goodness of fit criterion. **B:** Parameter sweep of HSA-Bilirubin binding constant from 0.5E7 to 4.15E8 1/M evaluated by percent error goodness of fit criterion. **C:** Model prediction compared to experimental result for kB,HSA = 4.15E8 1/M. Percent error for predicting the final value is 5.78%. Sum of squares error is 40.00. Error bars are standard deviation. The standard deviation shown is the standard deviation of n = 3 technical replicates. This setup was only run once. Where error bars are not shown, they would be smaller than the data point on the graph.

### 6.3.3 *Prediction of the Impact of BSA Concentration on Bilirubin Removal from HSA Solution*

To conserve HSA, a new experiment was created, using the F3 pediatric dialyzer and a smaller volume. $K_{free}A_{Qd=500}$ parameter was adjusted for area as shown in Equation 6-2. This condition was used for three setups (Setup 3-5) testing two BSA dialysate concentrations and one HSA dialysate control.

$$K_{free}A_{Qd=500,F3} = K_{free}A_{Qd=500,F6HPS} * \frac{A_{F3}}{A_{F6HPS}} = 2500\,\frac{mL}{min} * \frac{0.4\,m^2}{1.3\,m^2} \approx 769.23\,\frac{mL}{min} \quad \text{(Equation 6-2)}$$

Figure 6-2 shows the predicted impact of dialysate BSA concentration on bilirubin removal by BSA for the different binding constants previously discussed. The starting conditions for this simulation were the same as Setup 4, except that blood HSA concentration was set to exactly 2 g/dL and initial blood bilirubin concentration was set to exactly 20 mg/dL. As seen in Figure 6-2, the model predicted that at 2 g/dL dialysate side BSA, 16.2% would be removed. At 20 g/dL, 19.4% removal was predicted. Actual removal values were 12.1% and 21.2% respectively, supporting the trend predicted by the model.

Figure 6-3 A and B shows the results for blood bilirubin over time compared to the model predictions for conditions 4 and 5 (2 g/dL blood HSA vs. 2 and 20 g/dL dialysate BSA respectively). For both conditions the model predicts the final result with less than 5% error, and all data points are within one standard deviation of the model prediction.

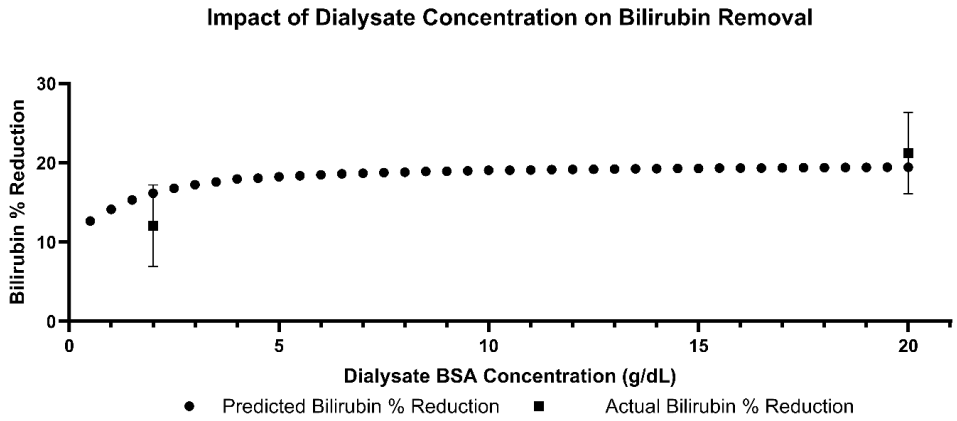


Figure 6-2: Parameter sweep of the impact of dialysate BSA concentration on bilirubin removal from 2 g/dL HSA solution using the kB,HSA value of 4.15E8 (1/M). Modeling predicts a significant improvement from increasing BSA from 2 g/dL to 20 g/dL. This motivated our experiments, and experimental data supported the model prediction. Experimental data is shown as mean ± standard deviation of n = 6 trials.

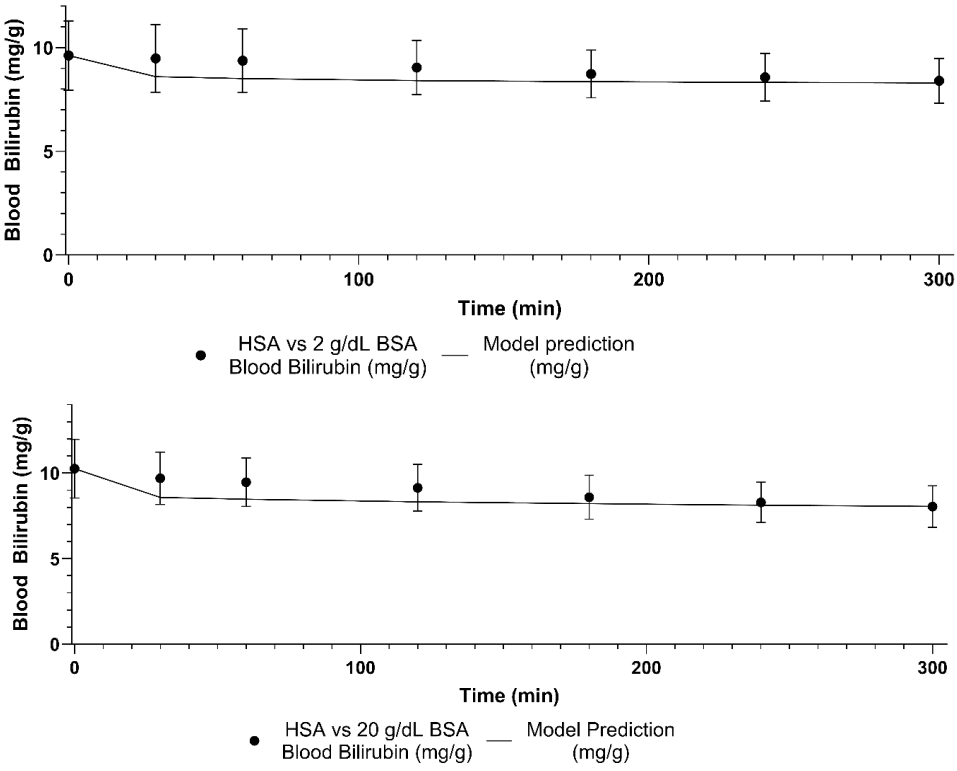


A

B

Figure 6-3: **A**: Model prediction compared to observed results for condition 4 (2 g/dL blood HSA vs. 2 g/dL dialysate BSA). Data is shown as mean ± standard deviation. The model predicts the final value with 1.25% error. Sum of Squares error was 2.12. **B**: Model prediction compared to observed results for condition 5 (2 g/dL blood HSA vs. 20 g/dL dialysate BSA). Data is shown as mean ± standard deviation. The model predicts the final value with 0.14% error. Sum of Squares error was 3.08.

### 6.3.4 *Comparison to HSA vs. HSA Positive Control (Bilirubin):*

A positive control (setup 3) was completed in which both sides had 2 g/dL HSA. Figure 6-4A shows the bilirubin % reduction for this trial, compared to the 2 g/dL BSA and the 20 g/dL BSA conditions. The 20 g/dL BSA dialysate removed significantly more bilirubin than the 2 g/dL BSA dialysate, as predicted by the model. The 20 g/dL BSA dialysate also removed significantly more bilirubin than the positive control. The model predicted the positive control average final blood bilirubin concentration with a -1.73% error (Figure 6-4B) and each predicted time point was within one standard deviation of the observed values. This provides independent validation of the model's predictive power.

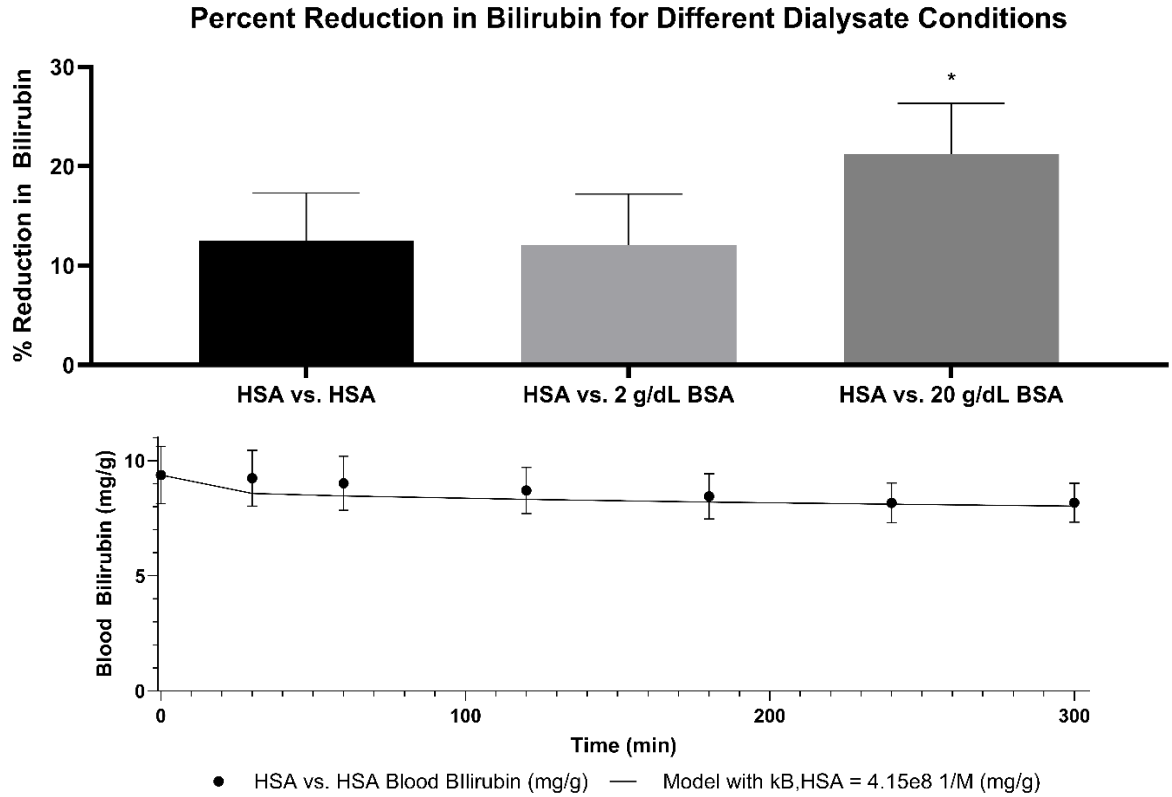


Figure 6-4: **A:** Average ± standard deviation of % reduction in bilirubin. n = 6 for all conditions. * indicates $p < 0.05$. The 20 g/dL BSA dialysate removed significantly more bilirubin than the 2 g/dL BSA dialysate ($p = 0.012$) and the positive control ($p = 0.013$). **B:** Model prediction compared to observed results for positive control (condition 3, 2 g/dL blood HSA vs. 2 g/dL dialysate HSA). Data is shown as mean ± standard deviation. The model predicts the final value with a 1.73% error. Sum of Squares error was 0.97.

### 6.3.5 *Initial Conditions for Modeling (Cholic Acid):*

Table 6-6 summarizes measured average starting cholic acid and albumin concentrations for all five setups. These values were used for modeling to avoid error caused by variations in the initial solution.

Table 6-6: Average initial cholic acid and albumin concentration. $C_{atlb}$ is initial albumin concentration in blood. $C_{atld}$ is initial albumin concentration in dialysate. For Condition 1, n = 3. For Condition 2, n = 1. For Conditions 3-5, n = 6. Values are shown as mean ± standard deviation, except for condition 2.

| Condition | Starting Blood Cholic Acid (mg/dL) | Starting Blood Albumin (g/dL) | Starting Dialysate Albumin (g/dL) |
|---|---|---|---|
| 1 (F6HPS, $C_{atlb}$ = 2 g/dL (BSA), $C_{atld}$ = 2 g/dL (BSA)) | 0.92 ± 0.38 | 2.24 ± 0.37 | 1.77 ± 0.41 |
| 2 (F6HPS, $C_{atlb}$ = 2 g/dL (HSA), $C_{atld}$ = 2 g/dL (BSA)) | 0.70 | 1.76 | 1.84 |
| 3 (F3, $C_{atlb}$ = 2 g/dL (HSA), $C_{atld}$ = 2 g/dL (HSA)) | 0.43 ± 0.08 | 2.07 ± 0.07 | 2.12 ± 0.11 |
| 4 (F3, $C_{atlb}$ = 2 g/dL (HSA), $C_{atld}$ = 2 g/dL (BSA)) | 0.38 ± 0.05 | 2.10 ± 0.21 | 2.19 ± 0.14 |
| 5 (F3, $C_{atlb}$ = 2 g/dL (HSA), $C_{atld}$ = 20 g/dL (BSA)) | 0.48 ± 0.07 | 1.99 ± 0.09 | 21.84 ± 3.10 |

### 6.3.6 *$K_{free}A$ and kB Parameter Sweep (Cholic Acid):*

The optimal values of kB,BSA, $K_{free}A_{Qd=500}$, and $\beta_{Q_d}$ for cholic acid removal in Setup 1 were found to be kB,BSA = 3.4E4 (1/M) and $K_{free}A_{Qd=500}$= 40 mL/min for the F6HPS, and $\beta_{Q_d} = 0.35$ for the F3 dialyzer and 0.05544 for the F6HPS. The F6HPS parameter is based on the literature value obtained for a similar parameter for urea (221). Parameter sweeps are reported in Chapter 5. Next, we conducted a pilot study (Setup 2) to determine the optimal value of kB,HSA. Because of limited HSA, this was only done once. BSA was used on the dialysate side, while blood side solution was prepared with HSA. Results are shown in Figure 6-5. The sum of squares and percent error criteria yield different optimal values. Given that the final cholic acid concentration is small, meaning small changes in concentration will produce large swings in the percent error

criterion, the sum of squares criteria is preferable. Thus, the value of kB,HSA for cholic acid that best explains the data is 10^(2.55) 1/M.

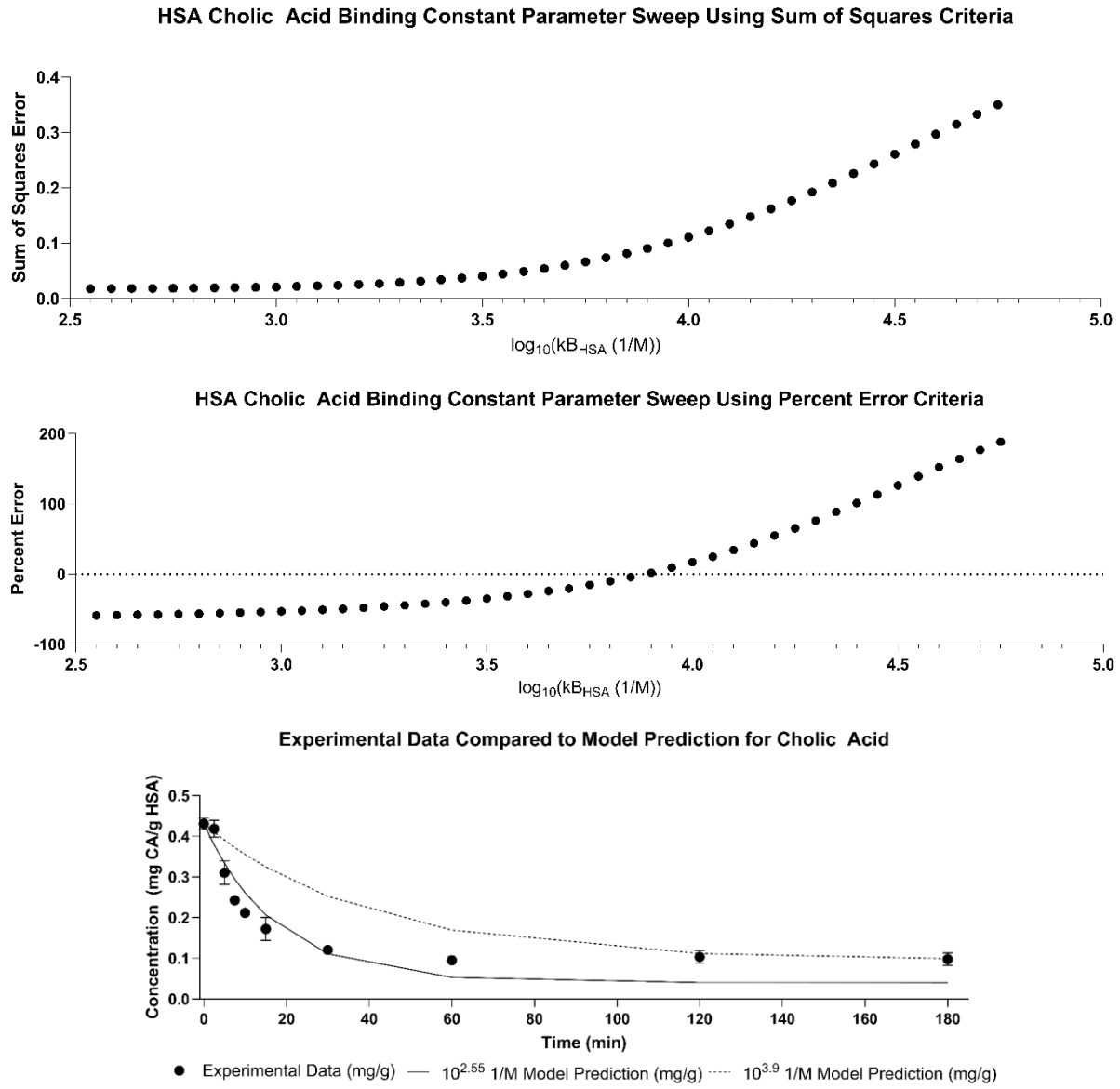


Figure 6-5: **A:** Parameter sweep of log10(HSA-Cholic Acid binding constant in 1/M) from 2.55 to 4.75 evaluated by least squares goodness of fit criterion. **B:** Parameter sweep of log10(HSA-Cholic Acid binding constant in 1/M) from 2.55 to 4.75 evaluated by percent error goodness of fit criterion. **C:** Model prediction compared to experimental result for kB,HSA = 10^(2.55) 1/M and kB,HSA = 10^(3.9) 1/M which are optimal according to the sum of squares and percent error criteria, respectively. Percent error for predicting the final value is -58.8% and 1.78% respectively. Sum of squares error is 0.0177 and 0.0905 respectively. Error bars are standard deviation. The standard deviation shown is the standard deviation of n = 3 technical replicates. This setup was only run once. Where error bars are not shown, they would be smaller than the data point on the graph.

### 6.3.7 *Impact of BSA Concentration on Cholic Acid Removal from HSA Solution*

Figure 6-6 A and B shows the results for blood cholic acid over time compared to the model predictions for conditions 4 and 5 (2 g/dL blood HSA vs. 2 and 20 g/dL dialysate BSA respectively). For both conditions the model predicts the final result with very low sum of squares error (<0.002). The percent error is high because the final values are very small, meaning a small deviation causes a large shift according to this metric.

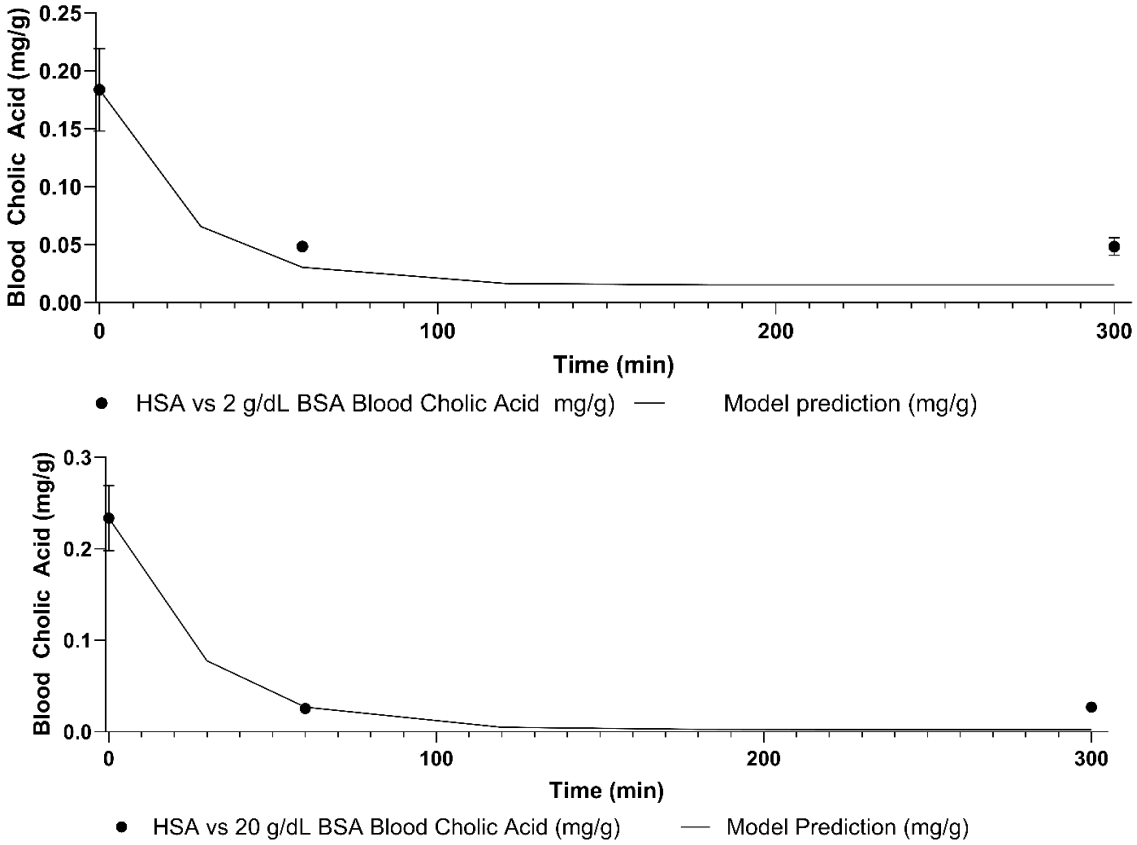


Figure 6-6: **A**: Model prediction compared to observed results for condition 4 (2 g/dL blood HSA vs. 2 g/dL dialysate BSA). Data is shown as mean ± standard deviation. The model predicts the final value with 68.24% error. Sum of Squares error was 0.0014. **B**: Model prediction compared to observed results for condition 5 (2 g/dL blood HSA vs. 20 g/dL dialysate BSA). Data is shown as mean ± standard deviation. The model predicts the final value with 91.13% error. Sum of Squares error was 0.000602.

### 6.3.8 *Comparison to HSA vs. HSA Positive Control (Cholic Acid):*

A positive control (setup 3) was completed in which both sides had 2 g/dL HSA. Figure 6-7 A shows the cholic acid % reduction for this trial, compared to the 2 g/dL BSA and the 20 g/dL BSA conditions. The 20 g/dL BSA dialysate removed significantly more cholic acid than the 2 g/dL BSA dialysate, as predicted by the model. The 20 g/dL BSA dialysate also removed significantly more cholic acid than the positive control. The model predicted the positive control average final blood cholic acid concentration with a 35.90% error (B) and low sum of squares error (<0.003). The low sum of squares error independently validates the model's predictive power.

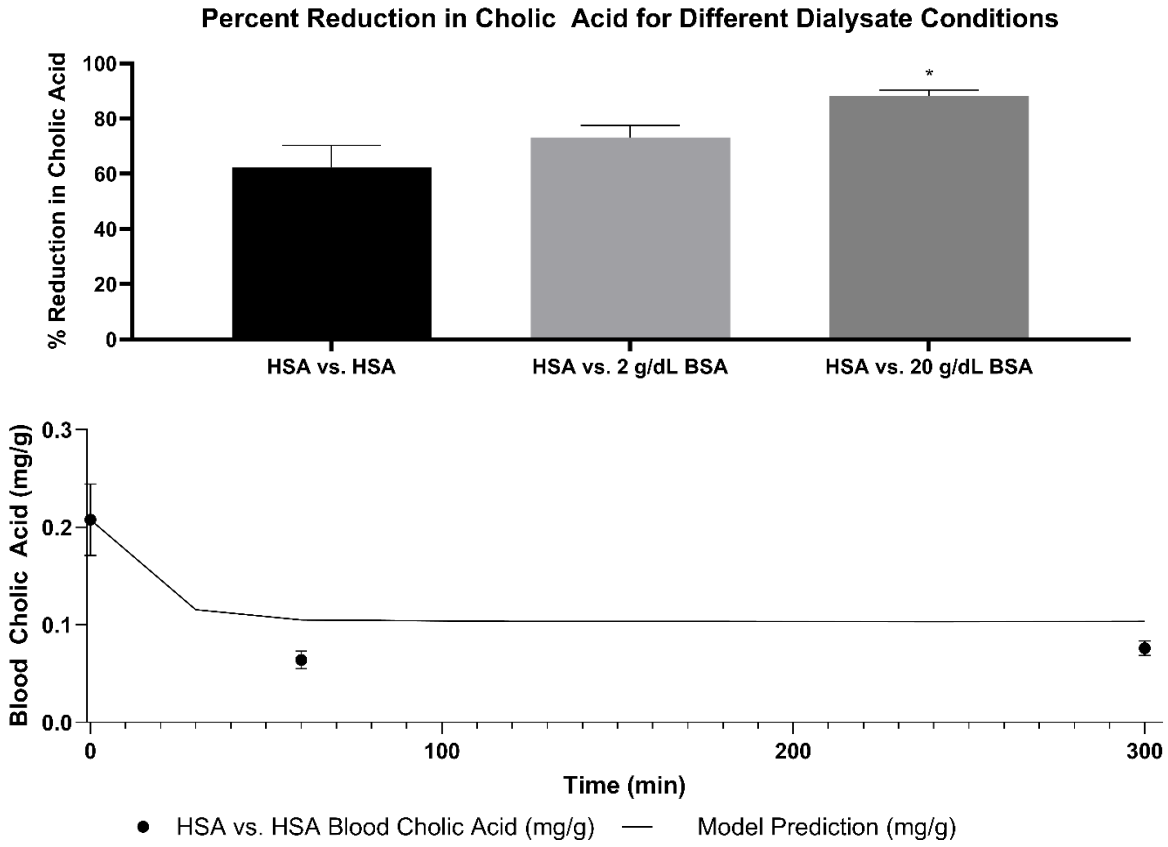


Figure 6-7: **A**: Average ± standard deviation of % reduction in cholic acid. n = 6 for all conditions. * indicates $p < 0.05$. The 20 g/dL BSA dialysate removed significantly more cholic acid than the 2 g/dL BSA dialysate ($p = 1E\text{-}4$) and the positive control ($p = 0.00033$). **B**: Model prediction compared to observed results for positive control (condition 3, 2 g/dL blood HSA vs. 2 g/dL dialysate HSA). Data is shown as mean ± standard deviation. The model predicts the final value with a 35.90% error. Sum of Squares error was 0.002422.

### 6.3.9 *Initial Conditions for Modeling (Indoxyl Sulfate):*

Table 6-7 summarizes measured average starting indoxyl sulfate and albumin concentrations for all five setups. These values were used for modeling to avoid error caused by variations in the initial solution.

Table 6-7: Average initial indoxyl sulfate and albumin concentration. $C_{atlb}$ is initial albumin concentration in blood. $C_{atld}$ is initial albumin concentration in dialysate. For Condition 1, n = 3. For Condition 2, n = 1. For Conditions 3-5, n = 6. Values are shown as mean ± standard deviation, except for condition 2.

| Condition | Starting Blood Indoxyl Sulfate (mg/dL) | Starting Blood Albumin (g/dL) | Starting Dialysate Albumin (g/dL) |
|---|---|---|---|
| 1 (F6HPS, $C_{atlb}$ = 2 g/dL (BSA), $C_{atld}$ = 2 g/dL (BSA)) | 2.27 ± 0.67 | 2.24 ± 0.37 | 1.77 ± 0.41 |
| 2 (F6HPS, $C_{atlb}$ = 2 g/dL (HSA), $C_{atld}$ = 2 g/dL (BSA)) | 2.62 | 1.76 | 1.84 |
| 3 (F3, $C_{atlb}$ = 2 g/dL (HSA), $C_{atld}$ = 2 g/dL (HSA)) | 2.95 ± 0.60 | 2.07 ± 0.07 | 2.12 ± 0.11 |
| 4 (F3, $C_{atlb}$ = 2 g/dL (HSA), $C_{atld}$ = 2 g/dL (BSA)) | 2.66 ± 0.11 | 2.10 ± 0.21 | 2.19 ± 0.14 |
| 5 (F3, $C_{atlb}$ = 2 g/dL (HSA), $C_{atld}$ = 20 g/dL (BSA)) | 2.90 ± 0.29 | 1.99 ± 0.09 | 21.84 ± 3.10 |

### 6.3.10 *$K_{free}A$ and kB Parameter Sweep (Indoxyl Sulfate):*

The optimal values of kB,BSA, $K_{free}A_{Qd=500}$, and $\beta_{Q_d}$ for indoxyl sulfate removal in Setup 1 were found to be kB,BSA = $10^{4.9}$ (1/M) and $K_{free}A_{Qd=500}$= 1500 mL/min for the F6HPS, and $\beta_{Q_d} = 0.0$ for the F3 dialyzer and 0.05544 for the F6HPS. The F6HPS parameter is based on the literature value obtained for a similar parameter for urea (221). Parameter sweeps are reported in Chapter 5.

Next, we conducted a pilot study (Setup 2) to determine the optimal value of kB,HSA. Because of limited HSA, this was only done once. BSA was used on the dialysate side, while blood side solution was prepared with HSA. Results are shown in Figure 6-8. The conditions with a log10(kB,HSA) of 3.7, 3.9, 4.0, and 4.4 could not be simulated due to numerical instability. The

percent error condition was minimized by a log10(kB,HSA) value of 4.9. The sum of squares error condition was minimized by a log10(kB,HSA) value of 5.0. Since it considers all available data, the sum of squares condition is preferrable. Thus, the value of kB,HSA for indoxyl sulfate that best explains the data is 10E5 1/M. This value is close to the value of KB,BSA for indoxyl sulfate (10^4.9 1/M).

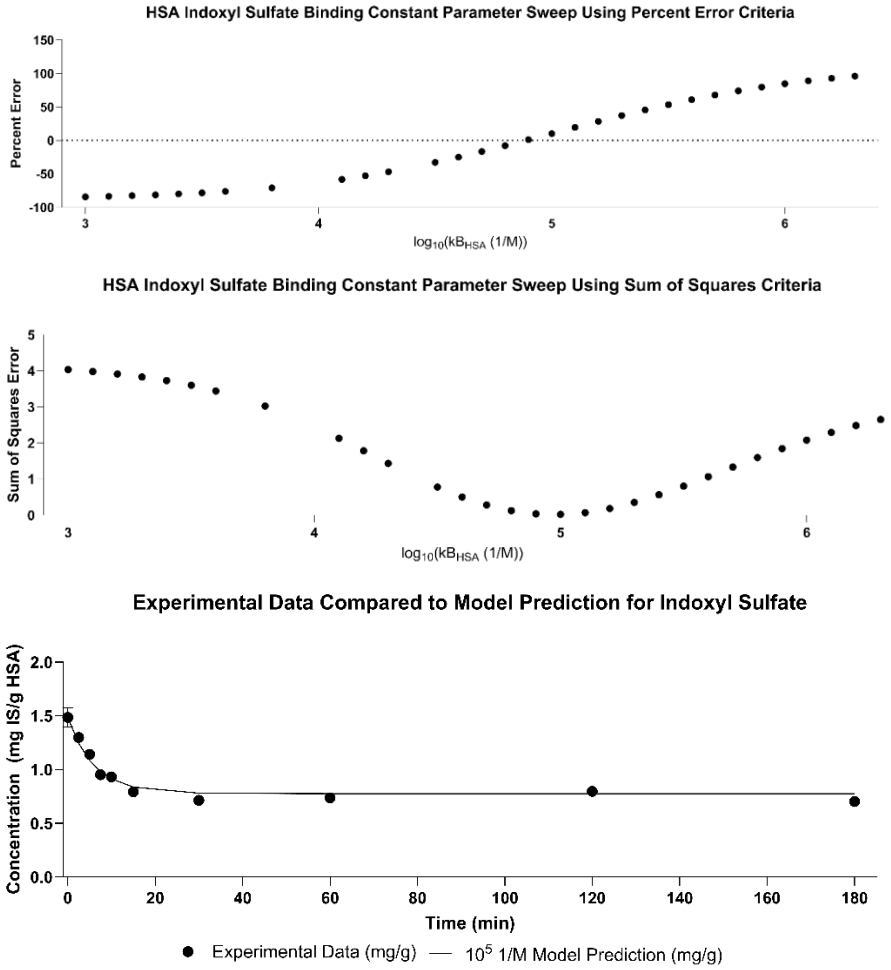


Figure 6-8: **A:** Parameter sweep of log10(HSA-Indoxyl Sulfate binding constant in 1/M) from 3.1 to 6.3 evaluated by least squares goodness of fit criterion. **B:** Parameter sweep of log10(HSA-Indoxyl Sulfate binding constant in 1/M) from 3.1 to 6.3 evaluated by percent error goodness of fit criterion. **C:** Model prediction compared to experimental result for kB,HSA = 10^(5) 1/M. Percent error for predicting the final value is 10.29%. Sum of squares error is 0.021. Error bars are standard deviation. The standard deviation shown is the standard deviation of n = 3 technical replicates. This setup was only run once. Where error bars are not shown, they would be smaller than the data point on the graph.

### 6.3.11 *Impact of BSA Concentration on Indoxyl Sulfate Removal from HSA Solution*

Figure 6-9 A and B shows the results for blood indoxyl sulfate over time compared to the model predictions for conditions 4 and 5 (2 g/dL blood HSA vs. 2 and 20 g/dL dialysate BSA respectively). For both conditions the model predicts the final result with a sum of squares error < 0.04. The percent error is relatively high (up to 35%) because the final value is small. The model demonstrates good predictive power for the impact of dialysate side albumin concentration on indoxyl sulfate removal.

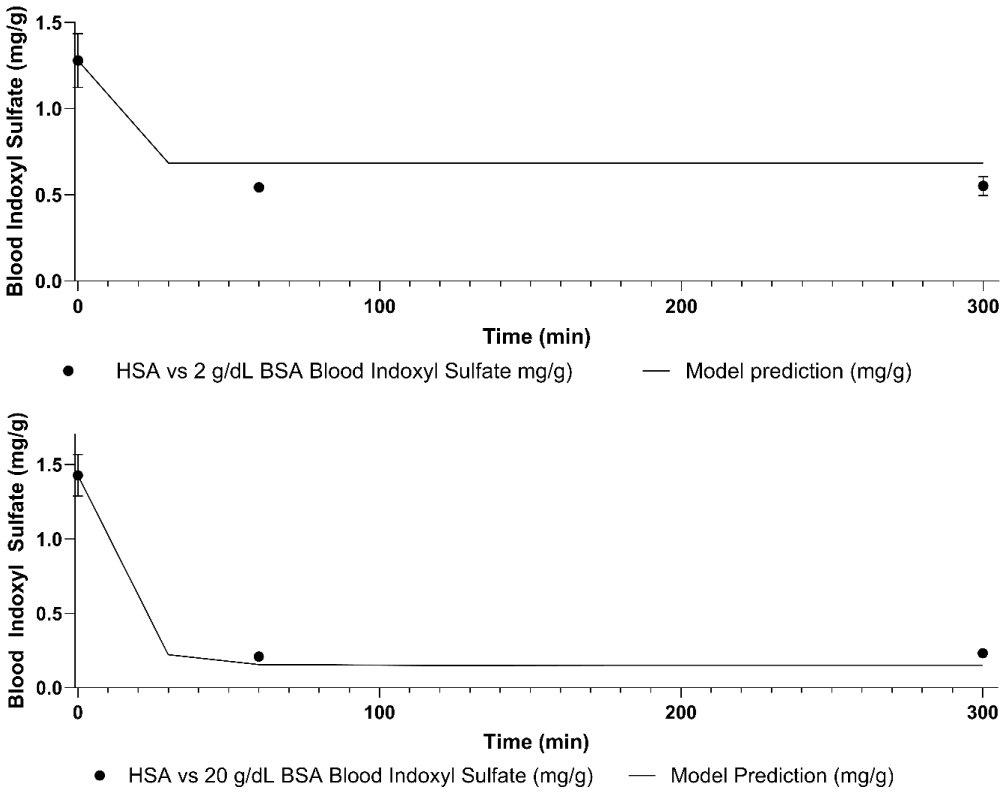


Figure 6-9: **A**: Model prediction compared to observed results for condition 4 (2 g/dL blood HSA vs. 2 g/dL dialysate BSA). Data is shown as mean ± standard deviation. The model predicts the final value with 23.85% error. Sum of Squares error was 0.0369. **B**: Model prediction compared to observed results for condition 5 (2 g/dL blood HSA vs. 20 g/dL dialysate BSA). Data is shown as mean ± standard deviation. The model predicts the final value with 34.6% error. Sum of Squares error was 0.00938.

### 6.3.12 *Comparison to HSA vs. HSA Positive Control (Indoxyl Sulfate):*

A positive control (setup 3) was completed in which both sides had 2 g/dL HSA. Figure 6-10 A shows the indoxyl sulfate % reduction for this trial, compared to the 2 g/dL BSA and the 20 g/dL BSA conditions. The 20 g/dL BSA dialysate removed significantly more indoxyl sulfate than the 2 g/dL BSA dialysate, as predicted by the model. The 20 g/dL BSA dialysate also removed significantly more indoxyl sulfate than the positive control. The model predicts the outcome of the positive control with a 0.064 sum of squares error and a 30.74% percent error.

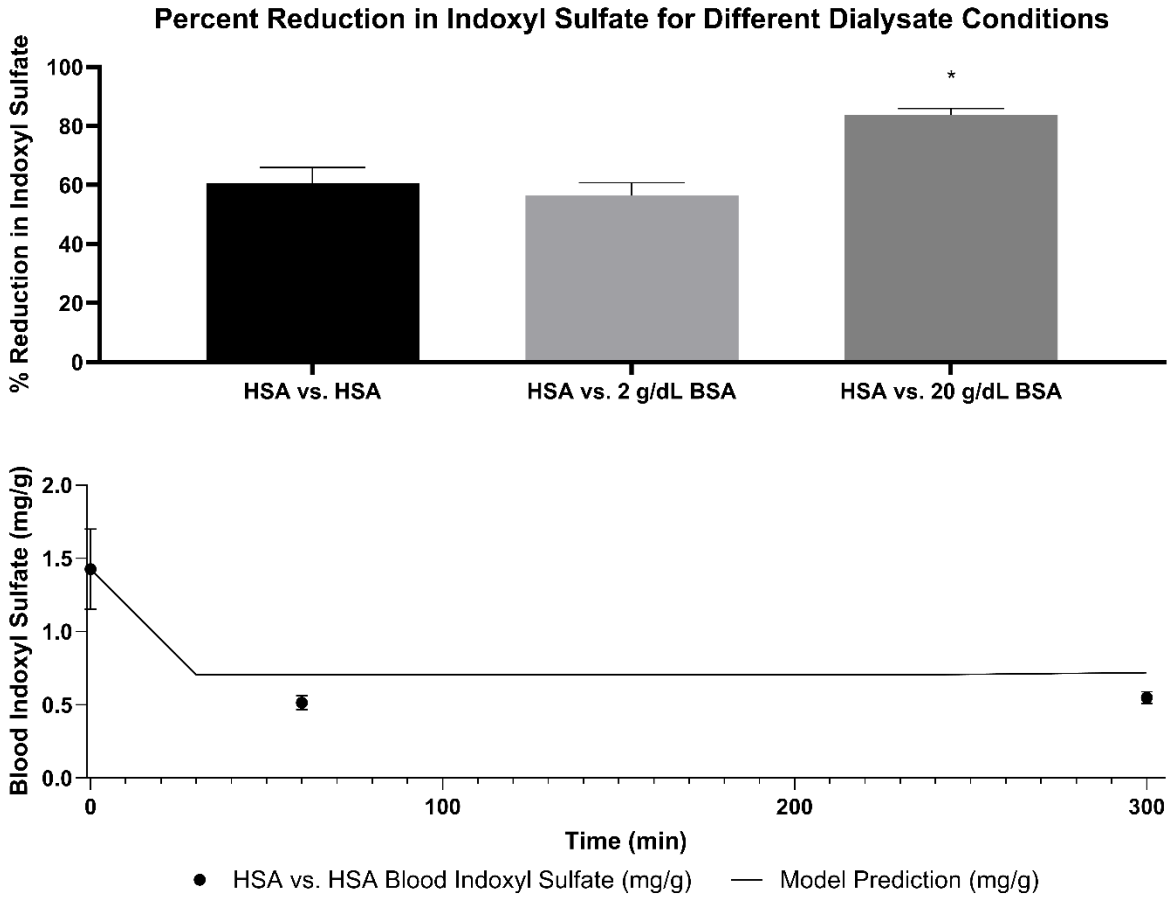


Figure 6-10: **A**: Average ± standard deviation of % reduction in indoxyl sulfate. n = 6 for all conditions. * indicates $p < 0.05$. The 20 g/dL BSA dialysate removed significantly more indoxyl sulfate than the 2 g/dL BSA dialysate ($p = 1.25E-6$) and the positive control ($p = 2.98E-5$). **B**: Model prediction compared to observed results for positive control (condition 3, 2 g/dL blood HSA vs. 2 g/dL dialysate HSA). Data is shown as mean ± standard deviation. The model predicts the final value with a 30.74% error. Sum of Squares error was 0.064.

### 6.3.13 *Copper Removal from HSA Solution:*

Table 6-8 summarizes measured average starting copper and albumin concentrations for all five setups. The analysis in this section is preliminary, based on the first three trials of each condition. Thus, n = 3 instead of n = 6 as for other analogous tables in this chapter. As shown in Figure 6-11, the pilot study showed no copper removal from HSA blood solution by BSA dialysate across an F6HPS dialyzer. Because of this, the pilot study could not be used to fit a kB,HSA value for modeling. Thus, the experimental work on copper removal from HSA blood solutions by BSA and HSA dialysate is presented on its own, without mathematical modeling. For conditions 3-5, no trends in copper reduction could be identified from the data collected so far. This is shown in Figure 6-12.

Table 6-8: Average Initial copper and albumin concentration. $C_{atlb}$ is initial albumin concentration in blood. $C_{atld}$ is initial albumin concentration in dialysate. For Condition 1 and 3-5, n = 3. For Condition 2, n = 1. Values are shown as mean ± standard deviation, except for condition 2.

| Condition | Starting Blood Copper (mg/dL) | Starting Blood Albumin (g/dL) | Starting Dialysate Albumin (g/dL) |
|---|---|---|---|
| 1 (F6HPS, $C_{atlb}$ = 2 g/dL (BSA), $C_{atld}$ = 2 g/dL (BSA)) | 0.24 ± 0.12 | 2.24 ± 0.37 | 1.77 ± 0.41 |
| 2 (F6HPS, $C_{atlb}$ = 2 g/dL (HSA), $C_{atld}$ = 2 g/dL (BSA)) | 0.33 | 1.76 | 1.84 |
| 3 (F3, $C_{atlb}$ = 2 g/dL (HSA), $C_{atld}$ = 2 g/dL (HSA)) | 0.12 ± 0.01 | 2.11 ± 0.05 | 2.17 ± 0.05 |
| 4 (F3, $C_{atlb}$ = 2 g/dL (HSA), $C_{atld}$ = 2 g/dL (BSA)) | 0.15 ± 0.05 | 1.96 ± 0.10 | 2.15 ± 0.11 |
| 5 (F3, $C_{atlb}$ = 2 g/dL (HSA), $C_{atld}$ = 20 g/dL (BSA)) | 0.13 ± 0.03 | 2.04 ± 0.07 | 27.30 ± 4.05 |

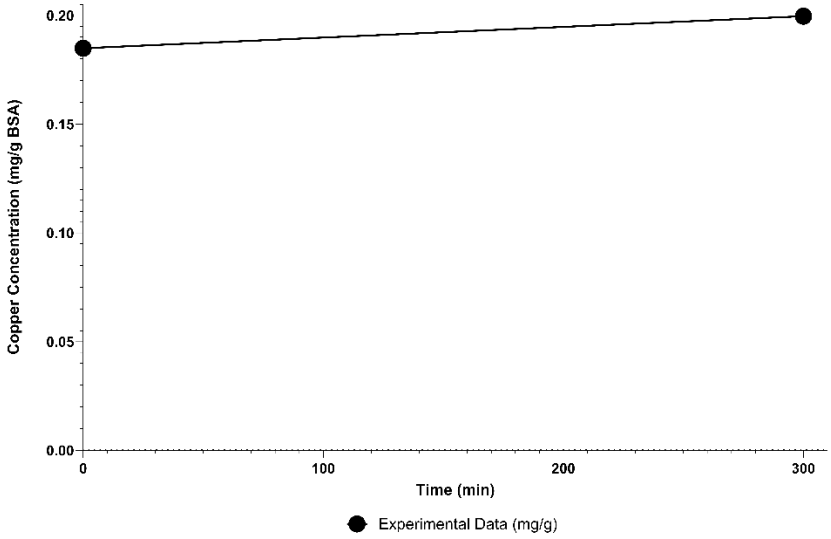


Figure 6-11: Blood side copper in Condition 2. No copper removal occurred in the pilot study.

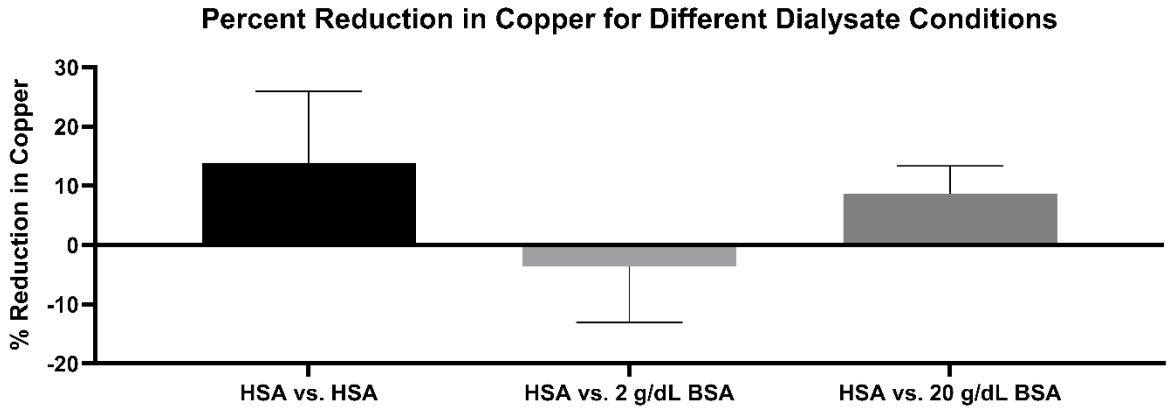


Figure 6-12: Percent reduction in copper for different dialysis conditions. No statistically significant trends were identified.

### 6.3.14 *Manganese Removal from HSA Solution:*

Table 6-9 summarizes measured average starting manganese and albumin concentrations for all five setups. The analysis in this section is preliminary, based on the first three trials of each condition. Thus, n = 3 instead of n = 6 as for other analogous tables in this chapter. Previously, we did not detect a significant impact on manganese removal from adding BSA to dialysate (Section 5.8).

Thus, no value for kB,BSA could be fit and modeling could not be done. The experimental work on manganese removal from HSA blood solutions by BSA and HSA dialysate is presented on its own, without mathematical modeling. In the pilot study, manganese concentration in HSA blood solution declined by 44.8% when dialyzed against 2 g/dL BSA dialysate. This result is consistent with past work with BSA blood solutions, BSA dialysate, and dialysate without sorbents. This data is shown in Figure 6-13. When comparing conditions 3-5, identification of statistically significant trends was compromised by large variation between trials. The data is shown in Figure 6-14. Increasing dialysate side BSA concentration from 2 g/dL to 20 g/dL increased the percent removal of manganese from 31.1% to 53.9%, with a p value of 0.052. This falls short of the prespecified threshold for statistical significance, but indicates that a study with a larger, prospectively constrained sample size may identify a trend. Observing a dose response for manganese removal by dialysate BSA would support the hypothesis that manganese is a protein-bound toxin which can be removed effectively by sorbent dialysis.

Table 6-9: Average initial manganese and albumin concentration. $C_{atlb}$ is initial albumin concentration in blood. $C_{atld}$ is initial albumin concentration in dialysate. For Condition 1 and 3-5, n = 3. For Condition 2, n = 1. Values are shown as mean ± standard deviation, except for condition 2.

| Condition | Starting Blood Manganese (mg/dL) | Starting Blood Albumin (g/dL) | Starting Dialysate Albumin (g/dL) |
|---|---|---|---|
| 1 (F6HPS, $C_{atlb}$ = 2 g/dL (BSA), $C_{atld}$ = 2 g/dL (BSA)) | 0.0155 ± 0.0051 | 2.24 ± 0.37 | 1.77 ± 0.41 |
| 2 (F6HPS, $C_{atlb}$ = 2 g/dL (HSA), $C_{atld}$ = 2 g/dL (BSA)) | 0.0226 | 1.76 | 1.84 |
| 3 (F3, $C_{atlb}$ = 2 g/dL (HSA), $C_{atld}$ = 2 g/dL (HSA)) | 0.00977 ± 0.0025 | 2.11 ± 0.05 | 2.17 ± 0.05 |
| 4 (F3, $C_{atlb}$ = 2 g/dL (HSA), $C_{atld}$ = 2 g/dL (BSA)) | 0.0119 ± 0.0026 | 1.96 ± 0.10 | 2.15 ± 0.11 |
| 5 (F3, $C_{atlb}$ = 2 g/dL (HSA), $C_{atld}$ = 20 g/dL (BSA)) | 0.0130 ± 0.0031 | 2.04 ± 0.07 | 27.30 ± 4.05 |

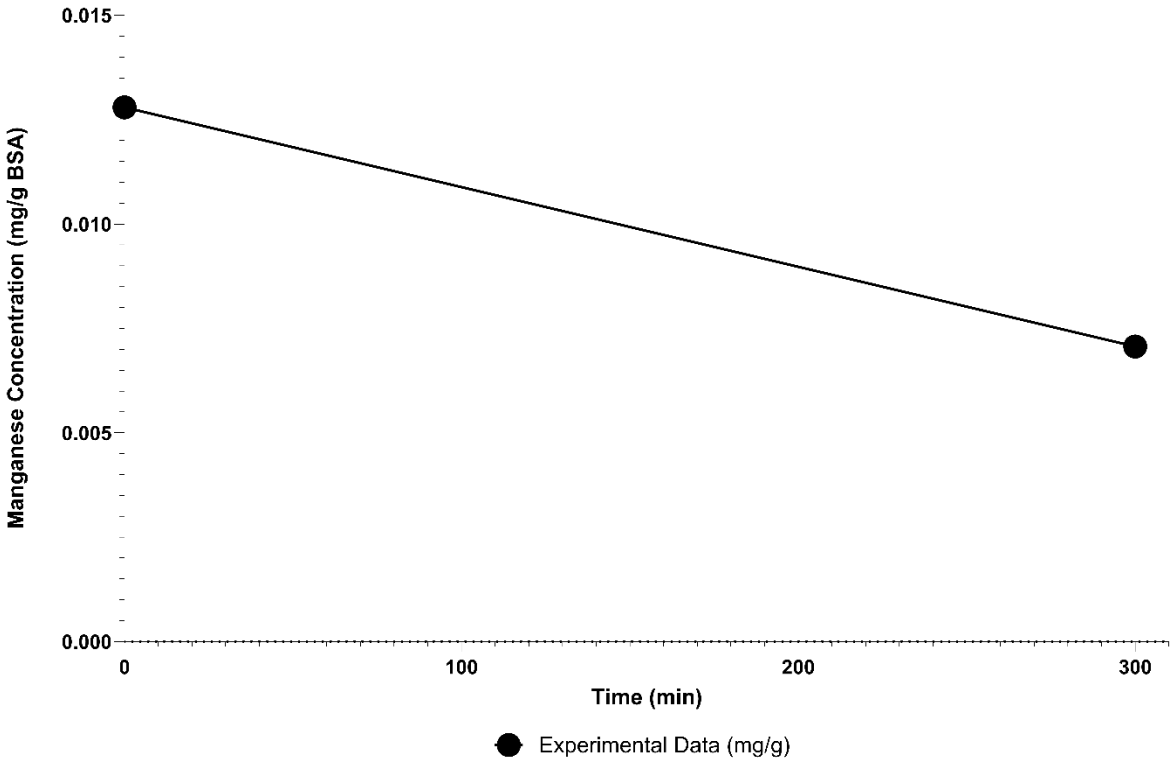


Figure 6-13: Blood side manganese removal in Condition 2. Manganese declined by 44.8%.

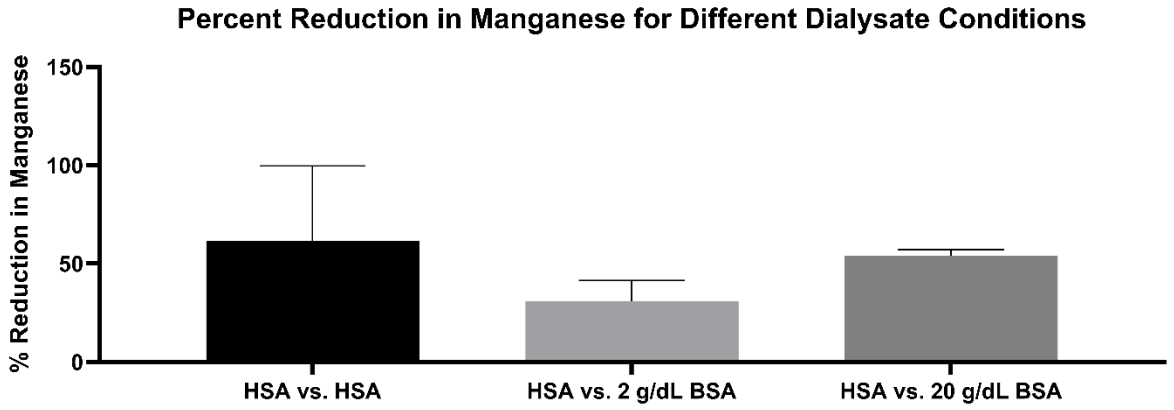


Figure 6-14: Percent reduction in manganese for different dialysis conditions. No comparisons reached the prespecified 0.05 threshold for statistical significance. The comparison between 2 g/dL BSA and 20 g/dL BSA had a p value of 0.052, indicating that a larger study with a prospectively constrained sample size may be informative.

## 6.4 DISCUSSION

This work demonstrates that BSA in high concentrations can remove bilirubin, cholic acid, and indoxyl sulfate from an HSA solution. It also validates a computational model that can be used to rationally design albumin dialysis. This paves the way for optimization of an albumin dialysis system for protein bound toxin removal. It also creates the potential for personalized dialysis regiments, where patients are given flow rate conditions and dialysate compositions tailored to their body volume and toxin concentrations.

This chapter only analyzed the model's ability to predict the impact of changes in albumin concentration. Further work is in progress to predict the impact of changes in other parameters and at larger scales.

Our group recently published a new Advanced Multi-Organ Replacement System (AMOR) (2). This device bridged critically ill multi-organ failure patients to liver transplant or recovery in a pilot study at the University of Washington, with greater excess fluid removal than previously observed. In that study, we published data demonstrating the impact of dialysate HSA concentration on bilirubin removal in a clinical setting. Models such as this one can be used to provide personalized medicine dosing of the AMOR system or provide standardized criteria to improve its clinical usage. Other binder dialysis devices can also be modeled in this way.

The model overestimates the rate at which bilirubin is transported across the membrane, even though it makes accurate predictions about equilibrium values. This has been observed previously with our model (Chapter 5), and similar models (147). Modeling membrane absorption may improve the capability to accurately predict bilirubin removal kinetics. This would enable coupling with a charcoal column model, such as the one developed by our group (307), to model a complex clinical system such as AMOR.

This mode of clinical binder dialysis systems could improve liver failure treatment by accurately predicting post-treatment concentrations. This work also demonstrates that BSA provides an alternative to scarce and expensive HSA with comparable or greater bilirubin removal. Additionally, we can simulate other dialysate binder molecules that may replace albumin. This would mitigate the costs and drawbacks of allogenic or xenogeneic albumin. This manuscript provides a proof of concept demonstrating these applications.

# Chapter 7. CHARCOAL COLUMNS FOR ALBUMIN REGENERATION AND RINSING SOLUTIONS FOR CHARCOAL COLUMN REGENERATION

## 7.1 BACKGROUND

As discussed in Chapter 1, existing albumin dialysis systems recirculate dialysate side albumin to reduce costs. Without some mechanism to regenerate albumin, it becomes rapidly saturated, greatly limiting toxin removal. The addition of resin and charcoal columns on the dialysate side allows the regeneration of albumin, because toxins from the albumin cross onto the charcoal and resin.

However, adding a charcoal column means that the saturation of the column now limits how much toxin can be removed. Previous work by our group suggested that charcoal columns can be rinsed to remove toxin (183). This has been demonstrated previously with urea (308). However, a previous effort to implement this with bilirubin was unsuccessful (309). This attempt involved a chitosan-encapsulated activated charcoal column. The authors used phosphate buffer to rinse their charcoal, aiming to desorb bilirubin. Our protocol instead utilized dialysate (*in vitro*) and D5NS saline (*in vivo*).

In our Advanced Multi-Organ Replacement (AMOR) system, an Adsorba 300 charcoal column was added to the dialysate circuit (2). The Adsorba 300 is chosen because it is FDA approved. We have published a study showing that rinsing improves the rate of bilirubin removal from a saturated Adsorba 300 column *in vitro* (2). This work is presented here alongside similar data for the other protein bound toxins we tested.

In addition, we measured the removal of albumin during BSA solution flow through an Adsorba 300 column over time. Albumin loss has been previously observed with MARS (75). Thus, reporting albumin loss data is important for characterizing and optimizing a novel system.

## 7.2 METHODS

### 7.2.1 *Charcoal Column Trial Setup*

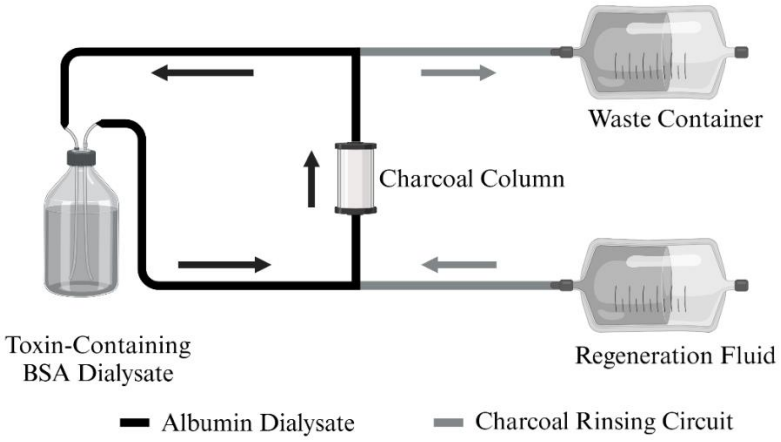


Figure 7-1: Charcoal column regeneration in vitro test setup. The main detoxification circuit is in black. The rinsing circuit is in grey. Figure from (2).

Figure 7-1 shows a schematic of our charcoal column set-up to test the efficacy of regeneration of charcoal column. Adsorba 300 columns (Baxter, Deerfield, IL, USA) were used to remove toxins from the dialysate with toxins and BSA. Columns were primed according to the instructions using glucose solution and saline. After the priming, 500 mL of BSA dialysate were introduced. Priming fluid was discarded into a waste container until yellow pigment was seen at

the column outlet. Now the system was switched into detoxification mode. BSA dialysate was recirculated through the column for 3 hours. Samples were taken at the inlet and outlet. The column dead volume was determined using the volume of priming fluid. In all setups care was taken to protect the setup from light.

### 7.2.2 *Charcoal Column Regeneration Using Dialysate Solution*

After 3 hours of toxin laden BSA flow at 120 ml/min, regeneration began at 50 mL/min with outflow to waste for 30 minutes using dialysate without albumin and toxins. Simultaneously, used BSA dialysate in the column was discarded.

After regeneration, the column was reconnected to the BSA circuit with a 120 mL/min flow rate, with regeneration fluid discarded to prevent toxin loss in experimental tubing. Discarding stopped when yellow pigment appeared in the charcoal column outlet, measuring column dead volume. Once regeneration fluid was removed, toxin-laden BSA dialysate continued to recirculate for another 3 hours as previously. 120 mL/min was chosen as the toxin removal flow rate because it is the recommended flow rate in the Instructions for Use for the Adsorba 300 column.

### 7.2.3 *Flow Rate Comparison*

Subsequently, a second set of experiments was run with the flow rate during toxin removal at 20 mL/min. All other parameters (toxin removal time, regeneration time, regeneration flow rate) were the same as in the 120 mL/min setup.

### 7.2.4 *Statistics*

Charcoal column regeneration was analyzed using slopes between the first and last points of specific time periods: "First Hour" (0 to 60 minutes), "Pre-regeneration" (120 to 180 minutes), and "Post-regeneration" (210 to 270 minutes).

Concentration reduction was defined as follows:

$$\%\ Reduction = \frac{\left(C(t=390\ min) - C(t=0)\right) * 100\%}{C(t=0)} \text{ (Equation 7-1)}$$

Clearance was calculated as follows:

$$Clearance = \frac{(C_{i-1} * V_{i-1} - C_i * V_i)}{C_{i-1} * (t_i - t_{i-1})} \text{ (Equation 7-2)}$$

Here, C corresponds to concentration. V corresponds to volume. t is time. i refers to a time point and i - 1 refers to the previous time point.

Comparisons were made using unpaired two-tailed t-tests without assuming equal variance. A $p < 0.05$ was considered statistically significant.

## 7.3 RESULTS

### 7.3.1 *Bilirubin*

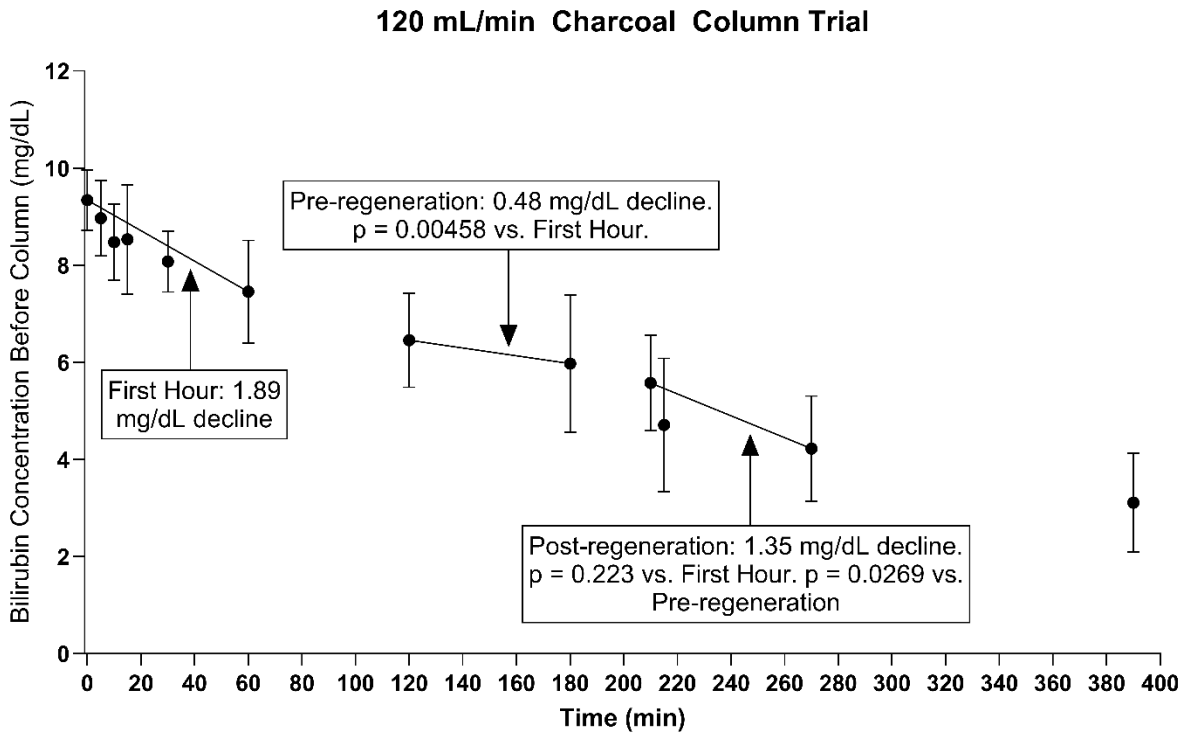


Figure 7-2: Change in bilirubin concentration over time before and after regeneration of the charcoal column for the 120 mL/min flow rate. Error bars are standard deviation.

Figure 7-2 shows bilirubin concentration over time during the albumin regeneration experiment using the Adsorba 300 charcoal column at a 120 mL/min flow rate. In the first hour of the experiments, the bilirubin concentration declined at a rate of 1.89 mg/dL/hr. Through the hour "pre-regeneration", this rate decreased to 0.48 mg/dL/hr, which is significantly lower than the first hour ($p = 0.0046$). During the hour of "post-regeneration", the concentration declined at a rate of 1.35 mg/dL/hr. This rate was a significant increase from the "pre-regeneration" period ($p = 0.027$). The "post regeneration" bilirubin decline rate did not differ significantly from the first hour observation ($p = 0.22$). The dead volume of the charcoal column discarded during regeneration was 207 mL ± 12 mL. For concentration decline measurements, five experiments were conducted.

#### 7.3.1.1 Flow Rate Comparison

Figure 7-3 shows bilirubin concentration over time during the experiment with a 20 mL/min flow rate. In the first hour of the experiments, the bilirubin concentration declined at a rate of 1.38 mg/dL/hr. Through the hour "pre-regeneration", this rate decreased to 0.53 mg/dL/hr, which is significantly lower than the first hour ($p = 0.00215$). The hour "post-regeneration" was impacted by a significant outlier measurement at 210 min (Figure 7-3). This is because mixing between leftover regeneration fluid and fluid entering the column was more difficult to avoid with the slower flow rate. Thus, we report the concentration change from 180 minutes to 270 minutes. The concentration doesn't change between 210 and 180 minutes during regeneration, so these definitions are equivalent, except in how they account for the impact of transient regeneration fluid in the circuit at 210 minutes. From 210 to 270 minutes the concentration declined by 0.35 mg/dL, which did not significantly differ from the pre-regeneration hour ($p = 0.94$) or the initial hour ($p = 0.65$) because of wide confidence intervals. From 180 to 270 minutes the concentration declined by 1.4 mg/dL. This rate was a significant increase from the "pre-regeneration" period ($p = 0.00026$). The "post regeneration" bilirubin decline rate did not differ significantly from the first hour observation ($p = 0.86$). The dead volume of the charcoal column discarded during regeneration was 200.33 mL $\pm$ 4.73 mL. For 20 mL/min flow rate measurements, three experiments were conducted. Figure 7-4 shows a comparison between the % bilirubin reduction in the 20 mL/min trials and the 120 mL/min trials.

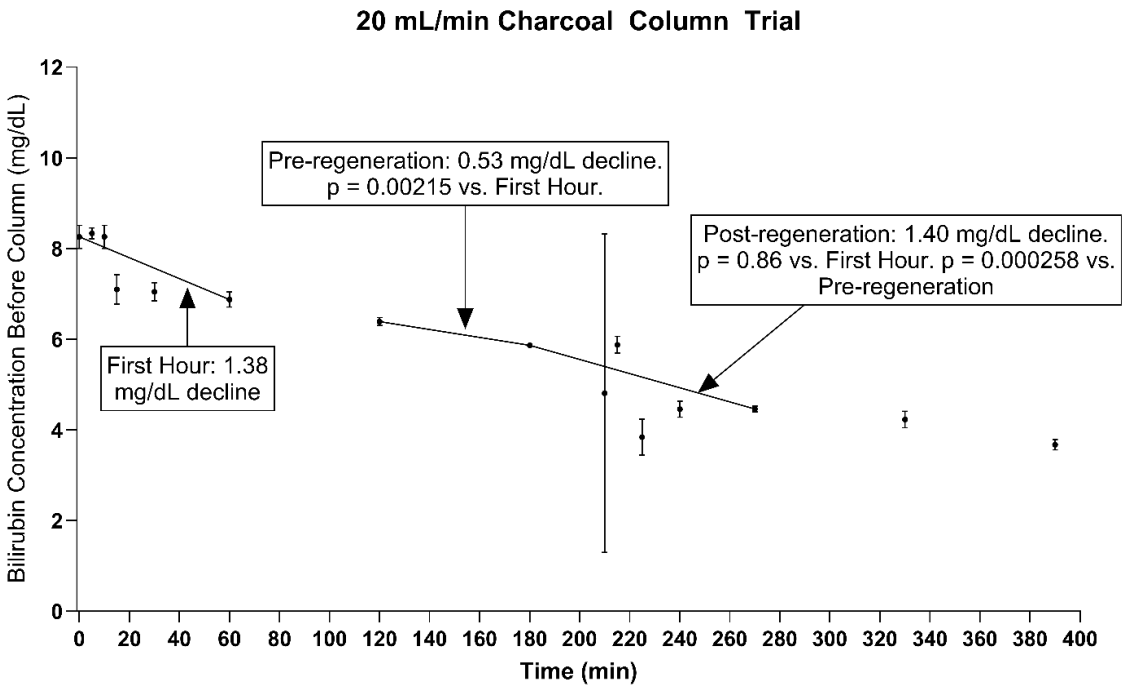


Figure 7-3: Change in bilirubin concentration over time before and after regeneration of the charcoal column for the 20 mL/min flow rate. Error bars are standard deviation. Where error bars are not shown, the standard deviation would fall within the graphed data point.

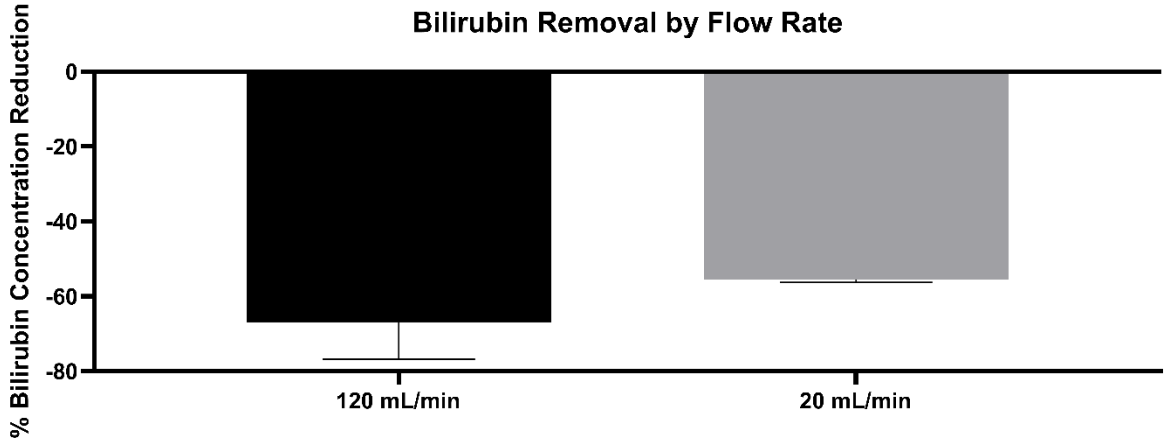


Figure 7-4: Comparison between the % reduction in bilirubin in the 120 mL/min trial (n = 5) and the 20 mL/min trial (n = 3). Error bars are standard deviation. In the first condition, bilirubin % reduction was 66.9%. In the second condition, average bilirubin % reduction was 55.5%. The difference narrowly failed to reach statistical significance (p = 0.061).

As seen in Figure 7-4, the concentration decline at the higher flow rate appears greater, but this difference did not attain statistical significance. Since this was only a small sample (n = 3) limited by the availability of expired Adsorba 300 columns at UW medicine, further trials are

warranted. If additional Adsorba 300 columns become available, we would conduct a statistical power calculation to predict the needed sample size and conduct additional trials.

#### 7.3.1.2 Analysis of Clearance

Because a significant volume of solution is discarded during regeneration, we compared bilirubin clearance before and after regeneration and between the 120 mL/min and 20 mL/min flow rates to account for the change in volume. This is because reducing the concentration of a 500 mL solution by 1 mg/dL entails twice as much toxin removed as reducing the concentration of a 250 mL solution. Thus, we analyzed clearance as a means of measuring the toxin removal capacity of the charcoal column in a way that controls for the change in volume. The results are summarized in Figure 7-5.

For the 120 mL/min flow rate, for the first 60 minutes (fresh column) clearance was 1.91 mL/min. Between 120 and 180 minutes (saturated column) clearance was 0.72 mL/min. Between 210 and 270 minutes (regenerated column), clearance was 1.52 mL/min. This calculation uses the 180 minute concentration value as the baseline since no toxin removal takes place between 180 and 210 minutes, and the 210 minute measurement was unreliable in the 20 mL/min condition. The fresh column clearance was significantly ($p = 0.023$) greater than the saturated column clearance and did not significantly differ from the post-regeneration clearance ($p = 0.28$). The difference between the saturated column clearance and regenerated column clearance did not attain statistical significance ($p = 0.052$). This result merits further study with a sample size prospectively determined to be large enough to be adequately powered to test this hypothesis.

For the 20 mL/min study, the fresh column bilirubin clearance was 1.62 mL/min. The saturated column clearance was 0.71 mL/min. The regenerated column clearance was 1.89 mL/min. The fresh column clearance was significantly greater than the saturated column clearance

($p = 0.0005$) and did not significantly differ from the regenerated column clearance ($p = 0.52$). The regenerated column clearance did not attain statistically significant differentiation from the saturated column clearance ($p = 0.073$). As before, further study with a larger, prospectively determined sample size, is needed. When comparing the same time point, the comparison between the 20 mL/min and 120 mL/min clearance did not attain statistical significance for any time period. P values were 0.39, 0.97, and 0.41 for the fresh, saturated, and post-regeneration columns respectively.

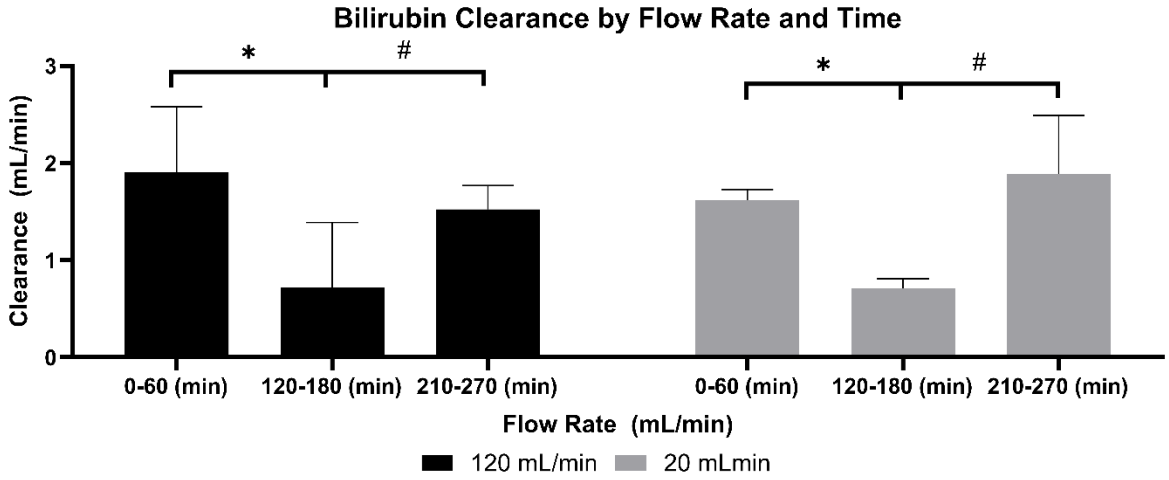


Figure 7-5: Clearance of Bilirubin by the Adsorba 300 during the initial phase (0-60 minutes), after saturation (120-180 minutes), and after regeneration (210-270 minutes). * indicates a p value < 0.05. # indicates $p < 0.1$, which did not attain our prespecified threshold for significance. A larger study with a prospectively determined sample size adequately powered to test this hypothesis is merited. n = 5 for the 120 mL/min flow rate study and n = 3 for the 20 mL/min flow rate study. No comparison between the 120 mL/min and 20 mL/min condition for the same time point had $p < 0.1$. Error bars are standard deviation.

### 7.3.2 *Albumin*

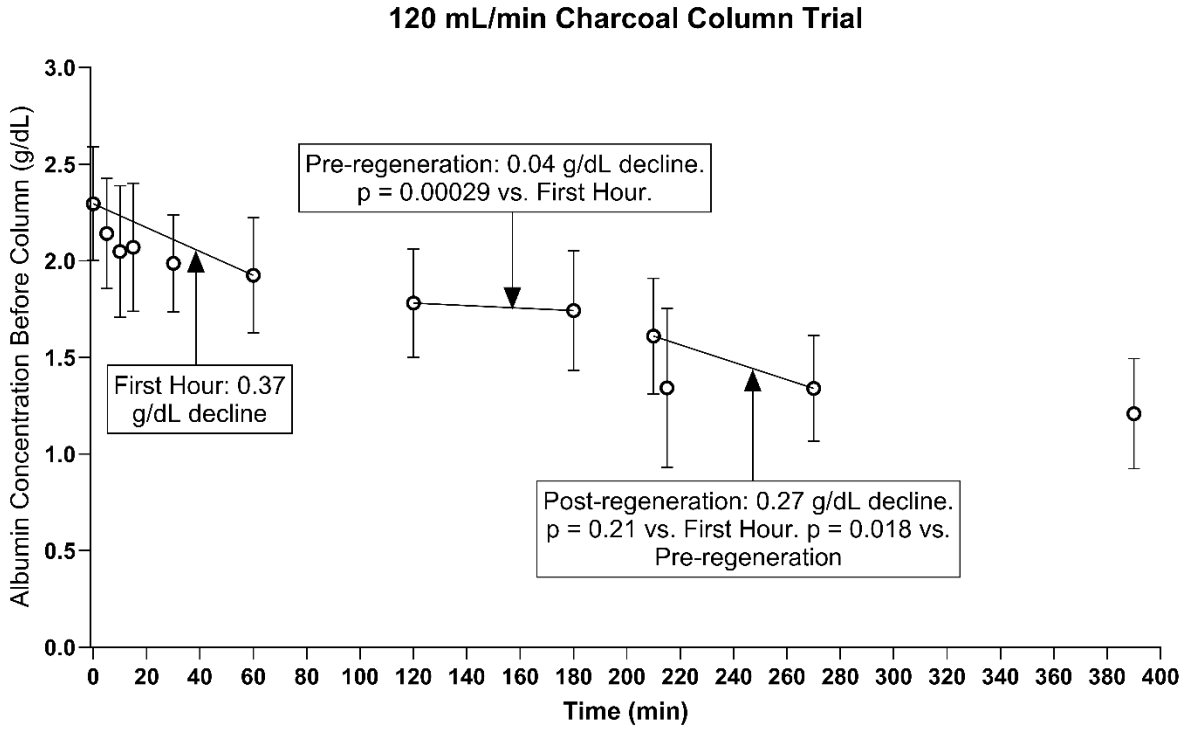


Figure 7-6: Change in albumin concentration over time before and after regeneration of charcoal column. Flow rate = 120 mL/min. n = 5. Error bars are standard deviation.

Figure 7-6 shows albumin concentration over time during the albumin regeneration experiment using the Adsorba 300 charcoal column with the 120 mL/min flow rate. In the first hour of the experiments, the albumin concentration declined at a rate of 0.37 g/dL/hr. Through the hour "pre-regeneration", this rate decreased to 0.04 g/dL/hr, which is significantly lower than the first hour ($p = 0.00029$). During the hour of "post-regeneration", the concentration declined at a rate of 0.27 g/dL/hr. This rate was a significant increase from the "pre-regeneration" period ($p = 0.018$). The "post regeneration" bilirubin decline rate did not differ significantly from the first hour observation ($p = 0.21$).

#### 7.3.2.1 Flow Rate Comparison

Figure 7-7 shows albumin concentration over time during the experiment with a 20 mL/min flow rate. In the first hour of the experiments, the albumin concentration declined at a rate of 0.31

g/dL/hr. Through the hour "pre-regeneration", this rate decreased to 0.09 g/dL/hr, which is significantly lower than the first hour ($p = 0.028$). The hour "post-regeneration" was impacted by a significant outlier measurement at 210 min (Figure 7-7). This is because mixing between leftover regeneration fluid and fluid entering the column was more difficult to avoid with the slower flow rate. Thus, we report the concentration change from 180 minutes to 270 minutes. As noted before, the concentration doesn't change between 210 and 180 minutes during regeneration, so these definitions are equivalent, except to exclude the impact of transient regeneration fluid in the circuit at 210 minutes. From 180 to 270 minutes the concentration declined by 0.27 g/dL. This rate was a significant increase from the "pre-regeneration" period ($p = 0.0009$). The "post regeneration" albumin decline rate did not differ significantly from the first hour observation ($p = 0.66$). For concentration decline measurements, three experiments were conducted. Figure 7-8 shows a comparison between the % albumin reduction in the 20 mL/min trials and the 120 mL/min trials. There was no difference between the two conditions in the amount of albumin loss.

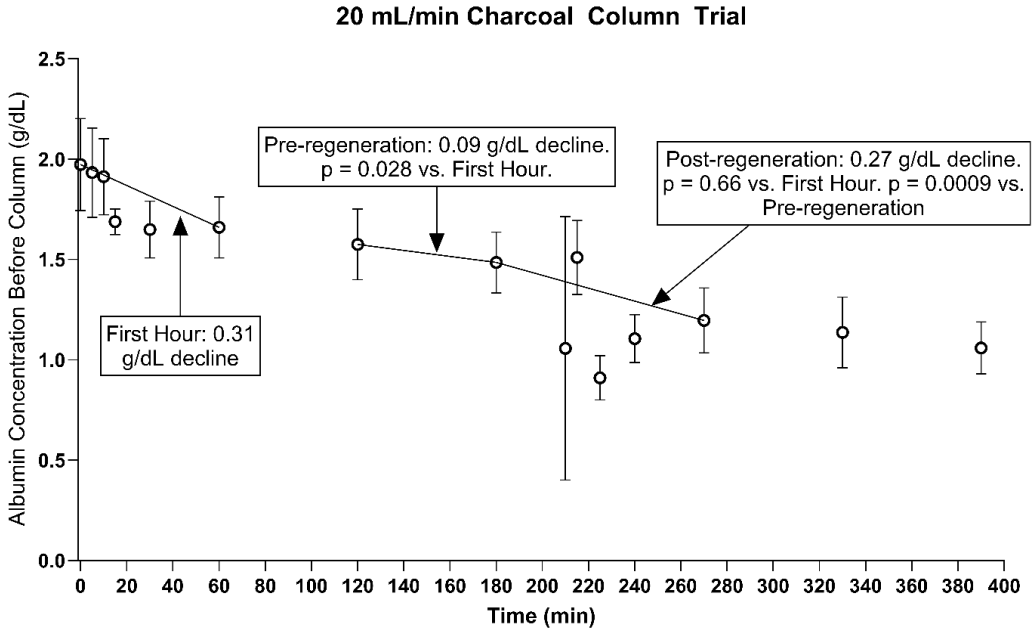


Figure 7-7: Change in albumin concentration over time before and after regeneration of charcoal column. Flow rate = 20 mL/min. n = 3. Error bars are standard deviation.

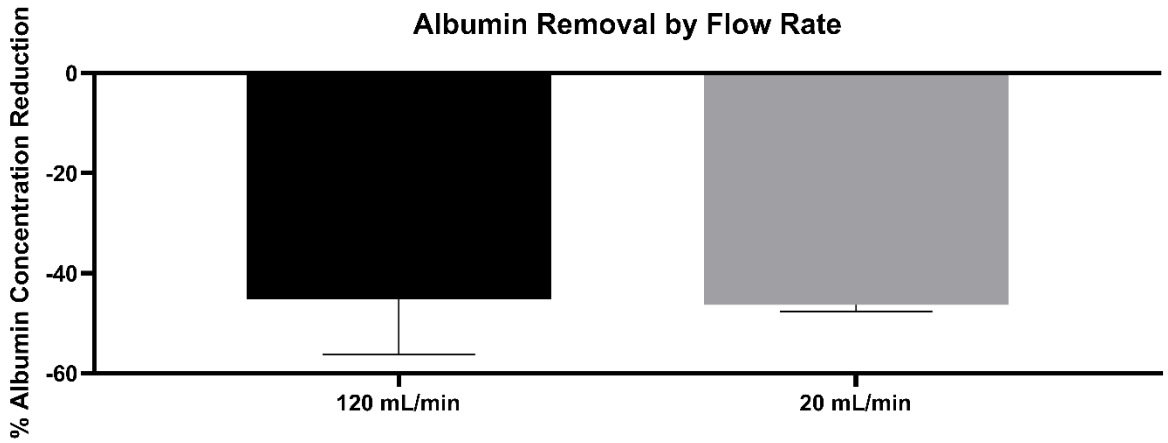


Figure 7-8: Comparison between the % reduction in albumin in the 120 mL/min trial (n = 5) and the 20 mL/min trial (n = 3). Error bars are standard deviation. In the first condition, albumin % reduction was 45.2%. In the second condition, average albumin % reduction was 46.3%. This difference was not statistically significant (p = 0.83).

## 7.4 CONCLUSION

Our experiments demonstrated that the Adsorba 300 removes bilirubin, with more than 2/3 concentration reduction in the best performing condition (120 mL/min flow rate). Albumin loss was also observed in all conditions. Regeneration restored the rate of bilirubin (and albumin) concentration decline to that observed with a fresh column. A larger study is needed to confirm these findings. Important comparisons in terms of toxin clearance (which accounts for volume changes), and between the two flow rates, fell within the $0.05 < p < 0.1$ range. This could indicate either spurious trends emerging by chance, or a study that was insufficiently powered to detect trends genuinely present in the underlying process. Since this was the first pilot study in which this protocol was assessed, follow-up is warranted.

# Chapter 8. ALBUMIN ALTERNATIVES

## 8.1 BACKGROUND

Replacing Human Serum Albumin (HSA) with an alternative that is not restricted by the availability of donor blood plasma is greatly desirable to bring down costs and enable liver dialysis to be implemented on a large scale. In Chapter 6, bovine serum albumin (BSA) was evaluated as an HSA alternative. This molecule has the advantage of being used in existing cell therapies (275), but disadvantages include concerns about allergies, and concerns about zoonotic diseases such as prion diseases from animal derived products (310,311). These concerns can be mitigated, for example through rapid detection of leaks in dialysis membranes, or the use of animal sources that have been confirmed to be free of known zoonotic agents. However, mitigations increase cost and regulatory burden. Thus, there is merit to considering other albumin alternatives. A combination of albumin alternatives has the potential to enable personalized medicine, where optimal binders are used depending on a patient's toxin profile.

Porcine serum albumin (PSA) is another promising animal albumin candidate, with a potential advantage over HSA. PSA has been indirectly used in previous liver support systems because it is produced by porcine hepatocytes which were used in the Phase 3 trial of HepatAssist (312). This trial failed because of lack of efficacy, not safety concerns. However, in theory, the same concerns about allergy and zoonosis apply.

Other molecules may be good candidates as long as they meet the following criteria: First, they must bind the toxin of interest. Second, they must be at least 65 kDa in size to minimize entry into the bloodstream via the pores of the dialysis membrane. Third, they must be soluble in sufficiently high concentrations to allow clinically relevant toxin removal. Fourth, they must be FDA approved, or have a good safety record of use in human clinical trials. Fifth, they must either

have a low cost, or have the potential to have their cost brought down without new technological innovations.

Carbohydrate polymers are one potential source of candidate molecules. β-cyclodextrin and similar polymers have been studied for the removal of PBTs such as bilirubin (313). They have also been functionalized onto iron to enable reuse of binders by magnetic separation from spent dialysate (314). However, novel polymer systems face regulatory and logistical challenges. Dextran and iron dextran are widely available, and FDA approved. While they are expected to remove less toxin per milligram than novel engineered binders, high concentrations can be added to dialysate cheaply, potentially allowing greater overall toxin removal. We thus studied whether dextran removes PBTs.

Polystyrene Sulfonate Sodium (PSS) and charcoal are of interest because they have previously been used in BioLogic-DT (51). This system was FDA approved until it was withdrawn due to fluid control issues, problems with its old cellulose membrane, and supply chain issues (89,315).

Lipid particles are of interest because lipid dialysate has been previously used to treat poisonings with hydrophobic toxins in veterinary contexts (316). Lecithin liposomes have been used to remove protein bound toxins in animal studies (317). Existing FDA approved liposomes used in other applications such as drug delivery are promising candidates.

Here we report preliminary work to test albumin alternatives of interest for the removal of our toxins of interest.

70 kDa Dextran is FDA approved as a volume expander (318). It is injected intravenously to increase oncotic pressure, allowing the movement of fluid from the interstitial space into the blood vessels. It is a polymer of glucose. It is produced by the lactic acid bacterium *Leuconostoc*

*Mesenteroides*, in the order Lactobacillales. While it is FDA approved and used intravenously, accidental release into the blood poses some hazards. Larger dextrans can interfere with normal coagulative function and induce anaphylaxis in 20% of the population. Thus, 70 kDa is selected because it exceeds the Molecular Weight Cut-Off (MWCO) of dialysis membranes. 70 kDa dextran is soluble up to 15 g/dL, which means it can be used in concentrations that exceed blood albumin concentrations (204).

Dextran Sulphate is an anionic dextran, making it potentially a good candidate for binding cationic metal ions. Copper (319) and manganese (320) form complexes with Dextran Sulphate. Sigma Aldrich supplies it in a 500 kDa formulation. Dextran Sulphate has been FDA approved in the past as an anticoagulant under the brand name Usherdex (321), although it is no longer FDA approved (FDA, personal communication). Its maximum solubility is 10 g/dL (322).

20% Intralipid is administered intravenously as a source of calories and essential fatty acids. Its constituents include soybean oil (20%), egg yolk phospholipids (1.2%), glycerin (2.25%) and water (323). Intralipid is FDA approved. Its pH range is 6-8.9. It is hydrophobic, which makes it a promising candidate to bind hydrophobic toxins such as bilirubin and cholic acid. There is veterinary experience using lipid dialysis to eliminate hydrophobic toxins (316). The distributor (Sigma Aldrich) does not provide information on the size of the lipid molecules. Since intralipid is commonly used intravenously, some crossing the membrane into the patient should not pose a safety risk, but characterization is important because the loss of dialysate binder could reduce effectiveness. We used the Beckman Coulter lipemia/turbidity, icterus, and hemolysis (LIH) reagent (OSR62166) to give a preliminary estimate on lipid crossing into the blood side.

Porcine serum albumin is likely to pose little risk, because patients would have been exposed to it in the use of HepatAssist (312). It’s ability to bind bilirubin is reported in Table 8-1.

Hence our focus was to determine its ability to remove bilirubin and other toxins from an HSA blood analog solution.

Table 8-1: Reported values of bilirubin-PSA binding constant

| Study | Primary Bilirubin-BSA Binding Constant (1/M) | Temperature (ºC) | Solution | pH |
|---|---|---|---|---|
| Chen, 1973 (224) | 1.8E7 | 25 | 0.1 M Potassium Phosphate Buffer | 7.4 |
| Harmatz, 1975 (324) | 1E6 | 27 | NaCl, 0.1 M; Tris-HCl buffer, 0.02 M; | 7.4 |
| Athar, 1999 (282) | 4.41E7 | 28 | Tris-HCl buffer, Ionic strength 0.15 | 8.0 |

## 8.2 METHODS

### 8.2.1 *Experimental Setup*

Four pilot studies were conducted using a setup similar to setups 2-6 in Chapter 6. They were compared to the negative control (setup 6) in Chapter 5 in terms of toxin removal. Table 8-2 summarizes the setups. In all setups care was taken to protect the setup from light.

Table 8-2: Setups Used for Albumin Alternatives Study

| | Dextran 70 | Dextran Sulphate | Intralipid | Porcine Serum Albumin |
|---|---|---|---|---|
| Duration (hr) | 5 | 5 | 5 | 5 |
| Solution Volumes (mL) | 200 | 200 | 200 | 200 |
| Blood and dialysate flow rate (mL/min) | 150 | 150 | 150 | 150 |
| Ultrafiltration rate (mL/min) | 0 | 0 | 0 | 0 |
| Blood Albumin Concentration (g/dL) | 2 | 2 | 2 | 2 |
| Dialysate Binder Concentration (g/dL) | 2 | 2 | 5% | 2 |
| Blood Albumin | BSA | BSA | BSA | HSA |
| Dialysate Binder | Dextran 70 | Dextran Sulphate | Intralipid | PSA |
| Dialyzer | F3 | F3 | F3 | F3 |
| Material | Polysulfone | Polysulfone | Polysulfone | Polysulfone |
| Number of Fibers | 2304 (253) | 2304 (253) | 2304 (253) | 2304 (253) |
| Hollow Fiber Inner Radius (μm) | 100 (255) | 100 (255) | 100 (255) | 100 (255) |
| Hollow Fiber Outer Radius (μm) | 140 (256) | 140 (256) | 140 (256) | 140 (256) |
| Hollow Fiber Length (cm) | 20 (255) | 20 (255) | 20 (255) | 20 (255) |
| Area ($m^2$) | 0.4 (255) | 0.4 (255) | 0.4 (255) | 0.4 (255) |
| Housing Inner Radius (mm) | 11 (measured) | 11 (measured) | 11 (measured) | 11 (measured) |
| Bilirubin Reflection Coefficient (assumed (158)) | 0 | 0 | 0 | 0 |
| Reflection Coefficients for Other Toxins (Assumed) | 0 | 0 | 0 | 0 |

### 8.2.2 *Reagents*

Four molecules with a history of FDA approval or use in humans were selected for this pilot study. 70 kDa Dextran from Leuconostoc Ssp. was purchased from Sigma Aldrich (Product number 31390-25G). Dextran Sulphate was purchased from Sigma Aldrich (Product number D6001). 20% Intralipid stock was purchased from Sigma Aldrich (Product number I141). Porcine

Serum Albumin (PSA) was purchased from Sigma Aldrich (Product number A1830-10G, purity 98%).

### 8.2.3 *Statistics*

Percent reduction was calculated as follows:

$$\%\ Reduction = \frac{\left(C(t=300\ min) - C(t=0)\right) * 100\%}{C(t=0)} \text{ (Equation 8-1)}$$

If the pilot studies only had n = 1 (this is the case for the intralipid for all toxins, and dextran sulphate and PSA for copper and manganese), significance compared to the negative control was assessed by computing a t-score reflecting the probability that this result would arise by chance from the distribution of negative control results. This computation was performed as follows:

$$t = \frac{\bar{x} - \mu_0}{s/\sqrt{n}} \text{ (Equation 8-2)}$$

Here $\bar{x}$ is the mean of the % toxin reduction in the negative control. $\mu_0$ is the reported outcome of the pilot study. s is the standard deviation of the negative controls. n is the sample size of the negative controls (n = 3). The T.DIST function in Microsoft Excel is then used to convert this score to a "significance estimate". The number of degrees of freedom is assigned to n – 1 = 2. The Cumulative parameter is assigned to TRUE to obtain the cumulative probability in the left tail of the T-distribution. The outcome guides decisions regarding follow-up work. Because the pilot study was only done once, this score should be interpreted as an indicator of whether further research is fruitful, not a finalized statistical significance estimate.

If the pilot study had n = 3 (porcine serum albumin, dextran, dextran sulphate) statistics were completed using the unpaired Student's t-test as previously described (e.g. section 5.3.3).

## 8.3 RESULTS

### 8.3.1 *Bilirubin*

Figure 8-1 shows the % reduction of blood side bilirubin in BSA solution for the albumin alternatives studied. N = 3 for all tests except intralipid, for which N = 1 due to supply chain limitations. The negative control and 2 g/dL BSA conditions are the 150 mL/min dialysate side flow rate conditions from Chapter 5. In addition to BSA, 2 g/dL dextran 70 removed significantly more bilirubin than the negative control. Percent reduction with BSA dialysate was 46.4% while with Dextran 70 dialysate it was 23.9%. Modeling will be done to predict the impact of higher Dextran 70 dialysate concentrations and those concentrations will be tested to determine whether Dextran 70 is a viable replacement for BSA in albumin dialysis. The observation that dextran 70 removed significantly more bilirubin than the negative control while dextran sulphate did not supports the hypothesis that the charge of the binder molecule is significant to its toxin removal capacity. Dextran sulphate and bilirubin are both anions, meaning there is a risk of electrostatic repulsion. Dextran 70 is neutral. We hypothesize that a cationic dextran may be a better bilirubin binder.

Figure 8-2 shows the % reduction of blood side bilirubin in 2 g/dL HSA blood analog solution by 2 g/dL PSA dialysis compared with % blood side bilirubin reduction for 2 g/dL BSA and HSA dialysate. N = 3 for PSA and N = 6 for BSA and HSA. The performance of the three albumins was comparable, suggesting that PSA may be a viable alternative to BSA and HSA for bilirubin removal by albumin dialysis. Testing of higher PSA concentrations is needed.

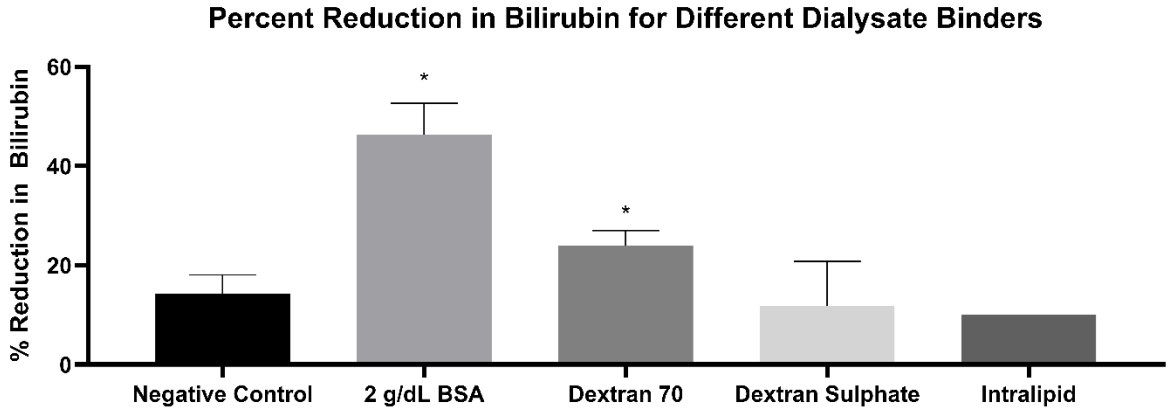


Figure 8-1: Percent reduction in bilirubin in BSA blood analog solution for different dialysate binders. N = 3 for all conditions except intralipid, where n = 1. Values are mean ± standard deviation. * indicates $p < 0.05$ compared to the negative control. BSA and Dextran 70 removed significantly more bilirubin than the negative control ($p = 0.0035$ and 0.029 respectively).

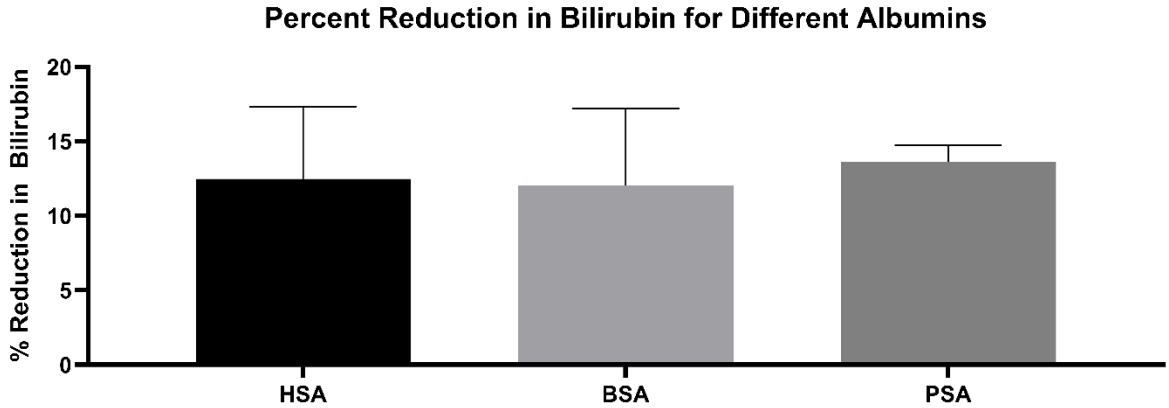


Figure 8-2: Percent reduction in bilirubin in HSA blood analog solution for different dialysate binders. No significant differences were detected between the three albumins studied. N = 6 for HSA and BSA and N = 3 for PSA. Values are mean ± standard deviation.

### 8.3.2 *Cholic Acid*

Figure 8-3 shows the % reduction of blood side cholic acid in BSA solution for the albumin alternatives studied. N = 3 for all tests except intralipid, for which N = 1 due to supply chain limitations. The negative control and 2 g/dL BSA conditions are the 150 mL/min dialysate side flow rate conditions from Chapter 5. None of the substances studied reached the prespecified threshold for statistical significance of $p = 0.05$ for cholic acid removal relative to the negative

control, with BSA coming the closest at p = 0.055. It would be beneficial to perform a larger trial for using BSA dialysate to remove cholic acid from BSA blood analog solution with a prospectively constrained sample size. No albumin alternative approached the outcome observed with BSA.

Figure 8-4 shows the impact of different dialysate side albumins on cholic acid removal from HSA blood analog solution. N = 3 for PSA and N = 6 for BSA and HSA. BSA and PSA removed significantly more cholic acid than HSA (p = 0.019 and 0.011 respectively). This indicates that these animal albumins may be superior binders for cholic acid removal compared to HSA.

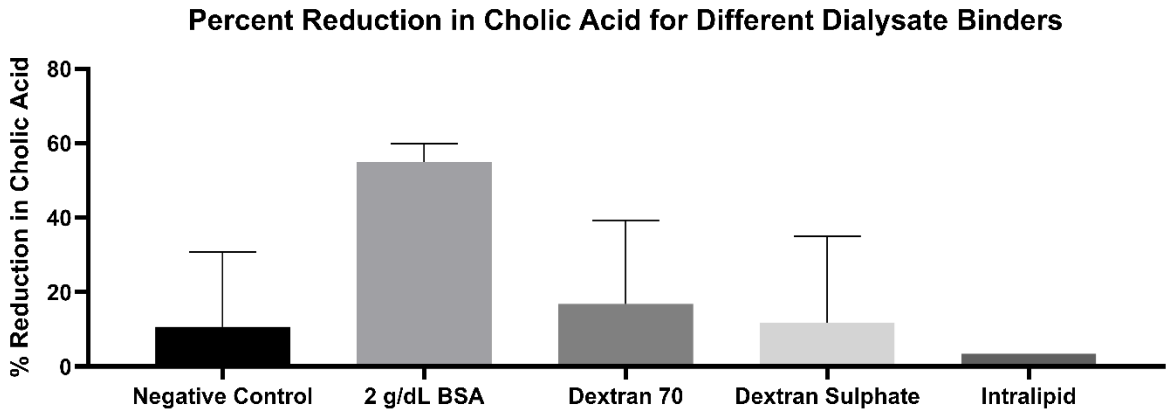


Figure 8-3: Percent reduction in cholic acid in BSA blood analog solution for different dialysate binders. N = 3 for all conditions except intralipid, where n = 1. Values are mean ± standard deviation.

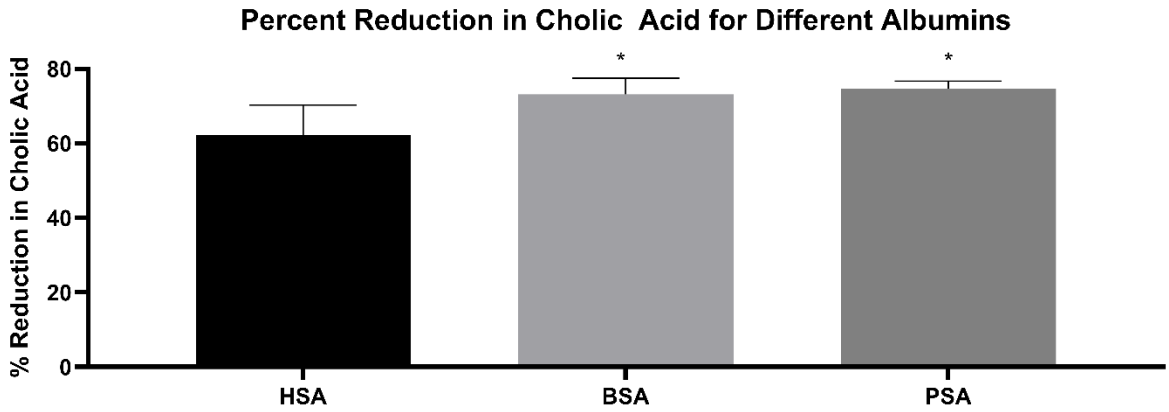


Figure 8-4: Percent reduction in cholic acid in HSA blood analog solution for different dialysate binders. * indicates $p < 0.05$ compared to HSA. BSA and PSA removed significantly more cholic acid ($p = 0.019$ and 0.011 respectively). N = 6 for HSA and BSA and N = 3 for PSA. Values are mean ± standard deviation.

### 8.3.3 *Indoxyl Sulfate*

Figure 8-5 shows the % reduction of blood side indoxyl sulfate in BSA solution for the albumin alternatives studied. N = 3 for all tests except intralipid, for which N = 1 due to supply chain limitations. The negative control and 2 g/dL BSA conditions are the 150 mL/min dialysate side flow rate conditions from Chapter 5. For all binders tested, indoxyl sulfate removal was greater than the negative control, but only the BSA attained the prespecified significance threshold, removing 46.3% ± 5.3% compared to a 39.1% ± 4.7% reduction in the negative control ($p = 0.048 < 0.05$). Dextran 70 removed 50.6% ± 9.4% ($p = 0.080$). Dextran sulphate removed 41.7% ± 11.7% ($p = 0.41$). Intralipid removed 46.4% ($p = 0.14$). The large variances and high percent removals observed in these conditions suggest that a study with a larger, prospectively constrained, sample size should be attempted to determine if any of these binders provide a low cost, FDA approved alternative to albumin for indoxyl sulfate removal.

Figure 8-6 shows the impact of different dialysate side albumins on indoxyl sulfate removal from HSA blood analog solution. N = 3 for PSA and N = 6 for BSA and HSA. There were no

significant differences between albumins from different species in removing indoxyl sulfate from HSA blood analog solution.

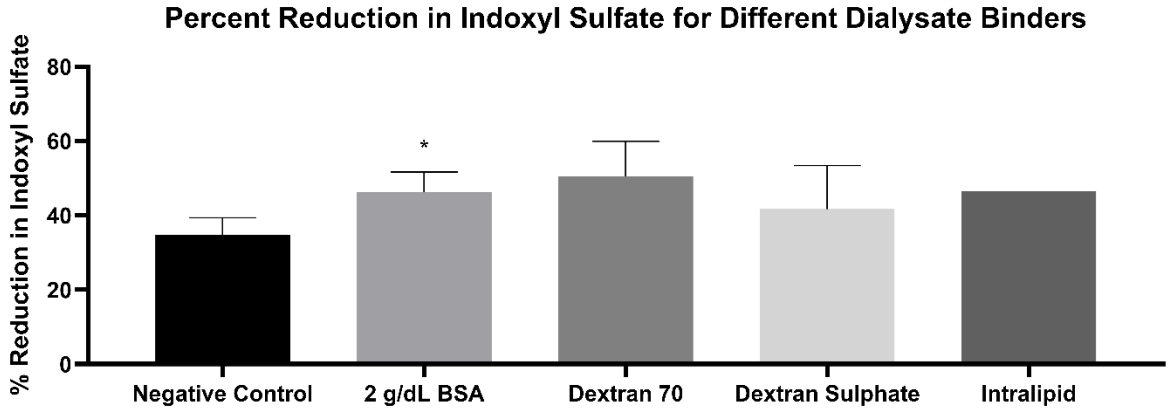


Figure 8-5: Percent reduction in indoxyl sulfate in BSA blood analog solution for different dialysate binders. N = 3 for all conditions except intralipid, where n = 1. Values are mean ± standard deviation. * indicates $p < 0.05$ compared to the negative control. 2 g/dL BSA removed significantly more indoxyl sulfate ($p = 0.048$).

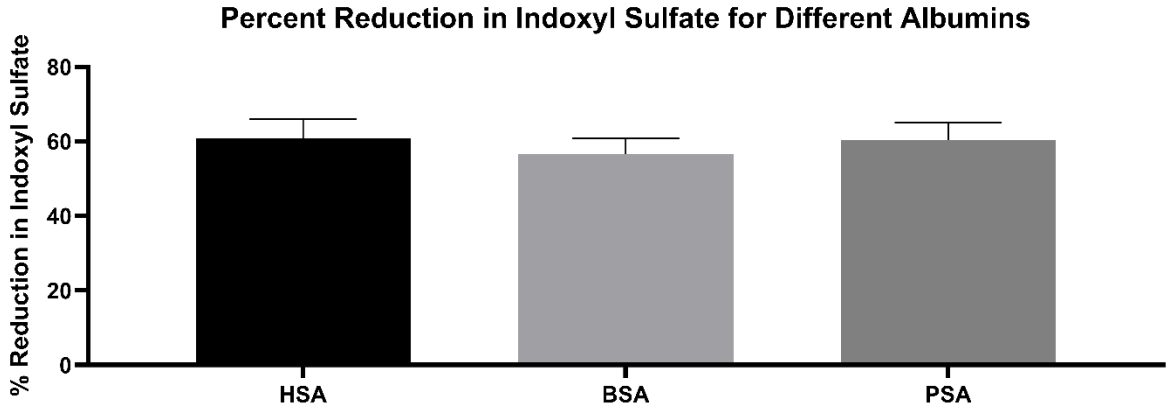


Figure 8-6: Percent reduction in indoxyl sulfate in HSA blood analog solution for different dialysate binders. N = 6 for HSA and BSA and N = 3 for PSA. Values are mean ± standard deviation.

### 8.3.4 *Copper*

Figure 8-7 shows the % reduction of blood side copper in BSA solution for the albumin alternatives studied. N = 3 for all tests except intralipid and dextran sulphate, for which N = 1. The negative control and 2 g/dL BSA conditions are the 150 mL/min dialysate side flow rate conditions from Chapter 5. The 2 g/dL BSA and dextran sulphate removed significantly more copper than the

negative control, with 19.6% ± 7.8% and 16.7% reduction compared to 3.4% ± 2.4% reduction respectively (p = 0.048 and 0.034). Additional replicates are needed for the dextran sulphate condition, since it is based on an N = 1 pilot study. Additionally, Dextran 70 removed 32.1% of copper on average, but large variance (37.1%) meant this did not attain statistical significance. Investigation into sources of variation is needed.

Figure 8-8 shows the impact of different dialysate side albumins on copper removal from HSA blood analog solution. N = 3 for BSA and HSA and N = 1 for PSA. No albumin dialysate tested removed significant copper concentrations from HSA blood analog solution. This conflicts with the results obtained for BSA dialysate and BSA blood analog solution, indicating that significantly higher HSA copper affinity may prevent BSA from being an effective low-cost model in this case.

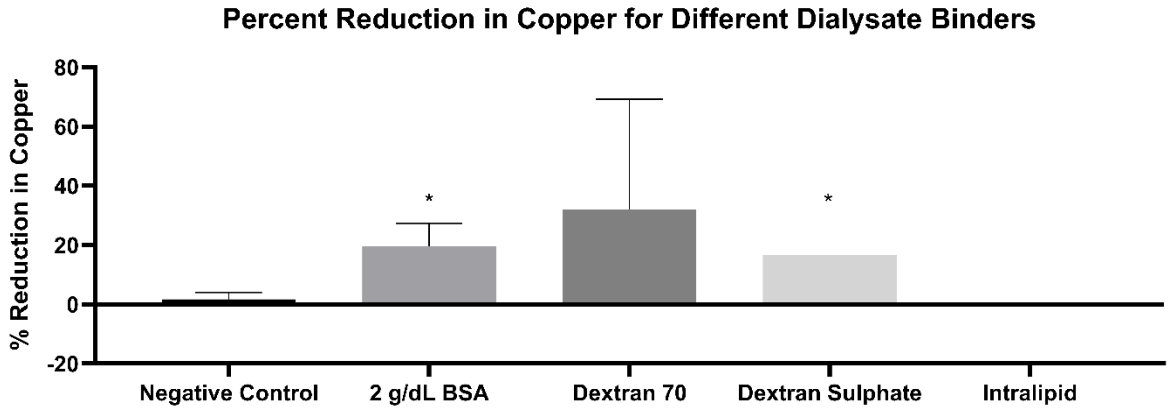


Figure 8-7: Percent reduction in copper in BSA blood analog solution for different dialysate binders. N = 3 for all conditions except intralipid and dextran sulphate, where n = 1. Values are mean ± standard deviation. * indicates p < 0.05 compared to the negative control. 2 g/dL BSA removed significantly more copper (p = 0.048), as did the dextran sulphate pilot study (p = 0.034).

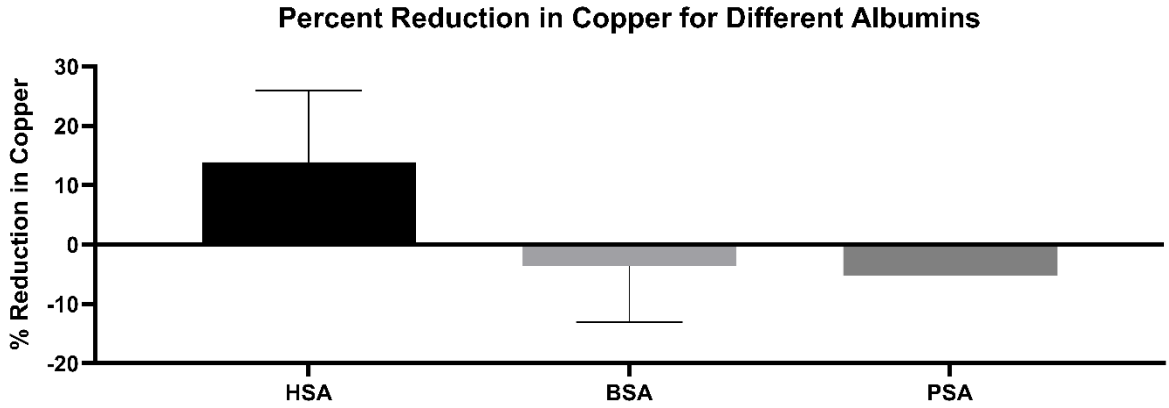


Figure 8-8: Percent reduction in copper in HSA blood analog solution for different dialysate binders. N = 3 for BSA and HSA and N = 1 for PSA. Values are mean ± standard deviation.

### 8.3.5 *Manganese*

Figure 8-9 shows the % reduction of blood side manganese in BSA solution for the albumin alternatives studied. N = 3 for all tests except intralipid and dextran sulphate, for which N = 1. The negative control and 2 g/dL BSA conditions are the 150 mL/min dialysate side flow rate conditions from Chapter 5. No albumin alternative produced a statistically significant increase in manganese removal. Protocol refinements to reduce variance are needed.

Figure 8-10 shows the impact of different dialysate side albumins on manganese removal from HSA blood analog solution. N = 3 for BSA and HSA and N = 1 for PSA. No significant trends were observed in this data.

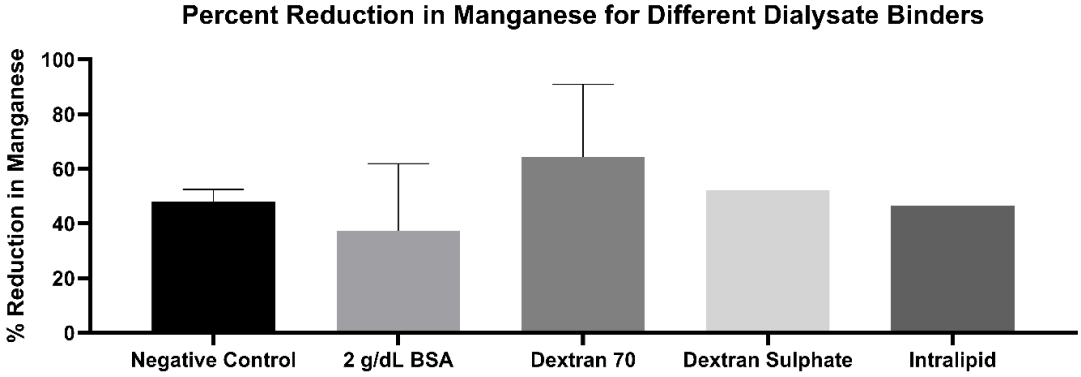


Figure 8-9: Percent reduction in manganese in BSA blood analog solution for different dialysate binders. N = 3 for all conditions except intralipid and dextran sulphate, where n = 1. Values are mean ± standard deviation.

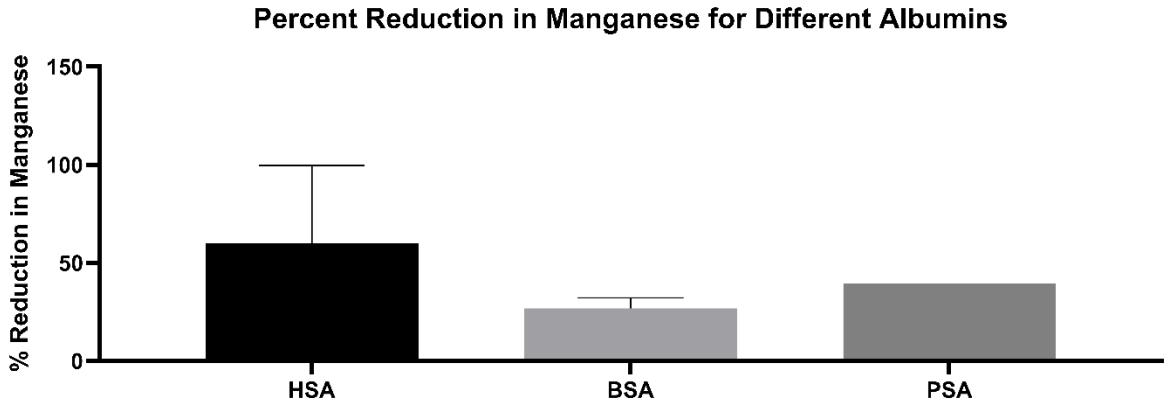


Figure 8-10: Percent reduction in manganese in HSA blood analog solution for different dialysate binders. N = 3 for BSA and HSA and N = 1 for PSA. Values are mean ± standard deviation.

### 8.3.6 *Lipid Transfer Across the Dialysis Membrane in Intralipid Trial*

The LIH reading remained positive on the dialysate side and negative on the blood side for the entire 5 hour intralipid trial, indicating that there was limited transfer of lipid from blood to dialysate.

## 8.4 DISCUSSION

From our limited pilot study, dextrans were the most promising albumin alternatives. Dextran 70 removed significantly more bilirubin from BSA blood analog solution than the negative control. Dextran sulphate removed significantly more copper than the negative control, although only one Dextran sulphate trial could be analyzed due to budget and facility constraints. Dextran sulphate is negatively charged, so we anticipate it would be effective for removing cations such as copper. Further study with a larger sample size is needed. Intralipid did not increase the removal of any toxins of interest.

Porcine serum albumin (PSA) removes substances of interest. Along with BSA, it removed significantly more cholic acid from HSA blood analog solution than HSA dialysate did. For other

toxins, its removal capabilities were comparable to HSA and BSA. This demonstrates the potential of tailoring dialysate binder mixtures to maximize toxin removal for a particular patient.

No albumin alternative was successful in removing significantly more manganese than the negative control, but manganese removal in our negative control approached 50%. This is uncharacteristic of an albumin-bound toxin. It is possible that our test setup did not accurately mimic manganese loading onto albumin *in vivo*.

# Chapter 9. POLYSULFONE MEMBRANE BINDING OF BILIRUBIN

## 9.1 BACKGROUND

In some of our trials, we observed a mismatch between bilirubin in dialysate and bilirubin loss from blood. In particular, as noted in Chapter 5, negative control experiments with no dialysate albumin still had significant bilirubin losses. In addition, we observed that the dialyzer membrane transfer coefficient ($K_{free}A$) for free bilirubin was extremely high. This phenomenon has been previously suggested to occur because of bilirubin binding to the dialyzer membrane (147). We had two dialyzers: an F3 polysulfone dialyzer, and an F6HPS dialyzer. The F6HPS is reported to be a polysulfone dialyzer.

We hypothesize that bilirubin binds polysulfone. Peng et al report a small, but nonzero binding of bilirubin to unmodified polysulfone (161). Polysulfone membranes are highly hydrophobic, despite a thin coating of poylvinylpyrolidone (PVP) which increases surface hydrophilicity (164). These membranes have been shown to be highly absorbant of β2-microglobulin. Thus, we conducted a study to determine the removal of polysulfone from solution containing only bilirubin and albumin, to test this hypothesis and determine the absorption capacity of our membrane for bilirubin. This would allow extending the model to include membrane

absorption, as has been previously done by Snisarenko and colleagues for a different membrane/toxin combination (263).

## 9.2 TEST SETUP

### 9.2.1 *Analysis of negative control and membrane fouling test data*

We started by analyzing the results of the negative control studies and membrane fouling tests. Negative control studies done with the F3 dialyzer have been previously described (Chapter 5). There were earlier negative controls using the F3 dialyzer and smaller blood and dialysate side volumes whose unexpected outcome originally prompted this investigation. A single negative control was also done with the F6HPS dialyzer, using the F6HPS dialyzer setup shown in Chapter 5 with no albumin on the dialysate side. Additionally, membrane fouling tests were done before the bilirubin removal tests described in Chapter 5, Setup 1. These tests consisted of the blood analog solution running through the primed blood side of the F6HPS dialyzer for 30 minutes while there was no flow on the dialysate side. Priming fluid (dialysate with no added sorbents) was present on the dialysate side and the dialysate side tubing was clamped to prevent ultrafiltration. This was done for both trials with HSA on the blood side and trials with BSA on the blood side. Thus, the four setups are summarized in Table 9-1. F6HPS dialyzers were reused after being cleaned according to established clinical protocols (260,261). The number of reuses is reported. In all setups care was taken to protect the setup from light.

Statistical comparisons were done between the sample at $t = 0$ and the sample at $t = t_{end}$. Each sample was taken in triplicate, so the unpaired two-tailed students t-test was used to test for a significant difference between the triplicates. In one case, when triplicates were not available, the t-score formula was used. It is shown as Equation 9-1. In all cases significance was set at 0.05.

$$t = \frac{\bar{x}-\mu_0}{s/\sqrt{n}}$$ (Equation 9-1)

Table 9-1: Test setups where membrane binding was the only potential method for bilirubin removal from blood

| | Test 1: F6HPS Negative Control | Test 2: F6HPS Membrane Fouling Test Data: BSA | Test 3: F6HPS Membrane Fouling Test Data: HSA | Test 4: F3 Negative Control, low volumes | Test 5: F3 Negative Control |
|---|---|---|---|---|---|
| Duration (hr) | 3 | 0.5 | 0.5 | 5 | 5 |
| Blood Analog Solution Volume (mL) | 660 | 610 | 610 | 120 | 200 |
| Dialysate Volume (mL) | 610 | NA | NA | 120 | 200 |
| Blood flow rate (mL/min) | 180 | 180 | 180 | 30 | 150 |
| Dialysate flow rate (mL/min) | 90 | NA | NA | 30 | 150 |
| Ultrafiltration rate (mL/min) | 0 | 0 | 0 | 0 | 0 |
| Blood Albumin Concentration (g/dL) | 2 | 2 | 2 | 2 | 2 |
| Blood Albumin | BSA | BSA | HSA | BSA | BSA |
| Dialyzer | F6HPS | F6HPS | F6HPS | F3 | F3 |
| Material | Polysulfone | Polysulfone | Polysulfone | Polysulfone | Polysulfone |
| Number of Fibers | 8400 (253) | 8400 (253) | 8400 (253) | 2304 (253) | 2304 (253) |
| Hollow Fiber Inner Radius (µm) | 100 (254) | 100 (254) | 100 (254) | 100 (255) | 100 (255) |
| Hollow Fiber Outer Radius (µm) | 140 (254) | 140 (254) | 140 (254) | 140 (256) | 140 (256) |
| Hollow Fiber Length (cm) | 21 (257) | 21 (257) | 21 (257) | 20 (255) | 20 (255) |
| Area ($m^2$) | 1.3 (254) | 1.3 (254) | 1.3 (254) | 0.4 (255) | 0.4 (255) |
| Housing Inner Radius (mm) | 20 (254) | 20 (254) | 20 (254) | 11 (measured) | 11 (measured) |
| Bilirubin Reflection Coefficient (assumed (158)) | 0 | 0 | 0 | 0 | 0 |

### 9.2.2 *Dedicated test of bilirubin binding to polysulfone dialyzer*

The setup for the dedicated study was the same as the typical F3 dialyzer setup except that both sides contained only albumin (BSA) dialysate with 20 mg/dL bilirubin and 2 g/dL BSA. The two solutions had a 120 mL volume. Thus, there was no concentration gradient for free bilirubin transport across the membrane, eliminating the possibility of bilirubin removal by any means besides membrane binding. To control for light exposure, during each trial three tubes of starting solution were aliquoted. One was frozen immediately (starting solution). One was kept in the dark cabinet (fume hood with cardboard panels to block light) covered in foil. The other was kept in the cabinet with no foil. If confounding by light exposure was avoided, none of the tubes should differ significantly in bilirubin concentration from the starting solution.

Statistical comparisons were done using the unpaired two-tailed students t-test. To determine whether bilirubin removal by the membrane was significantly greater than zero, Equation 9-1 was applied, along with a right-tailed student's T-Test. This is because membrane bilirubin removal over time could only be positive or zero. The membrane would not release bilirubin into the solution from its initial configuration. In all cases significance was set at 0.05.

## 9.3 RESULTS

### 9.3.1 *Analysis of negative control and membrane fouling test data*

Table 9-2 shows the results of the analysis of negative control trials and membrane fouling tests which were not done with the specific objective of analyzing bilirubin removal by the polysulfone, but nonetheless provide insight on this question because they are conditions in which other means of bilirubin removal have been excluded.

In all but two trials, the bilirubin concentration decreased significantly at the end of the test period compared to the beginning, even though there was no binder in the dialysate, and, for conditions 2 and 3, no dialysate flow. This strongly suggests bilirubin binds polysulfone but gives little information on binding capacity because of the heterogeneity of test conditions, membranes, and reuse conditions (for F6HPS). Thus, a dedicated study was initiated.

Table 9-2: Bilirubin removal results. Each data point is the mean of n = 3 technical replicates, except Condition 1 at t = 0. Due to an error that sample was not available for analysis, and the target bilirubin concentration (20 mg/dL) is assumed instead. For this case only, p-value is evaluated using the t-score formula. Otherwise, an unpaired two-tailed student's t-test is done. NS refers to "not significant".

| Condition # | Dialyzer | Qb (mL/min) | Vb (mL) | t (hr) | Bilirubin (t = 0 (mg/g) | Bilirubin after (mg/dL) | P value |
|---|---|---|---|---|---|---|---|
| 1 | F6HPS, 2nd use | 180 | 660 | 3 | 10 | 8.05 ± 0.65 | NS |
| 2 | F6HPS, fresh | 180 | 610 | 0.5 | 5.86 ± 0.09 | 4.92 ± 0.08 | 0.0002 |
| 2 | F6HPS, 2nd use | 180 | 610 | 0.5 | 7.06 ± 0.11 | 6.54 ± 0.09 | 0.0038 |
| 3 | F6HPS, fresh | 180 | 610 | 0.5 | 11.61 ± 0.2 | 11.56 ± 0.04 | NS |
| 3 | F6HPS, fresh | 180 | 610 | 0.5 | 11.51 ± 0.09 | 11.09 ± 0.03 | 0.0074 |
| 4 | F3, fresh | 30 | 120 | 5 | 10.76 ± 0.25 | 6.46 ± 0.12 | 0.0017 |
| 4 | F3, fresh | 30 | 120 | 5 | 11.72 ± 0.17 | 6.97 ± 0.086 | 3.3 E-05 |
| 5 | F3, fresh | 150 | 200 | 5 | 6.78 ± 0.36 | 5.94 ± 0.11 | 0.046 |
| 5 | F3, fresh | 150 | 200 | 5 | 8.00 ± 0.24 | 6.52 ± 0.10 | 0.0034 |
| 5 | F3, fresh | 150 | 200 | 5 | 8.56 ± 0.19 | 7.60 ± 0.14 | 0.0031 |

### 9.3.2 *Dedicated test of bilirubin binding to polysulfone dialyzer*

Table 9-3 lists the amount of bilirubin removed from the blood and dialysate sides containing 20 mg/dL bilirubin solution in these trials. On average, 12.57 mg of bilirubin were removed. This was significantly different from 0 bilirubin removal (p = 0.036). The average

amount removed over time is shown in Figure 9-1. Table 9-4 shows the results for the light exposure controls, verifying that no bilirubin was lost due to photodegradation. The only statistically significant result was a value of bilirubin concentration that was greater than the initial solution.

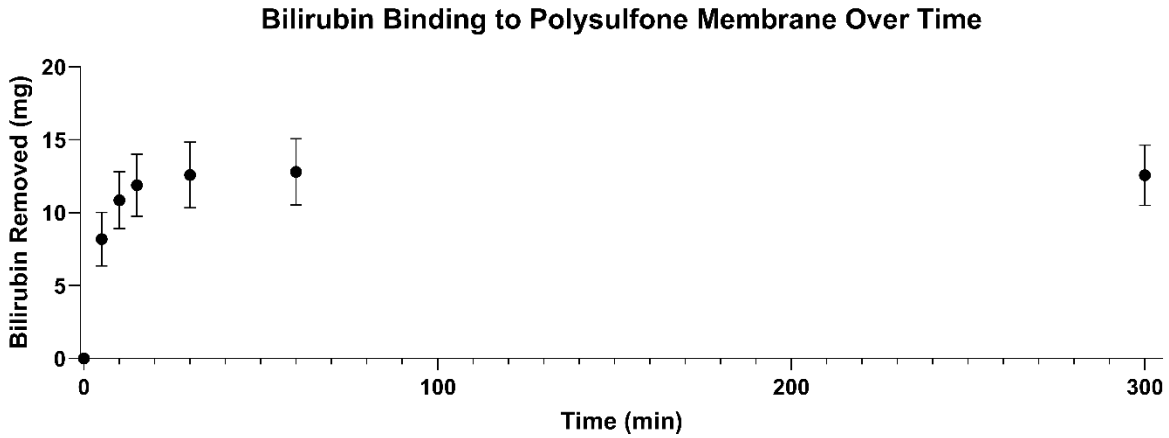


Figure 9-1: Bilirubin binding to polysulfone membrane over time. N = 3. Error bars show standard deviation.

Table 9-3: Bilirubin removed from blood and dialysate side in membrane absorption trials. All values are mean ± standard deviation of 3 technical replicates. * indicates p = 0.036

| Trial | Bilirubin Removed from Blood (mg) | Bilirubin Removed from Dialysate (mg) | Total Bilirubin Removed (mg) |
|---|---|---|---|
| 1 | 5.12 ± 0.27 | 5.44 ± 0.29 | 10.55 ± 0.55 |
| 2 | 7.32 ± 1.01 | 7.36 ± 0.35 | 14.68 ± 0.80 |
| 3 | 6.24 ± 0.27 | 6.24 ± 0.39 | 12.49 ± 0.60 |
| Average | 6.23 ± 1.10 | 6.34 ± 0.96 | 12.57 ± 2.07* |

Table 9-4: Photodegradation Control Results. All values are mean ± standard deviation of 3 technical replicates, except original solutions, which are mean ± standard deviation of 6 technical replicates (3 blood side and 3 dialysate side). * indicates p < 0. 05 compared to original solution.

| Trial | Original Solution (mg/dL) | Foil-Wrapped Tube, t = 5 hours (mg/dL) | Unwrapped Tube, t = 5 hours (mg/dL) |
|---|---|---|---|
| 1 | 15.90 ± 0.43 | 15.95 ± 0.22 | 15.91 ± 0.07 |
| 2 | 21.97 ± 0.36 | 21.84 ± 0.25 | 21.71 ± 0.14 |
| 3 | 18.62 ± 0.12 | 19.15 ± 0.20* | 19.24 ± 0.23* |

## 9.4 DISCUSSION

On average, the F3 polysulfone membrane removed 12.57 mg of bilirubin over 5 hours. Previous work suggests that the F6HPS polysulfone membrane also binds bilirubin. The density of polysulfone is 1.24 g/mL (325). The volume of polysulfone in the F3 pediatric dialyzer can be calculated as follows:

$$V_{dialyzer} = L * \pi * (r_0^2 - r_i^2) * n \text{ (Equation 9-2)}$$

n = 2304 (253). $r_i$ = 100 µm (255), $r_o$ = 140 µm (256), L = 20 cm (255). Thus, $V_{dialyzer}$ = 13.9 mL. The mass of the polysulfone in the F3 dialyzer is therefore 17.2 g. This means we removed 0.73 mg/g (bilirubin/polysulfone). This is similar to the results reported for bilirubin removal by polysulfone by Peng et al (161), and 2 orders of magnitude less than their custom-made polymer. However, polysulfone has the advantage of being inexpensive (so a large quantity can be used), validated as safe for use in humans, and FDA approved. The bilirubin binding affinity of polysulfone can be used to modify our albumin dialysis model to incorporate membrane absorption. This should improve its predictive power, especially for the kinetics of toxin transport, which the model currently overestimates.

# Chapter 10. CONCLUSION AND FUTURE WORK

In this thesis we review the history of artificial liver support systems. We then introduce a computational model of albumin dialysis based on the underlying physics of this process. We validate its ability to predict the impact of changing dialyzer flow rates, dialyzer setups, and albumin types. We introduce an FDA approved sorbent column (Adsorba 300) for toxin removal and demonstrate that it can be regenerated using dialysate. Next, we study alternatives to human and bovine serum albumin that have data supporting their use in humans. Finally, we demonstrate

data suggesting that polysulfone binds bilirubin, meaning an FDA approved material already in use in dialysis has the potential to eliminate an important protein bound toxin. This work supports the development of our novel artificial liver support system, the Advanced Multi-Organ Replacement System (AMOR), which has undergone preliminary human testing. In particular, the computational model of albumin dialysis will allow rational design of liver dialysis systems. This will maximize the benefit of this technology for patient care.

Future research will focus on modeling phenomena that are currently not accounted for. Membrane adsorption has been previously modeled by Snisarenko and colleagues (263). Charcoal columns have been modeled by Ding and colleagues (307). Modeling net ultrafiltration (as opposed to only local ultrafiltration) is another important aspect of a liver support device, given the importance of excess fluid removal in liver failure patients. Combining these components with the model presented here will permit the modeling of an entire binder dialysis device such as AMOR. This will allow clinical conditions to be simulated. Model predictions will need to be tested against realistic patient plasma volumes, non-Newtonian blood solutions, and other aspects that ensure relevance to patient care. Past clinical data may be used to fit model parameters and verify predictions. This will lead to the creation of a simulation that can optimize devices for protein bound toxin removal. Thus, devices can be optimized before entering clinical trials, maximizing the chance of success. Additionally, treatments can be personalized, such that a particular patient receives treatments that are best suited to their particular protein bound toxin milieu.

# Chapter 11. BIBLIOGRAPHY

1. Małkowski P. Human albumin: old, new, and emerging applications. Ann Transplant. 2013;18:205–17.

2. Ahmad S, Novokhodko A, Liou IW, Smith NC, Carithers RL, Reyes J, et al. Development and First Clinical Use of an Extracorporeal Artificial Multiorgan System in Acute-on-Chronic Liver Failure Patients. ASAIO J. 2024 Feb 29;

3. Naghavi M, Ong KL, Aali A, Ababneh HS, Abate YH, Abbafati C, et al. Global burden of 288 causes of death and life expectancy decomposition in 204 countries and territories and 811 subnational locations, 1990–2021: a systematic analysis for the Global Burden of Disease Study 2021. The Lancet. 2024 May;403(10440):2100–32.

4. Healthcare Cost and Utilization Project [Internet]. Rockville, MD: Agency for Healthcare Research and Quality; 2020. Available from: https://datatools.ahrq.gov/hcupnet

5. Shingina A, Mukhtar N, Wakim-Fleming J, Alqahtani S, Wong RJ, Limketkai BN, et al. Acute Liver Failure Guidelines. Am J Gastroenterol. 2023 Jul;118(7):1128–53.

6. Asrani SK, Devarbhavi H, Eaton J, Kamath PS. Burden of liver diseases in the world. Journal of Hepatology. 2019 Jan;70(1):151–71.

7. Kwong AJ, Kim WR, Lake JR, Schladt DP, Schnellinger EM, Gauntt K, et al. OPTN/SRTR 2022 Annual Data Report: Liver. American Journal of Transplantation. 2024 Feb;24(2):S176–265.

8. Torabi J, Todd R, Van Leeuwen LL, Bekki Y, Holzner M, Moon J, et al. A Decade of Liver Transplantation in the United States: Drivers of Discard and Underutilization. Transplantation Direct. 2024 May 3;10(6):e1605.

9. Cannon RM, Nassel A, Walker JT, Sheikh SS, Orandi BJ, Shah MB, et al. County-level Differences in Liver-related Mortality, Waitlisting, and Liver Transplantation in the United States. Transplantation. 2022 Sep;106(9):1799–806.

10. Tsipotis E, Shuja A, Jaber BL. Albumin Dialysis for Liver Failure: A Systematic Review. Advances in Chronic Kidney Disease. 2015 Sep;22(5):382–90.

11. Padmanabhan A, Connelly-Smith L, Aqui N, Balogun RA, Klingel R, Meyer E, et al. Guidelines on the Use of Therapeutic Apheresis in Clinical Practice – Evidence-Based Approach from the Writing Committee of the American Society for Apheresis: The Eighth Special Issue. J Clin Apher. 2019 Jun;34(3):171–354.

12. Larsen FS. Artificial liver support in acute and acute-on-chronic liver failure: Current Opinion in Critical Care. 2019 Apr;25(2):187–91.

13. Bai Z, Guo X, Tacke F, Li Y, Li H, Qi X. Association of serum albumin level with incidence and mortality of overt hepatic encephalopathy in cirrhosis during hospitalization. Therap Adv Gastroenterol. 2019 Jan;12:175628481988130.

14. Sarin SK, Choudhury A. Acute-on-chronic liver failure: terminology, mechanisms and management. Nat Rev Gastroenterol Hepatol. 2016 Mar;13(3):131–49.

15. Larsen FS, Schmidt LE, Bernsmeier C, Rasmussen A, Isoniemi H, Patel VC, et al. High-volume plasma exchange in patients with acute liver failure: An open randomised controlled trial. Journal of Hepatology. 2016 Jan;64(1):69–78.

16. Qin G, Shao JG, Wang B, Shen Y, Zheng J, Liu XJ, et al. Artificial Liver Support System Improves Short- and Long-Term Outcomes of Patients With HBV-Associated Acute-on-Chronic Liver Failure: A Single-Center Experience. Medicine. 2014 Dec;93(28):e338.

17. 2023 USRDS Annual Data Report: Epidemiology of kidney disease in the United States [Internet]. Bethesda, MD: National Institutes of Health, National Institute of Diabetes and Digestive and Kidney Diseases; 2023. (United States Renal Data System). Available from: https://usrds-adr.niddk.nih.gov/2023/suggested-citation

18. Giza H. Shaping the Future of Kidney Care: Annual Report 2023 [Internet]. Bad Homburg: Fresenius Medical Care; 2024. Available from: https://www.freseniusmedicalcare.com/fileadmin/data/com/pdf/Media_Center/Publications/Annual_Reports/FME_Annual_Report_2023_EN.pdf

19. Barreto FC, Barreto DV, Liabeuf S, Meert N, Glorieux G, Temmar M, et al. Serum Indoxyl Sulfate Is Associated with Vascular Disease and Mortality in Chronic Kidney Disease Patients. CJASN. 2009 Oct;4(10):1551–8.

20. Liabeuf S, Barreto DV, Barreto FC, Meert N, Glorieux G, Schepers E, et al. Free p-cresylsulphate is a predictor of mortality in patients at different stages of chronic kidney disease. Nephrology Dialysis Transplantation. 2010 Apr 1;25(4):1183–91.

21. Meijers BK, Weber V, Bammens B, Dehaen W, Verbeke K, Falkenhagen D, et al. Removal of the Uremic Retention Solute p-Cresol Using Fractionated Plasma Separation and Adsorption. Artificial Organs. 2008 Mar;32(3):214–9.

22. Butler DC, Berger T, Elmariah S, Kim B, Chisolm S, Kwatra SG, et al. Chronic Pruritus: A Review. JAMA [Internet]. 2024 May 29 [cited 2024 Jun 9]; Available from: https://jamanetwork.com/journals/jama/fullarticle/2819296

23. Tribe RM, Dann AT, Kenyon AP, Seed P, Shennan AH, Mallet A. Longitudinal Profiles of 15 Serum Bile Acids in Patients With Intrahepatic Cholestasis of Pregnancy. American Journal of Gastroenterology. 2010 Mar;105(3):585–95.

24. Akl EM, El-Eraki JM, Elfallah AA, Mohamed NH, Maher AM, Mansour AE, et al. Does Indoxyl Sulfate Have a Role in Uremic Pruritus? A Laboratory and Interventional Study. J Cutan Med Surg. 2024 Jan;28(1):44–50.

25. Bolanos CG, Pham NM, Mair RD, Meyer TW, Sirich TL. Metabolomic analysis of uremic pruritus in patients on hemodialysis. Millet O, editor. PLoS ONE. 2021 Feb 12;16(2):e0246765.

26. Cheungpasitporn W, Thongprayoon C, Zoghby ZM, Kashani K. MARS: Should I Use It? Advances in Chronic Kidney Disease. 2021 Jan;28(1):47–58.

27. De Geus H, Mathôt R, Van Der Hoven B, Tjoa M, Bakker J. Enhanced Paracetamol Clearance with Molecular Adsorbents Recirculating System (MARS®) in Severe Autointoxication. Blood Purif. 2010;30(2):118–9.

28. Lopez-Lopez V, Ros J, Ferreras D, Sanmartin J, Martinez M, Pons Miñano JA, et al. Molecular Adsorbent Recirculating System Treatment Can Reduce Blood Levels of N-Acetylcysteine in Patients With Acetaminophen Overdose: Case Reports. Transplantation Proceedings. 2018 Mar;50(2):687–9.

29. Scheiber IF, Brůha R, Dušek P. Pathogenesis of Wilson disease. In: Handbook of Clinical Neurology [Internet]. Elsevier; 2017 [cited 2024 Jun 9]. p. 43–55. Available from: https://linkinghub.elsevier.com/retrieve/pii/B9780444636256000057

30. Woimant F, Djebrani-Oussedik N, Poujois A. New tools for Wilson's disease diagnosis: exchangeable copper fraction. Ann Transl Med. 2019 Apr;7(S2):S70–S70.

31. Li N, Krishna SG, Hinton A, Conwell DL, Mumtaz K. Characteristics and outcomes of hospitalized patients with Wilson's disease in the United States: A national survey. Annals of Hepatology. 2021 Nov;25:100362.

32. Sandahl TD, Laursen TL, Munk DE, Vilstrup H, Weiss KH, Ott P. The Prevalence of Wilson's Disease: An Update. Hepatology. 2020 Feb;71(2):722–32.

33. Tuschl K, Clayton PT, Gospe SM, Gulab S, Ibrahim S, Singhi P, et al. Syndrome of Hepatic Cirrhosis, Dystonia, Polycythemia, and Hypermanganesemia Caused by Mutations in SLC30A10 , a Manganese Transporter in Man. The American Journal of Human Genetics. 2012 Mar;90(3):457–66.

34. Mercadante CJ, Prajapati M, Conboy HL, Dash ME, Herrera C, Pettiglio MA, et al. Manganese transporter Slc30a10 controls physiological manganese excretion and toxicity. Journal of Clinical Investigation. 2019 Nov 4;129(12):5442–61.

35. Jagadish S, Howard L, Thati Ganganna S. Atypical presentation of SLC30A10 gene mutation with hypermanganesemia, seizures and polycythemia. Epilepsy & Behavior Reports. 2021;16:100505.

36. Garg D, Yoganathan S, Shamim U, Mankad K, Gulati P, Bonifati V, et al. Clinical Profile and Treatment Outcomes of Hypermanganesemia with Dystonia 1 and 2 among 27 Indian Children. Movement Disord Clin Pract. 2022 Oct;9(7):886–99.

37. Hou H, Chen D, Liu J, Feng L, Zhang J, Liang X, et al. Clinical and Genetic Analysis in Neurological Wilson's Disease Patients With Neurological Worsening Following Chelator Therapy. Front Genet. 2022 Apr 4;13:875694.

38. Sen S, Felldin M, Steiner C, Larsson B, Gillett GT, Olausson M, et al. Albumin dialysis and Molecular Adsorbents Recirculating System (MARS) for acute Wilson's disease. Liver Transplantation. 2002 Oct;8(10):962–7.

39. Tcaciuc E, Podurean M, Tcaciuc A. Management of Crigler-Najjar syndrome. Med Pharm Rep. 2021 Aug;94(Suppl No 1):S64–7.

40. Roy-Chowdhury N, Roy-Chowdhury J. Crigler-Najjar syndrome. In: Rand E, Lindor K, Hoppin A, Robson K, editors. UpToDate [Internet]. 2024. Available from: https://www-uptodate-com.offcampus.lib.washington.edu/contents/crigler-najjar-syndrome?search=Crigler-Najjar%20syndrome&source=search_result&selectedTitle=1%7E13&usage_type=default&display_rank=1

41. Kiley JE, Pender JC, Welch HF, Welch CS. Ammonia Intoxication Treated by Hemodialysis. N Engl J Med. 1958 Dec 11;259(24):1156–61.

42. Sekandarzad A, Graf E, Prager EP, Luxenburger H, Staudacher DL, Wengenmayer T, et al. Cytokine adsorption in patients with acute-on-chronic liver failure ( CYTOHEP )—A single center, open-label, three-arm, randomized, controlled intervention pilot trial. Artificial Organs. 2024 May 21;aor.14774.

43. Maiwall R, Ashinikumar H, Chauhan N, Kumar A, Tevethia H, Rajan V, et al. Early versus late continuous renal replacement therapy in ACLF Patients with septic shock and acute kidney injury-a randomized. ICMx. 2023 Oct 24;11(S1):72, s40635-023-00546-y.

44. O'Brien Z, Cass A, Cole L, Finfer S, Gallagher M, McArthur C, et al. Higher versus Lower Continuous Renal Replacement Therapy Intensity in Critically ill Patients with Liver Dysfunction. Blood Purif. 2018;45(1–3):36–43.

45. Gish R, Regenstein F, Flamm S, Stravitz RT, Brothers J. Guidance for Coagulation Management in Patients With Acute or Chronic Liver Failure. Gastroenterology & Hepatology [Internet]. 2021 Jan;17(1S1). Available from: https://www.gastroenterologyandhepatology.net/supplements/guidance-for-coagulation-management-in-patients-with-acute-or-chronic-liver-failure/

46. Bai M, Yu Y, Zhao L, Tian X, Zhou M, Jiao J, et al. Regional Citrate Anticoagulation versus No Anticoagulation for CKRT in Patients with Liver Failure with Increased Bleeding Risk. CJASN [Internet]. 2023 Nov 23 [cited 2024 Sep 10]; Available from: https://journals.lww.com/10.2215/CJN.0000000000000351

47. Meijers B, Laleman W, Vermeersch P, Nevens F, Wilmer A, Evenepoel P. A prospective randomized open-label crossover trial of regional citrate anticoagulation vs. anticoagulation free liver dialysis by the Molecular Adsorbents Recirculating System. Crit Care. 2012;16(1):R20.

48. Jones RC, Strader LD, Berry WC. Peritoneal dialysis in liver coma. U S Armed Forces Med J. 1959 Aug;10:977–82.

49. Ring-Larsen H, Clausen E, Ranek L. Peritoneal Dialysis in Hyponatremia Due to Liver Failure. Scandinavian Journal of Gastroenterology. 1973 Jan 30;8(1):33–40.

50. Davenport A. Is there a role for continuous renal replacement therapies in patients with liver and renal failure? Kidney International. 1999 Nov;56:S62–6.

51. Patzer J. Principles of Bound Solute Dialysis. Therapher Dial. 2006 Apr;10(2):118–24.

52. Klammt S, Koball S, Hickstein H, Gloger M, Henschel J, Mitzner S, et al. Increase of Octanoate Concentrations During Extracorporeal Albumin Dialysis Treatments. Therapeutic Apheresis and Dialysis. 2009 Oct;13(5):437–43.

53. Sponholz C, Matthes K, Rupp D, Backaus W, Klammt S, Karailieva D, et al. Molecular adsorbent recirculating system and single-pass albumin dialysis in liver failure – a prospective, randomised crossover study. Crit Care. 2015 Dec;20(1):2.

54. Wallon G, Guth C, Guichon C, Thevenon S, Gazon M, Viale JP, et al. Extracorporeal Albumin Dialysis in Liver Failure with MARS and SPAD: A Randomized Crossover Trial. Blood Purif. 2021 Jun 17;1–8.

55. Hassanein TI, Tofteng F, Brown RS, McGuire B, Lynch P, Mehta R, et al. Randomized controlled study of extracorporeal albumin dialysis for hepatic encephalopathy in advanced cirrhosis. Hepatology. 2007 Dec;46(6):1853–62.

56. Bañares R, Nevens F, Larsen FS, Jalan R, Albillos A, Dollinger M, et al. Extracorporeal albumin dialysis with the molecular adsorbent recirculating system in acute-on-chronic liver failure: The RELIEF trial. Hepatology. 2013 Mar;57(3):1153–62.

57. Operating Instructions: MARS Monitor 1 TC and MARS Treatment Kit Type 1115/1-PrisMARS US Software version 4.04.15. Gambro; 2009.

58. Awad SS, Swaniker F, Magee J, Punch J, Bartlett RH. Results of a phase I trial evaluating a liver support device utilizing albumin dialysis. Surgery. 2001 Aug;130(2):354–62.

59. Kaps L, Ahlbrand CJ, Gadban R, Nagel M, Labenz C, Klimpke P, et al. Applicability and safety of discontinuous ADVanced Organ Support (ADVOS) in the treatment of patients with acute-on-chronic liver failure (ACLF) outside of intensive care. Kanda T, editor. PLoS ONE. 2021 Apr 1;16(4):e0249342.

60. Fuhrmann V, Perez Ruiz de Garibay A, Faltlhauser A, Tyczynski B, Jarczak D, Lutz J, et al. Registry on extracorporeal multiple organ support with the advanced organ support (ADVOS) system: 2-year interim analysis. Medicine. 2021 Feb 19;100(7):e24653.

61. Fuhrmann V, Weber T, Roedl K, Motaabbed J, Tariparast A, Jarczak D, et al. Advanced organ support (ADVOS) in the critically ill: first clinical experience in patients with multiple organ failure. Ann Intensive Care. 2020 Dec;10(1):96.

62. Huber W, Henschel B, Schmid R, Al-Chalabi A. First clinical experience in 14 patients treated with ADVOS: a study on feasibility, safety and efficacy of a new type of albumin dialysis. BMC Gastroenterol. 2017 Dec;17(1):32.

63. Sommerfeld O, Neumann C, Becker J, Von Loeffelholz C, Roth J, Kortgen A, et al. Extracorporeal albumin dialysis in critically ill patients with liver failure: Comparison of four different devices—A retrospective analysis. Int J Artif Organs. 2023 Sep;46(8–9):481–91.

64. Marangoni R, Bellati G, Castelli A, Romagnoli E. Development of High-Efficiency Molecular Adsorbent Recirculating System: Preliminary Report. Artificial Organs. 2014 Oct;38(10):879–83.

65. Sticova E. New insights in bilirubin metabolism and their clinical implications. WJG. 2013;19(38):6398.

66. Mitzner S, Stange J, Klammt S, Risler T, Erley C, Bader B, et al. Improvement of hepatorenal syndrome with extracorporeal albumin dialysis mars: Results of a prospective, randomized, controlled clinical trial. Liver Transplantation. 2000 May;6(3):277–86.

67. Stange J, Mitzner S, Klammt S, Loock J, Treichel U, Gerken G, et al. New extracorporeal liver support for chronic liver disease complicated by cholestasis-results of a prospective controlled randomized two center trial. Journal of Hepatology. 2001 Apr;34:45.

68. Heemann U, Treichel U, Loock J, Philipp T, Gerken G, Malago M, et al. Albumin dialysis in cirrhosis with superimposed acute liver injury: A prospective, controlled study. Hepatology. 2002 Oct;36(4):949–58.

69. Loock J, Heemann U, Mitzner S, Treichel U, Stange J, Peszynski P, et al. Are only bilirubin and bile acids removed by albumin dialysis? — observations of a randomized two center clinical trial. Journal of Hepatology. 2002 Apr;36:163.

70. Hu X, Zhou Y, Zhao Y, Liao M, He M, Wang M. Therapeutic application of the molecular adsorbent recirculating system in chronic severe hepatitis patients complicated with multiorgan failure. Crit Care. 2005;9(Suppl 1):P371.

71. Banayosy A, Cobaugh D, Pauly A, Kizner L, Körfer R. Albumindialyse bei Patienten mit sekundärem Leberversagen nach kardiogenem Schock. Intensivmed. 2007 Apr;44(3):149–57.

72. Saliba F, Camus C, Durand F, Mathurin P, Letierce A, Delafosse B, et al. Albumin Dialysis With a Noncell Artificial Liver Support Device in Patients With Acute Liver Failure: A Randomized, Controlled Trial. Ann Intern Med. 2013 Oct 15;159(8):522.

73. Fuhrmann V, Herkner H, Roedl K, Drolz A, Horvatits T, Horvatits K, et al. Treatment of hypoxic liver failure using molecular adsorbent recirculating system (MARS®) – a randomized controlled study. ICMx. 2019 Sep;7(S3):562.

74. Stange J, Ramlow W, Mitzner S, Schmidt R, Klinkmann H. Dialysis against a Recycled Albumin Solution Enables the Removal of Albumin-Bound Toxins. Artificial Organs. 1993 Sep;17(9):809–13.

75. Gong D, Ji D, Ren B, Tao J, Xu B, Ronco C, et al. Significant Decrease in Dialysate Albumin Concentration during Molecular Adsorbent Recirculating System (M.A.R.S.) Therapy. Int J Artif Organs. 2008 Apr;31(4):333–9.

76. MacDonald AJ, Subramanian RM, Olson JC, Speiser JL, Durkalski-Mauldin VL, Abraldes JG, et al. Use of the Molecular Adsorbent Recirculating System in Acute Liver Failure: Results of a Multicenter Propensity Score-Matched Study*. Critical Care Medicine. 2022 Feb;50(2):286–95.

77. Ahmad S, Liou I, Reyes J, Bakthavatsalam R, Smith N, Carithers R, et al. A Novel Liver Assist Device as a Bridge to Liver Transplantation in Acute on Chronic Liver Failure Patients with Multi-Organ Failure. In: American Journal of Transplantation [Internet]. 2021. (S3; vol. 21). Available from: https://atcmeetingabstracts.com/abstract/a-novel-liver-assist-device-as-a-bridge-to-liver-transplantation-in-acute-on-chronic-liver-failure-patients-with-multi-organ-failure/

78. Magosso E, Ursino M, Colì L, Baraldi O, Bolondi L, Stefoni S. A Modeling Study of Bilirubin Kinetics During Molecular Adsorbent Recirculating System Sessions. Artificial Organs. 2006 Apr;30(4):285–300.

79. Ash SR. Powdered Sorbent Liver Dialysis and Pheresis in Treatment of Hepatic Failure. Therapher Dial. 2001 Oct;5(5):404–16.

80. Stange J, Schmidt HHJ, Mitzner S, Koball S, Wilms C, Gerth H, et al. Randomized Controlled Trial to Compare Efficacy of Albumin Dialysis Using MARS versus New Adsorbent Recirculation for Pruritus Treatment [Internet]. European Association for the Study of the Liver; 2019 [cited 2021 Dec 27]; Rostock. Available from: https://s3.eu-central-1.amazonaws.com/meta-dcr/190410_6164_EASL_ILC_2019_Vienna/download/download_63788_un.pdf

81. Kortgen A, Stange J, Sponholz C, Schmidt HHJ, Wilms C, Gerth H, et al. Opal, but not MARS improves patients albumin binding function measured by Electron Spin Resonance (ESR) in a prospective multicenter trial. In: EASL. Paris: EASL; 2018.

82. Stange J, Sponholz C, Kortgen A, Schmidt HHJ, Dollinger M, Hassanein TI. Open albumin dialysis (OPAL) using new micro-structured charcoal adsorbents is significantly more effective in removing toxins and improving related complications of Aoclf than MARS-a multicenter trial. Hepatology. 2018 Oct;68(S1):180A.

83. Ash SR. Hemodiabsorption in Treatment of Acute Hepatic Failure and Chronic Cirrhosis with Ascites. Artificial Organs. 1994 May;18(5):355–62.

84. Ash SR, Steczko J, Knab WR, Blake DE, Carr DJ, Harker KD, et al. Push-Pull Sorbent-Based Pheresis and Hemodiabsorption in the Treatment of Hepatic Failure: Preliminary Results of a Clinical Trial with the BioLogic-DTPF System. Therapeutic Apheresis. 2000 Jun 1;4(3):218–28.

85. Ash SR, Steczko J, Levy H, Blake DE, Carr DJ. Treatment of Systemic Inflammatory Response Syndrome by Push-Pull Powdered Sorbent Pheresis: A Phase 1 Clinical Trial. Therapher Dial. 2001 Dec;5(6):497–505.

86. Mnasri N, Moussaoui Y, Elaloui E, Salem R ben, Lagerge S, Douillard JM, et al. Study of interaction between chitosan and active carbon in view of optimising composite gels devoted to heal injuries. EPJ Web of Conferences. 2012;29:00028.

87. Ash SR, Sullivan TA, Carr DJ. Sorbent Suspensions vs. Sorbent Columns for Extracorporeal Detoxification in Hepatic Failure. Therapher Dial. 2006 Apr;10(2):145–53.

88. Ash SR. The BioLogic-DT™ and the saga of Liver Dialysis™. Artificial Organs. 2022 Apr;46(4):715–9.

89. Carpentier B, Ash SR. Sorbent-based artificial liver devices: principles of operation, chemical effects and clinical results. Expert Review of Medical Devices. 2007 Nov;4(6):839–61.

90. O'Grady JG, Gimson AES, O'Brien CJ, Pucknell A, Hughes RD, Williams R. Controlled trials of charcoal hemoperfusion and prognostic factors in fulminant hepatic failure. Gastroenterology. 1988 May;94(5):1186–92.

91. Ocskay K, Tomescu D, Faltlhauser A, Jacob D, Friesecke S, Malbrain M, et al. Hemoadsorption in 'Liver Indication'—Analysis of 109 Patients' Data from the CytoSorb International Registry. JCM. 2021 Nov 5;10(21):5182.

92. Laleman W, Wilmer A, Evenepoel P, Elst I, Zeegers M, Zaman Z, et al. Effect of the molecular adsorbent recirculating system and Prometheus devices on systemic haemodynamics and vasoactive agents in patients with acute-on-chronic alcoholic liver failure. Crit Care. 2006;10(4):R108.

93. Iarustovskiĭ MB, Abramian MV, Komardina EV, Rep'eva EV, Nazarova EI, Krotenko NP, et al. [Extracorporeal methods of hematological correction in patients with acute liver insufficiency after cardiac surgery]. Anesteziol Reanimatol. 2014 Oct;59(5):4–10.

94. Kribben A, Gerken G, Haag S, Herget–Rosenthal S, Treichel U, Betz C, et al. Effects of Fractionated Plasma Separation and Adsorption on Survival in Patients With Acute-on-Chronic Liver Failure. Gastroenterology. 2012 Apr;142(4):782-789.e3.

95. Wan YM, Li YH, Xu ZY, Yang J, Yang LH, Xu Y, et al. Therapeutic plasma exchange versus double plasma molecular absorption system in hepatitis B virus-infected acute-on-chronic liver failure treated by entercavir: A prospective study. J Clin Apher. 2017 Dec;32(6):453–61.

96. Livigni S, Bertolini G, Rossi C, Ferrari F, Giardino M, Pozzato M, et al. Efficacy of coupled plasma filtration adsorption (CPFA) in patients with septic shock: A multicenter randomised controlled clinical trial. BMJ Open. 2014 Jan;4(1):e003536.

97. Viggiano D, de Pascale E, Marinelli G, Pluvio C. A comparison among three different apheretic techniques for treatment of hyperbilirubinemia. J Artif Organs. 2018 Mar;21(1):110–6.

98. Nakaji S, Hayashi N. Bilirubin Adsorption Column Medisorba BL-300. Therapher Dial. 2003 Feb;7(1):98–103.

99. Yadav M, Maiwal R, Kumar BR V, Tripathi G, Sharma N, Sharma N, et al. Comparative metabolome analysis reveals higher potential of haemoperfusion adsorption in providing favourable outcome in ACLF patients. Liver International. 2024 May;44(5):1189–201.

100. Shalimov SA, Zemskov VS, Kolesnikov EB. [Drainage of the thoracic lymphatic duct and lymphosorption in the combined treatment of obstruction of the bile ducts and liver failure]. Vestn Khir Im I I Grek. 1982 Feb;128(2):24–9.

101. Pirtskhalava TL, Granov DA. [A multilevel method of treatment of ascites with liver cirrhosis]. Vestn Khir Im I I Grek. 2003;162(5):36–9.

102. Mikhalovsky SV. Emerging technologies in extracorporeal treatment: focus on adsorption. Perfusion. 2003 Jan;18(1_suppl):47–54.

103. Hughes RD, Williams R. Selection of an adsorbent and hemoperfusion column design. Int J Artif Organs. 1981 Sep;4(5):224–9.

104. Skalsky M, Farrell PC. Adsorption of Selected Biochemicals onto coated and Uncoated Charcoal. Artificial Organs. 1979 Aug;3(3):258–64.

105. Hong SY, Yang JO, Lee EY, Kim SH. Effect of haemoperfusion on plasma paraquat concentration in vitro and in vivo. Toxicol Ind Health. 2003 Feb;19(1):17–23.

106. Ljunggren L, Ivanov AE, Gulalei F, Leistner A, Lehmann A, Klose-Stier A, et al. Effect of N-vinylimidazole comonomer on blood plasma protein and endogenous toxin adsorption on mesoporous copolymer beads. Biomedical Engineering Advances. 2022 Jun;3:100027.

107. Chen J, Han W, Chen J, Zong W, Wang W, Wang Y, et al. High performance of a unique mesoporous polystyrene-based adsorbent for blood purification. Regen Biomater. 2017 Feb;4(1):31–7.

108. Vienken J, Christmann H. How Can Liver Toxins be Removed? Filtration and Adsorption With the Prometheus System. Therapher Dial. 2006 Apr;10(2):125–31.

109. Donati G, Angeletti A, Gasperoni L, Piscaglia F, Croci Chiocchini AL, Scrivo A, et al. Detoxification of bilirubin and bile acids with intermittent coupled plasmafiltration and adsorption in liver failure (HERCOLE study). J Nephrol. 2021 Feb;34(1):77–88.

110. Ihara H, Shino Y, Hashizume N, Aoki T, Suzuki Y, Igarasi Y, et al. Decline in Plasma Retinol in Unconjugated Hyperbilirubinemia Treated with Bilirubin Adsorption Using an

Anion-Exchange Resin. Journal of Nutritional Science and Vitaminology, J Nutr Sci Vitaminol. 1998;44(2):329–36.

111. Nikolaev VG, Makhorin KE, Sergeev VP. Theoretical Aspects of Carbon Adsorbent Applications for Detoxification. Biomaterials, Artificial Cells and Artificial Organs. 1987 Jan;15(1):59–77.

112. Volfkovich YuM, Bagotzky VS, Sosenkin VE, Blinov IA. The standard contact porosimetry. Colloids and Surfaces A: Physicochemical and Engineering Aspects. 2001 Aug;187–188:349–65.

113. Nikolaev VG, Sarnatskaya VV, Sidorenko AN, Bardakhivskaya KI, Snezhkova EA, Yushko LA, et al. Deliganding Carbonic Adsorbents for Simultaneous Removal of Protein-Bound Toxins, Bacterial Toxins and Inflammatory Cytokines. In: Mikhalovsky S, Khajibaev A, editors. Biodefence [Internet]. Dordrecht: Springer Netherlands; 2011 [cited 2022 Aug 9]. p. 289–305. (NATO Science for Peace and Security Series A: Chemistry and Biology). Available from: http://link.springer.com/10.1007/978-94-007-0217-2_29

114. ГОГЕЛАШВИЛИ Г, ВАРТАПЕТЯН Р, ЛАДЫЧУК Д, ХОЗИНА Е, ГРУНИН Ю. Энергетические характеристики адсорбированной воды в активных углях по данным ЯМР-релаксации. ЖУРНАЛ ФИЗИЧЕСКОЙ ХИМИИ. 2010;84(2):327–31.

115. L.V. Pysarzhevsky Insitute of Physical Chemistry of National Academy of Sciences of Ukraine, Kapran AYu, Chedryk VI, L.V. Pysarzhevsky Insitute of Physical Chemistry of National Academy of Sciences of Ukraine, Alekseenko LM, L.V. Pysarzhevsky Insitute of Physical Chemistry of National Academy of Sciences of Ukraine, et al. Vapor-phase carbonylation of methanol on NiCl2-CuCl2(Sn)/AC(cordierite) catalysts. Him Fiz Tehnol Poverhni. 2020 Sep 30;11(3):378–87.

116. Zhou YD, Yang L, Han QF, Tang QB, Cheng YL, Shi JX. [Clinical effect of combined artificial extracorporeal liver support therapy for toxic hepatic failure]. Zhonghua Lao Dong Wei Sheng Zhi Ye Bing Za Zhi. 2017 Jan 20;35(1):51–3.

117. Vinay Kumar B, Maiwall R, Choudhury A, Bajpai M, Maras J, Kumar G, et al. A randomized controlled trial (RCT) of efficacy and safety of hemoperfusion or plasma exchange compared to standard medical therapy in patients with acute-on-chronic liver failure. Indian J Gastroenterol. 2020 Dec;39(S78):1–127.

118. Wu C, Peng W, Cheng D, Gu H, Liu F, Peng S, et al. Efficacy and Economic Evaluation of Nonbiological Artificial Liver Therapy in Acute-on-chronic Hepatitis B Liver Failure. J Clin Transl Hepatol. 2022 Jul 1;000(000):000–000.

119. Chang TMS. HÆMOPERFUSIONS OVER MICROENCAPSULATED ADSORBENT IN A PATIENT WITH HEPATIC COMA. The Lancet. 1972 Dec;300(7791):1371–2.

120. Ding WP, Zou LL, Pei YY, Sun SJ, Gao DY. Detoxification Capabilities of Adsorbents for Artificial Liver Support Devices: A Comparison. AMR. 2014 Jun;936:789–94.

121. Asanuma Y, Malchesky PS, Smith JW, Zawicki I, Carey WD, Ferguson DR, et al. Removal of Protein-Bound Toxins from Critical Care Patients. Clinical Toxicology. 1980 Jan;17(4):571–81.

122. Zhou PQ. Prognosis of acute-on-chronic liver failure patients treated with artificial liver support system. WJG. 2015;21(32):9614.

123. Falkenhagen D, Strobl W, Vogt G, Schrefl A, Linsberger I, Gerner FJ, et al. Fractionated Plasma Separation and Adsorption System: A Novel System for Blood Purification to Remove Albumin Bound Substances. Artificial Organs. 1999 Jan;23(1):81–6.

124. Dethloff T, Tofteng F, Frederiksen HJ, Hojskov M, Hansen BA, Larsen FS. Effect of Prometheus liver assist system on systemic hemodynamics in patients with cirrhosis: a randomized controlled study. World J Gastroenterol. 2008 Apr 7;14(13):2065–71.

125. Dong J, Huang L, Li C, Wu B, Yang X, Ge Y. Fractionated plasma separation and adsorption integrated with continuous veno-venous hemofiltration in patients with acute liver failure: A single center experience from China. J of Clinical Apheresis. 2024 Feb;39(1):e22100.

126. Du L, Ma Y, Zhou S, Chen F, Xu Y, Wang M, et al. A prognostic score for patients with acute-on-chronic liver failure treated with plasma exchange-centered artificial liver support system. Sci Rep. 2021 Jan 14;11(1):1469.

127. Spectra Optia® Apheresis System Operator's Manual [Internet]. Lakewood, CO, USA: Terumo BCT, Inc; 2018 May. Available from: https://www.ncbi.nlm.nih.gov/books/NBK572322/bin/fdacovideuas_136838.pdf

128. Akentiev S, Berezova M. CHANGING THE INDICATOR ENZYME LEVELS IN THE DETOXICATION PROCESS WITH INCLUSION OF PLASMA SORPTION IN THE STAGE OF INTENSIVE TREATMENT. Теория и практика современной науки. 2018;6(36):810–3.

129. Akentiev S, Berezova M. DYNAMICS OF PROTEIN LEVEL IN THE PROCEDURE OF THE DISCRETE VARIANT OF PLASMOSORPTION. Теория и практика современной науки. 2018;6(36):807–9.

130. Russell PS, Nachkebia S, Maldonado-Zimbron VE, Chuklin S, Gimel'farb G, Hong J, et al. Therapeutic thoracic duct drainage: A systematic review of the Eastern European experience and future potential. Lymphology. 2022;55(3):86–109.

131. Wang HW, Escott ABJ, Phang KL, Petrov MS, Phillips ARJ, Windsor JA. Indications, techniques, and clinical outcomes of thoracic duct interventions in patients: a forgotten literature? Journal of Surgical Research. 2016 Jul;204(1):213–27.

132. Lee C, Tink A. EXCHANGE TRANSFUSION IN HEPATIC COMA: REPORT OF A CASE. Medical Journal of Australia. 1958 Jan;1(2):40–2.

133. Redeker A, Yamahiro H. CONTROLLED TRIAL OF EXCHANGE-TRANSFUSION THERAPY IN FULMINANT HEPATITIS. The Lancet. 1973 Jan;301(7793):3–6.

134. Agarwal B, Cañizares RB, Saliba F, Ballester MP, Tomescu DR, Martin D, et al. Randomized, controlled clinical trial of the DIALIVE liver dialysis device versus standard of care in patients with acute-on- chronic liver failure. Journal of Hepatology. 2023 Jul;79(1):79–92.

135. Gong D, Ren B, Ji D, Tao J, Xu B, Liu Z, et al. Selective Albumin Exchange: A Novel and Simple Method to Remove Bilirubin. Int J Artif Organs. 2008 May;31(5):425–30.

136. Moreau R, Tonon M, Krag A, Angeli P, Berenguer M, Berzigotti A, et al. EASL Clinical Practice Guidelines on acute-on-chronic liver failure. Journal of Hepatology. 2023 Aug;79(2):461–91.

137. Sinha S, Sarin SK, Bajpai M, Arora V. Comparison of the efficacy and safety of plasma exchange compared to standard medical therapy in patients with severe drug induced liver injury-a randomized controlled trial. Hepatology. 2020 Nov;72(S1):620A.

138. Ye W jiang, Li L juan, Yu H yan, Zhang X ping, Tian J, Bai M hui. [Clinical research of plasma exchange with continuous veno-venous hemofiltration in treating mid- and late-stage chronic severe viral hepatitis B patients]. Zhonghua Gan Zang Bing Za Zhi. 2005 May;13(5):370–3.

139. Yang Y feng, Huang P, Zhang N, Gai X dong, Feng X ning, Zhong Y dan, et al. [Comparison of curative effect of low flow rate plasma exchange combined with hemofiltration for treatment of liver failure]. Zhongguo Wei Zhong Bing Ji Jiu Yi Xue. 2009 Feb;21(2):111–3.

140. Maiwall R, Bajpai M, Singh A, Agarwal T, Kumar G, Bharadwaj A, et al. Standard-Volume Plasma Exchange Improves Outcomes in Patients With Acute Liver Failure: A Randomized Controlled Trial. Clinical Gastroenterology and Hepatology. 2022 Apr;20(4):e831–54.

141. Pawaria A, Pandey S, Alam S, Khanna R. Efficacy and safety of high volume plasma exchange in children with acute liver failure - a prospective pilot study. Hepatol Int. 2019 Feb;13(S1):S253-S254.

142. Dai X, Zhang Y, Yu L, Jiang Y, Chen L, Chen Y, et al. Effect of artificial liver blood purification treatment on the survival of critical ill COVID-19 patients. Artif Organs. 2021 Jul;45(7):762–9.

143. Duan Z, Xin S, Zhang J, You S, Chen Y, Liu H, et al. Comparison of extracorporeal cellular therapy (ELAD®) vs standard of care in a randomized controlled clinical trial in treating Chinese subjects with acute-on-chronic liver failure. HMER. 2018 Nov;Volume 10:139–52.

144. APASL ACLF Research Consortium (AARC) for APASL ACLF working Party., Sarin SK, Choudhury A, Sharma MK, Maiwall R, Al Mahtab M, et al. Acute-on-chronic liver failure: consensus recommendations of the Asian Pacific association for the study of the liver (APASL): an update. Hepatol Int. 2019 Jul;13(4):353–90.

145. Anand AC, Nandi B, Acharya SK, Arora A, Babu S, Batra Y, et al. Indian National Association for the Study of Liver Consensus Statement on Acute Liver Failure (Part-2): Management of Acute Liver Failure. Journal of Clinical and Experimental Hepatology. 2020 Sep;10(5):477–517.

146. Connelly-Smith L, Alquist CR, Aqui NA, Hofmann JC, Klingel R, Onwuemene OA, et al. Guidelines on the Use of Therapeutic Apheresis in Clinical Practice – Evidence-Based Approach from the Writing Committee of the American Society for Apheresis: The Ninth Special Issue. J of Clinical Apheresis. 2023 Apr;38(2):77–278.

147. Patzer JF, Bane SE. Bound Solute Dialysis. ASAIO Journal. 2003 May;49(3):271–81.

148. Patzer JF, Safta SA, Miller RH. Slow Continuous Ultrafiltration with Bound Solute Dialysis. ASAIO Journal. 2006 Jan;52(1):47–58.

149. Annesini MC, Piemonte V, Turchetti L. ALBUMIN-BOUND TOXIN REMOVAL IN LIVER SUPPORT DEVICES: CASE STUDY OF BILIRUBIN ADSORPTION AND DIALYSIS. In: Biochemical Engineering. New York: Nova Science Publishers; 2009. p. 321–39. (Bioetchnology in Agriculture, Industry and Medicine Series).

150. Annesini MC, Piemonte V, Turchetti L. Artificial liver devices: A chemical engineering analysis. Asia-Pacific Jrnl of Chem Eng. 2011 Jul;6(4):639–48.

151. Annesini MC, Piemonte V, Turchetti L. Artificial liver support systems: a patient-device model. Asia-Pac J Chem Eng. 2014 May;9(3):390–400.

152. Annesini MC, Marrelli L, Piemonte V, Turchetti L. Artificial and Bio-Artificial Liver. In: Artificial Organ Engineering [Internet]. London: Springer London; 2017 [cited 2024 Nov 26]. p. 219–53. Available from: http://link.springer.com/10.1007/978-1-4471-6443-2_8

153. Maria Cristina Annesini, Vincenzo Morabito, Gilnardo Novelli, Vincenzo Piemonte, Luca Turchetti. Molecular adsorbent recirculating system (m.a.r.s.): a chemical engineering analysis of clinical data. Chemical Engineering Transactions. 2009 May;17:1095–100.

154. Liver Support Systems. In: Method of Lines PDE Analysis in Biomedical Science and Engineering [Internet]. Hoboken, NJ, USA: John Wiley & Sons, Inc; 2016 [cited 2022 Sep 16]. p. 165–204. Available from: https://onlinelibrary.wiley.com/doi/10.1002/9781119130499.ch6

155. Pei Y, Sun Y, Xu Y, Zhao G, Gao D, Ding W. A theoretical ultrafiltration model for albumin-bound toxin dialysis. In: 2013 ICME International Conference on Complex Medical Engineering [Internet]. Beijing: IEEE; 2013 [cited 2021 Oct 18]. p. 528–31. Available from: http://ieeexplore.ieee.org/document/6548306/

156. Pei YY, Xu Y, Sun YZ, Gao DY, Ding WP. Numerical Simulation and Experimental Validation of Bound Solute Dialysis in Artificial Liver Support Systems. AMR. 2014 Jun;971–973:107–10.

157. Pei YY, Sun YZ, Sun SJ, Gao DY, Ding WP. The Comparison of Albumin Dialysis between Open- and Closed-Loop Dialysis Modes. AMR. 2014 Jun;960–961:47–51.

158. Pei Y, Sun Y, Sun S, Gao D, Ding W. Albumin Dialysis in Artificial Liver Support Systems: Open-Loop or Closed-Loop Dialysis Mode? ASAIO Journal. 2015;61(3):324–31.

159. Villarroel F, Klein E, Holland F. SOLUTE FLUX IN HEMODIALYSIS AND HEMOFILTRATION MEMBRANES: ASAIO Journal. 1977;23(1):225–32.

160. Michaels AS. Operating parameters and performance criteria for hemodialyzers and other membrane-separation devices. Trans Am Soc Artif Intern Organs. 1966;12:387–92.

161. Peng Z, Yang Y, Luo J, Nie C, Ma L, Cheng C, et al. Nanofibrous polymeric beads from aramid fibers for efficient bilirubin removal. Biomater Sci. 2016;4(9):1392–401.

162. Ding W, Zhou X, Heimfeld S, Reems JA, Gao D. A Steady-State Mass Transfer Model of Removing CPAs From Cryopreserved Blood With Hollow Fiber Modules. Journal of Biomechanical Engineering. 2010 Jan 1;132(1):011002.

163. J.C., E. Comparative Study of Bisection, Newton-Raphson and Secant Methods of Root-Finding Problems. IOSRJEN. 2014 Apr;4(4):01–7.

164. Gao D, Huang Z. Artificial Kidney：Fundamentals, Research Approaches and Advances. Beijing: University of Science and Technology of China Press; 2009.

165. Meyer TW, Peattie JWT, Miller JD, Dinh DC, Recht NS, Walther JL, et al. Increasing the Clearance of Protein-Bound Solutes by Addition of a Sorbent to the Dialysate. JASN. 2007 Mar;18(3):868–74.

166. Yu J, Chitalia VC, Akintewe OO, Edwards A, Wong JY. Determinants of Hemodialysis Performance:Modeling Fluid and Solute Transport in Hollow-Fiber Dialyzers. Regen Eng Transl Med. 2021 Sep;7(3):291–300.

167. Hairer E, Wanner G. Solving ordinary differential equations. 2: Stiff and differential algebraic problems. 2., rev. ed., 1. softcover printing. Berlin Heidelberg: Springer; 2010. 614 p. (Springer series in computational mathematics).

168. Steinebach G. Construction of Rosenbrock–Wanner method Rodas5P and numerical benchmarks within the Julia Differential Equations package. Bit Numer Math. 2023 Jun;63(2):27.

169. Bezanson J, Edelman A, Karpinski S, Shah VB. Julia: A Fresh Approach to Numerical Computing. SIAM Rev. 2017 Jan;59(1):65–98.

170. Rackauckas C, Nie Q. DifferentialEquations.jl – A Performant and Feature-Rich Ecosystem for Solving Differential Equations in Julia. JORS. 2017 May 25;5(1):15.

171. Rackauckas C, Pal A, Raj Singh Y, Carlson S, Larsson, Qu Q, et al. SciML/NonlinearSolve.jl: v3.1.1 [Internet]. [object Object]; 2023 [cited 2024 Mar 12]. Available from: https://zenodo.org/doi/10.5281/zenodo.10397607

172. Mogensen PK, Carlsson K, Villemot S, Lyon S, Gomez M, Rackauckas C, et al. JuliaNLSolvers/NLsolve.jl: v4.5.1 [Internet]. [object Object]; 2020 [cited 2024 Mar 12]. Available from: https://zenodo.org/record/4404703

173. Verzani J. Root finding functions for Julia} [Internet]. 2020. Available from: https://github.com/JuliaMath/Roots.jl

174. Bieler J. linspace [Internet]. 2020. Available from: https://discourse.julialang.org/t/tl-dr-tips-for-julia-users-coming-from-matlab/41093/1

175. Franco M. remove [Internet]. 2019. Available from: https://stackoverflow.com/questions/35298809/delete-element-in-an-array-for-julia

176. myfind [Internet]. 2017. Available from: https://stackoverflow.com/questions/42232411/find-indices-of-non-zero-elements-from-1-2-0-0-4-0-in-julia-and-create-an-arrr

177. Hairer E, Wanner G. Stiff differential equations solved by Radau methods. Journal of Computational and Applied Mathematics. 1999 Nov;111(1–2):93–111.

178. Rackauckas C, Nie Q. Confederated modular differential equation APIs for accelerated algorithm development and benchmarking. Advances in Engineering Software. 2019 Jun;132:1–6.

179. Kalakonda A, Jenkins BA, John S. Physiology, Bilirubin. In: StatPearls [Internet]. Treasure Island (FL): StatPearls Publishing; 2024 [cited 2024 Mar 12]. Available from: http://www.ncbi.nlm.nih.gov/books/NBK470290/

180. Goncharova I, Orlov S, Urbanová M. The location of the high- and low-affinity bilirubin-binding sites on serum albumin: Ligand-competition analysis investigated by circular dichroism. Biophysical Chemistry. 2013 Oct;180–181:55–65.

181. Lakovic K, Ai J, D'Abbondanza J, Tariq A, Sabri M, Alarfaj AK, et al. Bilirubin and its Oxidation Products Damage Brain White Matter. J Cereb Blood Flow Metab. 2014 Nov;34(11):1837–47.

182. Dugdale D, Zieve D, Conaway B. Bilirubin blood test [Internet]. 2021. Available from: https://medlineplus.gov/ency/article/003479.htm

183. Weiping D. Development of an Optimal Artificial Liver Support System. 1st ed. Seattle: University of Washington; 2010. (PhD Thesis).

184. Senf R, Klingel R, Kurz S, Tullius S, Sauer I, Frei U, et al. Bilirubin-Adsorption in 23 Critically Ill Patients with Liver Failure. Int J Artif Organs. 2004 Aug;27(8):717–22.

185. Vaz FrédéricM, Ferdinandusse S. Bile acid analysis in human disorders of bile acid biosynthesis. Molecular Aspects of Medicine. 2017 Aug;56:10–24.

186. Fuchs CD, Trauner M. Role of bile acids and their receptors in gastrointestinal and hepatic pathophysiology. Nat Rev Gastroenterol Hepatol. 2022 Jul;19(7):432–50.

187. Chiang JYL, Ferrell JM. Bile Acid Metabolism in Liver Pathobiology. gene expr. 2018 May 18;18(2):71–87.

188. Rohacova J, Marin ML, Miranda MA. Complexes between Fluorescent Cholic Acid Derivatives and Human Serum Albumin. A Photophysical Approach To Investigate the Binding Behavior. J Phys Chem B. 2010 Apr 8;114(13):4710–6.

189. Horvatits T, Drolz A, Roedl K, Rutter K, Ferlitsch A, Fauler G, et al. Serum bile acids as marker for acute decompensation and acute-on-chronic liver failure in patients with non-cholestatic cirrhosis. Liver Int. 2017 Feb;37(2):224–31.

190. Lewis B, Panveliwalla D, Tabaqchali S, Wootton IDP. SERUM-BILE-ACIDS IN THE STAGNANT-LOOP SYNDROME. The Lancet. 1969 Feb;293(7588):219–20.

191. Watanabe H, Noguchi T, Miyamoto Y, Kadowaki D, Kotani S, Nakajima M, et al. Interaction between Two Sulfate-Conjugated Uremic Toxins, *p* -Cresyl Sulfate and Indoxyl Sulfate, during Binding with Human Serum Albumin. Drug Metab Dispos. 2012 Jul;40(7):1423–8.

192. Agarwal A. Correlation of Trace Elements in Patients of Chronic Liver Disease with Respect to Child- Turcotte- Pugh Scoring System. JCDR [Internet]. 2017 [cited 2021 Apr 24]; Available from: http://jcdr.net/article_fulltext.asp?issn=0973-709x&year=2017&volume=11&issue=9&page=OC25&issn=0973-709x&id=10655

193. Yu L, Liou IW, Biggins SW, Yeh M, Jalikis F, Chan L, et al. Copper Deficiency in Liver Diseases: A Case Series and Pathophysiological Considerations. Hepatol Commun. 2019 Aug;3(8):1159–65.

194. Nordberg G Fowler, Bruce A, Nordberg M. Handbook on the toxicology of metals [Internet]. Amsterdam: Academic Press; 2014 [cited 2021 Nov 21]. Available from: https://www.sciencedirect.com/science/book/9780444594532

195. Harris ED. Cellular Copper Transport and Metabolism. Annu Rev Nutr. 2000 Jul;20(1):291–310.

196. Al-Harthi S, Lachowicz JI, Nowakowski ME, Jaremko M, Jaremko Ł. Towards the functional high-resolution coordination chemistry of blood plasma human serum albumin. Journal of Inorganic Biochemistry. 2019 Sep;198:110716.

197. Rahelić D, Kujundzić M, Romić Z, Brkić K, Petrovecki M. Serum concentration of zinc, copper, manganese and magnesium in patients with liver cirrhosis. Coll Antropol. 2006 Sep;30(3):523–8.

198. Da Silva CJ, Da Rocha AJ, Jeronymo S, Mendes MF, Milani FT, Maia ACM, et al. A Preliminary Study Revealing a New Association in Patients Undergoing Maintenance Hemodialysis: Manganism Symptoms and T1 Hyperintense Changes in the Basal Ganglia. American Journal of Neuroradiology. 2007 Sep 1;28(8):1474–9.

199. Uchino S. Creatinine. Current Opinion in Critical Care. 2010 Dec;16(6):562–7.

200. Shahbaz H, Gupta M. Creatinine Clearance. In: StatPearls [Internet]. Treasure Island (FL): StatPearls Publishing; 2024 [cited 2024 Jun 10]. Available from: http://www.ncbi.nlm.nih.gov/books/NBK544228/

201. ul Amin N, Mahmood R, Asad MJ, Zafar M, Raja A. Evaluating Urea and Creatinine Levels in Chronic Renal Failure Pre and Post Dialysis: A Prospective Study. Journal of Cardiovascular Disease. 2014 Jul;2(4):182–5.

202. Varshney A, Rehan M, Subbarao N, Rabbani G, Khan RH. Elimination of Endogenous Toxin, Creatinine from Blood Plasma Depends on Albumin Conformation: Site Specific Uremic Toxicity & Impaired Drug Binding. Stultz C, editor. PLoS ONE. 2011 Feb 28;6(2):e17230.

203. Davis C, Shiel W. Creatinine Blood Test (Normal, Low, High Levels) [Internet]. 2022. Available from: https://www.medicinenet.com/creatinine_blood_test/article.htm

204. Specification Sheet Dextran from Leuconostoc spp. Mr ~70,000 [Internet]. Sigma Aldrich; 2022. Available from: https://www.sigmaaldrich.com/US/en/specification-sheet/SIGMA/31390

205. Han LW, Wang L, Shi Y, Dempsey JL, Pershutkina OV, Dutta M, et al. Impact of Microbiome on Hepatic Metabolizing Enzymes and Transporters in Mice during Pregnancy. Drug Metab Dispos. 2020 Aug;48(8):708–22.

206. Frei M. Centrifugation Basics [Internet]. MilliporeSigma; [cited 2021 Dec 29]. Available from: https://www.sigmaaldrich.com/US/en/technical-documents/technical-article/protein-biology/protein-pulldown/centrifugation-basics

207. Bower P. Method of Standard Addition. JoVE Science Education [Internet]. 2023; Available from: https://app.jove.com/v/10201/method-of-standard-addition

208. Cuhadar S, Koseoglu M, Atay A, Dirican A. The effect of storage time and freeze-thaw cycles on the stability of serum samples. Biochem Med. 2013;70–7.

209. Xiang X, Han Y, Neuvonen M, Laitila J, Neuvonen PJ, Niemi M. High performance liquid chromatography–tandem mass spectrometry for the determination of bile acid concentrations in human plasma. Journal of Chromatography B. 2010 Jan;878(1):51–60.

210. Al Za'abi M, Ali B, Al Toubi M. HPLC-Fluorescence Method for Measurement of the Uremic Toxin Indoxyl Sulfate in Plasma. Journal of Chromatographic Science. 2013 Jan 1;51(1):40–3.

211. Arnaud J. Stability of serum copper, selenium and zinc. TRACE ELEMENTS IN MEDICINE (MOSCOW). 2010;11(2):3.

212. Novokhodko A, Du N, Gao D. Bicarbonate concentrate stability in freezer. Cryobiology. 2022;109:59.

213. Wear J, McPherson TB, Kolling WM. Stability of sodium bicarbonate solutions in polyolefin bags. American Journal of Health-System Pharmacy. 2010 Jun 15;67(12):1026–9.

214. Naorungroj T, Neto AS, Fujii T, Jude B, Udy A, Bellomo R. Stability of bicarbonate in normal saline: a technical report. Critical Care and Resuscitation. 2020 Mar;22(1):83–5.

215. Hicks CI, Gallardo JPB, Guillory JK. Stability of Sodium Bicarbonate Injection Stored in Polypropylene Syringes. American Journal of Health-System Pharmacy. 1972 Mar 1;29(3):210–6.

216. Sayre BE, Prettyman T, Kaushal G. Extended Stability of Sodium Bicarbonate Infusions Prepared in Polyolefin Bags. Hosp Pharm. 2012 Jul;47(7):538–43.

217. Klein E, Holland FF, Donnaud A, Lebeouf A, Eberle K. Diffusive and hydraulic permeabilities of commercially available cellulosic hemodialysis films and hollow fibers,. Journal of Membrane Science. 1977 Jan;2:349–64.

218. Liao Z, Klein E, Poh C, Huang Z, Lu J, Hardy P, et al. Measurement of hollow fiber membrane transport properties in hemodialyzers. Journal of Membrane Science. 2005 Apr 7;S0376738805001602.

219. Benavente J, Jonsson G. Electrokinetic characterization of composite membranes: estimation of different electrical contributions in pressure induced potential measured across reverse osmosis membranes. Journal of Membrane Science. 2000 Jul 1;172(1–2):189–97.

220. Zepeda-Orozco D, Quigley R. Dialysis disequilibrium syndrome. Pediatr Nephrol. 2012 Dec;27(12):2205–11.

221. Depner TA, Greene T, Daugirdas JT, Cheung AK, Gotch FA, Leypoldt JK. Dialyzer Performance in the HEMO Study:In Vivo K 0 A and True Blood Flow Determined from a Model of Cross-Dialyzer Urea Extraction. ASAIO Journal. 2004 Jan;50(1):85–93.

222. Jacobsen J. STUDIES OF THE AFFINITY OF HUMAN SERUM ALBUMIN FOR BINDING OF BILIRUBIN AT DIFFERENT TEMPERATURES AND IONIC STRENGTH. International Journal of Peptide and Protein Research. 1977 Mar;9(3):235–40.

223. Weisiger RA, Ostrow JD, Koehler RK, Webster CC, Mukerjee P, Pascolo L, et al. Affinity of Human Serum Albumin for Bilirubin Varies with Albumin Concentration and Buffer Composition. Journal of Biological Chemistry. 2001 Aug;276(32):29953–60.

224. Chen RF. The Fluorescence of Bilirubin-Albumin Complexes. In: Thaer AA, Sernetz M, editors. Fluorescence Techniques in Cell Biology [Internet]. Berlin, Heidelberg: Springer Berlin Heidelberg; 1973 [cited 2022 Sep 19]. p. 273–82. Available from: http://link.springer.com/10.1007/978-3-642-49204-4_27

225. Faerch T, Jacobsen J. Determination of association and dissociation rate constants for bilirubin-bovine serum albumin. Archives of Biochemistry and Biophysics. 1975 Jun;168(2):351–7.

226. Rubaltelli FF, Jori G. VISIBLE LIGHT IRRADIATION OF HUMAN AND BOVINE SERUM ALBUMIN-BILIRUBIN COMPLEX*. Photochem Photobiol. 1979 May;29(5):991–1000.

227. Mir M, Fazili M, Qasim A. Chemical modification of buried lysine residues of bovine serum albumin and its influence on protein conformation and bilirubin binding. Biochimica et Biophysica Acta (BBA) - Protein Structure and Molecular Enzymology. 1992 Mar;1119(3):261–7.

228. Williams KR, Adhyaru B, Pierce RE, Schulman SG. The Binding Constant for Complexation of Bilirubin to Bovine Serum Albumin. An Experiment for the Biophysical Chemistry Laboratory. J Chem Educ. 2002 Jan;79(1):115.

229. Chen J, Song G, He Y, Yan Q. Spectroscopic analysis of the interaction between bilirubin and bovine serum albumin. Microchim Acta. 2007 Jun;159(1–2):79–85.

230. Ahmad S, Misra M, Hoenich N, Daugirdas JT. Equipo de hemodiálisis. In: Manual de Diálisis. 5th ed. Barcelona: Wolters Kluwer; 2015.

231. Pico GA, Houssier C. Bile salts-bovine serum albumin binding: spectroscopic and thermodynamic studies. Biochimica et Biophysica Acta (BBA) - Protein Structure and Molecular Enzymology. 1989 Nov;999(2):128–34.

232. Picó G. Use of 1-anilino-8-naphthalene sulfonate as a reporter molecule to study the bile salts-bovine serum albumin-binding. STUDIA BIOPHYSICA, AKADEMIE VERLAG, BERLIN. 1990;136(1):21–6.

233. Farruggia B, Picó G. Bile salts binding-induced alterations in ultraviolet absorption spectrum of bovine serum albumin. Gen Physiol Biophys. 1992 Apr;11(2):213–8.

234. Farruggia B, Picó G. Role of electrostatic forces in hydroxy and keto bile salt-albumin interactions: some experimental observations. Gen Physiol Biophys. 1992 Apr;11(2):219–24.

235. Davilas A, Koupparis M, Macheras P, Valsami G. In-vitro study on the competitive binding of diflunisal and uraemic toxins to serum albumin and human plasma using a potentiometric ion-probe technique. Journal of Pharmacy and Pharmacology. 2010 Feb 18;58(11):1467–74.

236. Moschen T, Grutsch S, Juen MA, Wunderlich CH, Kreutz C, Tollinger M. Measurement of Ligand–Target Residence Times by 1H Relaxation Dispersion NMR Spectroscopy. J Med Chem. 2016 Dec 8;59(23):10788–93.

237. Zhang Y, Wilcox DE. Thermodynamic and spectroscopic study of Cu(II) and Ni(II) binding to bovine serum albumin. J Biol Inorg Chem. 2002 Mar;7(3):327–37.

238. Singh A, Datta P, Pandey LM. Deciphering the mechanistic insight into the stoichiometric ratio dependent behavior of Cu(II) on BSA fibrillation. International Journal of Biological Macromolecules. 2017 Apr;97:662–70.

239. Arnquist IJ, Holcombe JA. Ultracentrifugation and inductively coupled plasma mass spectrometry for metal–protein equilibrium studies. Spectrochimica Acta Part B: Atomic Spectroscopy. 2012 Oct;76:140–6.

240. Zhang Y, Akilesh S, Wilcox DE. Isothermal Titration Calorimetry Measurements of Ni(II) and Cu(II) Binding to His, GlyGlyHis, HisGlyHis, and Bovine Serum Albumin: A Critical Evaluation. Inorg Chem. 2000 Jul 1;39(14):3057–64.

241. Liang H, Xin B, Wang X, Yuan Y, Zhou Y, Shen P. Equilibrium dialysis study on the interaction between Cu(II) and HSA or BSA. Chin Sci Bull. 1998 Mar;43(5):404–9.

242. Sommer-Knudsen J, Bacic A. A micro-scale method for determining relative metal-binding affinities of proteins. Mol Biotechnol. 1997 Dec;8(3):215–8.

243. Masuoka J, Hegenauer J, Van Dyke BR, Saltman P. Intrinsic stoichiometric equilibrium constants for the binding of zinc(II) and copper(II) to the high affinity site of serum albumin. Journal of Biological Chemistry. 1993 Oct;268(29):21533–7.

244. Zgirski A, Frieden E. Binding of Cu(II) to non-prosthetic sites in ceruloplasmin and bovine serum albumin. Journal of Inorganic Biochemistry. 1990 Jun;39(2):137–48.

245. Syvertsen C, Gaustad R, Schrøder K, Ljones T. Studies on the binding of copper to dopamine β-monooxygenase and other proteins using the Cu2+ ion-selective electrode. Journal of Inorganic Biochemistry. 1986 Jan;26(1):63–76.

246. Giroux E, Schoun J. Copper and zinc ion binding by bovine, dog, and rat serum albumins. Journal of Inorganic Biochemistry. 1981 Jan;14(4):359–62.

247. Ryall RG. Competitive Dialysis Studies of Metal-Protein Equilibria [Internet] [Ph.D.]. PQDT - Global. [Australia]: The Australian National University (Australia); 1974. Available from: https://www.proquest.com/dissertations-theses/competitive-dialysis-studies-metal-protein/docview/2606872698/se-2?accountid=14784

248. Rao MSN, Lal H. Metal Protein Interactions in Buffer Solutions. Part III. Interaction of $Cu^{II}$, $Zn^{II}$, $Cd^{II}$, $Co^{II}$ (and $Ni^{II}$) with Native and Modified Bovine Serum Albumins. J Am Chem Soc. 1958 Jul;80(13):3226–35.

249. Tanford C. The Effect of pH on the Combination of Serum Albumin with Metals1. J Am Chem Soc. 1952 Jan 1;74(1):211–5.

250. Klotz IM, Curme HG. The Thermodynamics of Metallo-protein Combinations. Copper with Bovine Serum Albumin. J Am Chem Soc. 1948 Mar;70(3):939–43.

251. Leypoldt JK, Cheung AK, Agodoa LY, Daugirdas JT, Greene T, Keshaviah PR, et al. Hemodialyzer mass transfer-area coefficients for urea increase at high dialysate flow rates. Kidney International. 1997 Jun;51(6):2013–7.

252. Battista J, De Luca D, Eleni Dit Trolli S, Allard L, Bacchetta J, Bouhamri N, et al. CARPEDIEM® for continuous kidney replacement therapy in neonates and small infants: a French multicenter retrospective study. Pediatr Nephrol. 2023 Aug;38(8):2827–37.

253. Fresenius Medical Care Renal Therapies Group Personal Communication. 2022.

254. Eloot S, Vos JY, Vos F, Hombrouckx R, Verdonck P. Middle molecule removal in low-flux polysulfone dialyzers: Impact of flows and surface area on whole-body and dialyzer clearances. Hemodialysis International. 2005 Oct;9(4):399–408.

255. Dukhin SS, Tabani Y, Lai R, Labib OA, Zydney AL, Labib ME. Outside-in hemofiltration for prolonged operation without clogging. Journal of Membrane Science. 2014 Aug;464:173–8.

256. Bieber S, Halldorson JB, Finn E, Ahmad S, Chamberlain JS, Odom GL. Extracorporeal Delivery of rAAV with Metabolic Exchange and Oxygenation. Sci Rep. 2013 Dec;3(1):1538.

257. Sangeetha MS, Kandaswamy A, Lakshmi Deepika C, Revanth CV. FINITE ELEMENT ANALYSIS FOR COMPARING THE PERFORMANCE OF STRAIGHT AND UNDULATED FIBERS IN ALTERING THE FILTERING EFFICIENCY OF HEMODIALYZER MEMBRANES. J Mech Med Biol. 2019 Aug;19(05):1850063.

258. Noh US, Yi JH, Han SW, Kim HJ. Varying Dialysate Bicarbonate Concentrations in Maintenance Hemodialysis Patients Affect Post-dialysis Alkalosis but not Pre-dialysis Acidosis. Electrolyte Blood Press. 2007;5(2):95.

259. Marano M, Marano S, Gennari FJ. Beyond bicarbonate: complete acid–base assessment in patients receiving intermittent hemodialysis. Nephrol Dial Transplant. 2016 Mar 21;gfw022.

260. Cheung AK, Agodoa LY, Daugirdas JT, Depner TA, Gotch FA, Greene T, et al. Effects of Hemodialyzer Reuse on Clearances of Urea and $\beta_2$-Microglobulin. JASN. 1999 Jan;10(1):117–27.

261. Leypoldt JK. Methods and Complications of Dialyzer Reuse. In: Handbook of Dialysis Therapy [Internet]. Elsevier; 2008 [cited 2021 Dec 29]. p. 469–77. Available from: https://linkinghub.elsevier.com/retrieve/pii/B9781416041979500363

262. Molina P, Gonzalez-Moya M, Vizcaıno B, Beltran S, Molina M, Sanchis I, et al. RELATIONSHIP BETWEEN PREDICTIVE KT/V AND CALCULATED KT/V ACHIEVED WITH NXSTAGE CYCLER IN SHORT-DAILY HOME HEMODIALYSIS PATIENTS. Nephrology Dialysis Transplantation. 2018 May 1;33(suppl_1):i505–6.

263. Snisarenko D, Pavlenko D, Stamatialis D, Aimar P, Causserand C, Bacchin P. Insight into the transport mechanism of solute removed in dialysis by a membrane with double functionality. Chemical Engineering Research and Design. 2017 Oct;126:97–108.

264. MacCoun R, Perlmutter S. Blind analysis: Hide results to seek the truth. Nature. 2015 Oct;526(7572):187–9.

265. Novokhodko A, Du N, Hao S, Wang Z, Shu Z, Ahmad S, et al. Predicting the Impact of Dialyzer Choice and Binder Dialysate Flow Rate on Bilirubin Removal [Internet]. bioRxiv; 2024 Sep. Available from: https://www.biorxiv.org/content/10.1101/2024.09.27.615470v1

266. Sharma R, Sharma S. Physiology, Blood Volume. In: StatPearls [Internet]. Treasure Island (FL): StatPearls Publishing; 2024 [cited 2024 Apr 23]. Available from: http://www.ncbi.nlm.nih.gov/books/NBK526077/

267. Li PKT, Cheng YL, Leung CB, Szeto CC, Chow KM, Kwan BCH, et al. Effect of Membrane Permeability on Inflammation and Arterial Stiffness: A Randomized Trial. Clinical Journal of the American Society of Nephrology. 2010 Apr;5(4):652–8.

268. Varchanis S, Dimakopoulos Y, Wagner C, Tsamopoulos J. How viscoelastic is human blood plasma? Soft Matter. 2018;14(21):4238–51.

269. Thomson NM, Stevens BJ, Humphery TJ, Atkins RC. Comparison of trace elements in peritoneal dialysis, hemodialysis, and uremia. Kidney International. 1983 Jan;23(1):9–14.

270. Gómez De Oña C, Martínez-Morillo E, Gago González E, Vidau Argüelles P, Fernández Merayo C, Álvarez Menéndez FV. Variation of trace element concentrations in patients undergoing hemodialysis in the north of Spain. Scandinavian Journal of Clinical and Laboratory Investigation. 2016 Aug 17;76(6):492–9.

271. Akcan E, Özkurt S, Sahin G, Yalcin AU, Adapinar B. The relation between brain MRI findings and blood manganese levels in renal transplantation, hemodialysis, and peritoneal dialysis patients. Int Urol Nephrol. 2018 Jan;50(1):173–7.

272. Prodanchuk M, Makarov O, Pisarev E, Sheiman B, Kulyzkiy M. Disturbances of trace element metabolism in ESRD patients receiving hemodialysis and hemodiafiltration. CEJU [Internet]. 2013 [cited 2024 Jun 18];66(04). Available from: http://ceju.online/journal/2013/trace-elements-end-stage-renal-disease-hemodyalisis-hemodiafiltration-307.php

273. Xu B, Zhang Y, Chen Y, Zeng M, Feng J, Tang J, et al. Simultaneous multielement analysis by ICP-MS with simple whole blood sample dilution and its application to uremic patients undergoing long-term hemodialysis. Scandinavian Journal of Clinical and Laboratory Investigation. 2020 Apr 2;80(3):247–55.

274. Li C, Xiang W, Wu M, Zhang H, Cheng J, Yang T, et al. A randomized dose-escalation study on the safety, tolerability, immunogenicity, pharmacokinetics and pharmacodynamics of a novel recombinant human albumin in healthy subjects. European Journal of Pharmaceutical Sciences. 2021 Oct;165:105923.

275. Minonzio G, Linetsky. The Use of Fetal Bovine Serum in Cellular Products for Clinical Applications: Commentary. CellR4. 2014;2(6):e1307.

276. Mackensen A, Dräger R, Schlesier M, Mertelsmann R, Lindemann A. Presence of IgE antibodies to bovine serum albumin in a patient developing anaphylaxis after vaccination with human peptide-pulsed dendritic cells. Cancer Immunology, Immunotherapy. 2000 May 22;49(3):152–6.

277. Gray RD, Stroupe SD. Kinetics and mechanism of bilirubin binding to human serum albumin. Journal of Biological Chemistry. 1978 Jun;253(12):4370–7.

278. Jacobsen J. Binding of bilirubin to human serum albumin - determination of the dissociation constants. FEBS Letters. 1969 Oct 21;5(2):112–4.

279. Beaven GH, D'Albis A, Gratzer WB. The Interaction of Bilirubin with Human Serum Albumin. Eur J Biochem. 1973 Mar;33(3):500–9.

280. Blauer G, Lavie E, Silfen J. Relative affinities of bilirubin for serum albumins from different species. Biochimica et Biophysica Acta (BBA) - Protein Structure. 1977 May;492(1):64–9.

281. Berde CB, Hudson BS, Simoni RD, Sklar LA. Human serum albumin. Spectroscopic studies of binding and proximity relationships for fatty acids and bilirubin. Journal of Biological Chemistry. 1979 Jan;254(2):391–400.

282. Athar H, Ahmad N, Tayyab S, Qasim MA. Use of fluorescence enhancement technique to study bilirubin–albumin interaction. International Journal of Biological Macromolecules. 1999 Aug;25(4):353–8.

283. Khan MohdM, Muzammil S, Tayyab S. Role of salt bridge(s) in the binding and photoconversion of bilirubin bound to high affinity site on human serum albumin. Biochimica et Biophysica Acta (BBA) - Protein Structure and Molecular Enzymology. 2000 Jun;1479(1–2):103–13.

284. Khan MA, Kumar Y, Tayyab S. Bilirubin binding properties of pigeon serum albumin and its comparison with human serum albumin. International Journal of Biological Macromolecules. 2002 Jun;30(3–4):171–8.

285. Tayyab S, Khan NJ, Khan MA, Kumar Y. Behavior of various mammalian albumins towards bilirubin binding and photochemical properties of different bilirubin–albumin complexes. International Journal of Biological Macromolecules. 2003 Jan;31(4–5):187–93.

286. Rudman D, Kendall FE. Bile Acid Content of Human Serum. II. The Binding of Cholanic Acids by Human Plasma Proteins1. J Clin Invest. 1957 Apr 1;36(4):538–42.

287. Kaur M, Bhattacharya M, Maity B. Deciphering conformational changes in human serum albumin induced by bile salts using spectroscopic and molecular modeling approaches. Journal of Molecular Liquids. 2023 Nov;390:123026.

288. Scagnolari F, Roda A, Fini A, Grigolo B. Thermodynamic features of bile salt-human serum albumin interaction. Biochimica et Biophysica Acta (BBA) - Protein Structure and Molecular Enzymology. 1984 Dec;791(2):274–7.

289. Roda A, Cappelleri G, Aldini R, Roda E, Barbara L. Quantitative aspects of the interaction of bile acids with human serum albumin. Journal of Lipid Research. 1982 Mar;23(3):490–5.

290. Burke CW, Lewis B, Panveliwalla D, Tabaqchali S. The binding of cholic acid and its taurine conjugate to serum proteins. Clinica Chimica Acta. 1971 Apr;32(2):207–14.

291. Deltombe O, De Loor H, Glorieux G, Dhondt A, Van Biesen W, Meijers B, et al. Exploring binding characteristics and the related competition of different protein-bound uremic toxins. Biochimie. 2017 Aug;139:20–6.

292. Sakai T, Takadate A, Otagiri M. Characterization of Binding Site of Uremic Toxins on Human Serum Albumin. Biological & Pharmaceutical Bulletin. 1995;18(12):1755–61.

293. Bergé-Lefranc D, Chaspoul F, Cérini C, Brunet P, Gallice P. Thermodynamic study of indoxylsulfate interaction with human serum albumin and competitive binding with p-cresylsulfate. J Therm Anal Calorim. 2014 Mar;115(3):2021–6.

294. Dehghan Niestanak V, Unsworth LD. Detailing Protein-Bound Uremic Toxin Interaction Mechanisms with Human Serum Albumin in the Pursuit of Designing Competitive Binders. IJMS. 2023 Apr 18;24(8):7452.

295. Li S, Tonelli M, Unsworth LD. Indoxyl and p-cresol sulfate binding with human serum albumin. Colloids and Surfaces A: Physicochemical and Engineering Aspects. 2022 Feb;635:128042.

296. Yamamoto S, Sasahara K, Domon M, Yamaguchi K, Ito T, Goto S, et al. pH-Dependent Protein Binding Properties of Uremic Toxins In Vitro. Toxins. 2021 Feb 4;13(2):116.

297. Kato S, Drout RJ, Farha OK. Isothermal Titration Calorimetry to Investigate Uremic Toxins Adsorbing onto Metal-Organic Frameworks. Cell Reports Physical Science. 2020 Jan;1(1):100006.

298. Zaidi N, Khan RH. A biophysical insight into structural and functional state of human serum albumin in uremia mimic milieu. International Journal of Biological Macromolecules. 2019 Jun;131:697–705.

299. De Loor H, Poesen R, De Leger W, Dehaen W, Augustijns P, Evenepoel P, et al. A liquid chromatography – tandem mass spectrometry method to measure a selected panel of uremic retention solutes derived from endogenous and colonic microbial metabolism. Analytica Chimica Acta. 2016 Sep;936:149–56.

300. Yu S, Schuchardt M, Tölle M, Van Der Giet M, Zidek W, Dzubiella J, et al. Interaction of human serum albumin with uremic toxins: a thermodynamic study. RSC Adv. 2017;7(45):27913–22.

301. Rueth M, Lemke H -D., Preisinger C, Krieter D, Theelen W, Gajjala P, et al. Guanidinylations of albumin decreased binding capacity of hydrophobic metabolites. Acta Physiologica. 2015 Sep;215(1):13–23.

302. Ascenzi P, Leboffe L, Di Masi A, Trezza V, Fanali G, Gioia M, et al. Ligand Binding to the FA3-FA4 Cleft Inhibits the Esterase-Like Activity of Human Serum Albumin. Permyakov EA, editor. PLoS ONE. 2015 Mar 19;10(3):e0120603.

303. Devine E, Krieter D, Rüth M, Jankovski J, Lemke HD. Binding Affinity and Capacity for the Uremic Toxin Indoxyl Sulfate. Toxins. 2014 Jan 24;6(2):416–29.

304. Viaene L, Annaert P, De Loor H, Poesen R, Evenepoel P, Meijers B. Albumin is the main plasma binding protein for indoxyl sulfate and *p* -cresyl sulfate. Biopharm & Drug Disp. 2013 Apr;34(3):165–75.

305. Zsila F. Subdomain IB Is the Third Major Drug Binding Region of Human Serum Albumin: Toward the Three-Sites Model. Mol Pharmaceutics. 2013 May 6;10(5):1668–82.

306. Sakai T, Yamasaki K, Sako T, Kragh-Hansen U, Suenaga A, Otagiri M. Interaction Mechanism Between Indoxyl Sulfate, a Typical Uremic Toxin Bound to Site II, and Ligands Bound to Site I of Human Serum Albumin. Pharmaceutical Research. 2001;18(4):520–4.

307. Ding W, Zou L, Sun S, Li W, Gao D. A New Method to Increase the Adsorption of Protein-Bound Toxins in Artificial Liver Support Systems: Preconcentration Method in Liver Support. Artificial Organs. 2014 Nov;38(11):954–62.

308. Giordano C, Esposito R, Bello P, Quarto E, Gonzalez FM. Cold Carbon Apparatus for Hemodialysis. Journal of Dialysis. 1976 Jan;1(2):165–79.

309. Chandy T, Sharma CP. Preparation and performance of chitosan encapsulated activated charcoal (ACCB) adsorbents for small molecules. Journal of Microencapsulation. 1993 Jan;10(4):475–86.

310. Debiec H, Lefeu F, Kemper MJ, Niaudet P, Deschênes G, Remuzzi G, et al. Early-Childhood Membranous Nephropathy Due to Cationic Bovine Serum Albumin. N Engl J Med. 2011 Jun 2;364(22):2101–10.

311. Restani P, Ballabio C, Cattaneo A, Isoardi P, Terracciano L, Fiocchi A. Characterization of bovine serum albumin epitopes and their role in allergic reactions. Allergy. 2004 Aug;59(s78):21–4.

312. Demetriou AA, Brown RS, Busuttil RW, Fair J, McGuire BM, Rosenthal P, et al. Prospective, Randomized, Multicenter, Controlled Trial of a Bioartificial Liver in Treating Acute Liver Failure. Annals of Surgery. 2004 May;239(5):660–70.

313. Wang Z, Wei H, Jia L, Xu L, Zou C, Xie J. Water-soluble adsorbent β-cyclodextrin-grafted polyethyleneimine for removing bilirubin from plasma. Transfusion and Apheresis Science. 2012 Oct;47(2):159–65.

314. Han L, Chu S, Wei H, Ren J, Xu L, Jia L. Functionalized Magnetic $Fe_3O_4$ - $\beta$ - Cyclodextran Nanoparticles for Efficient Removal of Bilirubin. j nanosci nanotechnol. 2016 Jun 1;16(6):5537–45.

315. Kramer L, Gendo A, Madl C, Mullen KD, Kaminski-Russ K, Sunder-Plassmann G, et al. A Controlled Study of Sorbent Suspension Dialysis in Chronic Liver Disease and Hepatic Encephalopathy. Int J Artif Organs. 2001 Jul;24(7):434–42.

316. Londoño LA, Buckley GJ, Bolfer L, Bandt C. Clearance of plasma ivermectin with single pass lipid dialysis in 2 dogs: Lipid dialysis for ivermectin toxicosis. Journal of Veterinary Emergency and Critical Care. 2017 Mar;27(2):232–7.

317. Shen Y, Wang Y, Shi Y, Tian H, Zhu Q, Ding F. Development of liposome as a novel adsorbent for artificial liver support system in liver failure. Journal of Liposome Research. 2020 Jul 2;30(3):246–54.

318. Naessens M, Cerdobbel A, Soetaert W, Vandamme EJ. Leuconostoc dextransucrase and dextran: production, properties and applications. J Chem Technol Biotechnol. 2005 Aug;80(8):845–60.

319. Glišić S, Nikolić G, Cakić M, Trutić N. Spectroscopic study of copper(II) complexes with carboxymethyl dextran and dextran sulfate. Russ J Phys Chem. 2015 Jul;89(7):1254–62.

320. Steffan G, Wulff S, Galla HJ. Divalent cation-dependent interaction of sulfated polysaccharides with phosphatidylcholine and mixed phosphatidylcholine/phosphatidylglycerol liposomes. Chemistry and Physics of Lipids. 1994 Dec;74(2):141–50.

321. Dextran Sulfate MeSH Descriptor Data 2023 [Internet]. National Library of Medicine; 2007. Available from: https://meshb-prev.nlm.nih.gov/record/ui?ui=D016264

322. Protein Pull-Down Techniques > Dextran Sulfate [Internet]. Sigma Aldrich; 2024. Available from: https://www.sigmaaldrich.com/US/en/technical-documents/protocol/protein-biology/protein-pulldown/dextran-sulfate

323. Intralipid® 20% NDA 18-449/S-039 NDA 17-643/S-072. US FDA; 2006.

324. Harmatz D, Blauer G. Optical properties of bilirubin-serum albumin complexes in aqueous solution. A comparison among albumins from different species. Archives of Biochemistry and Biophysics. 1975;170:375–83.

325. Sastri VR. High-Temperature Engineering Thermoplastics: Polysulfones, Polyimides, Polysulfides, Polyketones, Liquid Crystalline Polymers, and Fluoropolymers. In: Plastics in Medical Devices [Internet]. Elsevier; 2014 [cited 2024 Feb 10]. p. 173–213. Available from: https://linkinghub.elsevier.com/retrieve/pii/B9781455732012000082

# Chapter 12. APPENDIX A: BIORENDER FIGURE LICENSES

This section contains Figure License documents from BioRender.

49 Spadina Ave. Suite 200
Toronto ON M5V 2J1 Canada
www.biorender.com

# Confirmation of Publication and Licensing Rights

**July 21st, 2024**
**Science Suite Inc.**

| | |
|---|---|
| ***Subscription:*** | *Institution* |
| ***Agreement number:*** | *UP273801QU* |
| ***Journal name:*** | *Thesis* |

To whom this may concern,

This document is to confirm that Alexander Novokhodko has been granted a license to use the BioRender content, including icons, templates and other original artwork, appearing in the attached completed graphic pursuant to BioRender's Academic License Terms. This license permits BioRender content to be sublicensed for use in journal publications.

All rights and ownership of BioRender content are reserved by BioRender. All completed graphics must be accompanied by the following citation: "Created with BioRender.com".

BioRender content included in the completed graphic is not licensed for any commercial uses beyond publication in a journal. For any commercial use of this figure, users may, if allowed, recreate it in BioRender under an Industry BioRender Plan.

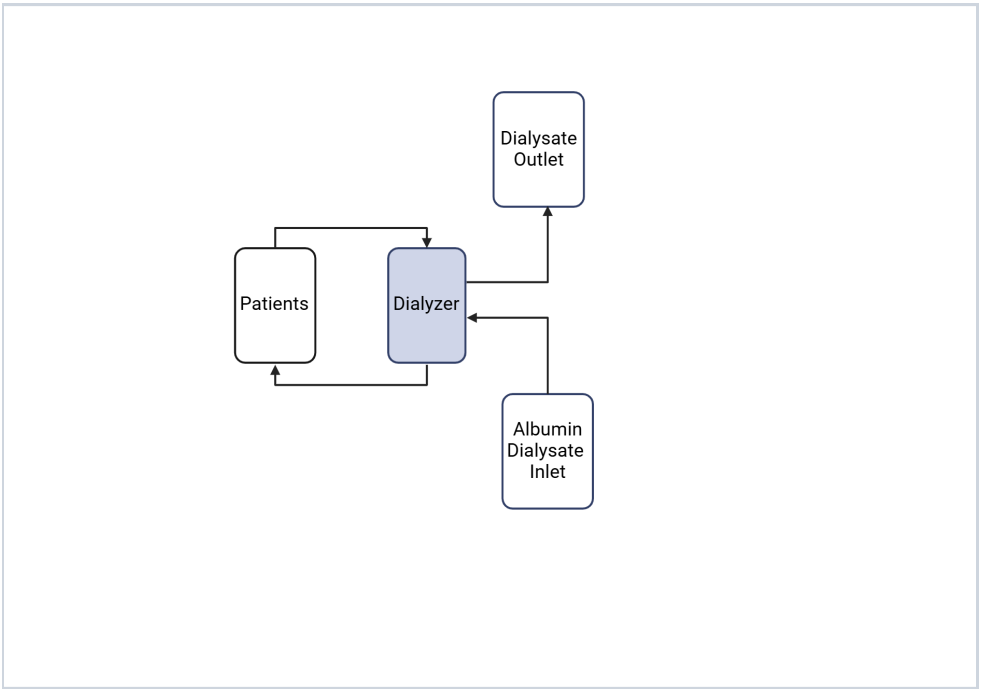


*For any questions regarding this document, or other questions about publishing with BioRender refer to our BioRender Publication Guide, or contact BioRender Support at support@biorender.com.*

49 Spadina Ave. Suite 200
Toronto ON M5V 2J1 Canada
www.biorender.com

# Confirmation of Publication and Licensing Rights

**July 21st, 2024**
**Science Suite Inc.**

| | |
|---|---|
| ***Subscription:*** | *Institution* |
| ***Agreement number:*** | *PS2738AE0S* |
| ***Journal name:*** | *Thesis* |

To whom this may concern,

This document is to confirm that Alexander Novokhodko has been granted a license to use the BioRender content, including icons, templates and other original artwork, appearing in the attached completed graphic pursuant to BioRender's Academic License Terms. This license permits BioRender content to be sublicensed for use in journal publications.

All rights and ownership of BioRender content are reserved by BioRender. All completed graphics must be accompanied by the following citation: "Created with BioRender.com".

BioRender content included in the completed graphic is not licensed for any commercial uses beyond publication in a journal. For any commercial use of this figure, users may, if allowed, recreate it in BioRender under an Industry BioRender Plan.

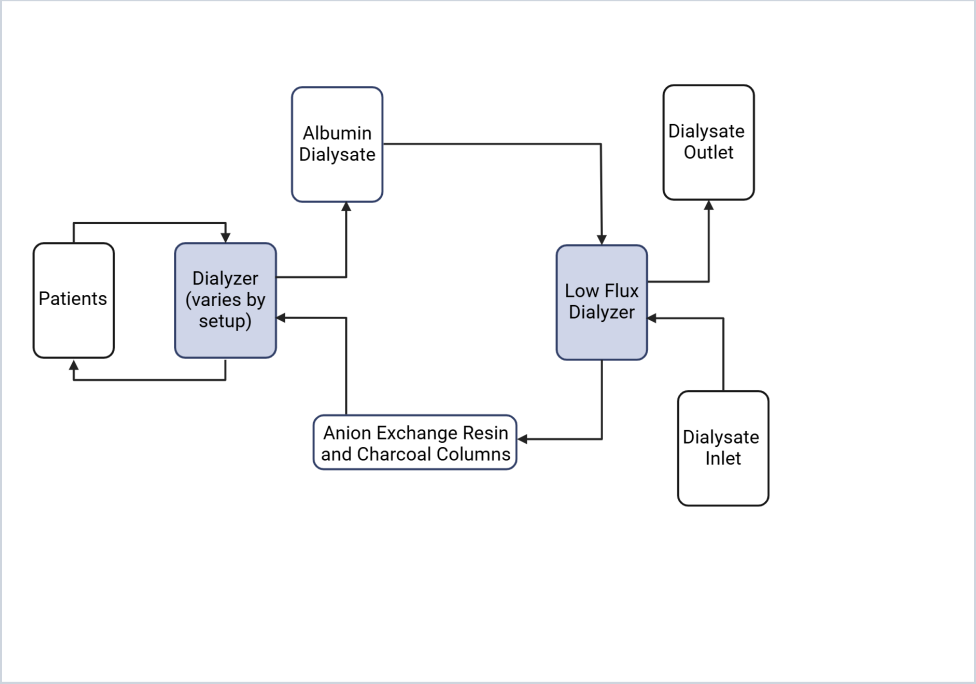


*For any questions regarding this document, or other questions about publishing with BioRender refer to our BioRender Publication Guide, or contact BioRender Support at support@biorender.com.*

49 Spadina Ave. Suite 200
Toronto ON M5V 2J1 Canada
www.biorender.com

# Confirmation of Publication and Licensing Rights

**July 21st, 2024**
**Science Suite Inc.**

| | |
|---|---|
| ***Subscription:*** | *Institution* |
| ***Agreement number:*** | *EF273887NN* |
| ***Journal name:*** | *Thesis* |

To whom this may concern,

This document is to confirm that Alexander Novokhodko has been granted a license to use the BioRender content, including icons, templates and other original artwork, appearing in the attached completed graphic pursuant to BioRender's Academic License Terms. This license permits BioRender content to be sublicensed for use in journal publications.

All rights and ownership of BioRender content are reserved by BioRender. All completed graphics must be accompanied by the following citation: "Created with BioRender.com".

BioRender content included in the completed graphic is not licensed for any commercial uses beyond publication in a journal. For any commercial use of this figure, users may, if allowed, recreate it in BioRender under an Industry BioRender Plan.

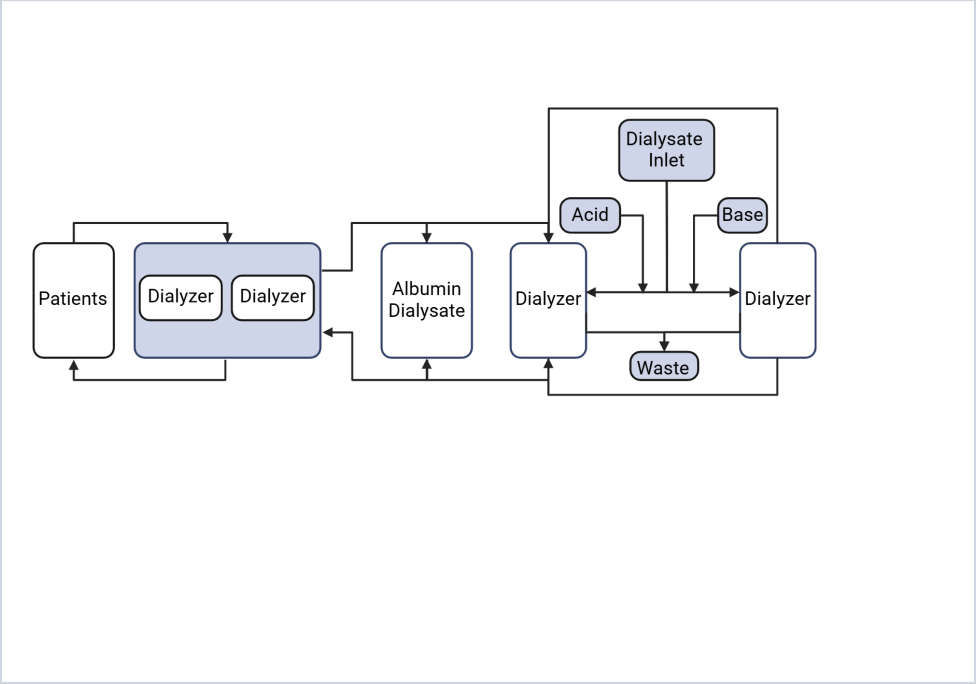


*For any questions regarding this document, or other questions about publishing with BioRender refer to our BioRender Publication Guide, or contact BioRender Support at support@biorender.com.*

49 Spadina Ave. Suite 200
Toronto ON M5V 2J1 Canada
www.biorender.com

# Confirmation of Publication and Licensing Rights

**July 21st, 2024**
**Science Suite Inc.**

| | |
|---|---|
| ***Subscription:*** | *Institution* |
| ***Agreement number:*** | *TE27389DEQ* |
| ***Journal name:*** | *Thesis* |

To whom this may concern,

This document is to confirm that Alexander Novokhodko has been granted a license to use the BioRender content, including icons, templates and other original artwork, appearing in the attached completed graphic pursuant to BioRender's Academic License Terms. This license permits BioRender content to be sublicensed for use in journal publications.

All rights and ownership of BioRender content are reserved by BioRender. All completed graphics must be accompanied by the following citation: "Created with BioRender.com".

BioRender content included in the completed graphic is not licensed for any commercial uses beyond publication in a journal. For any commercial use of this figure, users may, if allowed, recreate it in BioRender under an Industry BioRender Plan.

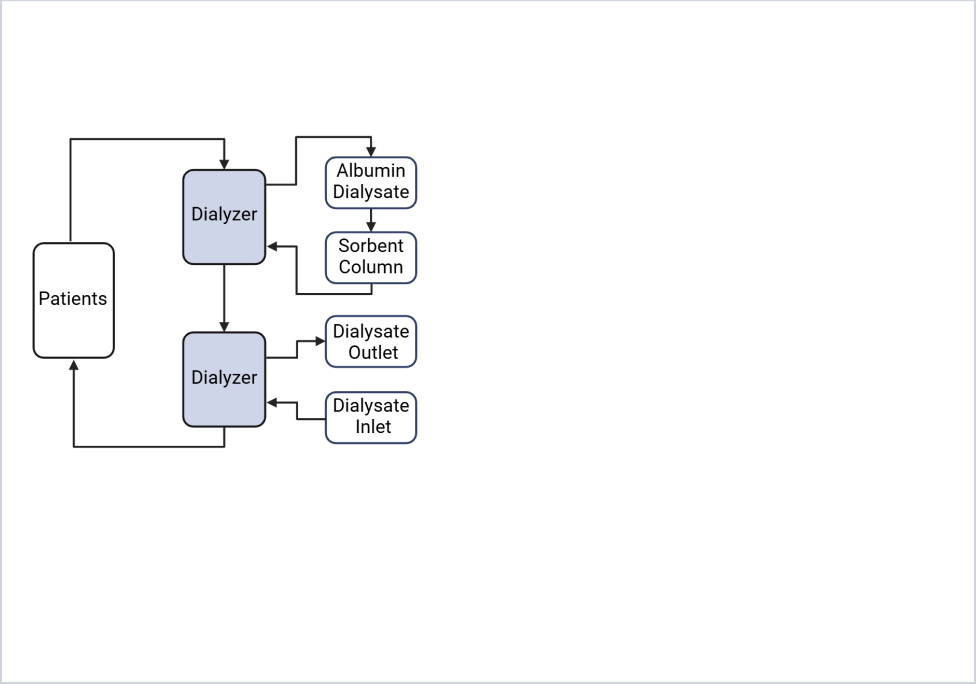


*For any questions regarding this document, or other questions about publishing with BioRender refer to our BioRender Publication Guide, or contact BioRender Support at support@biorender.com.*

49 Spadina Ave. Suite 200
Toronto ON M5V 2J1 Canada
www.biorender.com

# Confirmation of Publication and Licensing Rights

**July 21st, 2024**
**Science Suite Inc.**

| | |
|---|---|
| ***Subscription:*** | *Institution* |
| ***Agreement number:*** | *MG2738A0GW* |
| ***Journal name:*** | *Thesis* |

To whom this may concern,

This document is to confirm that Alexander Novokhodko has been granted a license to use the BioRender content, including icons, templates and other original artwork, appearing in the attached completed graphic pursuant to BioRender's Academic License Terms. This license permits BioRender content to be sublicensed for use in journal publications.

All rights and ownership of BioRender content are reserved by BioRender. All completed graphics must be accompanied by the following citation: "Created with BioRender.com".

BioRender content included in the completed graphic is not licensed for any commercial uses beyond publication in a journal. For any commercial use of this figure, users may, if allowed, recreate it in BioRender under an Industry BioRender Plan.

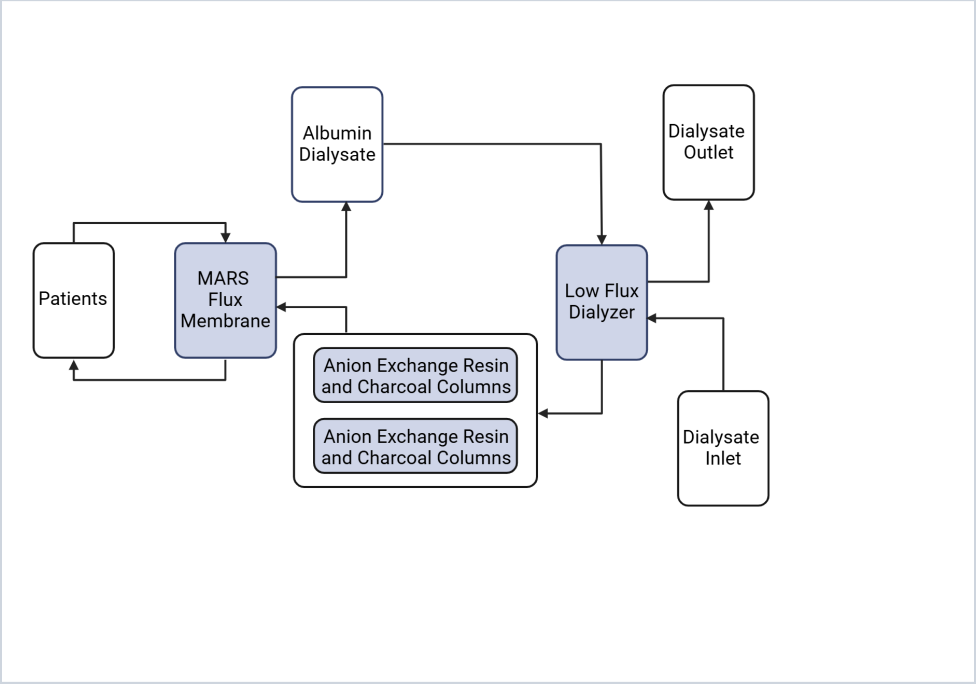


*For any questions regarding this document, or other questions about publishing with BioRender refer to our BioRender Publication Guide, or contact BioRender Support at support@biorender.com.*

49 Spadina Ave. Suite 200
Toronto ON M5V 2J1 Canada
www.biorender.com

# Confirmation of Publication and Licensing Rights

**August 10th, 2024**
**Science Suite Inc.**

| | |
|---|---|
| ***Subscription:*** | *Student Plan* |
| ***Agreement number:*** | *IB2763FWGS* |
| ***Journal name:*** | *PhD Thesis* |

To whom this may concern,

This document is to confirm that Alexander Novokhodko has been granted a license to use the BioRender content, including icons, templates, and other original artwork, appearing in the attached completed graphic pursuant to BioRender's Academic License Terms. This license permits BioRender content to be sublicensed for use in journal publications.

All rights and ownership of BioRender content are reserved by BioRender. All completed graphics must be accompanied by the following citation: "Created with BioRender.com".

BioRender content included in the completed graphic is not licensed for any commercial uses beyond publication in a journal. For any commercial use of this figure, users may, if allowed, recreate it in BioRender under an Industry BioRender Plan.

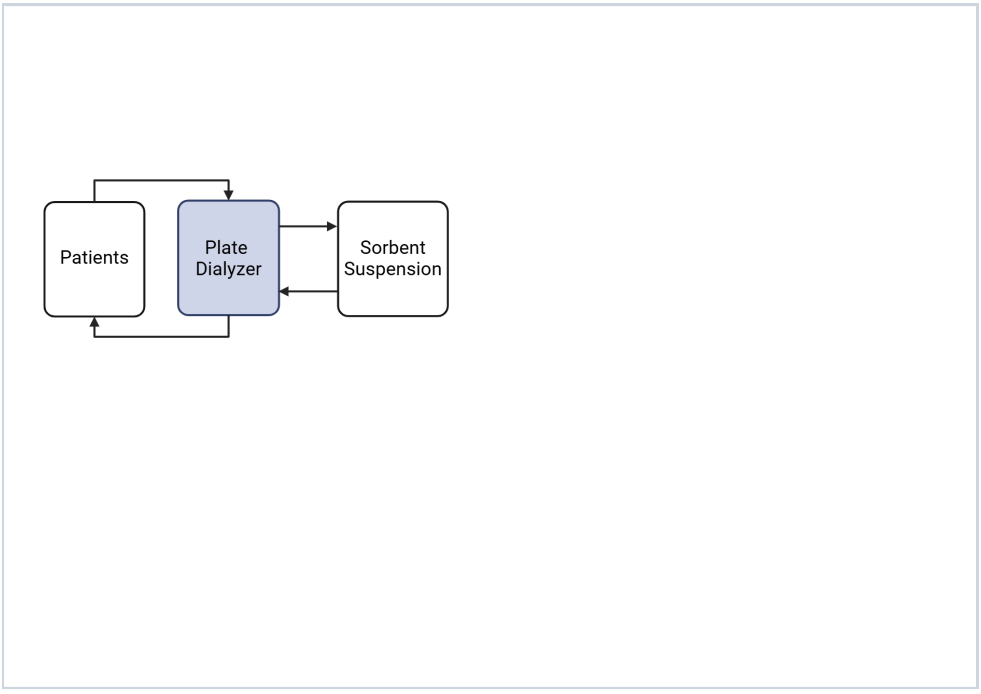


*For any questions regarding this document, or other questions about publishing with BioRender refer to our BioRender Publication Guide, or contact BioRender Support at support@biorender.com.*

49 Spadina Ave. Suite 200
Toronto ON M5V 2J1 Canada
www.biorender.com

# Confirmation of Publication and Licensing Rights

**August 10th, 2024**
**Science Suite Inc.**

| | |
|---|---|
| ***Subscription:*** | *Student Plan* |
| ***Agreement number:*** | *WD2763HG75* |
| ***Journal name:*** | *PhD Thesis* |

To whom this may concern,

This document is to confirm that Alexander Novokhodko has been granted a license to use the BioRender content, including icons, templates, and other original artwork, appearing in the attached completed graphic pursuant to BioRender's Academic License Terms. This license permits BioRender content to be sublicensed for use in journal publications.

All rights and ownership of BioRender content are reserved by BioRender. All completed graphics must be accompanied by the following citation: "Created with BioRender.com".

BioRender content included in the completed graphic is not licensed for any commercial uses beyond publication in a journal. For any commercial use of this figure, users may, if allowed, recreate it in BioRender under an Industry BioRender Plan.

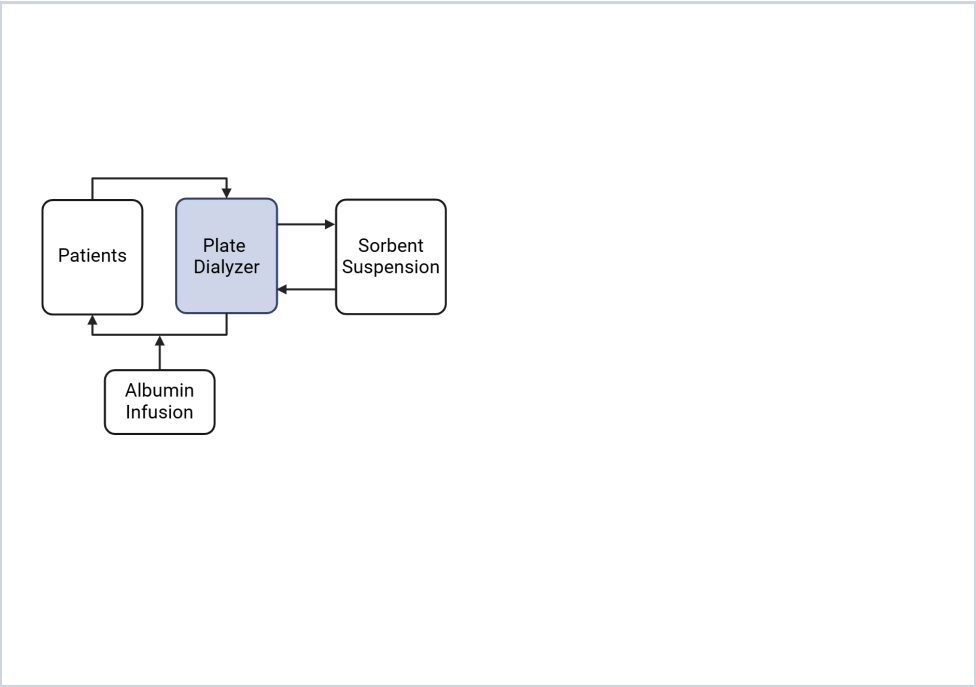


*For any questions regarding this document, or other questions about publishing with BioRender refer to our BioRender Publication Guide, or contact BioRender Support at support@biorender.com.*

49 Spadina Ave. Suite 200
Toronto ON M5V 2J1 Canada
www.biorender.com

# Confirmation of Publication and Licensing Rights

**August 10th, 2024**
**Science Suite Inc.**

| | |
|---|---|
| ***Subscription:*** | *Student Plan* |
| ***Agreement number:*** | *VI2763FI2V* |
| ***Journal name:*** | *PhD Thesis* |

To whom this may concern,

This document is to confirm that Alexander Novokhodko has been granted a license to use the BioRender content, including icons, templates, and other original artwork, appearing in the attached completed graphic pursuant to BioRender's Academic License Terms. This license permits BioRender content to be sublicensed for use in journal publications.

All rights and ownership of BioRender content are reserved by BioRender. All completed graphics must be accompanied by the following citation: "Created with BioRender.com".

BioRender content included in the completed graphic is not licensed for any commercial uses beyond publication in a journal. For any commercial use of this figure, users may, if allowed, recreate it in BioRender under an Industry BioRender Plan.

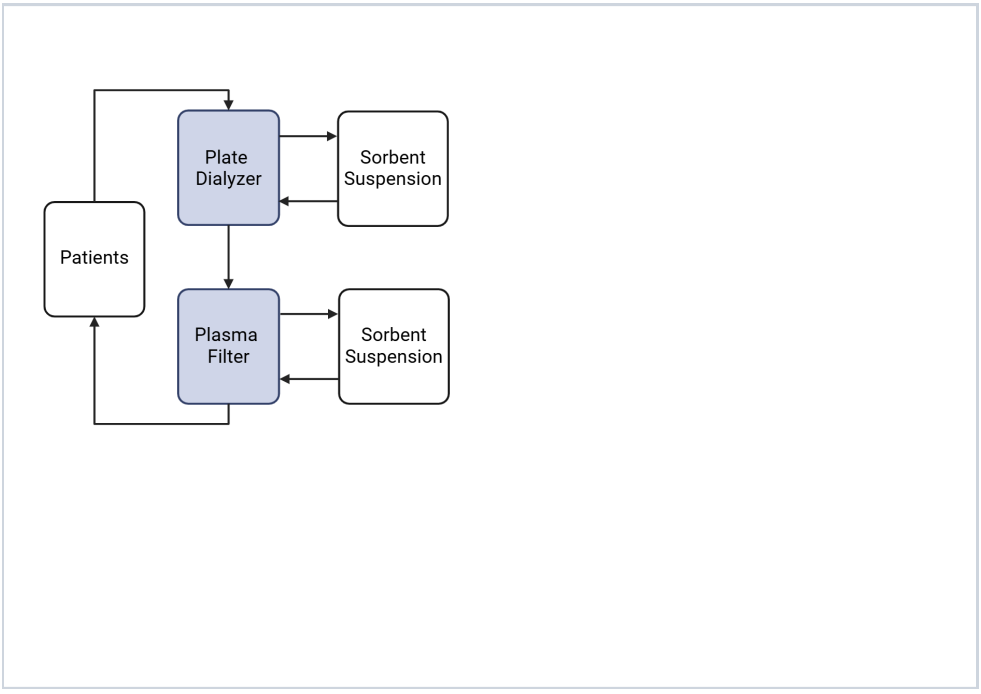


*For any questions regarding this document, or other questions about publishing with BioRender refer to our BioRender Publication Guide, or contact BioRender Support at support@biorender.com.*

49 Spadina Ave. Suite 200
Toronto ON M5V 2J1 Canada
www.biorender.com

# Confirmation of Publication and Licensing Rights

**August 10th, 2024**
**Science Suite Inc.**

| | |
|---|---|
| ***Subscription:*** | *Student Plan* |
| ***Agreement number:*** | *ZL2763BDSY* |
| ***Journal name:*** | *PhD Thesis* |

To whom this may concern,

This document is to confirm that Alexander Novokhodko has been granted a license to use the BioRender content, including icons, templates, and other original artwork, appearing in the attached completed graphic pursuant to BioRender's Academic License Terms. This license permits BioRender content to be sublicensed for use in journal publications.

All rights and ownership of BioRender content are reserved by BioRender. All completed graphics must be accompanied by the following citation: "Created with BioRender.com".

BioRender content included in the completed graphic is not licensed for any commercial uses beyond publication in a journal. For any commercial use of this figure, users may, if allowed, recreate it in BioRender under an Industry BioRender Plan.

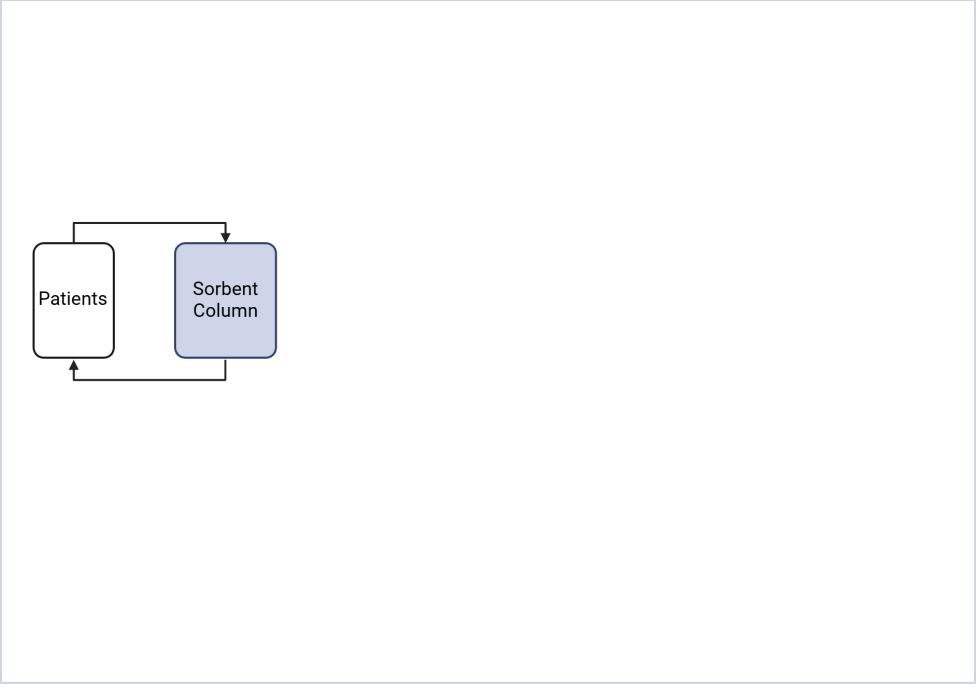


*For any questions regarding this document, or other questions about publishing with BioRender refer to our BioRender Publication Guide, or contact BioRender Support at support@biorender.com.*

49 Spadina Ave. Suite 200
Toronto ON M5V 2J1 Canada
www.biorender.com

# Confirmation of Publication and Licensing Rights

**August 10th, 2024**
**Science Suite Inc.**

| | |
|---|---|
| ***Subscription:*** | *Student Plan* |
| ***Agreement number:*** | *AN2763CSBC* |
| ***Journal name:*** | *PhD Thesis* |

To whom this may concern,

This document is to confirm that Alexander Novokhodko has been granted a license to use the BioRender content, including icons, templates, and other original artwork, appearing in the attached completed graphic pursuant to BioRender's Academic License Terms. This license permits BioRender content to be sublicensed for use in journal publications.

All rights and ownership of BioRender content are reserved by BioRender. All completed graphics must be accompanied by the following citation: "Created with BioRender.com".

BioRender content included in the completed graphic is not licensed for any commercial uses beyond publication in a journal. For any commercial use of this figure, users may, if allowed, recreate it in BioRender under an Industry BioRender Plan.

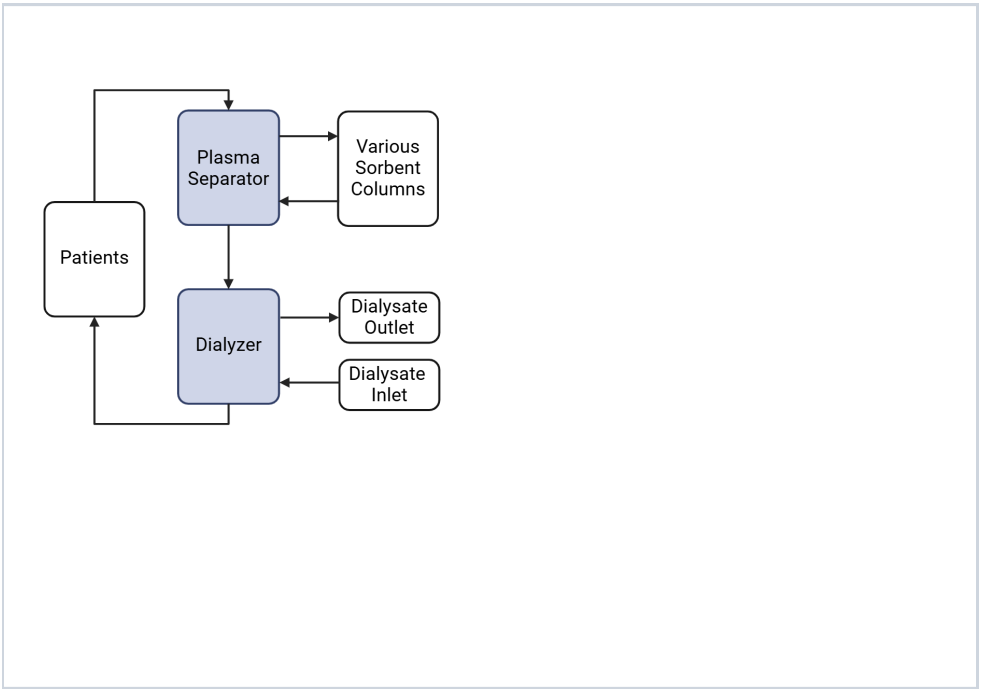


*For any questions regarding this document, or other questions about publishing with BioRender refer to our BioRender Publication Guide, or contact BioRender Support at support@biorender.com.*

49 Spadina Ave. Suite 200
Toronto ON M5V 2J1 Canada
www.biorender.com

# Confirmation of Publication and Licensing Rights

**August 10th, 2024**
**Science Suite Inc.**

| | |
|---|---|
| ***Subscription:*** | *Student Plan* |
| ***Agreement number:*** | *FI2763DNHR* |
| ***Journal name:*** | *PhD Thesis* |

To whom this may concern,

This document is to confirm that Alexander Novokhodko has been granted a license to use the BioRender content, including icons, templates, and other original artwork, appearing in the attached completed graphic pursuant to BioRender's Academic License Terms. This license permits BioRender content to be sublicensed for use in journal publications.

All rights and ownership of BioRender content are reserved by BioRender. All completed graphics must be accompanied by the following citation: "Created with BioRender.com".

BioRender content included in the completed graphic is not licensed for any commercial uses beyond publication in a journal. For any commercial use of this figure, users may, if allowed, recreate it in BioRender under an Industry BioRender Plan.

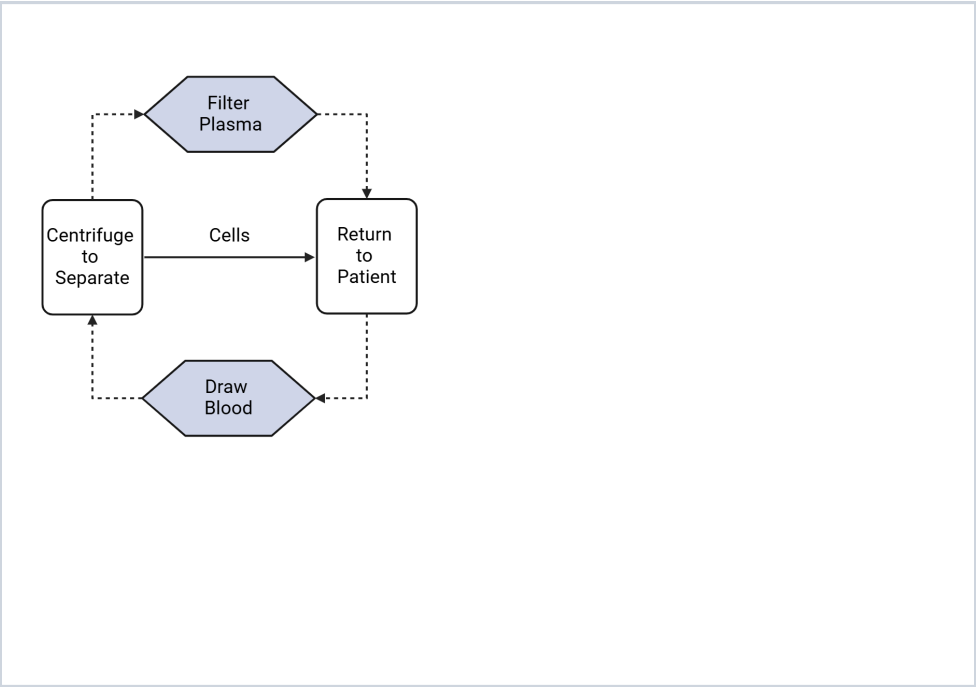


*For any questions regarding this document, or other questions about publishing with BioRender refer to our BioRender Publication Guide, or contact BioRender Support at support@biorender.com.*

49 Spadina Ave. Suite 200
Toronto ON M5V 2J1 Canada
www.biorender.com

# Confirmation of Publication and Licensing Rights

**August 10th, 2024**
**Science Suite Inc.**

| | |
|---|---|
| ***Subscription:*** | *Student Plan* |
| ***Agreement number:*** | *HP2763EDIV* |
| ***Journal name:*** | *PhD Thesis* |

To whom this may concern,

This document is to confirm that Alexander Novokhodko has been granted a license to use the BioRender content, including icons, templates, and other original artwork, appearing in the attached completed graphic pursuant to BioRender's Academic License Terms. This license permits BioRender content to be sublicensed for use in journal publications.

All rights and ownership of BioRender content are reserved by BioRender. All completed graphics must be accompanied by the following citation: "Created with BioRender.com".

BioRender content included in the completed graphic is not licensed for any commercial uses beyond publication in a journal. For any commercial use of this figure, users may, if allowed, recreate it in BioRender under an Industry BioRender Plan.

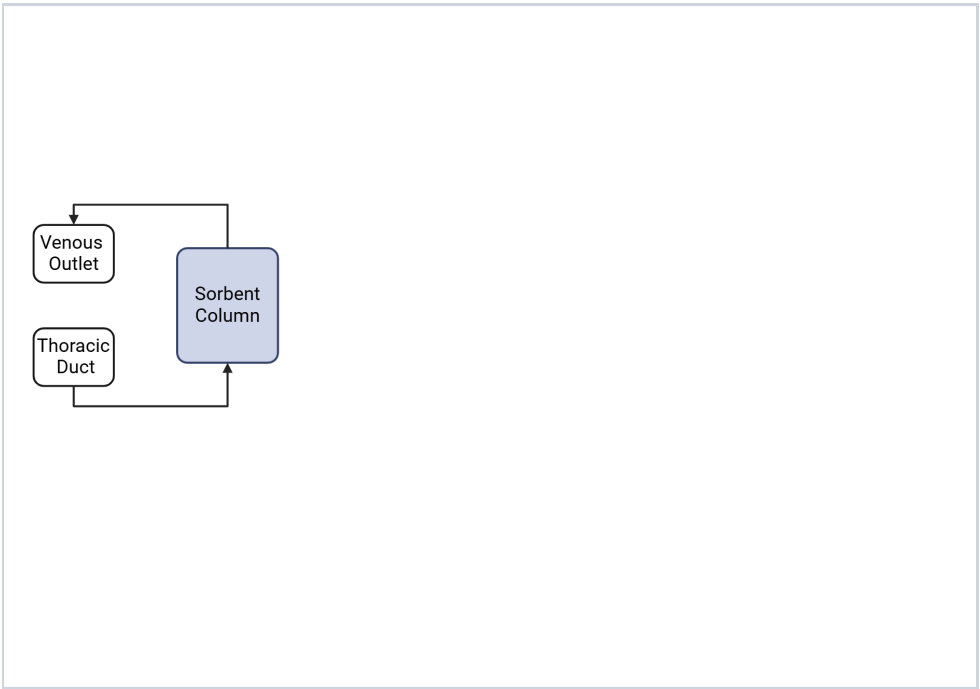


*For any questions regarding this document, or other questions about publishing with BioRender refer to our BioRender Publication Guide, or contact BioRender Support at support@biorender.com.*

49 Spadina Ave. Suite 200
Toronto ON M5V 2J1 Canada
www.biorender.com

# Confirmation of Publication and Licensing Rights

**December 9th, 2024**

| | |
|---|---|
| ***Subscription Type:*** | *Student Plan - Academic* |
| ***Agreement number:*** | *QJ27NDX922* |
| ***Publisher Name:*** | *University of Washington PhD Thesis* |
| ***Citation to Use:*** | *Created in BioRender. Novokhodko, A. (2024) https://BioRender.com/h29q605* |

To whom this may concern,

This document is to confirm that Alexander Novokhodko has been granted a license to use the BioRender Content, including icons, templates, and other original artwork, appearing in the attached Completed Graphic pursuant to BioRender's Academic License Terms. This license permits BioRender Content to be sublicensed for use in publications (journals, textbooks, websites, etc.).

All rights and ownership of BioRender Content are reserved by BioRender. All Completed Graphics must be accompanied by the following citation: "Created in BioRender. Novokhodko, A. (2024) https://BioRender.com/h29q605".

BioRender Content included in the Completed Graphic is not licensed for any commercial uses beyond use in a publication. For any commercial use of this figure, users may, if allowed, recreate it in BioRender under an Industry BioRender Plan.

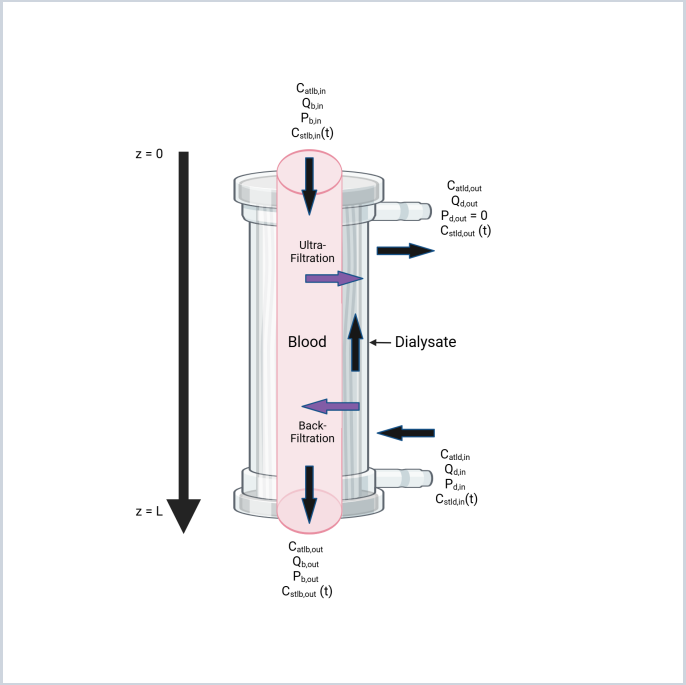


*For any questions regarding this document, or other questions about publishing with BioRender, please refer to our BioRender Publication Guide, or contact BioRender Support at support@biorender.com.*

49 Spadina Ave. Suite 200
Toronto ON M5V 2J1 Canada
www.biorender.com

# Confirmation of Publication and Licensing Rights

**June 14th, 2024**
**Science Suite Inc.**

| | |
|---|---|
| ***Subscription:*** | *Student Plan* |
| ***Agreement number:*** | *FE26XYDCVU* |
| ***Journal name:*** | *University of Washington PhD Thesis* |

To whom this may concern,

This document is to confirm that Alexander Novokhodko has been granted a license to use the BioRender content, including icons, templates and other original artwork, appearing in the attached completed graphic pursuant to BioRender's Academic License Terms. This license permits BioRender content to be sublicensed for use in journal publications.

All rights and ownership of BioRender content are reserved by BioRender. All completed graphics must be accompanied by the following citation: "Created with BioRender.com".

BioRender content included in the completed graphic is not licensed for any commercial uses beyond publication in a journal. For any commercial use of this figure, users may, if allowed, recreate it in BioRender under an Industry BioRender Plan.

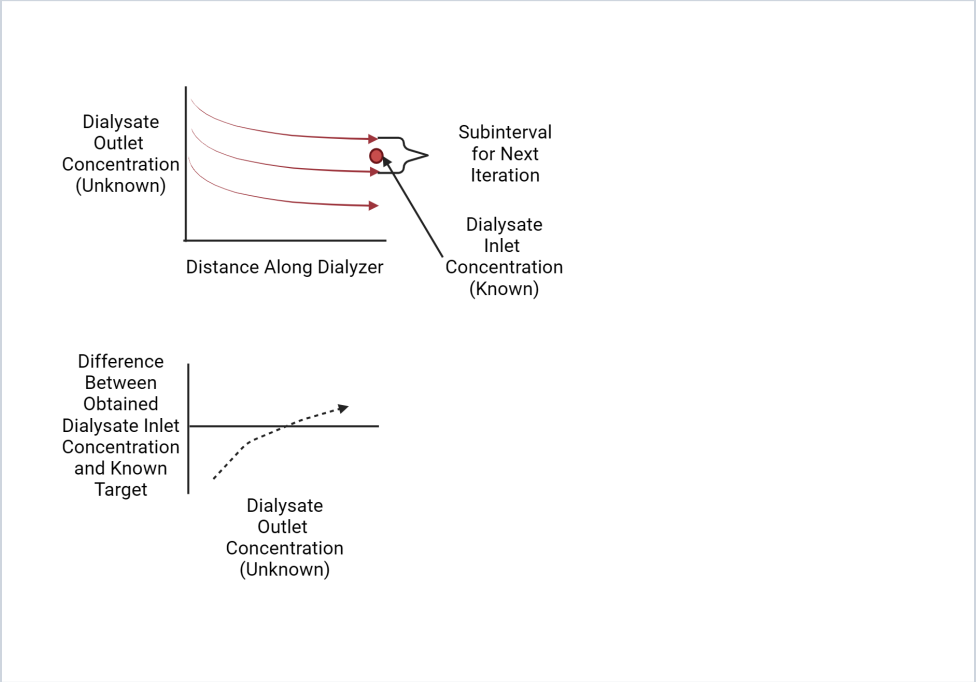


*For any questions regarding this document, or other questions about publishing with BioRender refer to our BioRender Publication Guide, or contact BioRender Support at support@biorender.com.*

49 Spadina Ave. Suite 200
Toronto ON M5V 2J1 Canada
www.biorender.com

# Confirmation of Publication and Licensing Rights

**June 14th, 2024**
**Science Suite Inc.**

| | |
|---|---|
| ***Subscription:*** | *Student Plan* |
| ***Agreement number:*** | *GV26XYJG0R* |
| ***Journal name:*** | *University of Washington PhD Thesis* |

To whom this may concern,

This document is to confirm that Alexander Novokhodko has been granted a license to use the BioRender content, including icons, templates and other original artwork, appearing in the attached completed graphic pursuant to BioRender's Academic License Terms. This license permits BioRender content to be sublicensed for use in journal publications.

All rights and ownership of BioRender content are reserved by BioRender. All completed graphics must be accompanied by the following citation: "Created with BioRender.com".

BioRender content included in the completed graphic is not licensed for any commercial uses beyond publication in a journal. For any commercial use of this figure, users may, if allowed, recreate it in BioRender under an Industry BioRender Plan.

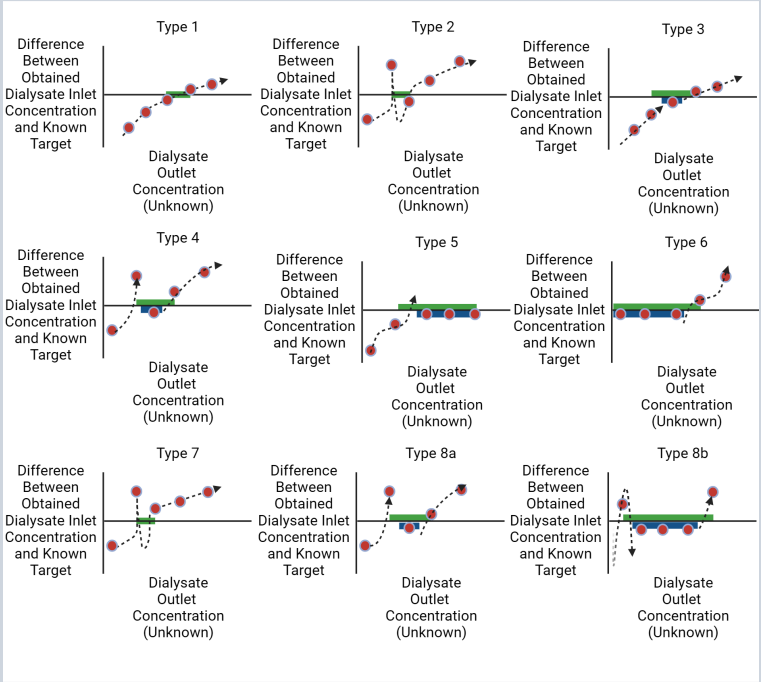


*For any questions regarding this document, or other questions about publishing with BioRender refer to our BioRender Publication Guide, or contact BioRender Support at support@biorender.com.*

49 Spadina Ave. Suite 200
Toronto ON M5V 2J1 Canada
www.biorender.com

# Confirmation of Publication and Licensing Rights

**December 9th, 2024**

| | |
|---|---|
| ***Subscription Type:*** | *Student Plan - Academic* |
| ***Agreement number:*** | *DB27NDZ9CY* |
| ***Publisher Name:*** | *University of Washington PhD Thesis* |
| ***Citation to Use:*** | *Created in BioRender. Novokhodko, A. (2024) https://BioRender.com/x85x842* |

To whom this may concern,

This document is to confirm that Alexander Novokhodko has been granted a license to use the BioRender Content, including icons, templates, and other original artwork, appearing in the attached Completed Graphic pursuant to BioRender's Academic License Terms. This license permits BioRender Content to be sublicensed for use in publications (journals, textbooks, websites, etc.).

All rights and ownership of BioRender Content are reserved by BioRender. All Completed Graphics must be accompanied by the following citation: "Created in BioRender. Novokhodko, A. (2024) https://BioRender.com/x85x842".

BioRender Content included in the Completed Graphic is not licensed for any commercial uses beyond use in a publication. For any commercial use of this figure, users may, if allowed, recreate it in BioRender under an Industry BioRender Plan.

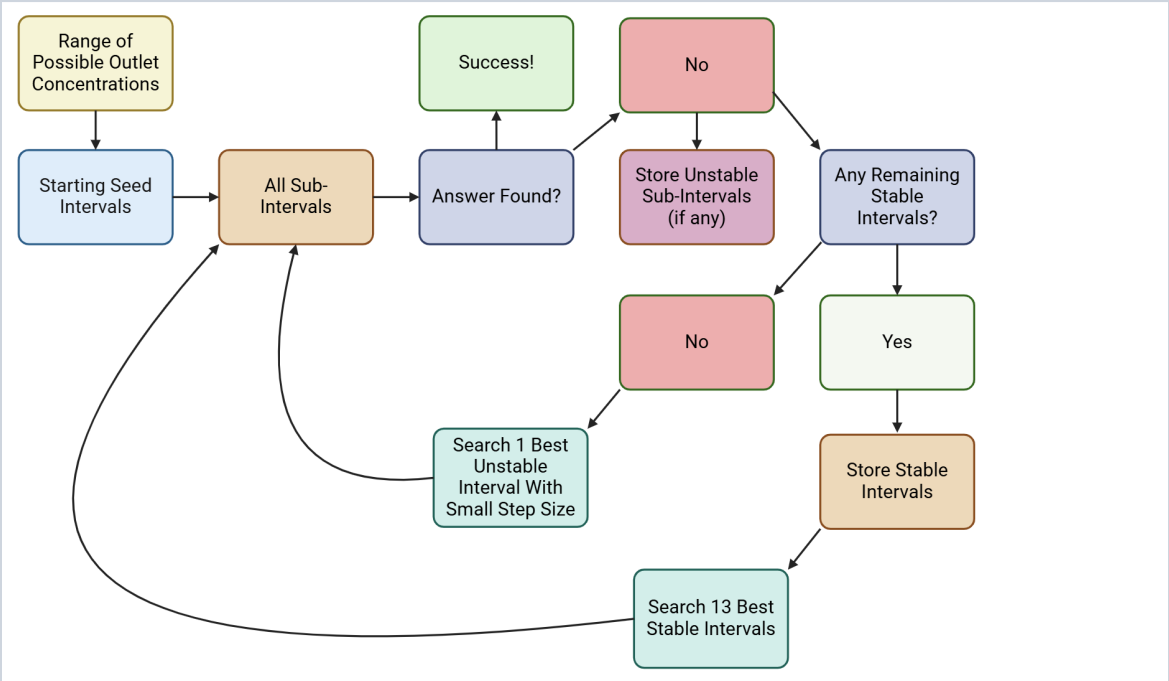


*For any questions regarding this document, or other questions about publishing with BioRender, please refer to our BioRender Publication Guide, or contact BioRender Support at support@biorender.com.*

49 Spadina Ave. Suite 200
Toronto ON M5V 2J1 Canada
www.biorender.com

# Confirmation of Publication and Licensing Rights

**December 9th, 2024**

| | |
|---|---|
| ***Subscription Type:*** | *Student Plan - Academic* |
| ***Agreement number:*** | *NC27NDZO6K* |
| ***Publisher Name:*** | *University of Washington PhD Thesis* |
| ***Citation to Use:*** | *Created in BioRender. Novokhodko, A. (2024) https://BioRender.com/d19h956* |

To whom this may concern,

This document is to confirm that Alexander Novokhodko has been granted a license to use the BioRender Content, including icons, templates, and other original artwork, appearing in the attached Completed Graphic pursuant to BioRender's Academic License Terms. This license permits BioRender Content to be sublicensed for use in publications (journals, textbooks, websites, etc.).

All rights and ownership of BioRender Content are reserved by BioRender. All Completed Graphics must be accompanied by the following citation: "Created in BioRender. Novokhodko, A. (2024) https://BioRender.com/d19h956".

BioRender Content included in the Completed Graphic is not licensed for any commercial uses beyond use in a publication. For any commercial use of this figure, users may, if allowed, recreate it in BioRender under an Industry BioRender Plan.

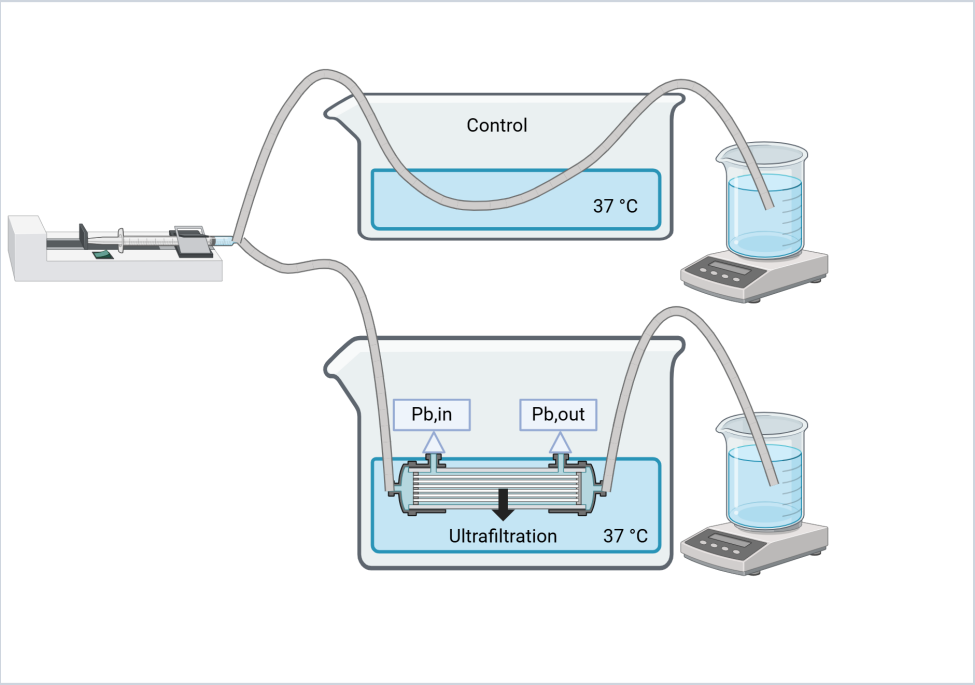


*For any questions regarding this document, or other questions about publishing with BioRender, please refer to our BioRender Publication Guide, or contact BioRender Support at support@biorender.com.*

49 Spadina Ave. Suite 200
Toronto ON M5V 2J1 Canada
www.biorender.com

# Confirmation of Publication and Licensing Rights

**August 21st, 2024**
**Science Suite Inc.**

| | |
|---|---|
| ***Subscription:*** | *Student Plan - Academic* |
| ***Agreement number:*** | *NR277MD3BP* |
| ***Publication name:*** | *PhD Thesis* |
| ***Citation to Use:*** | *Created with BioRender.com* |

To whom this may concern,

This document is to confirm that Alexander Novokhodko has been granted a license to use the BioRender Content, including icons, templates, and other original artwork, appearing in the attached Completed Graphic pursuant to BioRender's Academic License Terms. This license permits BioRender Content to be sublicensed for use in publications (journals, textbooks, websites, etc.).

All rights and ownership of BioRender Content are reserved by BioRender. All Completed Graphics must be accompanied by the following citation: "Created with BioRender.com".

BioRender Content included in the Completed Graphic is not licensed for any commercial uses beyond use in a publication. For any commercial use of this figure, users may, if allowed, recreate it in BioRender under an Industry BioRender Plan.

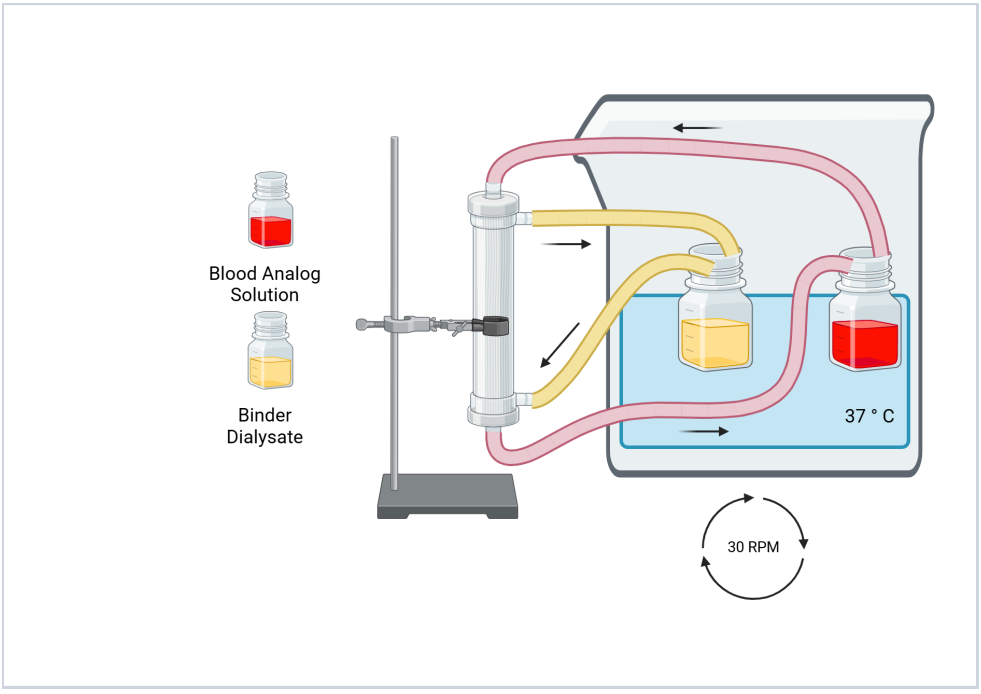


*For any questions regarding this document, or other questions about publishing with BioRender refer to our BioRender Publication Guide, or contact BioRender Support at support@biorender.com.*

49 Spadina Ave. Suite 200
Toronto ON M5V 2J1 Canada
www.biorender.com

# Confirmation of Publication and Licensing Rights

**June 15th, 2024**
**Science Suite Inc.**

| | |
|---|---|
| ***Subscription:*** | *Student Plan* |
| ***Agreement number:*** | *YX26Y3ARJJ* |
| ***Journal name:*** | *University of Washington PhD Thesis* |

To whom this may concern,

This document is to confirm that Alexander Novokhodko has been granted a license to use the BioRender content, including icons, templates and other original artwork, appearing in the attached completed graphic pursuant to BioRender's Academic License Terms. This license permits BioRender content to be sublicensed for use in journal publications.

All rights and ownership of BioRender content are reserved by BioRender. All completed graphics must be accompanied by the following citation: "Created with BioRender.com".

BioRender content included in the completed graphic is not licensed for any commercial uses beyond publication in a journal. For any commercial use of this figure, users may, if allowed, recreate it in BioRender under an Industry BioRender Plan.

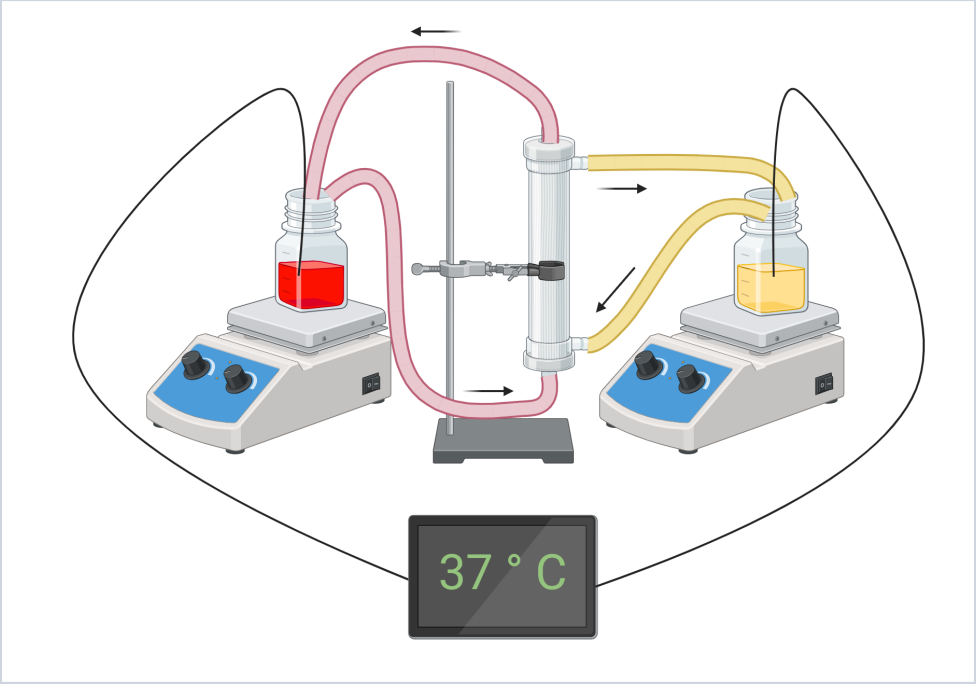


*For any questions regarding this document, or other questions about publishing with BioRender refer to our BioRender Publication Guide, or contact BioRender Support at support@biorender.com.*

# VITA

Alexander Novokhodko received a Masters Degree from the University of Washington (UW) in Mechanical Engineering in June 2022. Prior to that he graduated Cum Laude from the UW with dual Bachelor of Science degrees in Bioengineering and Biology in 2018. During this time, he completed a capstone in Dr. Ying Zheng's lab, titled "Design of a System to Study Endothelial Cell Adaptation in Response to Physiological Cues *in vitro*". He also worked in Dr. Barry Lutz's lab, co-authoring the manuscript "Fluidic Considerations of Measuring Intracranial Pressure Using an Open External Ventricular Drain".

He next worked at Seattle Children's Research Institute to study treatments for hemophilia A. This work led to the publication "Transcutaneous ultrasound mediated gene delivery into canine livers achieves therapeutic levels of FVIII expression".

Alexander begun his graduate studies in September 2019. Alexander was supported by the National Science Foundation Graduate Research Fellowship and the Ron and Wanda Crockett Endowed Fellowship in Mechanical Engineering. From Winter 2020 to Winter 2022, his studies were impacted by a global public health emergency. Despite this he was able to produce the research described here, which has been published as the *in vitro* portion of the study "Development and First Clinical Use of an Extracorporeal Artificial Multiorgan System in Acute-on-Chronic Liver Failure Patients". A second manuscript, "Non-cell-based extracorporeal artificial liver systems: historic perspectives, approaches and mechanisms, current applications, and challenges" has been accepted in the journal *Artificial Organs*. Another manuscript, "Predicting the Impact of Polysulfone Dialyzers and Binder Dialysate Flow Rate on Bilirubin Removal" is under review in the journal *Bioengineering*. A final manuscript is in preparation.

During the COVID-19 pandemic, when in-person research was not possible, Alexander contributed to a collaboration to computationally model the virus. His contributions appear in four manuscripts: "Controlling long-term SARS-CoV-2 infections can slow viral evolution and reduce the risk of treatment failure" and "Risk of rapid evolutionary escape from biomedical interventions targeting SARS-CoV-2 spike protein" and "Rapid relaxation of pandemic restrictions after vaccine rollout favors growth of SARS-CoV-2 variants: A model-based analysis" and "Endemicity is not a victory: the unmitigated downside risks of widespread SARS-CoV-2 transmission".